SYNTHESIS AND BIOLOGICAL ACTIVITY OF SCHIFF BASE AND RUTHENIUM *P*-CYMENE COMPLEXES CONTAINING ETHYNYL-PYRIDINE BRIDGED TO QUINAZOLINE DERIVATIVES

MASTER OF SCIENCE IN CHEMISTRY

DILEBO K.B

2019

SYNTHESIS AND BIOLOGICAL ACTIVITY OF SCHIFF BASE AND RUTHENIUM *P*-CYMENE COMPLEXES CONTAINING ETHYNYL-PYRIDINE BRIDGED TO QUINAZOLINE DERIVATIVES

BY

KABELO BRAMLEY DILEBO

[redacted]

A RESEARCH DISSERTATION SUBMITTED FOR THE DEGREE, MASTER OF SCIENCE IN CHEMISTRY, SCHOOL OF PHYSICAL AND MINERAL SCIENCES, FACULTY OF SCIENCE AND AGRICULTURE, UNIVERSITY OF LIMPOPO, SOUTH AFRICA

SUPERVISOR: Prof R.M. MAMPA

CO-SUPERVISORS: Prof W. NXUMALO

Prof B.O. OWAGA (UKZN)

2019

DEDICATION

I dedicate this work to:

- My baby sister Eucharia, my parents and my brothers.

DECLARATION

I declare that “Synthesis and biological activity of Schiff base and ruthenium *p*-cymene complexes containing ethynyl-pyridine bridged to quinazoline derivatives” is my own, unaided work submitted for the degree of Master Science at Limpopo. It has not been submitted for any degree or examination at any other University, and all sources I have used or quoted have been indicated and acknowledged through complete references.

…… 09/09/2019

Mr K.B Dilebo **Date**

ACKNOWLEDGEMENTS

This dissertation has become a reality with the kind support and help of my supervisors Prof R.M Mampa, Prof W Nxumalo and Prof B.O Owaga. I extend my sincere thanks to you all.

I also extend great thanks to the following individuals and institutions (in no order of importance) for the help offered where possible and for successful collaborations during the academic journey, this work is what it is because of your contributions:

- My family for their prayers, encouragement and support and the Almighty God who in his presence I have achieved a lot.
- The department of chemistry at the University of Limpopo for affording me the opportunity to enroll for postgraduate degrees.
- The NRF-Sasol Inzalo bursary for the financial support.
- Prof M.J Mphahlele for inspiring the project and providing financial support where necessary.
- Dr N.J Gumede for teaching and hosting me during molecular modelling training at the Mangosuthu University of Technology.
- Ms TG Ramakadi for her continuous guidance during the period of my postgraduate studies and for teaching and training me the running (experiments), maintenance and processing (data) of nuclear magnetic resonance (NMR) instrument.
- Prof T Matsebatlela for assisting with anticancer assay experimental data.
- The centre for drug delivery and development (H3-D) centre at the University of Cape Town for the anti-*Mycobaterium tuberculosis* assay experimental data.
- University of Stellenbosch for high resolution mass spectrometry analysis.
- Ms Bokome Shaku for her continuous support and encouragement, thanks nana!
- My labmates Ms L.A Raphoko, Mr N.R Moroane and Mr K Lekgau for making the lab space a fun place to be.
- My friends (Cry, Titelo, Msido-Sidwell, Ofentse, Marvelous, Lesedi and Louis) for always being there for me!

TABLE OF CONTENTS

SCIENTIFIC CONTRIBUTIONS

Conferences attended:

Oral presentation at:

9th Faculty of Sciences and Agriculture, University of Limpopo Research day Limpopo South Africa 2018

Title: Synthesis, characterisation, molecular docking and in vitro anti-*Mycobacterium tuberculosis* properties of 4-(pyridylamino) - and 4-(ethynylpyridine)quinazolines

Date: 20-21 September 2018

Synthesis, characterisation, molecular docking and in vitro anti-*Mycobacterium tuberculosis* properties of 4-(pyridylamino)- and 4-(ethynylpyridine)quinazolines

KB Dilebo[1], RM Mampa[1*], W Nxumalo[1], NR Moroane[1], BO Owaga[2], NJ Gumede[3]

[1]University of Limpopo Department of Chemistry, Private Bag x1106, Sovenga, 0727, [2]University of KwaZulu Natal, School of Chemistry and Physics, Private Bag X54001, Durban 4000, [3]Mangosuthu University of Technology, Department of Chemistry, PO Box 12363, Jacobs 4026.

email address: kbsebashe@gmail.com

A series of novel 4-(pyridylamino)- and 4-(ethynylpyridine)quinazolines were successfully prepared via Sonogashira cross-coupling and dechloro-amination reactions on the *C(4)-Cl* position of the requisite 2-(*p*-phenyl)-4-chloroquinazolines. The prepared compounds were characterized by way of (^{1}H, ^{13}C, COSY and HMBC) NMR, FTIR, Mass spectrometry and UV/Vis. Furthermore, the compounds were evaluated for potential in vitro anti-*Mycobacterium tuberculosis (Mtb)* properties employing rifampicin as a reference drug. Preliminary results from the Alamar Blue assay (*Mtb*. H_{37}Rv strain) revealed promising MIC_{90} ranging from 10 to 43 ug/ml. The possible mode of action against the *Mtb* was theoretically explained through molecular docking of *glutamine synthetase* (1HTO). These compounds were inductively docked into the 1HTO protein where a promising hint of the 4-(pyridylamino)- and 4-(ethynylpyridine)quinazolines ranging from -6.280 to -8.257 Kcal/ mol is observed.

Keywords: 4-(pyridylamino) and 4-(ethynylpyridine)quinazolines, 2-(*p*-phenyl)-4-chloroquinazolines, *Mycobacterium tuberculosis (Mtb)*, Molecular docking, *glutamine synthetase*

Oral presentation at:

43rd SACI National Convention, CSIR-ICC, Pretoria, South Africa 2018

Title: Synthesis, characterisation, molecular docking and in vitro anti-*Mycobacterium tuberculosis* properties of 4-(pyridylamino) - and 4-(ethynylpyridine)quinazolines

Date: 2-7 December 2018

Synthesis, characterisation, molecular docking and in vitro anti-*Mycobacterium tuberculosis* properties of 4-(pyridylamino)- and 4-(ethynylpyridine)quinazolines

Kabelo B Dilebo[a], Richard M Mampa[a*], Winston Nxumalo[a], Ngoako R Moroane[a], Bernard O Owaga[b] and Njabulo J Gumede[c]

[a]Department of Chemistry, University of Limpopo, Private Bag X 1106, Sovenga, Polokwane,
E-mail: richard.mampa@ul.ac.za
[b]University of KwaZulu Natal, School of Chemistry and Physics, Private Bag X54001, Durban 4000,
[c]Mangosuthu University of Technology, Department of Chemistry, PO Box 12363, Jacobs 4026.

Keywords: 4-(pyridylamino) and 4-(ethynylpyridine)quinazolines, 2-(p-phenyl)-4-chloroquinazolines, *Mycobacterium tuberculosis* (Mtb), Molecular docking, *glutamine synthetase*

A series of novel 4-(pyridylamino)- and 4-(ethynylpyridine)quinazolines were successfully prepared via Sonogashira cross-coupling and dechloro-amination reactions on the *C(4)-Cl* position of the requisite 2-(*p*-phenyl)-4-chloroquinazolines. The prepared compounds were characterized by way of ^{1}H-NMR, FTIR and Mass spectrometry. Furthermore, the compounds were evaluated for potential in vitro anti-*Mycobacterium tuberculosis (Mtb)* properties employing rifampicin as a reference drug. Preliminary results from the Alamar Blue assay (*Mtb*. H_{37}Rv strain) revealed promising MIC_{90} ranging from <0.244 to 43 ug/ml. The possible mode of action against the *Mtb* was theoretically explained through molecular docking of *glutamine synthetase* (1HTO). These compounds were inductively docked into the 1HTO protein where a promising hint of the 4-(pyridylamino)- and 4-(ethynylpyridine)quinazolines ranging from -6.280 to -8.257 Kcal/ mol is observed.

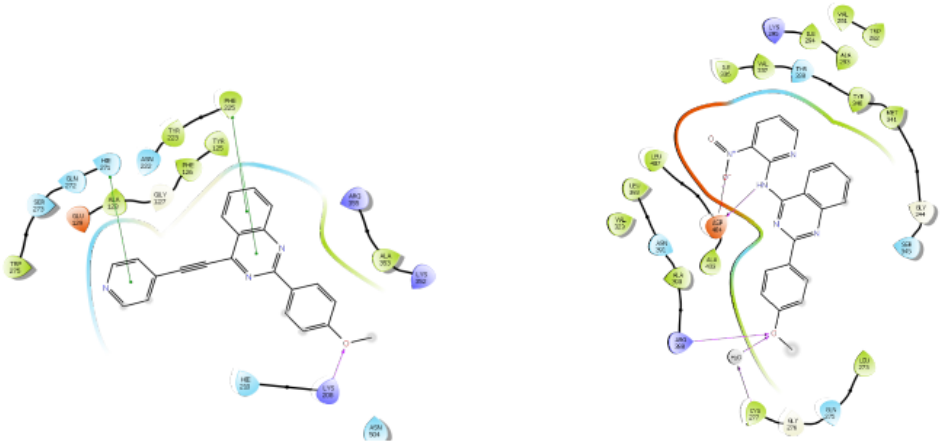

Figure 1&2: The 2D ligand interaction diagram of 4-(pyridylamino) and 4-(ethynylpyridine)quinazolines in *glutamine synthetase* (1HTO).

LIST OF FIGURES

LIST OF SCHEMES

LIST OF TABLES

LIST OF ABBREVIATIONS

A	
A431	Squamous Carcinoma
ATP	Adenosine Triphosphate
ADME	Absorption Distribution Metabolism Excretion
ALA	Alanine
ASP	Asparagine
ARG	Arginine
ADC	Antibody Drug Conjugate
ATNR	Amine Terminated Liquid Natural Rubber
B	
br-s	Broad Signal
C	
c-myc	Avian Myelocytomitosis
CAN	Cerium(IV) ammonium nitrate
COSY	Correlation Spectroscopy
CIS	Coordination Induced Shift
CAS	Central Asian Strain
CAN	Cerium Ammonium Nitrate
D	
DDQ	Dichloro Dicyano Benzoquinone
dd	Doublet Of Doublet
DNA	Deoxyribonucleic Acid
DCM	Dichloromethane
DMSO	Dimethylsulfoxide
DMF	Dimethylformamide
E	
EGFR	Epidermal Growth Factor Receptor
EGFR-TK	Epidermal Growth Factor Receptor Tyrosine Kinase
ES	Electrospray

F	
FTIR	Fourier Transform Infrared Spectroscopy
G	
GLN	Glutamine
GLY	Glycine
GFP	Green Fluorescent Protein
H	
HTVS	High Throughput Virtual Screening
HepG2	Hepatocellular Carcinoma Cell Line
HT29	Human Colon Adenocarcinoma Cells
HMBC	Heteronuclear Multiple Bond Correlation
HPLC	High Performance Liquid Chromatography
HIE	Histidine Neutral E-Protonated
HIV	Human Immunodeficiency Virus
I	
IFD	Induced Fit Docking
K	
Kcal	Kilocalvins
L	
Ligprep	Ligand Preparation
LBVS	Ligand Based Virtual Screening
LBDD	Ligand Based Drug Design
LYS	Lysine
LLC	Limited Liability Company
M	
MIC	Minimum Inhibitory Concentration
MHz	Megahertz
MDR	Multi-Drug Resistant
mg/mL	Milligram Per Milliliter

MCF-7	Michigan Cancer Foundation 7
Mtb	*Mycobacterium tuberculosis*
MCHRI	Melanin Concentrating Hormone Receptor
MS	Mass Spectrometry
mp	Melting Point
mol	Molecules
N	
NMR	Nuclear Magnetic Resonance
O	
OPLS	Optimised Potentials For Liquid Simulations
P	
PGM	Platinum Group Metals
ppm	Parts Per Million
PSCBH	Polymer-Supported Cyanoborohydride
p53	Protein 53
pH	Potential Hydrogen
PDB	Protein Data Bank
Q	
QSAR	Qualitative Structure Activity Relationship
R	
RET	Rational Emotive Therapy
RAQ	Ruthenium Arene Quinazolines
rt	Room Temperature
ROS	Reactive Oxygen Species
RAS	Ruthenium Arene Schiff Bases
S	
SAR	Structure Activity Relationship
SBDD	Structure Based Drug Design
SBVS	Structure Based Virtual Screening
T	

2D	Two Dimension
3D	Three Dimension
3CA	Three Component Assembly
TBABr	Tetrabutylammonium Bromide
TBAI	Tetrabutylammonium Iodide
TEA	Triethylamine
THF	Tetrahydrofuran
TYR	Tyrosine
TRP	Tryptophan
TB	Tuberculosis
U	
UCT	University of Cape Town
V	
VAL	Valine
VEGF	Vascular Endothelial Growth Factor Receptor
W	
WHO	World Health Organisation
X	
XP	Extra Precision

ABSTRACT

Imidazolyl-ethanamine Schiff base ligands of the *N^N* type were prepared by condensation reaction of histamine dihydrochloride with *para*-substituted aldehyde derivatives to yield: (E)-N-benzylidene-2-(1H-imidazol-4-yl)ethanamine **119a**, 4-((E)-(2-(1H-imidazol-4-yl)ethylimino)methyl)phenol **119b**, *E)*-N-(4-fluorobenzylidene)-2-(1H-imidazol-4-yl)ethanamine **119c** and (E)-N-(4-nitrobenzylidene)-2-(1H-imidazol-4-yl)ethanamine **119d**, which were characterised by ^{1}H and ^{13}C-NMR, FTIR specroscopy and HRMS. 2D-NMR experiments (^{1}H-^{1}H COSY and 2D-HMBC) for representative ligand **119b** were performed to qualify success in the condensation reaction. An attempted reaction to coordinate Schiff base ligand **119c** to zinc chloride was carried out in an NMR tube and traces of the product were observed between 12 and 24 h monitoring using ^{1}H-NMR. Iodine promoted cyclocondensation reaction of anthranilamide and *para*-substituted aldehyde derivatives afforded 2-aryl-quinazolin-4(3*H*)-ones **120a-e** and subsequent chloro-aromatisation reaction in $SOCl_2$ afforded electrophilic *C4-(Cl)* 2-aryl-4-chloro-quinazolines **121a-e** and the compounds were characterised by ^{1}H and ^{13}C-NMR and FTIR spectroscopic techniques. The 2-aryl-4-chloro-quinazolines served as prerequisites for de-chloro amination on the *C4-(Cl)* position by 2-amino-3-nitropyridine to yield 2-aryl-N-(3-nitropyridin-2-yl)quinazolin-4-amine derivatives **123a-e** in good yield and the derivatives were characterised by ^{1}H and ^{13}C-NMR, FTIR and HRMS spectroscopic techniques. The *C4-(Cl)* position further allowed for Sonogashira cross-coupling with ethynylpyridine to yield 2-aryl-4-(ethynylpyridine)quinazoline derivatives **125a-e** which were characterised by ^{1}H and ^{13}C-NMR, FTIR and HRMS spectroscopic techniques. The 2-aryl-4-(ethynylpyridine)quinazoline served as ligands for coordination to monomeric p-cymene ruthenium(ll) which yielded (η^6-*p*-cymene)$RuCl_2$-2-aryl-4-(ethynylpyridine)quinazoline derivatives **126a-e** in good yield. Compounds **126a-e** were characterised by ^{1}H and ^{13}C-NMR, FTIR and HRMS spectroscopic techniques**.** 2D-HMBC NMR of representative ligands **126c** and **126e** showed long range couplings from $^{1}J_{CH}$ to $^{9}J_{CH}$ and this was confirmed by coordination induced shifts (CIS) ranging from 1 ppm to 11 ppm.

Compounds **119a-d**, **123a-e** and **125a-e** were inductively docked into the active receptors of tyrosine kinase (PDB:2SRC), *glutamine synthetase* (PDB:1HTO) and

oxidoreductase (PDB:3F8P). The docking scores obtained gave hits ranging from -5 to -10 Kcal/mol.

Compounds **119a-d**, **121a-e**, **123a-e**, **125a-e** and **126a-e** were assayed employing the broth-dilution method which gave promising anti-*Mycobaterium tuberculosis* activity. Compound **125e** gave good activity of <0.244 µg/mL over 7 day and 14 day sampling. Coordination of ligands **125a-e** to Ru(ll) group resulted in loss of activity, notably for ligand **125e**.

CHAPTER 1: INTRODUCTION

Inorganic chemistry is a field that combines with biochemistry to examine the role of metals in biological cell lines by studying metalloproteins and artificially induced metals [1]. On the other hand, biochemistry is aimed at understanding biological processes in the living cell, through the action of prodrugs i.e. inorganic or organic compounds [2]. The latter fields have grown significantly over the previous 40 years in an excess of 2 million scientific literature reports [3]. There are numerous literature articles in which reports aimed at combating the development and persistence of infectious and deadly diseases such as cholera, human immunodeficiency virus (HIV), influenza, malaria, tuberculosis (TB) and cancer through chemotherapeutic techniques [4] have been recorded. Some of the successful drug candidates include transition metal containing cisplatin currently used to treat cancer [5]. Newly food and drug administration (FDA) approved drug candidates include vizimpro, pilifetro, krintafel and terizidone used to treat metastatic non-small-cell lung cancer, HIV-1 infection in adult patients, radical cure of plasmodium vivax malaria and multi-drug resistant (MDR) tuberculosis respectively [6].

A major challenge of the aforementioned drug regimen lies in the development of cellular mutations, wherein the prodrugs employed become inactive over time [7]. This has paved the way for drug-drug complementation in the form of molecular hybrids [8]. For example, ruthenium containing compounds (NAMI, NAMI-A, KP1019, KP1339 and KP418) have since entered phase ll of clinical trials and are reported to show excellent abnormal-DNA damage and low toxicity towards normal cells [9]. At the same time, drug delivery nanocomposites are being designed to improve targeted therapy [10]. Targeted therapy is a newer type of chemotherapeutic treatment approach which employs chemical compounds to precisely identify and attack infected cells in biological systems. This therapy is complemented by *in silico* studies such as molecular modelling which looks at molecular kinetics and dynamics under molecular docking conditions [11-12].

Molecular docking is a computational process to study protein-ligand interactions and has proven to be a game changer in drug design. The process employs approaches such as ligand preparations (ligprep), conformational search, protein preparation,

ligand docking, virtual screening work-flow (VSW), high-throughput virtual screening (HTVS), induced-fit docking (IFD) of either extracted or synthetic compounds, etc. [12].

Method development for synthesis of the desired active bioinorganic compounds may include one-pot or multi-step non-sequential [13] or sequential [14] synthesis of carbo-substituted heterocycles and coordination to transition metal compounds. Reaction procedures employed may include condensation, cyclondensation, dehydrogenation, oxidation, amination, cross-coupling, mesylation [15], neutral or oxidative coordination of polar ligands to transition metals [16], etc.

Reference

[1]. Constable, E.C., Housecroft, C.E., Creus, M., Gademann, K., Giese, B., Ward, T.R., Woggon, W.D. and Chougnet, A., 2010. Bioorganic and Bioinorganic Chemistry. *CHIMIA International Journal for Chemistry*, *64*(12), pp.846-854.

[2]. Davis, T.A., Volesky, B. and Mucci, A., 2003. A review of the biochemistry of heavy metal biosorption by brown algae. *Water Research*, *37*(18), pp.4311-4330.

[3]. Kaim, W., Schwederski, B. and Klein, A., 2013. *Bioinorganic Chemistry--Inorganic Elements in the Chemistry of Life: An Introduction and Guide*. John Wiley & Sons.

[4]. Kiserud, T., Benachi, A., Hecher, K., Perez, R.G., Carvalho, J., Piaggio, G. and Platt, L.D., 2018. The World Health Organization fetal growth charts: concept, findings, interpretation, and application. *American Journal of Obstetrics and Gynecology*, *218*(2), pp.S619-S629.

[5]. Dutta, S., Rivetti, C., Gassman, N.R., Young, C.G., Jones, B.T., Scarpinato, K. and Guthold, M., 2018. Analysis of single, cisplatin-induced DNA bends by atomic force microscopy and simulations. *Journal of Molecular Recognition*, p.e2731.

[6]. Mullard, A., 2018. 2017 FDA drug approvals. Accessed, 05 December 2018.

[7]. Lackner, M., Amler, L.C., Cavet, G., O'brien, C. and Pandita, A., Genentech Inc, 2018. *Genetic Variations Associated with Drug Resistance*. U.S. Patent 9,879,267.

[8]. Catto, M., Trisciuzzi, D., Alberga, D., Mangiatordi, G.F. and Nicolotti, O., 2018. *Multitarget Drug Design for Neurodegenerative Diseases*.

[9]. Zia, M.K., Siddiqui, T., Ali, S.S., Rehman, A.A., Ahsan, H. and Khan, F.H., 2018. Chemotherapeutic Drugs and Plasma Proteins: Exploring New Dimensions. *Current Protein and Peptide Science*, *19*(10), pp.937-947.

[10]. Chopra, D.S., 2018. Nanocomposites in Drug Delivery and Imaging Applications. In *Multifunctional Nanocarriers for Contemporary Healthcare Applications* (pp. 415-430). IGI Global.

[11]. Hinrichs, C.S., 2018. Cell-based molecularly targeted therapy: targeting oncoproteins with T cell receptor gene therapy. *The Journal of Clinical Investigation*, *128*(4).

[12]. Filipovič, J., Vávra, O., Plhák, J., Bednář, D., Marques, S.M., Brezovský, J., Matyska, L. and Damborský, J., 2018. A Novel Method for Analysis of Ligand Binding and Unbinding Based on Molecular Docking. *Journal of Computational Chemistry*, *19*(14), pp.1639-1662.

[13]. Ghosh, M. and De Sarkar, S., 2018. meta-and para-Selective C− H Functionalization using Transient Mediators and Noncovalent Templates. *Asian Journal of Organic Chemistry*, *7*(7), pp.1236-1255.

[14]. Hayashi, Y., Okano, K. and Mori, A., 2018. Synthesis of Thieno [3, 2-b] indoles via Halogen Dance and Ligand-Controlled One-Pot Sequential Coupling Reaction. *Organic letters*, *20*(4), pp.958-961.

[15]. O'Donnel, C.J. and Burke, S.D., 1998. Selective Mesylation of Vicinal Diols: A Systematic Case Study. *The Journal of Organic Chemistry*, *63*(23), pp.8614-8616.

[16]. Megger, D.A., Lax, P.M., Paauwe, J., Guerra, C.F. and Lippert, B., 2018. Mixed guanine, adenine base quartets: possible roles of protons and metal ions in their stabilization. *Journal of Biological Inorganic Chemistry*, *23*(1), pp.41-49.

CHAPTER 2: LITERATURE REVIEW

2.1 Structure and Chemistry of Schiff base compounds

2.1.1 Schiff base ligands

Schiff bases were discovered as azomethine conformers bearing an imino group of the form (-RN=CH-) in 1864 by a German scientist named Hugo Schiff [1]. Schiff base compounds are well studied due to their attractive chemical (catalysis, dyes and corrosion inhibition), physical (photophysics – emission and absorption) and biological (antitubercular, anticancer and antimalarial) properties [2]. The structural conformation of Schiff base ligands plays an important role in developing stable Schiff base transition metal complexes. The chelating ability of the Schiff base ligands is augmented by the presence of *pi*-electrons in the sp^2-hybridised nitrogen of the azomethino group. The azomethino group imparts excellent chelating ability when combined with one or more electron donor atoms (sulphur, nitrogen, oxygen and phosphorous) to yield bi- **1**, tri- **3**, tetra- **3** and polydentate **4** coordination systems (**Figure 2.1)**.

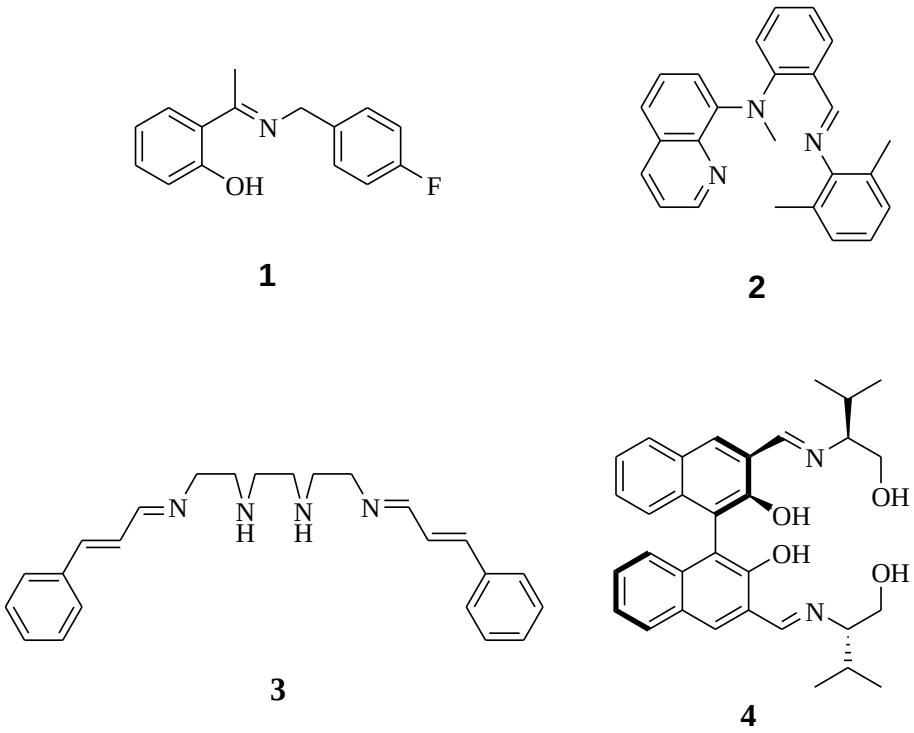

Figure 2.1: Schiff base ligands with different coordination geometries.

Salicylaldimine or salen-type Schiff base ligands as shown in **Figure 2.2** are widely studied due to their ease of preparation. The condensed ligands produce a di-nitrogeno-dioxo N_2O_2 or *N^N^O^O* coordination system. These type of ligands accommodate transition metals with high oxidation numbers. The most popular type of coordination system is the tetradentate bis-Schiff base ligands [3].

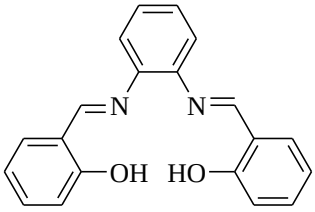

5

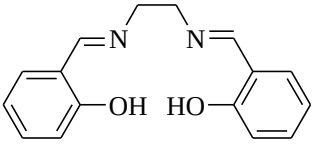

6

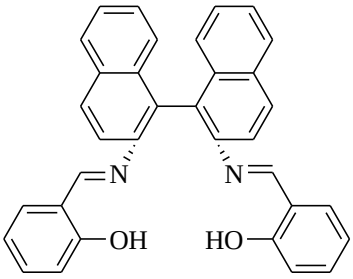

7

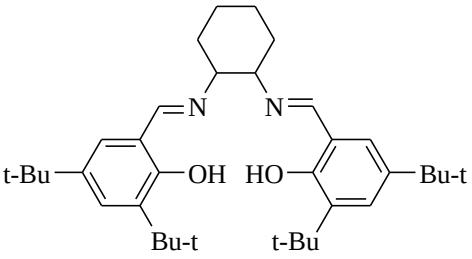

8

Figure 2.2: Salen-type Schiff base ligands

2.1.2 Schiff base complexes

The aforementioned Schiff base ligands can coordinate a variety of transition metals to yield stable Schiff base complexes with various geometries (**Figure 2.3)** and redox properties. The oxidation and reduction states provides knowledge on stability and geometry of a metal complex. When the sp^2-hybridised nitrogen of the azomethino group donates electrons towards the metal centre, *pi*-back donation from the metal is triggered and such electronic transitions can be registered as absorption or emission spectra [4-10].

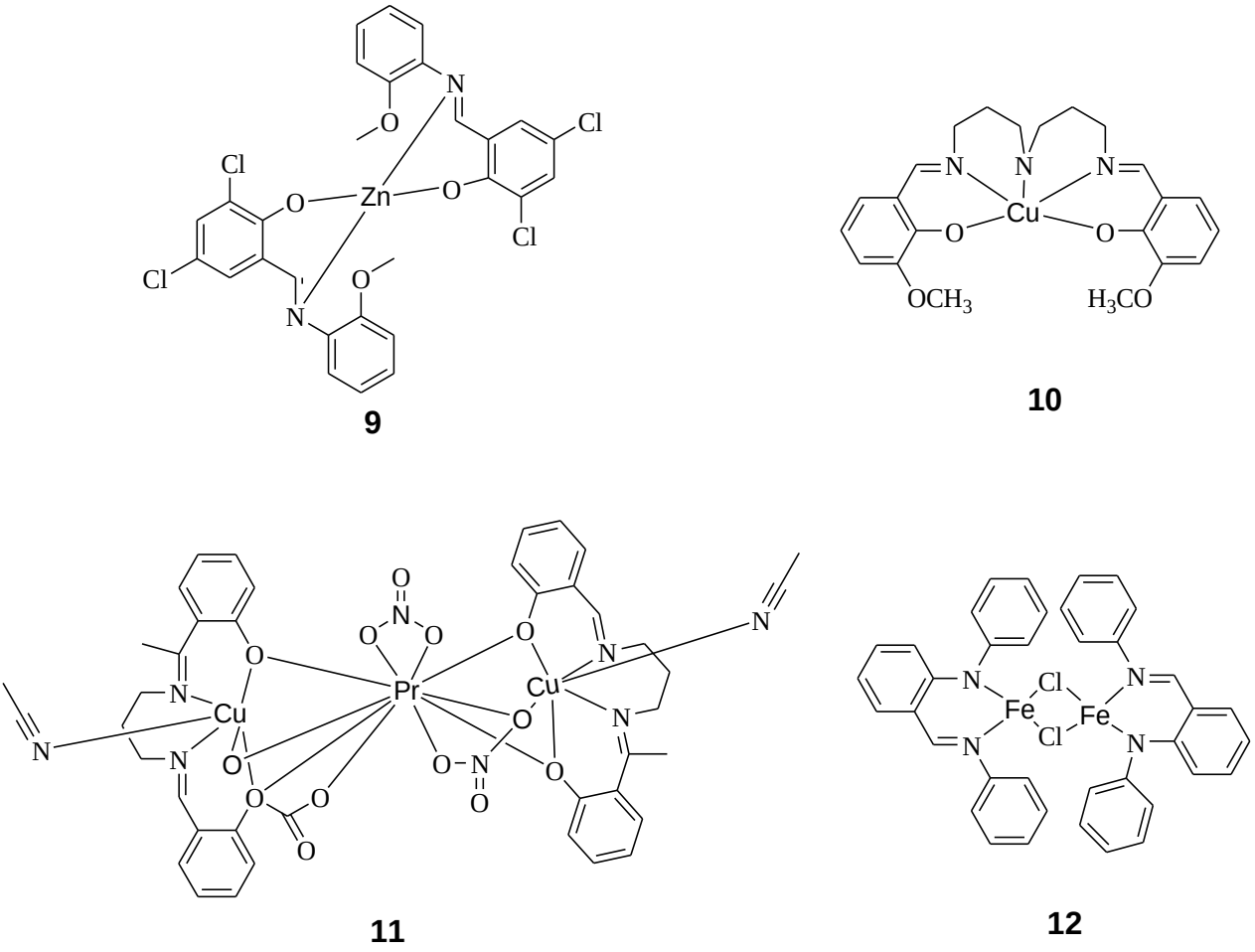

Figure 2.3: Schiff base complexes of different geometry.

2.1.3 Biological application of Schiff base ligands and their complexes

Schiff base complexes possess biological activities including cardiovascular, antimycobacterial, anticancer, ant-inflammatory, anti-leukemic and antibacterial activities depending on the type of metal present in the complex [11-17]. For example, *3d*-transition metal Schiff base complexes containing metals such as copper, nickel, chromium, iron, cobalt and zinc have been reported to chelate DNA of various diseased cells [18-25].

Kumar and co-workers [26] reported *N^N-O^O*-tretracoordinated acyclic chromium(lll) Schiff base complexes with antimicrobial activity. The antimicrobial activity of the [Cr(lll)-(*N,N'*-bis(5-methyl-salicylaldimine)-*N,N'*-bis-(3-amino-propyl)-ethylene-

diamine)$(H_2O)_2]^+$ **13** was demonstrated by *in vitro* testing against *Escherichia coli*, *Staphylococcus aureus* and *Pseudomonas aeruginosa*. The latter demonstrated promising activity with inhibition zones ranging from 18 to 36 mg/mL. In addition, Pervez and co-workers [27] reported salen-derived copper(ll) complexes as urease inhibitors. Urease is a nickel ion (Ni^{2+}) dependent natural enzyme which catalyses the rate of urea hydrolysis to ammonia (NH_3) and carbon dioxide (CO_2) in bacteria, fungi and plants [28].

Medically, ureases have become important therapeutic targets for treatment of disease caused by urease-dependent pathogenic microorganisms [29]. Likewise, the antecedent copper(ll) complexes *i.e.,* the dioxo-di-nitrogeno tetracoordinated bipyrimidal Bis-(3Z)-3,3′-[(4-methyl-1,3-phenylene)dinitrilo]bis(1,3-dihydro-2H-indol-2-one) copper(II) chloride complex **14** was tested against *Helicobacter pylori* cells and the latter demonstrated excellent anti-urease activity with an inhibition concentration (IC_{50}) of 0.03 µM [27]. Furthermore, a bidentate, thiocarbohydrazone zinc(ll) Schiff base complex, *i.e.* (1E,5E)-1,5-bis((furan-2-yl)methylene)-thiocarbono-hydrazide-zinc(ll) chloride **15** was synthesised and tested for antibacterial activity against *Acinetobacter septicaemia* and *Staphylococcus aureus*. The complex **15** tested positive against *Acinetobacter septicaemia,* with inhibition zones ranging from 8 – 16 mm [30]. Although the complexes in (**Figure 2.4)** demonstrate promising pharmaceutical importance, key candidates of the transition metal containing bioactive compounds have come from the platinum group metals (PGMs) [31]. Metals such as platinum (Pt) and ruthenium (Ru) are present in drug candidates applied in cancer treatment and some in clinical trials respectively [32].

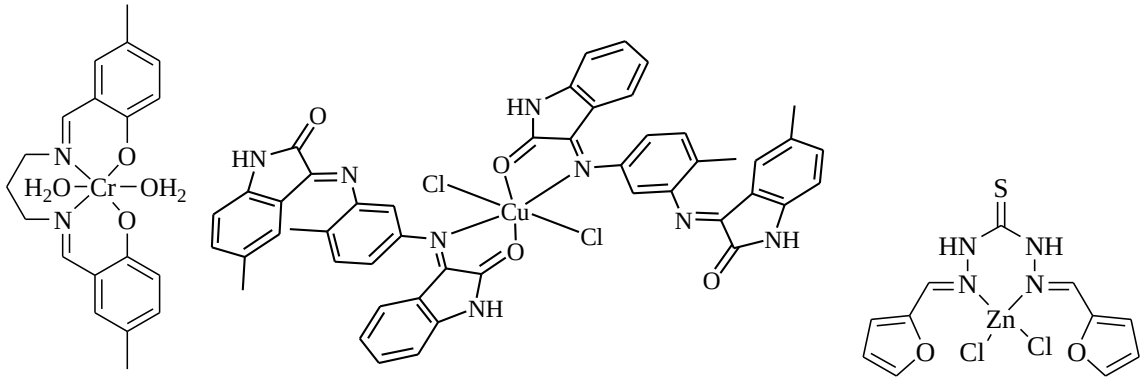

13 **14** **15**

Figure 2.4: Biologically active *3d*-transition metal Schiff base complexes.

Bioinorganic Schiff base complexes containing the PGMs (**Figure 2.5**) are applied mostly in cancer therapy [33]. The motivation behind this application arises from the success of cisplatin **16,** however its use results in side effects such as hair loss, constipation, normal cell death and diarrhoea [34]. The coordination chemical properties of the Schiff base ligands plays an important role for targeted therapy. For example, Peng Wu and co-workers [35] designed and synthesised platinum(ll) complexes with the ability to bind and inhibit *c-myc* by way of stabilising G-quadruplex DNA. The *c-myc* is a gene that encodes DNA-binding to proteins and promotes development of cancers when overexpressed in cells [36]. In this project, the authors tested the corresponding [N,N'-Bis(salicylidene)-4,5-methoxy-1,2-phenylenediamine] platinum(ll) **17** against human hepatocellular carcinoma (HepG2) and the Pt(ll) complex proved cytotoxic with an inhibitory concentration of 1.09 ± 0.14 µM. In addition, Mun and co-workers [37] reported p53 independent ruthenium(ll) arene Schiff base (RAS) complexes with promising anticancer activity. The p53 gene is a tumor suppressor involved in the intercession of cellular DNA repair and neurotoxicity of anticancer drugs. However, it can be deactivated due to mutations. The antecedent RAS complexes are p53 independent, meaning, their mechanism of action is non-binding to the p53 gene. To qualify their theory, the authors designed and prepared "three-legged piano-stool" quinolone derived ruthenium(ll) arene Schiff base complexes, *i.e*. [(η^6-1,3,5-Triisopropybenzene)RuCl(N-(2-quinolinylmethylene)-1-naphthyl-amine)]Cl **18** which was tested against MCF7 human cancer cell lines and tested active with IC_{50} of 2.93 ± 0.21 µM. The promising anticancer activity of these PGMs proved insightful and opened doors for research in the coordination chemistry and biological evaluation of Lanthanide Schiff base complexes thereof [38].

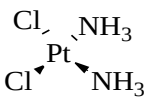

16

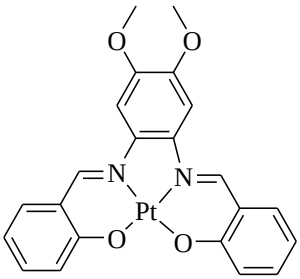

17

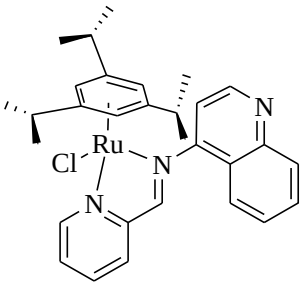

18

Figure 2.5: Cisplatin and biological active PGM Schiff base complexes.

Lanthanides are commonly referred to as rare earth elements and comprise of 15 elements. Lanthanide(lll) coordinated compounds play an important role as antibacterial agents, in cancer diagnosis and for imaging diagnostics therapy [41]. Radioactive lanthanides and their complexes are reported to find application in neoplastic diseases [42]. For instance, a heptagonal gadolinium(lll) complex bearing texaphyrin produces reactive oxygen species (ROS) such as O_2^-, H_2O_2 or OH when reacted with antioxidants. The generated species bind proteins and lead to their destruction and cell apoptosis [43]. Likewise, the Gd(lll) Schiff base complex *i.e.* gadolinium(lll) texaphyrin **19** (**Figure 2.6**) was evaluated for anticancer activity against human colon cancer cell lines (HT29) *in vitro* [44] and the study revealed progressive cell killing at a concentration of 2.2 ± 0.03 µM. Similarly, Andiappan and co-workers [45] prepared distorted square planar erbium(lll) Schiff base complexes and the corresponding [bis-((15E,22E)-N^2-((anthracen-10-yl)methylene)-N^3-((anthracen-9-yl)methylene) pyridine-2,3-diamine)erbium(lll)]nitrate **20** (**Figure 2.6**)was tested against MCF7 cancer cell lines. The latter proved cytotoxic by killing 20% of cancerous cells at 10 µg/mL.

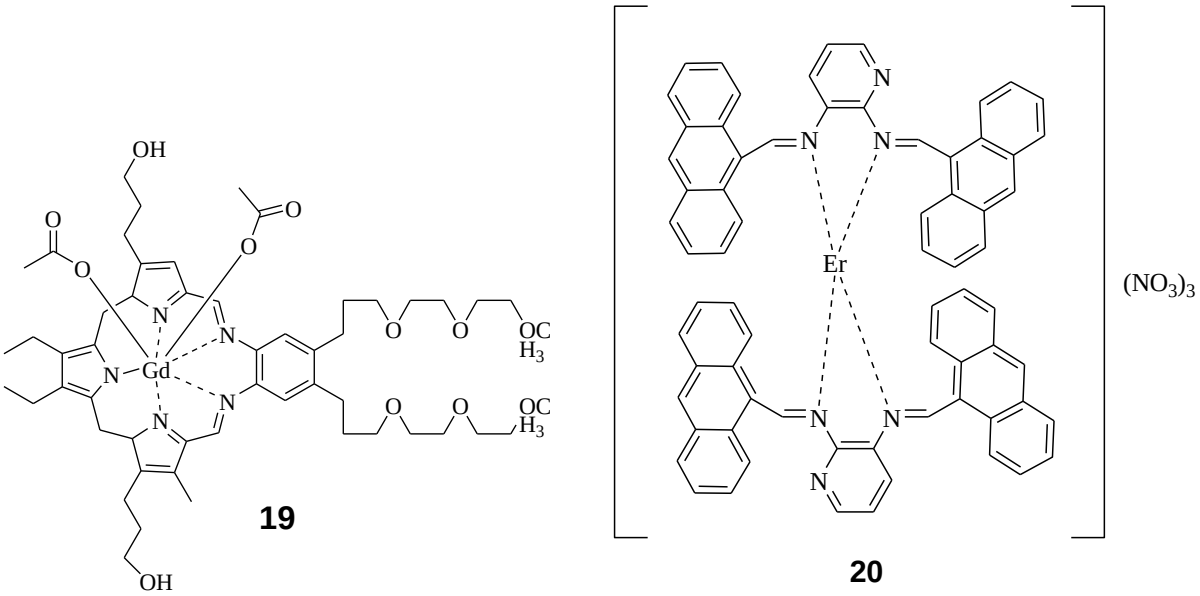

Figure 2.6. Anticancerous lanthanide (lll) Schiff base complexes.

2.1.4 Industrial application of Schiff base complexes

2.1.4.1 Catalysts

Hydroxy benzaldehyde derived Co(lll), Fe(lll) and Ru(lll) Schiff base complexes are used in hydrogen peroxide promoted aerobic oxidation of cyclohexane to cyclohexanol and cyclohexanone [46-47]. In addition, chromium-salen complexes **21** (**Figure 2.7**) are reported to take part in heterogeneous catalysis, [48] by catalysing epoxidation of cis-oflefins. Furthermore, *N^N*-bischelated nickel(ll) Schiff base complexes **22** (**Figure 2.8**) are reported to act as effective catalytic precursors for active olefin oligomerisation [49].

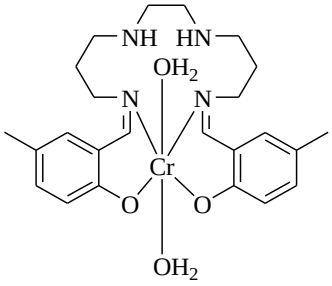

21

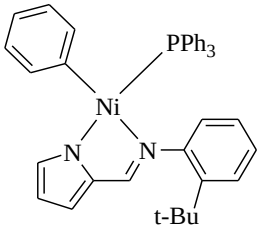

22

Figure 2.7: Schiff base complexes with catalytic activity.

2.1.4.2 Schiff base compounds as dyes

Azomethine complexes of chromium and cobalt are reported to give fast colours to wools, leathers and food packages [50]. Similarly, chromium(lll) azo-Schiff base complexes **23** (**Figure 2.8**) are applied as dyes for cellulose polyester textiles [51]. Some cobalt(ll) complexes **24** (**Figure 2.8**) reported are used in dying mass polyfibres [52].

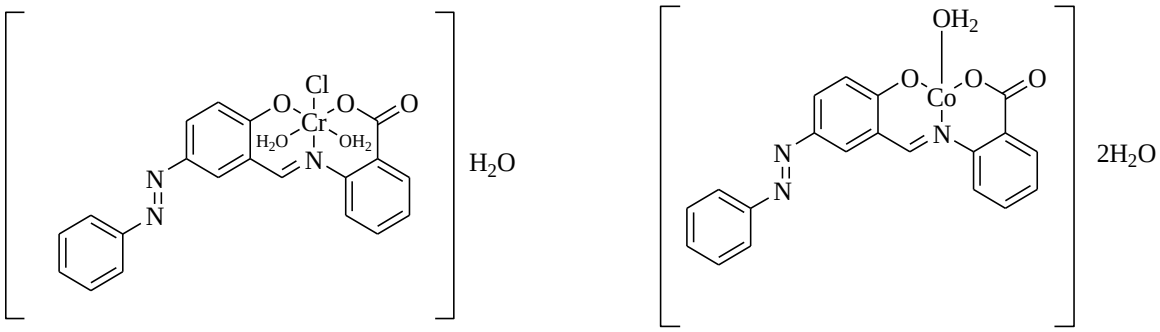

23 **24**

Figure 2.8: Dyes of Schiff base complexes.

2.1.4.3 Schiff base compounds as polymeric materials

Ethylenediamine promotes photochemical degration of natural rubber to produce amine terminated liquid natural rubber (ATNR) in solution [53]. The reaction between ATNR and glyoxial polymeric Schiff bases **25** (**Figure 2.9**) enhances aging resistance [54]. Nickel(lll) Schiff base complexes with a tridentate coordination system **26** (**Figure 2.9**) are reported to initiate emulsion and co-polymerisation of dienyl and vinyl monomers [55].

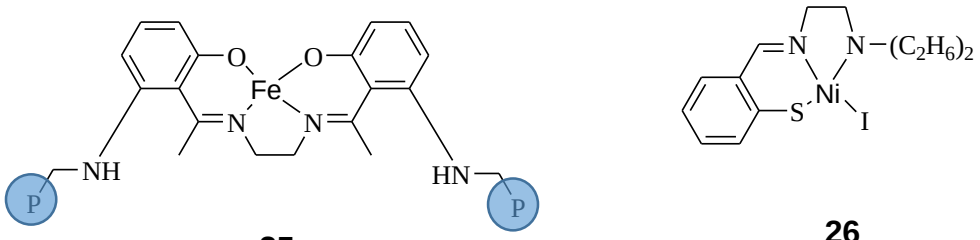

25 **26**

Figure 2.9: Schiff base complexes with polymerisation properties.

2.2 Synthesis of Schiff base ligands

The general method for the synthesis of Schiff base or imine derivatives involves a direct condensation reaction between a primary amine and an aldehyde derivative in basic or acidic conditions [56]. The original synthesis reported by Hugo Schiff involved the condensation of a carbonyl compound with an amine under azeotropic distillation [1] conditions. Molecular sieves were then used to completely remove the by-product (water) formed during the reaction. In the 1990s, an *in situ* method for drying water

was applied using salts such as sodium hydrogen carbonate ($NaHCO_3$), sodium carbonate (Na_2CO_3) and magnesium sulphate ($MgSO_4$) [5]. In 2004, Chakraborti and co-workers [16] revealed that the competence of these methods is dependent on the use of highly electrophilic carbonyl compounds and strongly nucleophilic amines. They proposed as an alternative, the use of substances that function as Bronsted-Lowry or Lewis acids to activate the carbonyl group of aldehydes and catalyse the nucleophilic attack by amines, and dehydrate the system, thus eliminating water as the final step.

2.2.1 Methods for the synthesis of *n*-carbon spacer Schiff base ligands (n = 1, 2 and 3)

Multiple synthetic approaches towards Schiff base derivatives have been described in literature [57]. Problems such as hydrolysis [61] and moisture susceptibility [62] are reported to bring about structural decomposition and encouraging reverse reaction. Synthetic approaches such as racemization by aza-Michael/ retro-aza-Michael addition [58], aerobic oxidation [59], amine reduction [60] etc, are aimed at solving the problems associated with the *imine* bond of the Schiff base compounds. Safa and co-workers [63] reported organosilicon type Schiff base derivatives, prepared by a direct condensation of 4-(2,2-bis(trimethylsilyl)vinyl)benzaldehyde **27** and 4-aminophenol **28** refluxed in ethanol for 15 hours to afford the corresponding (E)-4-(4-(2,2-bis(trimethylsilyl)vinyl)-benzylideneamino)-phenol **29** in low yields ranging from 33 - 45% (**Scheme 2.1**.

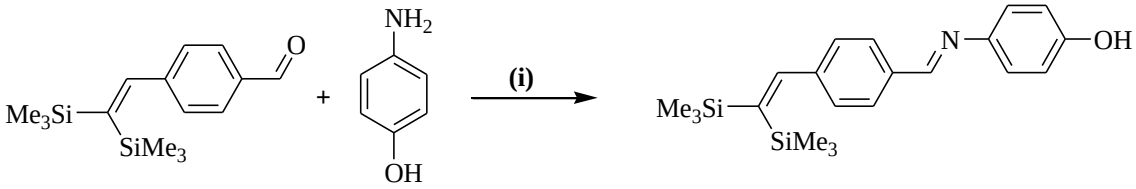

27 **28** **29**

Reagents and conditions: (i) Ethanol, reflux, 24 h.

Scheme 2.1: Synthesis of (E)-4-(4-(2,2-bis(trimethylsilyl)vinyl)benzylideneamino)-phenol **29** via a direct condensation reaction of organosilicon aldehyde derivatives and a primary amine.

A facile and heatless metathesis reaction of aryl isocyanates and aldehydes yielding imino derivatives of Schiff bases was described by Kumar and Samuelson [64]. The metathesis reaction is catalysed by square planar, group IV metal alkoxides. The

reaction time is accelerated by an insertion step leading to the formation of carbamate. As a demonstration, the authors reacted 1-isocyanato-4-methoxybenzene **30** and *para*-cyanobenzaldehyde derivatives **31** in the presence of $Zr(OMe)_4$, solvated by a combination of THF and water v/v 3:1. The reaction was then stirred at room temperature for 60 h to yield 70% of the corresponding (E)-4-(4-methoxy-benzylideneamino)benzonitrile **32** (**Scheme 2.2**).

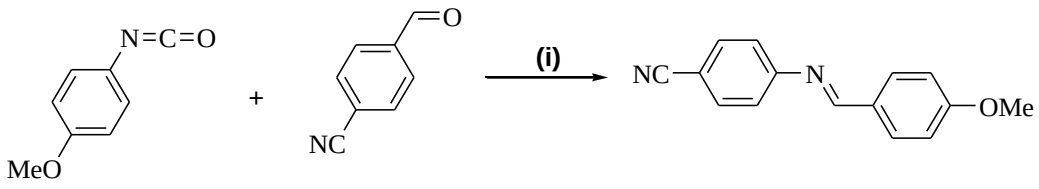

30 **31** **32**

Reagents and conditions: (i) $Zr(OMe)_4$, rt, 60 h, THF-H_2O.

Scheme 2.2: Group IV metal alkoxide catalysed synthesis of corresponding (E)-4-(4-methoxybenzylideneamino)benzonitrile **32**.

A combination of polymer-supported cyanoborohydride (PSCBH) and manganese dioxide in a one-pot type conversion of alcohols into imines was reported by Blackburn and Taylor [65]. The manganese oxide acts as an oxidant *in situ* and thus adhering to the oxidation-imine formation-reduction sequence and converts the alcohols to tertiary amines. As an example, the authors reacted 2-phenylethanol **33** and cyclohexanamine **34** in the presence of MnO/ PSCBH in two portions at reflux temperature in DCM to afford 95% of the corresponding (E)-N-(2-phenylethylidene)cyclohexanamine **35** (**Scheme 2.3**).

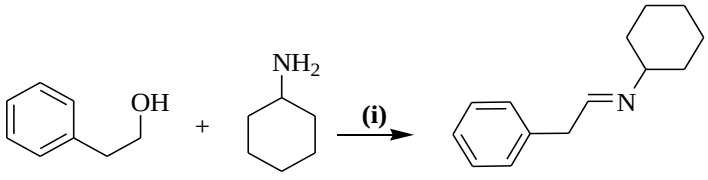

33 **34** **35**

Reagents and conditions: (i) MnO/PSCBH, 60 ^oC, 24 h, DCM.

Scheme 2.3: Manganese oxide catalysed one-pot oxidation-imine formation-reduction of alcohols to imines.

2.2.2. Indirect methods for the synthesis of Schiff base derivatives

Amines undergo aerobic oxidation to afford *imino* Schiff base derivatives by way of introducing unsaturation between the amino *C-sp*^{3}-carbon and nitrogen [66]. For example, Wang and co-workers [67] presented a palladium catalysed selective aerobic oxidation reaction of N-benzylnaphthalen-1-amine **36** to yield 99% of the corresponding (Z)-N-benzylidenenaphthalen-1-amine **36** (**Scheme 2.4**). Synthesis of **37** involves palladium(ll) chloride ($PdCl_2$) as catalyst, sodium acetate (NaOAc) as a base, triphenyphosphine (PPh_3) as a ligand, oxygen (O_2) and dimethylformamide (DMF) as a solvent. The aforementioned reagents were stirred at room temperature for 16 hours in the presence of **36**.

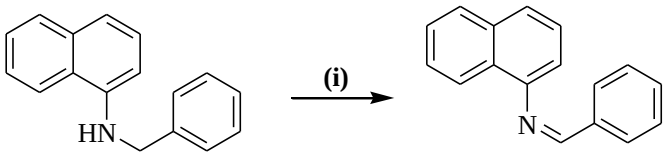

36 **37**

Reagents and conditions: (i) $PdCl_2$, NaOAc, PPh_3, O_2, rt, DMF.

Scheme 2.4: Palladium catalysed aerobic oxidation of amines to *imino* Schiff base derivatives.

2.3 Synthesis of Schiff base complexes

The synthesis of Schiff base complexes generally involves treatment of metal salts with Schiff base ligands under moisture free conditions [68]. However, for Schiff base complexes with catalytic application, a *one-pot* reaction procedure is followed [69]. For example, a purification free, three-component assembly (3CA) of dichloro-(*p*-cymene)-ruthenium(ll) dimer **38**, picolinaldehyde **39** and 4-aminobenzamidine **41** afforded 74% of the corresponding [(η^6-*p*-cymene)RuCl((E)-4-((pyridin-2-yl)methyleneamino) benzamidine]Cl **42** (**scheme 2.5**). The synthesis of **42** is effected by continuous stirring at room temperature for 36 h in DMSO-d_6/D_2O mixture 1:1 v/v [70].

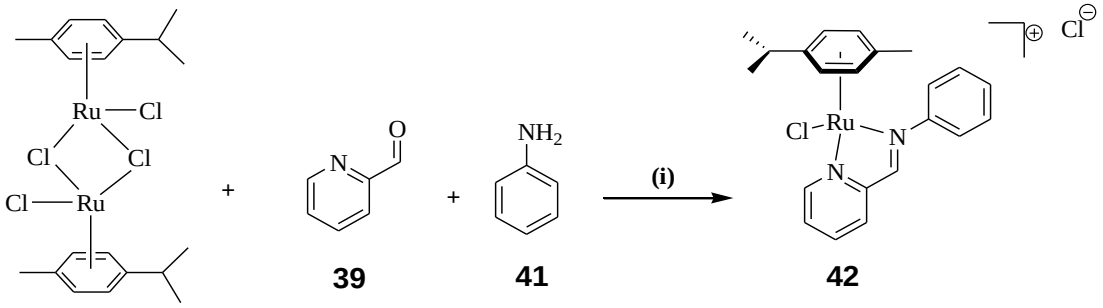

38 **39** **41** **42**

Reagents and conditions: (i) DMSO-d_6/D_2O (1:1 v/v), 36 h, rt.

Scheme 2.5: One-pot, three-component assembly (3CA) synthesis of RAS complex.

A one-pot preparation of ternary pyridyl copper(ll) Schiff base complexes was reported by Banerjee and co-workers [71]. The pre-mentioned Cu(ll) complexes were prepared in a basic medium by refluxing 1:1 mmol of salicyaldehyde **43** and histamine dyhrochloride **44** in methanol for 1 h, after which another 1:1 solution of copper(ll) nitrate and 2-(pyridin-2-yl)pyridine **45** was added slowly and the solution was stirred for an additional 1 h (**scheme 2.6**) to yield 78% of 2-(pyridin-2-yl)pyridine-2-((E)-(2-(1H-imidazol-4-yl)ethylimino)methyl)phenol Cu(ll) chloride **46**.

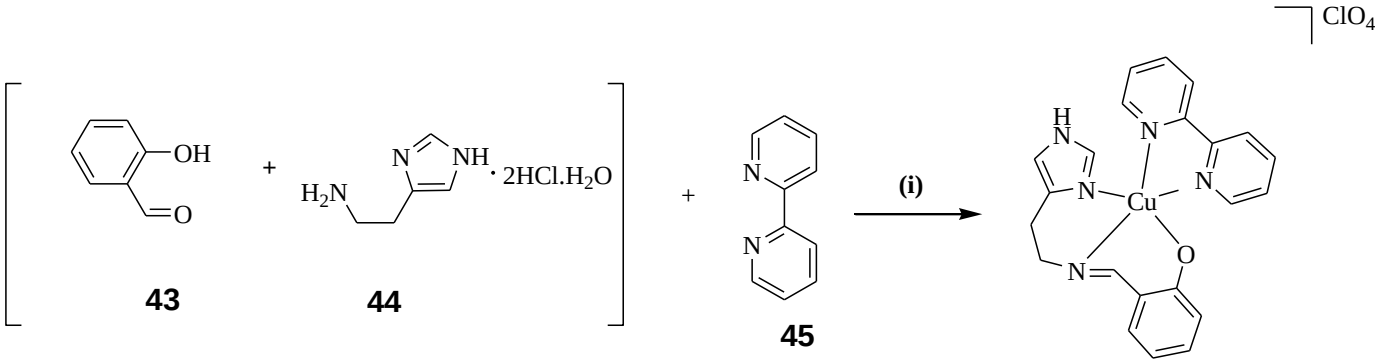

43 **44** **45** **46**

Reagents and conditions: (i) TEA, $Cu(OAc)_2.H_2O$, MeOH, heat 1h, rt 1h.

Scheme 2.6: One-pot synthesis of ternary pyridyl copper(ll) complexes.

Tajuddin and co-workers [72] described square planar palladium(ll) complexes with potential catalytic activity in Suzuki coupling reactions. The tetracoordinated Pd(ll) complexes were synthesised by refluxing the corresponding 2-((E)-1-(4-fluorobenzylimino)ethyl)phenol **47** and palladium(ll) acetate **48** in ethanol for 5 h

(**Scheme 2.7**) to yield 87.8% of bis-2-((E)-1-(4-fluorobenzylimino)ethyl)phenolpalladium(ll) **49**.

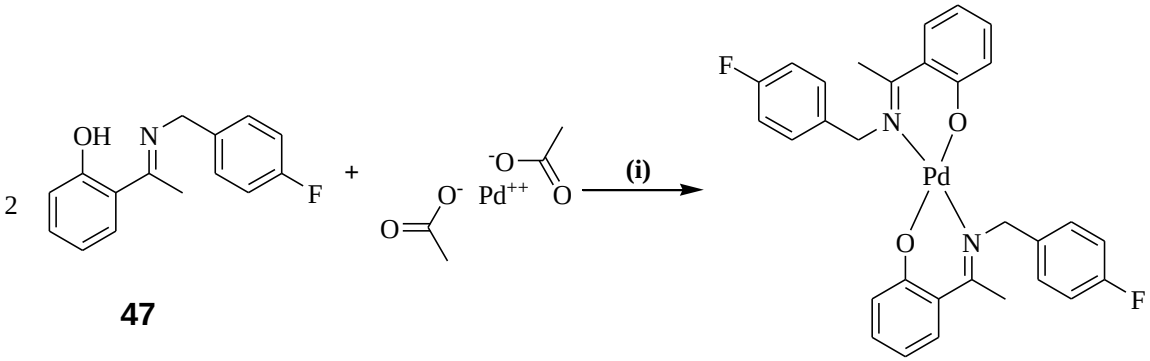

47 **48**

Reagents and conditions: (i) Ethanol, 5 h, heat.

Scheme 2.7: Square planar palladium(ll) Schiff base complexes.

2.4 Quinazolines

2.4.1 Structure and biological application of quinazoline derivatives

Nitrogen-containing heterocyclic compounds exert a global dominance in organic chemistry research because of their important biological and medicinal applications [73-74]. Among the pharmaceutically essential organo-nitrogen heterocycles, fused pyrimidines formally found in a variety of natural products possess a broad spectrum of biological properties. These consist of antibacterial, antifungal, antiviral, antimalarial, anticancer, anti-inflammatory and analgesics, antidepressant, anticonvulsant, antioxidant, antileshmanial and antiobesity activities [75-76] Quinazolines which form part of this investigation, are made up of two fused six-membered simple aromatic rings, a benzene ring and a pyrimidine ring with one carbonyl group, [i.e. 2,3-dihydroquinazoline-4(1*H*)-one **49**, quinazolin-4(3*H*)-one **50**, 3,4-dihydroquinazoline-2(1*H*)-one **51**] or two carbonyl groups [i.e. quinazoline-2,4(1*H*, 3*H*)-dione **52**] on the pyrimidine framework (**Figure 2.10**).

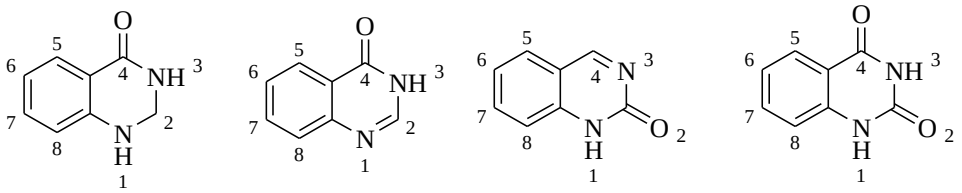

49 **50** **51** **52**

Figure 2.10: Generalised examples of the quinazoline framework.

Quinazoline frameworks, the 2,3-dihydroquinazolin-4(1*H*)-ones and quinazolin-4(3*H*)-one are the most experimented due to their biological properties and potential application in material sciences [77]. The quinazoline alkaloid termed Febrifugine **53a** (**Figure 2.11**), for example, was the first to be discovered as an extract from the Chinese plant *Dichora Fibrifuga* in 1950 and was reported to exhibit antimalarial activity [78]. A drawback was revealed in its clinical trials as the latter was found to cause gastrointestinal disorders [79]. This drawback made way for the search of Febrifugine analogues with escalated effectiveness and reduced side effects [80]. A hydrated and aminated Febrifugine derivative, Diproqualone **53b** (**Figure 2.11**), was synthesised and is currently used for the treatment of inflammatory pain resulting from osteoarthritis and rheumatoid arthritis [81]. Methaqualone **54a**, an important derivative

in the field of synthetic anticonvulsants was reported was reported by Arora and co-workers [82]. The modification of **54a** was carried out by El-Azab and co-workers [83] to obtain quinazolinone scaffold **54b** which proved to be 2-fold more active than **54a**. According to the findings of El-Azab and co-workers, 8-substituted-4(3*H*)-quinazolinone **54c** was demonstrated to be a better anticonvulsant activity with lower toxicity than **54a** and **54b**.

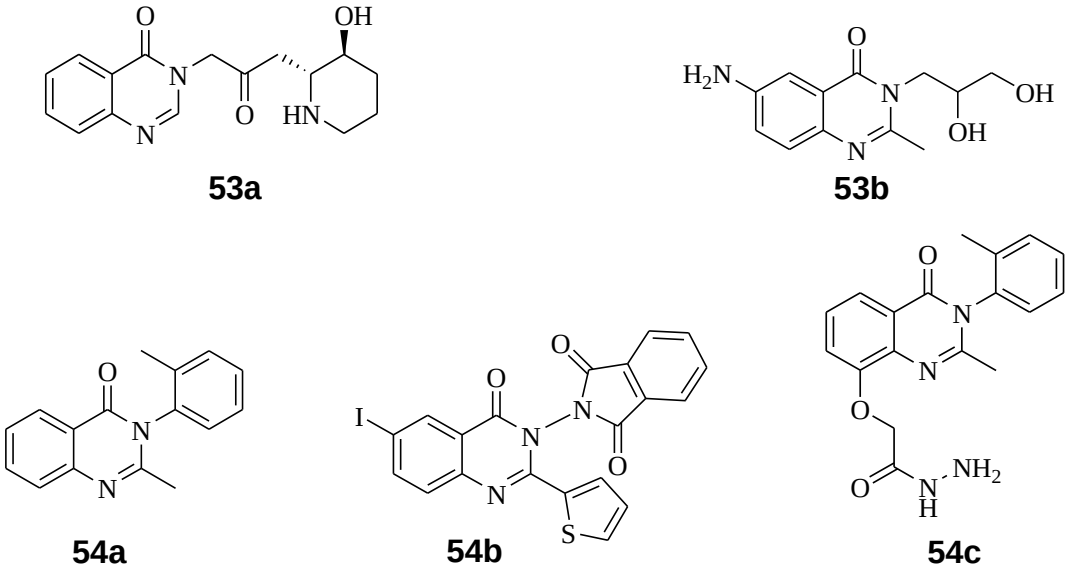

53a **53b**

54a **54b** **54c**

Figure 2.11: Examples of biologically active derivatives of febrifugine.

The 2,3-dihydroquinazolin-4(1*H*)-one framework offers the opportunity for introduction of a vast degree of unsaturation in the heterocyclic ring through dehydration and subsequent aromatisation to afford corresponding quinazolin-4(3*H*)-ones and quinazoline derivatives respectively. Quinazoline-4(3*H*)-one based compounds are reported to possess antitubercular activity [84-85] with some derivatives exhibiting sedative properties [86]. For exmpale, 4-(isopropylthio)quinazoline **55** (**Figure 2.12**) previously prepared by acylation of the corresponding quinazoline-4-thiol with 2-chloropropane was reported to display significant antibacterial activities against *Mycobaterium tuberculosis* strains [88]. In addition, 6,8-dichloro-3-phenylquinazoline-2,4(1H,3H)-dione **56** prepared by chlorination of the corresponding antharalic acid, followed by cyclisation and acylation of the corresponding 6,8-dichloro-3H-benzo[e][1,3]oxazine-2,4-dione with chlorobenzene was reported to show activity against Multi-Drug resistant MDR-TB [87].

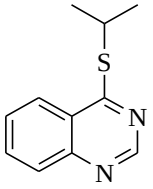

55

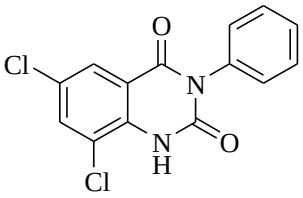

56

Figure 2.12: Examples of biologically active quinazoline derivatives

The *keto*-group of the quinazoline-4-ones was reported to be a crucial DNA-chelator during *in silico* studies [89]. As a result, many quinazoline compounds holding the *keto*-group, particularly on the 4-position have been reported to demonstrate anticancer, anti-proliferative, anti-sedative, anti-inflammatory and antibacterial activities [90]. For example two derivatives, 2-(2-methoxystyryl)-6-chloro-3-(pyrimidin-2-yl)quinazolin-4(3H)-one **57** and 2-(2-methoxystyryl)-6-chloro-3-(5-methylisoxazol-3-yl)quinazolin-4(3H)-one **58** previously prepared by an acetic acid supported reflux of the corresponding 2-methylquinazolines with benzoic aldehyde derivatives were tested for anti-leukemic activity and the latter reported good activity [91]. Moreover, Patel and co-workers [92] reported 2-(2-(2,6-dichlorophenylamino)benzyl)-3-(4,5-dihydro-5-phenyl-1H-pyrazol-3-ylamino)-6-iodoquinazolin-4(3H)-one **59** derivatives which showed positive *in vitro* antibacterial activity against both gram negative and gram positive. In addition to quinazolinone containing bactericides, Cakici and co-workers [93] reported 2-(4-nitrophenoxy)-N-(4-oxo-2-phenylquinazolin-3(4H)-yl)acetamide **60** which was prepared by reacting the corresponding 2-chloro-N-(4-oxo-2-phenylquinazolin-3(4H)-yl)acetamide with different substituted benzyl alcohols. The latter was tested for antibacterial activity against *Salmonella typhimurium* by employing a cup plate method measuring inhibition zone, the compound casted excellent antibacterial activity.

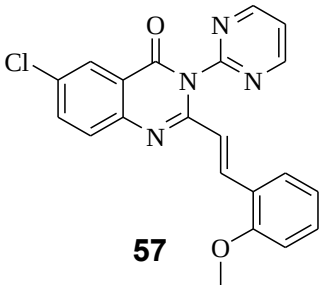

57

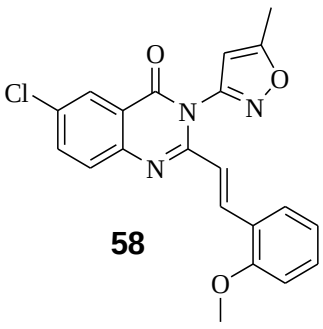

58

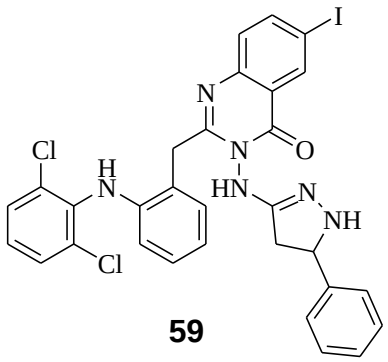

59

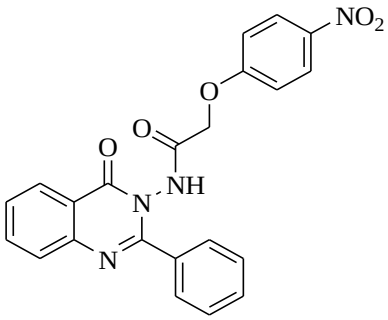

60

Figure 2.13: Examples of biologically active quinazoline-4-ones.

4-methylquinazolines are a rare class of quinazoline analogues which are not as documented as the 4-quinazolinone derivatives. The (Z)-N-(2-(3-hydroxypropylamino)-4-methylquinazolin-6-yl)-3-(4-chlorophenyl)acrylamide **61** and (Z)-3-(4-chlorophenyl)-N-(2-(4-cyclopropyl-4-hydroxypiperidin-1-yl)-4-methyl-quinazolin-6-yl)-acrylamide **62** were reported to act as antagonists for melanin concentrating hormone receptor 1 (MCHR1) *in vivo* and were therefore applied as antiobesity agents [94].

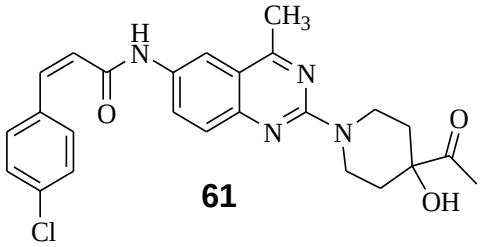

61

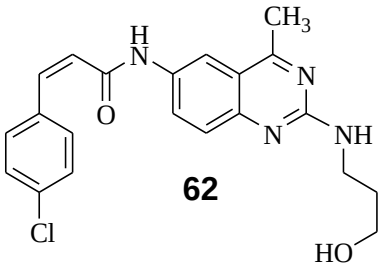

62

Figure 2.14: Examples of biologically active 4-methylquinazolines.

4-Anilinoquinazolines extensively studies as a results of bioactive quinazoline analogues due to their activity against EGFR (Epidermal Growth Factor Receptor), reversible and irreversible kinase inhibition capabilities [95]. The 4-anilinoquinazolines are reported to exhibit anticancer activity against lung, breast, prostate, brain and liver cancer cells [96]. For example, the N^6-(4-chlorobenzyl)-N^4-(3-bromophenyl)quinazoline-4,6-diamine **63** was tested for the ability to prompt apoptosis in the Hep G2 liver cancer cell lines. Both *in silico* and *in vitro* studies qualified the latter as having both antiproliferative and EGFR-TK inhibitory activity [97]. In addition, N-(4-(3-chloro-4-fluorophenylamino)quinazolin-6-yl)-3-bromopropanamide **64** showed

anti-cell proliferation against A431 breast cancer cell lines and is also reported to participate in cell proliferation and autophoshorylation inhibition of EGFR *in vitro* [98].

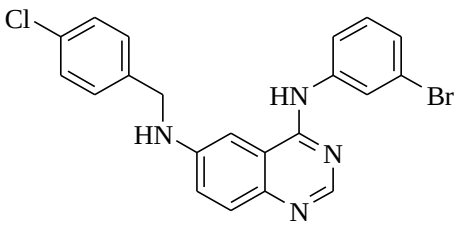

63

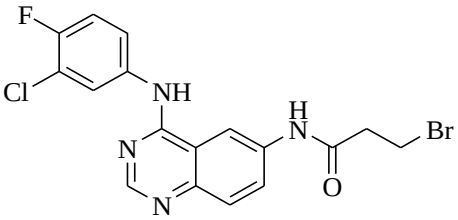

64

Figure 2.15: Examples of 4-anilinoquinazolines with EGFR inhibitory properties.

The study of 4-anilinoquinazoline derivatives as inhibitors of tyrosine kinase activity of EGFR resulted in the approval of Gefitinib **65** for the treatment of lung cancer [99]. Protein tyrosine kinases are enzymes involved in many cellular processes and are known to be activated in cancer cells to drive tumour growth and progression. Blocking tyrosine kinase activity therefore represents a coherent approach to cancer therapy. Erlotinib or Tarceva **66**, a 4-anilinoquinazoline derivative bearing an alkynyl moiety on the aniline ring, is also known as a tyrosine kinase inhibitor which acts on the epidermal growth factor receptor [100]. A multiple approach by a marketed drug vandetanib **67** is reported to act against three targets (1) vascular endothelial growth factor receptor (VEGFR), (2) EGFR and (3) inhibits RET-tyrosine kinase activity, an important growth driver in certain types of thyroid cancer [101].

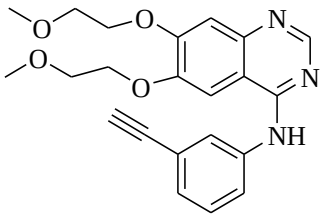

65

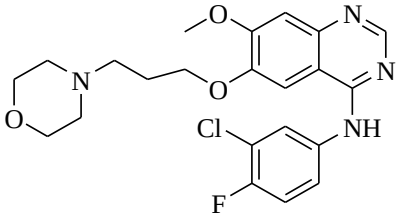

66

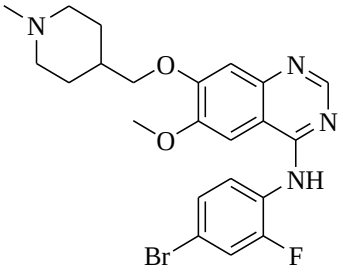

67

Figure 2.16: Examples of cancer active marketed 4-anilinoquinazoline derivatives.

2.4.2 Synthesis of quinazolin-4-one derivaties

The primary method for the preparation of quinazoline derived chemical compounds involves the cyclocondensation of anthranilamide and aldehyde derivatives in the presence of iodine [102], phosgene [103], NaOBr [104] to name a few.

2.4.2.1 Methods for the synthesis of quinazolin-4(1*H*)-ones

A variety of methods for the synthesis of quinazolin-4(1*H*)-ones have been presented in literature including cyclisation, amidation and metal promoted reactions. Tajbakhsh and co-workers [105] described a straightforward procedure for the synthesis of 2,3-dihydroquinazolinones. The reaction mixture involves an inexpensive and non-toxic catalyst *i.e* $H_3PW_{12}O_{40}$ (1 mol%) which aids a cyclisation reaction at reflux temperature in water between antharanialmide **68**, aldehyde derivative and 4-formylbenzonitrile **69** to afford the corresponding 4-(3,4-dihydro-4-oxoquinazolin-2-yl)benzonitrile **70** in high yields (**Scheme 2.8**). The catalytic system holds several advantages including short reaction time of 2 h, easy work-up and green procedure avoiding toxic solvents.

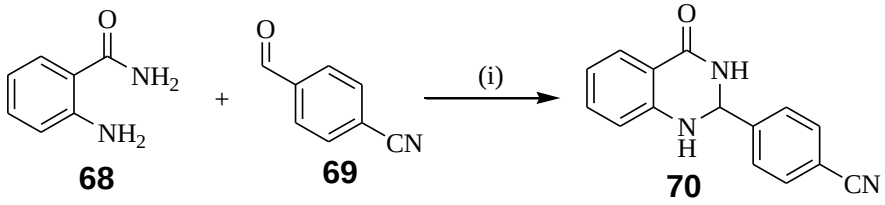

Reagents and conditions: (i) $H_3PW_{12}O_{40}$ (1 mol%), 80 °C, reflux, 2 h.

Scheme 2.8: $H_3PW_{12}O_{40}$ catalysed synthesis of 4-(3,4-dihydro-4-oxoquinazolin-2-yl)benzonitrile **70**.

Metal-free cyclisation of anthranilamide **68** and aldehyde derivatives **71** using SO_3-H-functionalised ionic liquid catalysts under solvation-induced proton transfer afforded 2,3-dihydroquinazolin-4(1*H*)-one derivatives **72** (**Scheme 2.9, on page 23**) [106]. Methane-sulfonic acid is a Brønsted acid which promotes cyclo-condensation via aerobic oxidation.

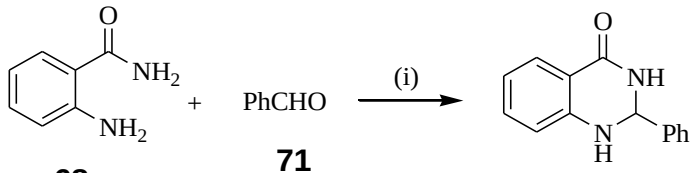

68 **71** **72**

Reagents and conditions: (i) Methane-sulfonic acid, O_2, EtOH, reflux, 2 h.

Scheme 2.9: Brønsted acid-promoted aerobic oxidation via solvation-induced proton transfer: Metal-free construction of dihydroquinazolinones

With the escalating amount of organic pollutants found in drinking water, green chemistry has been documented as the future of science in organic synthesis [107]. Wang and co-workers [108], reported a novel synthetic procedure for the synthesis of 2,3-dihydroquinazolin-4(1*H*)-ones **73**, which involves the grinding of anthranilamide **68** with aldehyde derivatives **71** at ambient temperature in the presence of cerium(IV) ammonium nitrate (CAN) and water. The reaction is driven to completion by heating at 60 ^{0}C (**Scheme 2.10**). Cerium(IV) ammonium nitrate (CAN) is a flexible single-electron oxidant which promotes the cyclisation of anthranilamide **68** derivatives with carbonyl containing compounds. The grinding step was found to be vital in increasing the surface area and resulted in high yields.

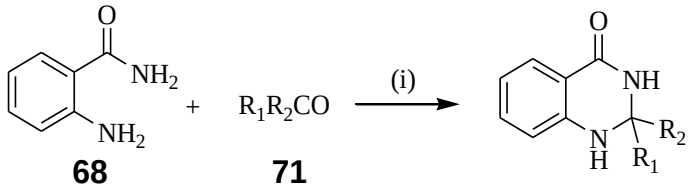

68 **71** **73**

Reagents and conditions: (i) CAN, Grinding.

Scheme 2.10: CAN-mediated synthesis of dihydroquinazolin-4(1*H*)-ones

2.4.2.2 Methods for the synthesis of quinazolin-4(3*H*)-ones

Dihydroquinazolin-4(1*H*)-ones undergo tautomerism to afford the corresponding quinazolin-4(3*H*)-ones through dehydrogenation aided by oxidising agents introducing unsaturation between *N*-1 and C-2 of the scaffold. Otherwise, quinazolin- 4(3*H*)-ones can prepared directly in a single-pot procedure from anthranilamide derivatives and various carbonyl compounds by oxidative cyclocondensation or transition metal-catalyzed reactions [109].

2.4.2.3 Indirect methods involving dehydrogenation of quinazolin-4(1*H*)-ones

The 2-phenylquinazolin-4(3H)-one derivatives serve as an example as they are prepared by the oxidation of dihydrogenated derivatives **74** with potassium permanganate in acetone under reflux (**Scheme 2.11**) [110]. Potassium permanganate serves as an oxidising reagent to bring about unsaturation between *N*-1 and C-2. Hitherto, two forms of quinazolin-4-ones were reported namely: the lactam (major) **76** and iminol form (minor) **75**. [111].

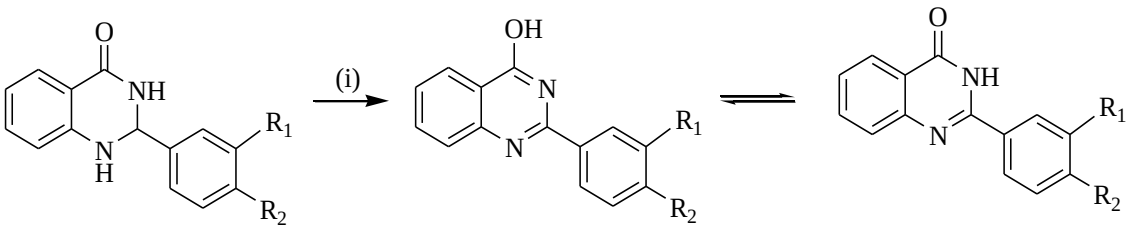

74 **75** (iminol) **76** (lactam)

Reagents and conditions: (i) $KMnO_4$, Me_2CO, reflux.

Scheme 2.11: Synthesis of 2-phenylquinazolin-4(3H)-ones with $KMnO_4$

By the same token, the oxidation of 2,3-dihydroquinazolin-4(1*H*)-ones **77** with tertiary-butyloxide (2 equiv.) as an oxidising agent under refluxed furnished 2-substituted quinazolin-4(3*H*)-ones **78** yielding between 75 to 93% (**Scheme 2.12**) [112].

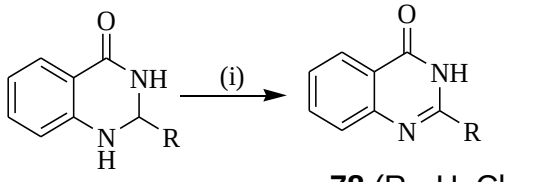

77 **78** (R=-H, Cl, -OMe)

Reagents and conditions: (i) *t*BuO, reflux.

Scheme 2.12: Oxidation of 2,3-dihydroquinazolin-4(1*H*)-ones with *t*BuO

Although the synthesis of quinazolin-4(3*H*)-ones by dehydrogenation of the parallel quinazolin-4(1*H*)-ones has been effective, the majority of these procedures include the use of non-environmentally, non-friendly oxidising agents in large excess. As an attempt to minimise the risk of pollution, one-pot synthesis methods continue to spark interest in literature.

2.4.2.4 Direct methods for the synthesis of quinazolin-4(3*H*)-ones

A single pot reaction between 2-amino-N-methoxybenzamide **79** and 4-bromobenzaldehyde **80**, in acetone refluxed at 100 ºC for 12 h was reported to undergo a cascade cyclisation sequence to yield the corresponding 2-(4-bromophenyl)quinazolin-4(3H)-one **81** by 81% (**Scheme 2.13**) [113].

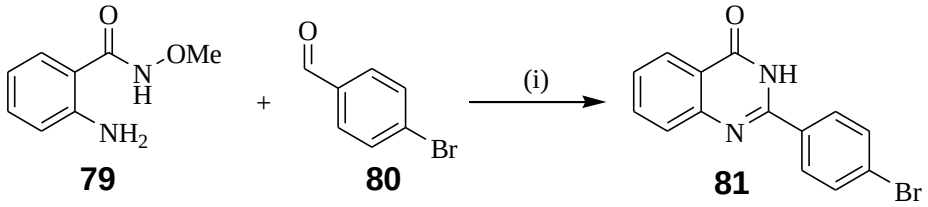

Reagents and conditions: (i) 90 ºC, acetone, 12 h.

Scheme 2.13: Single-pot cyclisation of 2-amino-N-methoxybenzamide with 4-bromobenzaldehyde.

A mixture of anthranilamide **68**, ethynylbenzene **82** and tosylazide **83** in acetonitrile at room temperature for 10 h afforded 2-benzylquinazolin-4(3H)-one **84** in 91% yield. The latter was produced after 8 h in the presence of copper(i) iodide (10 mol%), triethylamine (3 equiv) in acetonitrile (**Scheme 2.14**) [114]. The reaction was found to proceed through two crucial steps involving 1,3-dipolar cycloaddition and intramolecular cyclisation. Though complex, this procedure gave high yields at low temperature. The use of high temperature was dubbed to produce complex decomposed mixtures [115].

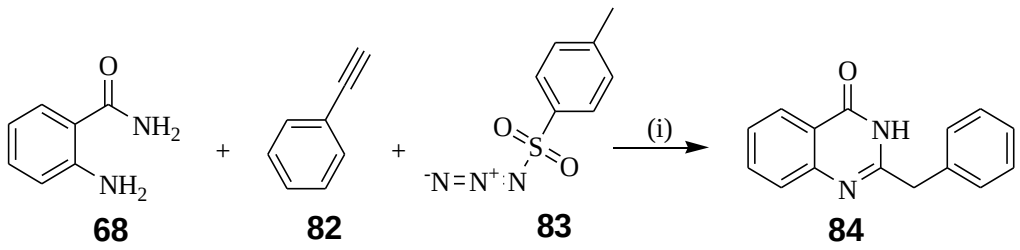

Reagents and conditions: (i) CuI, TEA, rt, CH_3CN, 10 h

Scheme 2.14: Copper catalysed one-pot synthesis of 2-substituted quinazoline 4-(3H)-one.

Romero and co-workers [116] described a simple one-pot synthetic procedure for quinazolin-4(3*H*)-ones by the reaction of 2-nitrobenzamide **85** with 3-fluorobenzaldehyde **86** in the presence of sodium dithionite (3.5 equiv). Sodium dithionite is a reducing agent of the nitro group and it thus decomposes *in situ* in

aqueous DMF-H_2O (9:1) at 90 ^oC (reflux) for 5 h (**Scheme 2.15**), leading to an oxidation step that yields the desired 2-(3-fluorophenyl)quinazolin-4(3H)-one 99% **87**. The reaction is accelerated by the addition of water.

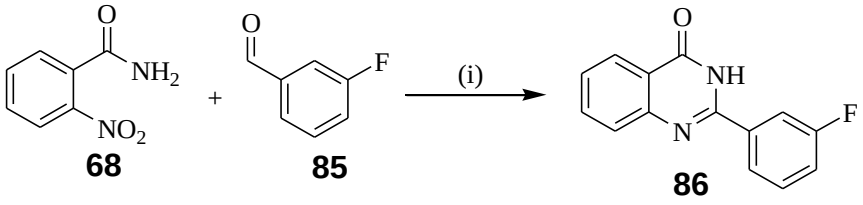

Reagents and conditions: (i) $Na_2S_2O_4$, DMF-H_2O, 90 ^oC, reflux, 5 h

Scheme 2.15: One-pot synthesis of quinazolin-4(3*H*)-ones from 2-nitrobenzamide using sodium dithionite

Parua and co-workers [117] reported an environmental friendly and mild approach for the synthesis of quinazolin-4(3*H*)-ones via a square-planar nickel(II) complex-catalysed acceptor-less dehydrogenative cyclisation of anthranilamide **68** with (4-methoxyphenyl)methanol **88** (**Scheme 2.16**). The reaction proceeds in xylene with sodium butaoxide (1.5 equiv) as a base, Ni-catalyst (5 mol%) at a reflux temperature of 100 ^oC for 36 h. The approach yielded 74% of 2-(4-methoxyphenyl)quinazolin-4(3H)-one **89**. The by-product of this particular procedure was reported to be a hydrogen gas.

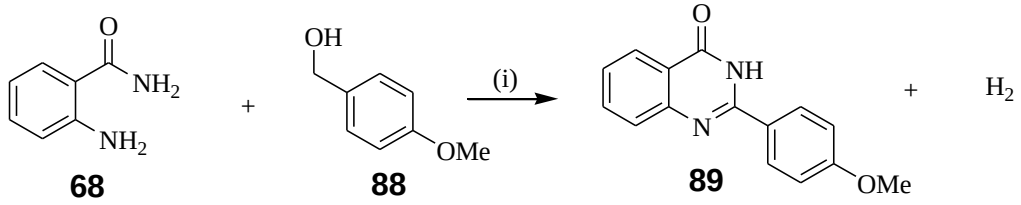

Reagents and conditions: (i) [Ni(MeTAA)], Na^{t}OBu, xylene, 100 ^oC, 36 h

Scheme 2.16: One-pot Nickel-catalysed synthesis of quinazolin-4(3*H*)-ones

As an addition to eco-friendly reaction conditions, Fang [118] described the synthesis of quinazolin-4(3*H*)-ones via a homogeneous transition metal catalysed acceptor- less dehydrogenative alcohol oxidation which produces water via nitrile **90** hydrolysis and later hydrogen via a dehydrogenative oxidation step. The procedure involves the cyclocondensation of anthranilamide **68** derivatives with oxidised alcohols (i.e. aldehydes) **71**. The reaction takes place in water as a solvent at room temperature

while stirring for 3 h (**Scheme 2.17**), and is therefore catalysed by a water soluble Iridium-catalyst $[CpIrCl_2]_2$ (5 mol%) to yield 70-81% of 2-substituted quinazolin-4-ones **91**.

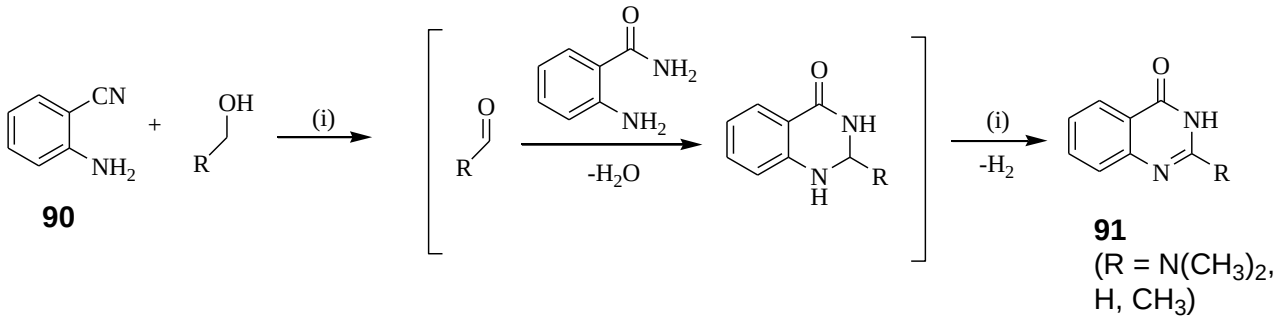

90

91
(R = $N(CH_3)_2$, H, CH_3)

Reagents and conditions: (i) $[CpIrCl_2]_2$, water, rt, 3 h

Scheme 2.17: One-pot Iridium-catalysed synthesis of 2-substituted quinazolin-4(3*H*)-ones

2.4.3 Synthesis of quinazolines

An assortment of synthetic methods leading to the synthesis of quinazoline framework have been reported in literature by employing different starting materials, for instance *N*-substituted anthranilamide, isatoic anhydride derivatives and the heavily documented quinazolin-4(3*H*)-ones.

2.4.3.1 Oxidative-aromatisation of quinazolin-4(3*H*)-ones derivatives

The 4-halogenoquinazolines have proven to be an important class of intermediates in the construction of quinazoline analogues owing to the C-X (X=Cl, Br, I) bond towards various nucleophiles. For example, the conjoint method for the synthesis of 4-chloroquinazoline derivatives involves oxidative aromatisation of the analogous quinazolin-4(3*H*)-ones using reagents such as thionyl chloride ($SOCl_2$) in DMF [119], phosphoryl chloride ($POCl_3$) [120] and at times the combination of phosphoryl chloride ($POCl_3$) and pentachloride (PCl_5) [121]. The synthesis of 6,8-dibromo-4-chloro-2-(4-methoxyphenyl)quinazoline **92**, for example was prepared by aromatisation of the 6,8-dibromo-2-(4-methoxyphenyl)quinazolin-4(3H)-one **93** (a quinazolin-4(3*H*)-one framework) using $SOCl_2$ and DMF as a solvent [122] (**Scheme 2.18**).

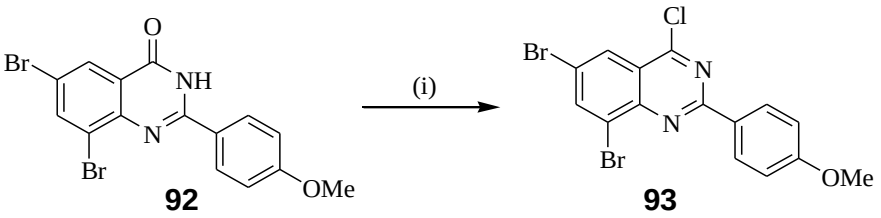

Reagents and conditions: (i) $SOCl_2$, DMF, 80 ^oC.

Scheme 2.18: Oxidative aromatisation of **92** with $SOCl_2$ and DMF as a solvent.

The treatment of 2-trichloromethylquinazolin-4(3*H*)-one **94** in the presence of phosphorous pentoxide (P_2O_5) in toluene with either tetrabutylammonium bromide (TBABr) or tetrabutylammonium iodide (TBAI) can result in oxidative aromatisation by bromination or iodination to yield quinazoline derivatives **95** and **96** respectively (**Scheme 2.19**) [123].

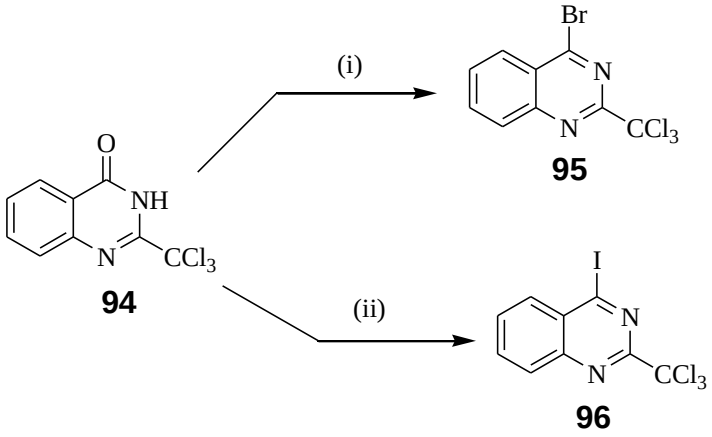

Reagents and conditions: (i) TBABr, P_2O_5 (ii) TBAI, P_2O_5

Scheme 2.19: Oxidative aromatisation by halogenation in the presence of phosphorous pentoxide (P_2O_5).

2.4.3.2 Direct synthesis of quinazolines from substituted anthranilamide derivatives

A new, direct and very convenient procedure to synthesise quinazoline derivatives from substituted anthranilamide derivatives was discovered by Koutentis and co-workers [124]. The authors reported synthesis of 3-aryl-4-imino-3,4-dihydroquinazoline-2-carbonitriles **99a-b** from 2-amino-*N'*-arylbenzamidines **97a-b** with 4,5-dichloro-1,2,3-dithiazolium chloride **98** (Appel salt) in the presence of Hünig's

base (2 equiv.). Target compounds were obtained in one-step process in moderate to good yields of 51 to 86% (**Scheme 2.20**). The reaction provides an expedient synthetic route to C-2 cyano substituted quinazolin-4(3H)-imines

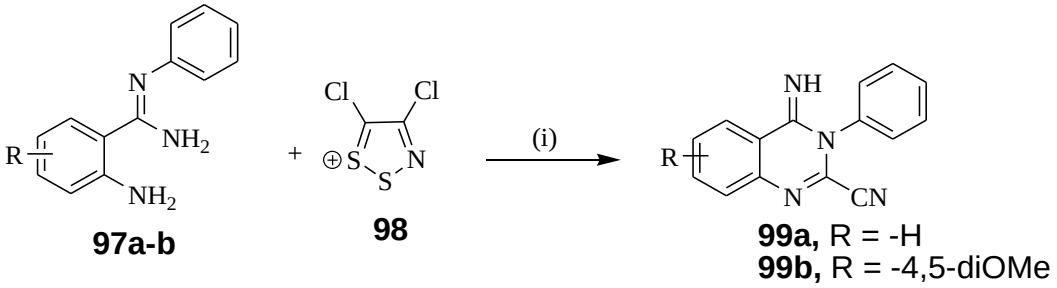

97a-b **98** **99a,** R = -H
99b, R = -4,5-diOMe

Reagents and conditions: (i) *i*-Pr$_2$Net (2 equiv.), DCM, 20 ^{o}C, 2h.

Scheme 2.20: Hünig's base promoted synthesis of 3-aryl-4-imino-3,4-dihydroquinazoline-2-carbonitriles.

An atom-efficient, atom-economic, eco-friendly, solvent-free, high yielding, multicomponent green strategy to synthesise the highly functionalised 2-(4-chlorophenyl)-6-nitro-4-phenylquinazoline **102** through a magnetic ionic liquid (IL), butylmethylimidazolium tetrachloroferrate (bmim [FeCl$_4$]) aided one-pot reaction of 2-aminobenzophenone **100**, aromatic aldehyde **71**, and ammonium acetate **101** (**Scheme 2.21**) was reported by Saha and Panja [125]. The presence of a nitro group at C-5 position of the corresponding (2-amino-5-nitrophenyl)(phenyl)methanone **100** affects the reaction time significantly.

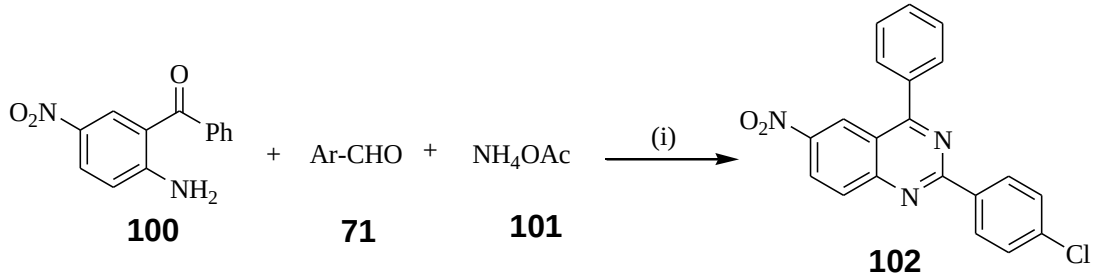

100 **71** **101** **102**

Reagents and conditions: (i) *i*-Pr$_2$NEt (2 equiv.), DCM, 20 ^{o}C, 2h.

Scheme 2.21: Magnetic IL, butylmethylimidazolium tetrachloroferrate (bmim [FeCl$_4$]) aided one-pot preparation of 2-(4-chlorophenyl)-6-nitro-4-phenylquinazoline **102.**

2.4.3.3 Metal-catalysed cross-coupling reactions aiding the synthesis of carbo-substituted quinazoline derivatives.

The assortment of transition metal-catalysed cross-coupling reactions can easily be regarded as a foundation of construction leading to highly substituted heterocycles in organic synthesis [126]. Kumada, Negishi, Suzuki-Miyaura, Stille, and Sonogashira cross-coupling reactions represent a direct approach towards the synthesis of new carbon-carbon (Csp^2-Csp) bonds [127-130]. The mechanism for metal-catalysed cross-coupling follows three steps, namely, oxidative addition, transmetallation and reductive elimination. In the case of palladium cross-coupling reaction conditions, a catalytically active 14-electron Pd(0) species supplied by $Pd(PPh_3)_4$, $PdCl_2(PPh_3)_2$, $Pd(OAc)_2$ is generated by ligand dissociation for Pd(0) (**Scheme 2.22**) or by palladium reduction for Pd(II) (**Scheme 2.23**). $Pd(PPh_3)_4$ is most commonly used because of the increased reactivity of palladium which is already in a zero oxidation state. Concurrently, $PdCl_2(PPh_3)_2$ and $Pd(OAc)_2$ plus an additional PPh_3 or other phosphine ligands have also been reported efficient since they are non-hydroscopic and can be reduced to the active Pd(0) complexes with stoichiometric additions of phosphines.

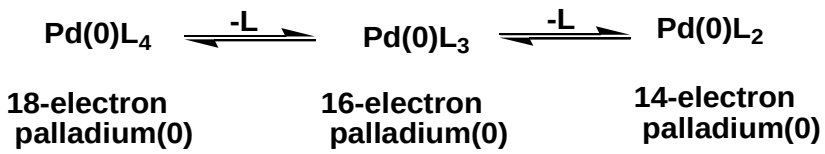

Scheme 2.22: Ligand dissociation off palladium species

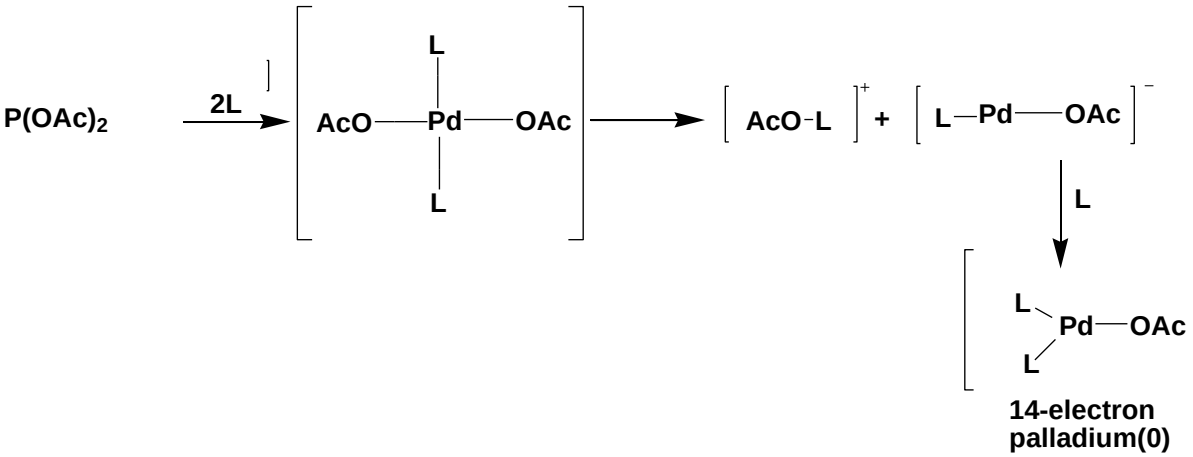

Scheme 2.23: Reduction of palladium(ll) to palladium(0) on Pd(ll)$(OAc)_2$

The palladium cross-coupling catalytic cycle starts with oxidative addition of the active palladium(0) complex Pd(0)L_2 **A** to the aryl halide (**Figure 2.17**). During this step, the Csp^2-X bond breaks forming a palladium(II) complex conforming to *trans*-R_1Pd(II)L_2X **B** containing aryl and halide ligands. The rate of the oxidative addition is accelerated by the reactivity of the aryl halide and the type of ligand present in the palladium(0) precursor [131]. The periodic order of electronegativity in aryl halides is in agreement with the C-X bond strengths. Likewise, alkylphosphine ligands are reported to increase the electron density by *σ*-complexation-dehydropalladation-reductive elimination of palladium and thus, accelerate the oxidative addition step. The palladium(II) complex **B** formed is a 16-electron square-planar complex which undergoes transmetallation *via* a ligand exchange process with the aid of a base to form an organopalladium(II) complex R_1Pd(II)L_2Nu **C** (**Figure 2.17**). The ligands of compound **C** are *trans* oriented and are converted to *cis* in a *trans-cis* isomerization to form isomer **D**. The final step, known as reductive elimination, the organopalladium(II) complex *cis*-R_1Pd(II)L_2Nu **D** dissociates the coupled product and regenerates the catalyst Pd(0). The increase of the electron density at the metal centre accelerates the reductive elimination. Alkylphosphine ligands are known to coordinate with palladium and increase its electron density more than arylphosphines. The general catalytic cycle for such reactions is represented as follows:

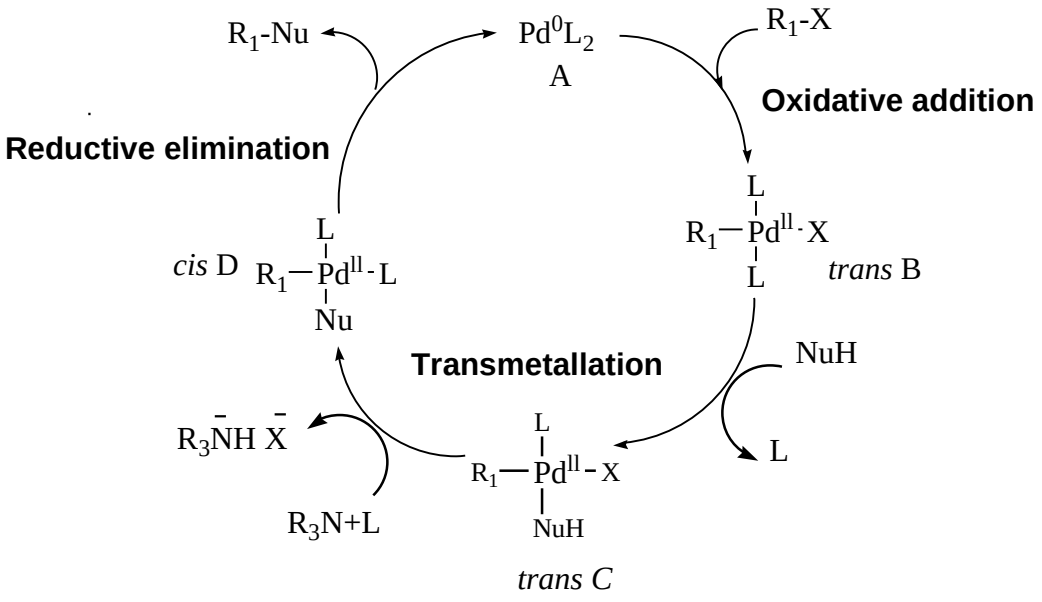

Figure 2.17: Generalised mechanism for Csp^2-Csp cross-coupling reactions.

In addition to the cross-coupling reaction conditions, the Sonogashira cross-coupling reaction has since dominated the field of organic synthesis due to the ease of synthesis leading to carbon-carbon bonds. The cross-coupling reaction involves a copper(I) salt which serves as a co-catalyst. The palladium catalytic cycle in this type of reaction is very much similar to the general palladium reaction which involves 3 catalytic steps (1) oxidative addition (2) transmetallation (3) reductive elimination. The copper co-catalysed Sonogashira reaction takes place in two independent catalytic cycles, where the tertiary amine (R_3N) is represented as base. The palladium catalytic cycle follows the one described in **Figure 2.18**. Akin to the palladium cycle, the copper cycle follows three steps, a copper acetylide ($Nu\text{-}Cu^{+}\ X^{-}$) **E**, is formed in the presence of copper(I) salt in solution. The base then abstracts the proton of the alkyne derivative leading to the *π*-alkyne-Cu complex **F**. The third step is transmetallation between the *trans* palladium complex **B** after which the copper(I) salt **D** is regenerated and the cycle continues.

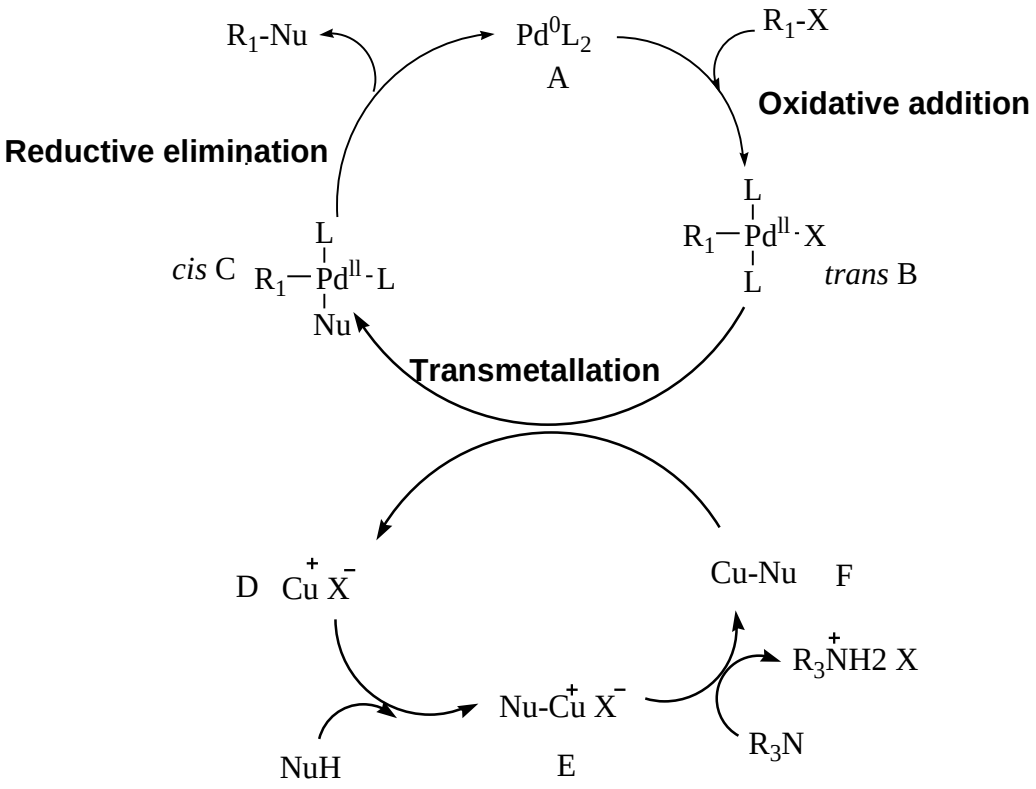

Figure 2.18: Generalised Sonogashira copper co-catalysed reaction mechanism for C*sp*^{2}-C*sp* cross-coupling.

2.4.3.4. Sonogashira cross-coupling reaction

The trend in reactivity of the Csp^2–halogen bonds in Sonogashira cross-coupling reaction of halogenated quinazoline compounds follows, Csp^2-I > C(4)-Cl > Csp^2-Br > C(2)-Cl > C-sp^2-Cl > Csp^2–F in relation to the different bond dissociation energies which favours substitution of iodine in the presence of Br, Cl and the C(4)-Cl [132]**.** The Sonogashira cross-coupling reaction between 6-bromo-2,4-dichloroquinazoline **103** and terminal alkynes **104** catalysed by $PdCl_2(PPh_3)_2$ as Pd(0) source and CuI co-catalysed in triethylamine (Et_3N), favoured cross-coupling at the more electrophilic C(4)-Cl position rather than the less activated Csp^2(6)–Br bond yielding 78-86% of the corresponding 6-bromo-2-chloro-4-(hex-1-ynyl)quinazoline **105** (**Scheme 2.24**) [133].

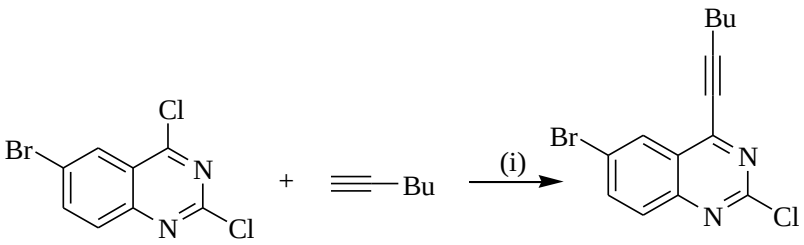

103 **104** **105**

Reagents and conditions: (i) $PdCl_2(PPh_3)_2$, CuI, Et_3N, rt.

Scheme 2.24: Sonogashira coupling reaction of **103** and **104**.

Attempted Sonogashira cross-coupling reaction between 4-chloro-2-trichloromethyl-quinazoline **106** and phenylacetylene **107** using triethylamine as a base, tetrakis(triphenyl-phosphine)palladium(0) [$Pd(PPh_3)_4$] as a source of a reactive Pd(0) species and copper(I) iodide (CuI) in THF under nitrogen atmosphere did not afford the expected cross-coupled product [134]. The presence of the trichloromethyl group at the 2-position was found to interfere with the outcome of this reaction. The use of cesium carbonate (Cs_2CO_3) as a base and palladium(II) acetate [$Pd(OAc)_2$] as a source of Pd(0) in dimethylformamide (DMF), on the other hand, afforded the cross-coupled product **108** in low yield (15%) along with other undesirable products (**Scheme 2.25**).

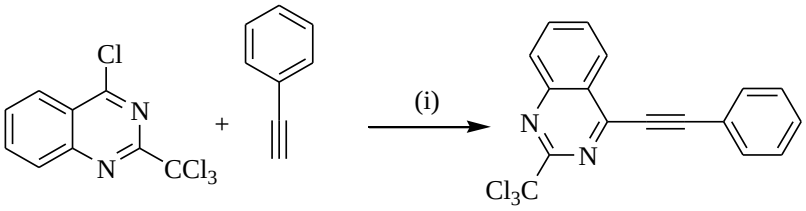

106 **107** **108**

Reagents and conditions: (i) Cs_2CO_3, $Pd(OAc)_2$, CuI, DMF, N_2, rt, 3 h.

Scheme 2.25: Sonogashira cross-coupling reaction of 4-chloro-2-trichloromethylquinazoline.

A good demonstration of the reactivity trend in Sonogashira coupling reaction leading to the Csp^2-Csp bond was shown during a reaction between 4-chloro-6-iodo-2-(4-methoxyphenyl)quinazoline **109** and phenylacetylene **110**. The reaction was catalysed by Pd(ll)$Cl_2(PPh_3)_2$ and CuI in the presence of Cs_2CO_3 under nitrogen atmosphere at room temperature. The reaction conditions favoured cross-coupling at the C(6)sp^2-I position rather than the C(4)-Cl position to yield 75% of the corresponding 4-chloro-2-(4-methoxyphenyl)-6-(2-phenylethynyl)quinazoline **111** (**Scheme 2.26**) [135].

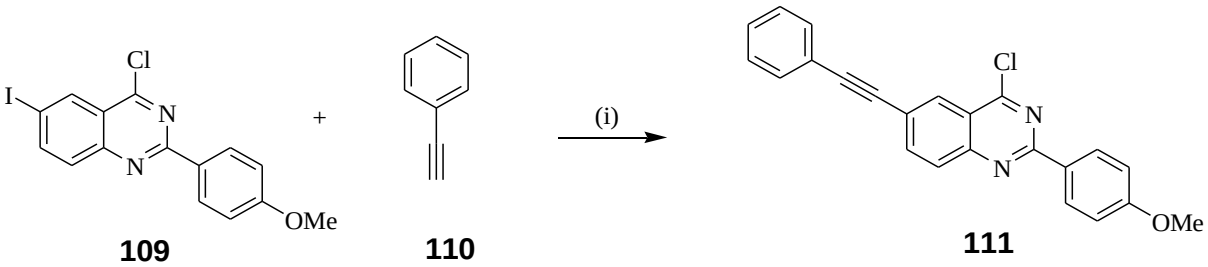

109 **110** **111**

Reagents and conditions: (i) Cs_2CO_3, Pd(ll)$Cl_2(PPh_3)_2$, CuI, THF, N_2, rt, 18 h.

Scheme 2.26: Sonogashira cross-coupling reaction of 4-chloro-6-iodo-2-(4-methoxyphenyl)quinazoline **111** on the C(6)sp^2-I position.

2.4 Quinazoline derivatives as intermediates in coordination chemistry including their synthesis and biological application.

The field of bioinorganic chemistry has been at the highest receiving end of chemistry research attention over the past 3 decades [136-137]. The research interest in this field is amplified by the unending increase in activity of heterocyclic compounds with anticancer, anti-inflammatory, antimalarial, antibacterial and anti-proliferative

properties [138]. Of these highly biologically active heterocycles, pyrimidine derivatives, particularly quinazoline bearing derivatives have been under massive exploration both *in silico* and *in vitro* studies [139].

The literature on transition metal containing quinazoline complexes is limited, hence indicative of perhaps, difficulty in synthesising the complexes or area unexplored. The synthesis or coordination of quinazoline derivatives requires knowledge in ligand behaviour, coordination modes, general understanding of coordination chemistry, etc. The type of geometrical arrangement around the metal centre is key in avoiding steric hindrance, hence contributing to the stability of the complex. For example, poly-nuclear silver(I) quinazoline containing derivatives **114** were reported by Glišić and co-workers [140] to possess activity against the pathogenic *Pseudomonas aeruginosa* strains *in silico* and *in vitro*. The Ag(I) complexes were synthesised by refluxing 2 mmol of quinazoline **112** and 1 mmol of $AgCF_3SO_3$ **113** in ethanol for 8 h to yield 42% of the corresponding tetrahedral Silver(I) quinazoline complex (**Scheme 2.27**) **114**.

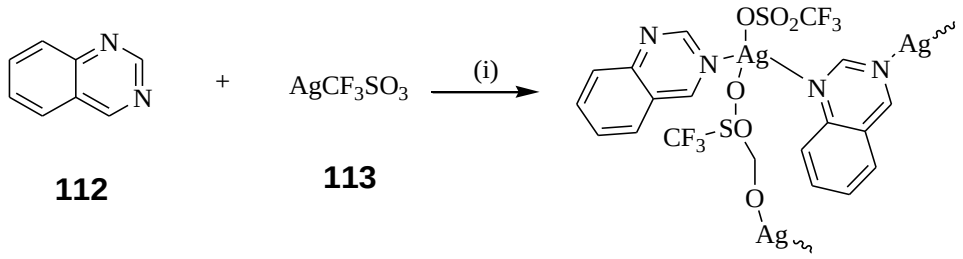

112 **113** **114**

Reagents and conditions: (i) $AgBF_4$, ethanol, heat, 8 h.

Scheme 2.27: Synthesis of silver(I) quinazoline complexes with antimicrobial activity.

A three-legged piano stool ruthenium(II) quinazoline complex possessing oncotherapeutic antiplatelet activity was reported by Kharamang and co-workers [141]. The ruthenium arene quinazoline (RAQ) complex is reported to hinder ATP release and $[Ca^{2+}]$, and therefore decrease Akt/JNK signals. Akt/JNK pathways are involved in autophagy [142] process. Autophagy is a homeostatic, catabolic degradation process whereby cellular proteins and organelles are engulfed into autophagosomes, digested in lysosomes and recycled to sustain cellular metabolism [143]. Targeting these pathways represents an ideal strategy towards cancer cell lysis. Experimental synthesis of the RAQ complex was achieved by stirring dichloro-(p-

cymene)-ruthenium(ll) dimer **38** and corresponding 4-phenyl-2-(pyridin-2-yl)quinazoline **115** ligand in methanol at room temperature for 24 h to yield 87% of [(η^6-*p*-cymene)RuCl4-phenyl-2-(pyridin-2-yl)quinazoline]tetrafluoroborate **116** (**Scheme 2.28**). Likewise, the RAQ complex inhibited platelet aggregation in washed human platelets while stimulated by collagen in a concentratrion-dependent manner (1 – 5 uM).

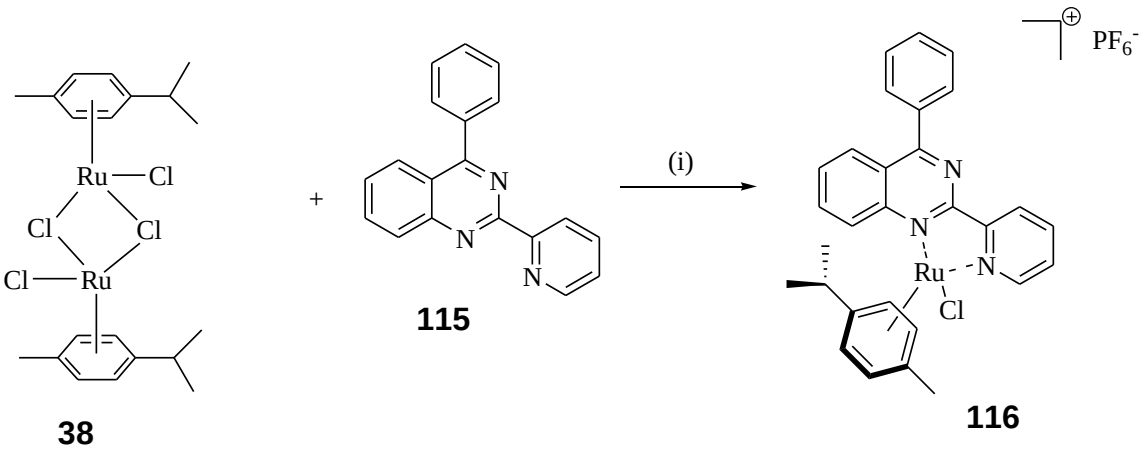

Reagents and conditions: (i) $NaBF_4$, methanol, rt, 24 h.

Scheme 2.28: Synthesis of ruthenium(ll) arene quinazoline complexes with antiplatelet activity.

A new, dual-targeting, piano stool ruthenium(ll) complex possessing anticancer properties was developed by Zhang and co-workers [144]. The corresponding RAQ complex was synthesised by stirring 6-(2-(2-aminoethylamino)ethoxy)-4-(3'-chloro-4'-fluoroanilino)-7-methoxy-quinazoline **117** and dichloro-(p-cymene)-ruthenium(ll) dimer **38** in methanol for 24 h to yield 31.2 % of [(η^6-*p*-cymene)RuCl6-(2-(2-aminoethylamino)ethoxy)-4-(3'-chloro-4'-fluoroanilino)-7-methoxy-quinazoline]hexa-fluorophosphate **118** (**Scheme 2.29**). The antecedent RAQ complex is reported to exhibit 29-fold IC_{50} against HeLa cell lines i.e. 1.36 uM compared to the ligand precursor **117** i.e. 29.5 uM.

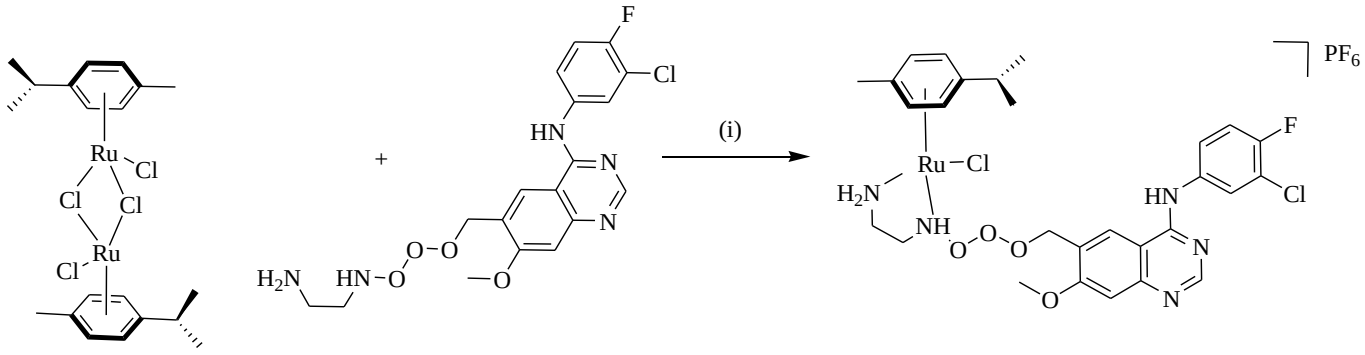

38 **117** **118**

Reagents and conditions: (i) KPF_6, methanol, rt, 24 h.

Scheme 2.29: Synthesis of ruthenium(ll) erlotinib complex with improved anticancer activity.

The synthesis of biologically active compounds is a challenging and costly process, in the 1960's researchers would blindly screen hundred thousands of natural and synthetic compounds for possible biological activity. Upon viewing activity, medicinal chemists would synthesise a library of compounds for further biological exploration [145]. This method, termed "traditional drug design" is costly as out of 100 thousand compounds only 25 would register the desired property investigated [146]. Previous sources estimated the cost to be ranging from $200-$500 million each year worldwide [147]. To ameliorate this injustice, scientists have since developed a computer programme called molecular docking.

2.5 Molecular docking

Molecular docking is a modern medicinal chemistry tool which investigates pharmacodynamical data and pharmacokinetic properties through structure activity relationship (SAR) of prodrugs [148]. The pharmacodynamical data includes potency, selectivity, affinity and efficacy of prodrugs [149], on the other hand pharmacokinetic properties investigated include ADME-Tox (absorption, distribution, metabolism, excretion and toxicity) of the prepared prodrugs [150]. The progression of this field is complemented by advances in biomolecular spectroscopic methods such as X-ray crystallography and nuclear magnetic resonance techniques (NMR) [151]. These techniques have produced over 100 000 three-dimensional (3D) protein structures, brewing influential information on macromolecular drug targets [152]. The

incorporation of computational (*in silico*) and experimental (*in vitro*) methods have provided a broad understanding of the complex aspects of intermolecular recognition [153].

Within the pre-described concept, structure-based design (SBDD) methods such as molecular kinetics, molecular dynamics and structure-based virtual screening (SBVS) are employed to aid molecular recognition events such as binding energy, molecular interactions and induced conformational changes [154]. A defined approach in drug design encompasses biologically active small molecule libraries [155]. The unique diversity available in these libraries (co-crystallised ligands within proteins) represents the active site to which ligands target [156]. This application is limited to ligand-based drug design (LBDD) methods. Similarly, ligand-based virtual screening (LBVS), conformational searching and quantitative structure activity relationship (QSAR) modelling are the most used LBDD methods [157]. The SBDD and LBDD methods are the most encountered in computer aided drug-design and have proved valuable to both academia and industry [158].

2.6 Purpose of the study

Infectious airborne and neoplastic diseases are the two causes of illness and mortality in developing and developed countries, respectively [159]. This section covers the challenges faced by chemotherapeutic techniques applied to treat specifically Tuberculosis (TB) and cancer.

2.6.1. Tuberculosis (TB)

Tuberculosis (TB) is an airborne disease caused by *Myobacterium tuberculosis* (*Mtb*) [1]. The world health organisation (WHO) has reported that TB remains one of the modern day killer bacteria in the world, where treatment and management of the infection remains a big challenge [160]. In 2017 (latest statistics), TB was reported to be the biggest killer disease in the country (South Africa) and unfortunately more and more people are infected daily at an alarming rate [160]. Several TB drugs, such as Isoniazid, Rifampicin, Pyrazinamide, Ethambutol and Streptomycin, are administered to treat the TB disease at different stages (i.e. for latent TB, MDR-TB and XDR-TB). Even though the antecedent drugs have several advantages such as low cost, effectiveness and limited host toxicity, the country is still burdened with increased new

infections. This is because of the prolonged treatment period of six (6) months, during which mutations of the *Mtb* resistant strains occurs if care is not taken during the six (6) months period [161]. Recently, drugs by names Delamanid and Bedaquiline have been unveiled as the most progressive treatment for the resistant TB, the major limitation being the QT-prolongation side effect [162]. The QT-prolongation is a serious disturbance of the heart's electrical rhythm. Other side effects include the liver toxicity, deafness, accumulation of phospholipids in cells and even death [162].

2.6.2 Cancer

Cancer is defined as a group of unrelated diseases that affect any part of the human body. According to the world health organisation (WHO), cancer is one of the leading causes of death worldwide and it has been responsible for 9.6 million deaths in 2018 [163]. The development of cancer strategies over the years have employed chemotherapy combined with radiotherapy, surgery and targeted therapy [164]. Chemotherapeutic drugs currently employed to treat this burden include *Cis*platin, cobimetinib and elronitib [165]. These drugs, though effective to some extent, pose severe side effects such as hair loss, stroke and vomiting due to their non-selectivity towards normal cells [166]. Apart from the pre-mentioned drawbacks and lack of alternatives, they still find application.

Herein we hypothesise a possible strategy on eliminating the problems described in subsections **2.6.1** and **2.6.2**. Schiff base and quinazoline structure activity relationship (SAR) of ruthenium(ll) *p*-cymene bioinorganic molecular hybrids with plausible mimic of synergy in cancerous and *Mycobacterium tuberculosis* cell lines. In this project, we employ Sonogashira cross-coupling at the *C(4)-Cl* to introduce electron-donating ethynylpyridine bridge, which is used as a link between the quinazoline and the ruthenium(ll) *p*-cymene moieties. For the Schiff base groups, a similar idea is hoped to stabilise the ligands in biological solutions such as DMSO and water, and thus improving binding in the active site. Molecular docking is used to better understand the possible interactions in the binding site of cancer and *Mtb* proteins 3F8P and 2SRC belonging to the Tyrosine kinase and oxidoreductase family and the 1HTO of *glutamine synthetase* respectively. In this way, we hope to gain control of the hydrophilicity and size of the complexes in the delivery system, where the two parts of

the compound complement each other to exhibit different interactions in the binding site. Thus, the aim and the objectives of the study are therefore defined as follows:

2.7 Aim

The aim of this study was to synthesise, characterise, and perform biological evaluation of *p*-cymene ruthenium(ll) complexes of imidazolyl-ethanamine-Schiff bases and 4-ethynylpyridine *cross-coupled* quinazolines.

2.8 The objectives were to:

i. Synthesise imidazolyl-ethanamine-Schiff bases and their M(ll) complexes
ii. Synthesise ethynylpyridine bridged quinazolines and their *p*-cymene ruthenium(ll) complexes
iii. Evaluate the anticancer properties of the synthesised compounds *in vitro*
iv. Evaluate the anti-*Mycobacterium tuberculosis* properties of the synthesised compounds *in vitro*
v. Perform molecular docking of the synthesised compounds in 1HTO, 2RSC and 3F8P

Reference

[1]. Tidwell, T.T., 2008. Hugo (Ugo) Schiff, Schiff Bases, and a Century of β-Lactam Synthesis. *Angewandte Chemie International Edition*, *47*(6), pp.1016-1020.

[2]. Kumar, S., Dhar, D.N. and Saxena, P.N., 2009. Applications of metal complexes of Schiff bases-A review. *Journal of Scientific and Industrial Research, 68*, pp. 181-187.

[3]. Cao, Y., Varo, G., Chang, M., Ni, B., Needleman, R. and Lanyi, J.K., 1991. Water is required for proton transfer from aspartate-96 to the bacteriorhodopsin Schiff base. *Biochemistry*, *30*(45), pp.10972-10979.

[4]. Glomb, M.A. and Monnier, V.M., 1995. Mechanism of protein modification by glyoxal and glycolaldehyde, reactive intermediates of the Maillard reaction. *Journal of Biological Chemistry*, *270*(17), pp.10017-10026.

[5]. Deng, H., Huang, L., Callender, R. and Ebrey, T., 1994. Evidence for a bound water molecule next to the retinal Schiff base in bacteriorhodopsin and rhodopsin: a resonance Raman study of the Schiff base hydrogen/deuterium exchange. *Biophysical Journal*, *66*(4), pp.1129-1136.

[6]. Balan, K., Ratha, P., Prakash, G., Viswanathamurthi, P., Adisakwattana, S. and Palvannan, T., 2017. Evaluation of invitro α-amylase and α-glucosidase inhibitory potential of N2O2 schiff base Zn complex. *Arabian Journal of Chemistry*, *10*(5), pp.732-738.

[7]. Gupta, 1.K. and Sutar, A.K., 2008. Catalytic activities of Schiff base transition metal complexes. *Coordination Chemistry Reviews*, *252*(12-14), pp.1420-1450.

[8]. Cozzi, P.G., 2004. Metal–Salen Schiff base complexes in catalysis: practical aspects. *Chemical Society Reviews*, *33*(7), pp.410-421.

[9]. Holm, R.H., Everett Jr, G.W. and Chakravorty, A., 1966. Metal complexes of Schiff bases and β-ketoamines. *Progress in Inorganic Chemistry*, pp.83-214.

[10]. Nishinaga, A. and Tomita, H., 1980. Model catalytic oxygenations with Co (II)—schiff base complexes and the role of cobalt-oxygen complexes in the oxygenation process. *Journal of Molecular Catalysis*, *7*(2), pp.179-199.

[11]. Eichhorn, G.L. and Trachtenberg, I.M., 1954. Catalysis of Schiff Base Hydrolysis by Metal Ions1, 2. *Journal of the American Chemical Society*, *76*(20), pp.5183-5185.

[12]. Zolezzi, S., Spodine, E. and Decinti, A., 2002. Electrochemical studies of copper (II) complexes with Schiff-base ligands. *Polyhedron*, *21*(1), pp.55-59.

[13]. Hamilton, D.E., Drago, R.S. and Zombeck, A., 1987. Mechanistic studies on the cobalt (II) Schiff base catalyzed oxidation of olefins by O2. *Journal of the American Chemical Society*, *109*(2), pp.374-379.

[14]. Hung, W.C. and Lin, C.C., 2008. Preparation, characterization, and catalytic studies of magnesium complexes supported by NNO-tridentate Schiff-base ligands. *Inorganic Chemistry*, *48*(2), pp.728-734.

[15]. Sreekala, R. and Yusuff, K.K., 1995. Catalytic activity of five coordinate cobalt (II) complexes for the decomposition of hydrogen peroxide.Indian *Journal of Chemistry*, *34*(12), pp.994-996.

[16]. Chakraborti, A.K., Bhagat, S. and Rudrawar, S., 2004. Magnesium perchlorate as an efficient catalyst for the synthesis of imines and phenylhydrazones. *Tetrahedron Letters*, *45*(41), pp.7641-7644.

[17]. Dubrovsky, L., Ulrich, P., Nuovo, G.J., Manogue, K.R., Cerami, A. and Bukrinsky, M., 1995. Nuclear localization signal of HIV-1 as a novel target for therapeutic intervention. *Molecular Medicine*, *1*(2), p.217.

[18]. Raman, N., Kulandaisamy, A., Shunmugasundaram, A. and Jeyasubramanian, K., 2001. Synthesis, spectral, redox and antimicrobial activities of Schiff base complexes derived from 1-phenyl-2, 3-dimethyl-4-aminopyrazol-5-one and acetoacetanilide. *Transition Metal Chemistry*, *26*(1-2), pp.131-135.

[19]. DharmaraJ, N., Viswanathamurthi, P. and NataraJan, K., 2001. Ruthenium (II) complexes containing bidentate Schiff bases and their antifungal activity. *Transition Metal Chemistry*, *26*(1-2), pp.105-109.

[20]. Apostolopoulos, V., Barnes, N., Pietersz, G.A. and McKenzie, I.F., 2000. Ex vivo targeting of the macrophage mannose receptor generates anti-tumor CTL responses. *Vaccine*, *18*(27), pp.3174-3184.

[21]. Ali, M.A., Mirza, A.H., Butcher, R.J., Tarafder, M.T.H., Keat, T.B. and Ali, A.M., 2002. Biological activity of palladium (II) and platinum (II) complexes of the acetone Schiff bases of S-methyl-and S-benzyldithiocarbazate and the X-ray crystal structure of the [Pd (asme) 2](asme= anionic form of the acetone Schiff base of S-methyldithiocarbazate) complex. *Journal of Inorganic Biochemistry*, *92*(3), pp.141-148.

[22]. Segura, J.L., Mancheño, M.J. and Zamora, F., 2016. Covalent organic frameworks based on Schiff-base chemistry: synthesis, properties and potential applications. *Chemical Society Reviews*, *45*(20), pp.5635-5671.

[23]. Gündüzalp, A.B., Özsen, İ., Alyar, H., Alyar, S. and Özbek, N., 2016. Biologically active Schiff bases containing thiophene/furan ring and their copper (II) complexes: Synthesis, spectral, nonlinear optical and density functional studies. *Journal of Molecular Structure*, *1120*, pp.259-266.

[24]. Abu-Dief, A.M. and Mohamed, I.M., 2015. A review on versatile applications of transition metal complexes incorporating Schiff bases. *Beni-suef university Journal of Basic and Applied Sciences*, *4*(2), pp.119-133.

[25]. Latha, R. and Umadevi, M., 2017. Synthesis, Characterization, and Biological Evaluation of Some 3d-Metal Complexes of Schiff Base Derived from Sulfonamide Drug. *Journal of Advanced Applied Scientific Research*, *1*(9), pp. 62-67.

[26]. Kumar, S.P., Suresh, R., Giribabu, K., Manigandan, R., Munusamy, S., Muthamizh, S. and Narayanan, V., 2015. Synthesis and characterization of chromium (III) schiff base complexes: Antimicrobial activity and its electrocatalytic sensing ability of catechol. *Spectrochimica Acta Part A: Molecular and Biomolecular Spectroscopy*, *139*, pp.431-441.

[27]. Pervez, H., Ahmad, M., Zaib, S., Yaqub, M., Naseer, M.M. and Iqbal, J., 2016. Synthesis, cytotoxic and urease inhibitory activities of some novel isatin-derived bis-Schiff bases and their copper (II) complexes. *Medicinal Chemistry Communications*, *7*(5), pp.914-923.

[28]. Kappaun, K., Piovesan, A.R., Carlini, C.R. and Ligabue-Braun, R., 2018. Ureases: historical aspects, catalytic and non-catalytic properties-a review. *Journal of Advanced Research*, *13*, pp. 3-17.

[29]. Boer, J.L., Mulrooney, S.B. and Hausinger, R.P., 2014. Nickel-dependent metalloenzymes. *Archives of Biochemistry and Biophysics*, *544*, pp.142-152.

[30]. Esmadi, F., Khabour, O.F., Albarqawi, A.I., Ababneh, M. and Al-Talib, M., 2013. Synthesis and Characterization of Some Transition Metal Complexes of Thiocarbohydrazone Schiff Bases. *Jordan Journal of Chemistry*, *146*(895), pp.1-13

[31]. Curini, M., Epifano, F., Maltese, F. and Marcotullio, M.C., 2002. Novel chiral Schiff base ligands from amino acid amides and salicylaldehyde. *Tetrahedron Letters*, *43*(21), pp.3821-3823.

[32]. Zhang, C.X. and Lippard, S.J., 2003. New metal complexes as potential therapeutics. *Current Opinion in Chemical Biology*, *7*(4), pp.481-489.

[33]. Fisher, J.M., Potter, R.J. and Barnard, C.F.J., 2004. Applications of Coordination Complexes. *Platinum Metals Review*, *48*(3), pp.101-104.

[34]. Wozniak, A.J., Crowley, J.J., Balcerzak, S.P., Weiss, G.R., Spiridonidis, C.H., Baker, L.H., Albain, K.S., Kelly, K., Taylor, S.A., Gandara, D.R. and Livingston, R.B., 1998. Randomized trial comparing cisplatin with cisplatin plus vinorelbine in the treatment of advanced non-small-cell lung cancer: a Southwest Oncology Group study. *Journal of Clinical Oncology*, *16*(7), pp.2459-2465.

[35]. Wu, P., Ma, D.L., Leung, C.H., Yan, S.C., Zhu, N., Abagyan, R. and Che, C.M., 2009. Stabilization of G-Quadruplex DNA with Platinum (II) Schiff Base Complexes: Luminescent Probe and Down-Regulation of c-myc Oncogene Expression. *Chemistry–A European Journal*, *15*(47), pp.13008-13021.

[36]. Chen, H., Liu, H. and Qing, G., 2018. Targeting oncogenic Myc as a strategy for cancer treatment. *Signal Transduction and Targeted Therapy*, *3*(1), p.5.

[37]. Chow, M.J., Babak, M.V., Wong, D.Y.Q., Pastorin, G., Gaiddon, C. and Ang, W.H., 2016. Structural determinants of p53-independence in anticancer ruthenium-arene schiff-base complexes. *Molecular Pharmaceutics*, *13*(7), pp.2543-2554.

[38]. Feng, J. and Zhang, H., 2013. Hybrid materials based on lanthanide organic complexes: a review. *Chemical Society Reviews*, *42*(1), pp.387-410.

[39]. Guan, Q.L., Xing, Y.H., Liu, J., Wei, W.J., Zhang, R., Wang, X. and Bai, F.Y., 2013. Application of multiple parallel perfused microbioreactors: Synthesis, characterization and cytotoxicity testing of the novel rare earth complexes with indole acid as a ligand. *Journal of Inorganic Biochemistry*, *128*, pp.57-67.

[40]. Zhou, J., An, L., Liu, X., Zou, H., Hu, F. and Liu, C., 2012. One unprecedented 1-D europium thioindate-thioantimonate based on heterometallic mixed nitro-thioclusters with photoluminescent properties. *Chemical Communications*, *48*(19), pp.2537-2539.

[41]. Ban, S., Suzuki, S., Kubota, K., Ohshima, S., Satoh, H., Imada, H. and Ueda, Y., 2017. Gastric mucosal status susceptible to lanthanum deposition in patients treated with dialysis and lanthanum carbonate. *Annals of Diagnostic Pathology*, *26*, pp.6-9.

[42]. Haley, P.J., 1991. Pulmonary toxicity of stable and radioactive lanthanides. *Health Physics*, *61*(6), pp.809-820.

[43]. Mody, T.D., Fu, L. and Sessler, J.L., 2001. Texaphyrins: synthesis and development of a novel class of therapeutic agents. *Progress in Inorganic Chemistry*, pp.551-598.

[44]. Storr, T., Thompson, K.H. and Orvig, C., 2006. Design of targeting ligands in medicinal inorganic chemistry. *Chemical Society Reviews*, *35*(6), pp.534-544.

[45]. Andiappan, K., Sanmugam, A., Deivanayagam, E., Karuppasamy, K., Kim, H.S. and Vikraman, D., 2018. In vitro cytotoxicity activity of novel Schiff base ligand–lanthanide complexes. *Scientific Reports*, *8*(1), p.3054.

[46]. Tümer, M., Akgün, E., Toroğlu, S., Kayraldiz, A. and Dönbak, L., 2008. Synthesis and characterization of Schiff base metal complexes: their antimicrobial, genotoxicity and electrochemical properties. *Journal of Coordination Chemistry*, *61*(18), pp.2935-2949.

[47]. Deligönül, N., Tümer, M. and Serin, S., 2006. Synthesis, characterization, catalytic, electrochemical and thermal properties of tetradentate Schiff base complexes. *Transition Metal Chemistry*, *31*(7), pp.920-929.

[48]. Aranha, P.E., dos Santos, M.P., Romera, S. and Dockal, E.R., 2007. Synthesis, characterization, and spectroscopic studies of tetradentate Schiff base chromium (III) complexes. *Polyhedron*, *26*(7), pp.1373-1382.

[49]. Champouret, Y.D., Fawcett, J., Nodes, W.J., Singh, K. and Solan, G.A., 2006. Spacially confined M2 centers (M= Fe, Co, Ni, Zn) on a sterically bulky binucleating support: Synthesis, structures and ethylene oligomerization studies. *Inorganic Chemistry*, *45*(24), pp.9890-9900.

[50]. Prakash, A. and Adhikari, D., 2011. Application of Schiff bases and their metal complexes-A Review. *International Journal of ChemTech Research*, *3*(4), pp.1891-1896.

[51]. Mennicke, W., 1986. Westphal, Mixtures of 1: 2 chromium complex dyes, Ger Offen3, 409,082 (to Bayer AG) 19 Sep. 1985, DE Appl, 13 Mar 1984. In *Chemistry Abstracts* (Vol. 104, p. 111359).

[52]. Dehnert, J. and Juchemann, W., 1985. Azo group containing metal complex dyes, Ger Offen3, 337,591 (to BASF AG) 25 April. 1985, Appl 15 Oct. 1983. In *Chemistry Abstracts* (Vol. 103, p. 106288).

[53]. Manju, Kishore, D. and Kumar, D., 2011. Cadmium and tin complexes of Schiff-base ligands. *Journal of Coordination Chemistry*, *64*(12), pp.2130-2156.

[54]. Cozzi, P.G., 2004. Metal–Salen Schiff base complexes in catalysis: practical aspects. *Chemical Society Reviews*, *33*(7), pp.410-421.

[55]. Gradinaru, J., Forni, A., Druta, V., Tessore, F., Zecchin, S., Quici, S. and Garbalau, N., 2007. Structural, spectral, electric-field-induced second harmonic, and theoretical study of Ni (II), Cu (II), Zn (II), and VO (II) complexes with [N2O2] unsymmetrical schiff bases of S-methylisothiosemicarbazide derivatives. *Inorganic Chemistry*, *46*(3), pp.884-895.

[56]. O'Donnell, M.J. and Polt, R.L., 1982. A mild and efficient route to Schiff base derivatives of amino acids. *The Journal of Organic Chemistry*, *47*(13), pp.2663-2666.

[57]. Arulmurugan, S., Kavitha, H.P. and Venkatraman, B.R., 2010. Biological activities of Schiff base and its complexes: a review. *Rasayan Journal of Chemistry*, *3*(3), pp.385-410.

[58]. Wang, J., Li, P., Choy, P.Y., Chan, A.S. and Kwong, F.Y., 2012. Advances and Applications in Organocatalytic Asymmetric aza-Michael Addition. *ChemCatChem*, *4*(7), pp.917-925.

[59]. Patil, R.D. and Adimurthy, S., 2011. Copper-catalyzed aerobic oxidation of amines to imines under neat conditions with low catalyst loading. *Advanced Synthesis & Catalysis*, *353*(10), pp.1695-1700.

[60]. Cheng, C. and Brookhart, M., 2012. Iridium-catalyzed reduction of secondary amides to secondary amines and imines by diethylsilane. *Journal of the American Chemical Society*, *134*(28), pp.11304-11307.

[61]. Machado, V.G., Nascimento, M.G. and Rezende, M.C., 1993. Metal ion catalysis in the hydrolysis of imines. *Journal of Brazilian Chemical Society*, *4*, pp.76-79.

[62]. Sadeghi-Kiakhani, M., Gharanjig, K. and Arami, M., 2015. Grafting of prepared chitosan–poly (propylene) imines dendrimer hybrid as a biopolymer onto cotton and

its antimicrobial property. *Journal of Industrial and Engineering Chemistry*, *28*, pp.78-85.

[63]. Safa, K.D., Mardipour, J.V. and Oskoei, Y.M., 2011. Synthesis of new imines and amines containing organosilicon groups. *Journal of Organometallic Chemistry*, *696*(3), pp.802-806.

[64]. Kumar, A. and Samuelson, A.G., 2011. Metathesis of carbon dioxide and phenyl isocyanate catalysed by group (IV) metal alkoxides: An experimental and computational study. *Journal of Chemical Sciences*, *123*(1), pp.29-36.

[65]. Blackburn, L. and Taylor, R.J., 2001. In situ oxidation− imine formation− reduction routes from alcohols to amines. *Organic Letters*, *3*(11), pp.1637-1639.

[66]. Gu, X.Q., Chen, W., Morales-Morales, D. and Jensen, C.M., 2002. Dehydrogenation of secondary amines to imines catalyzed by an iridium PCP pincer complex: initial aliphatic or direct amino dehydrogenation?. *Journal of Molecular Catalysis A: Chemical*, *189*(1), pp.119-124.

[67]. Wang, J.R., Fu, Y., Zhang, B.B., Cui, X., Liu, L. and Guo, Q.X., 2006. Palladium-catalyzed aerobic oxidation of amines. *Tetrahedron letters*, *47*(47), pp.8293-8297.

[68]. Chow, M.J., Licona, C., Yuan Qiang Wong, D., Pastorin, G., Gaiddon, C. and Ang, W.H., 2014. Discovery and investigation of anticancer ruthenium–arene Schiff-Base complexes via water-promoted combinatorial three-component assembly. *Journal of Medicinal Chemistry*, *57*(14), pp.6043-6059.

[70]. Banerjee, S., Dixit, A., Maheswaramma, K.S., Maity, B., Mukherjee, S., Kumar, A., Karande, A.A. and Chakravarty, A.R., 2016. Photocytotoxic ternary copper (II) complexes of histamine Schiff base and pyridyl ligands. *Journal of Chemical Sciences*, *128*(2), pp.165-175.

[71]. Tajuddin, A.M., Bahron, H., Kassim, K., Ibrahim, W.N. and Yamin, B.M., 2012. Synthesis and characterization of paladium (II) Schiff base complexes and their catalytic activities for Suzuki coupling reaction. *The Malaysian Journal of Analytical Sciences*, *16*(1), pp.79-87.

[72]. Namiecinska, E., Sobiesiak, M., Malecka, M., Guga, P., Rozalska, B. and Budzisz, E., 2018. Antimicrobial and structural properties of metal ions complexes with

thiosemicarbazide motif and related heterocyclic compounds. *Current medicinal chemistry*.

[73]. Choudhary, S., Silakari, O. and Singh, P.K., 2018. New Insights into Chemistry and Biological Potential of Thiazine Scaffold: A Review. *Mini Reviews in Medicinal Chemistry*, 18(17), pp.1452-1478.

[74]. Hameed, A., Al-Rashida, M., Uroos, M., Ali, S.A., Arshia, Ishtiaq, M. and Khan, K.M., 2018. Quinazoline and quinazolinone as important medicinal scaffolds: a comparative patent review (2011–2016). *Expert Opinion on Therapeutic Patents*, *28*(4), pp.281-297.

[75]. Patil, S.B., 2018. Biological and Medicinal Significance of Pyrimidines: A Review. *International Journal of Pharmaceutical Sciences and Research*, *9*(1), pp.44-52.

[76]. Campos, J.F., Loubidi, M., Scherrmann, M.C. and Berteina-Raboin, S., 2018. A Greener and Efficient Method for Nucleophilic Aromatic Substitution of Nitrogen-Containing Fused Heterocycles. *Molecules*, *23*(3), p.684.

[77]. Witt, A. and Bergman, J., 2003. Recent developments in the field of quinazoline chemistry. *Current Organic Chemistry*, *7*(7), pp.659-677.

[78]. Jiang, S., Zeng, Q., Gettayacamin, M., Tungtaeng, A., Wannaying, S., Lim, A., Hansukjariya, P., Okunji, C.O., Zhu, S. and Fang, D., 2005. Antimalarial activities and therapeutic properties of febrifugine analogs. *Antimicrobial Agents And Chemotherapy*, *49*(3), pp.1169-1176.

[79]. Pines, M., 2014. Halofuginone for fibrosis, regeneration and cancer in the gastrointestinal tract. *World Journal of Gastroenterology: WJG*, *20*(40), p.14778.

[80]. Kikuchi, H., Tasaka, H., Hirai, S., Takaya, Y., Iwabuchi, Y., Ooi, H., Hatakeyama, S., Kim, H.S., Wataya, Y. and Oshima, Y., 2002. Potent antimalarial febrifugine analogues against the plasmodium malaria parasite. *Journal of Medicinal Chemistry*, *45*(12), pp.2563-2570.

[81]. Tiwari, V.K., Kale, R.R., Mishra, B.B. and Singh, A., 2008. A facile one-pot MW approach for 3-heteroaryl-2-thioxo-2, 3-dihydroquinazolin-4 (1H)-one. *Arkivoc*, *14*(11), pp.27-36.

[82]. Arora, R., Gill, N.S., Kapoor, A., Arora, R., Kapoor, A., Gill, N.S., Rana, A.C., Khalil, A.A., Hamide, S.A., El-Obeid, A.M. and El-Subbagh, H.I., 2011. Synthesis and anti-microbial screening of novel schiff bases of 3-amino-2-methyl quinazolin 4-(3H)-one. *Journal of Pharmacy and Allied Health Sciences*, *4*(1), pp.22-28.

[83]. El-Azab, A.S. and ElTahir, K.E., 2012. Design and synthesis of novel 7-aminoquinazoline derivatives: antitumor and anticonvulsant activities. *Bioorganic & Medicinal Chemistry Letters*, *22*(5), pp.1879-1885.

[84]. Asif, M., 2014. Chemical characteristics, synthetic methods, and biological potential of quinazoline and quinazolinone derivatives. *International Journal of Medicinal Chemistry*, *2014*(1), pp.395637.

[85]. Abida, P.N. and Arpanarana, M., 2011. An updated review: newer quinazoline derivatives under clinical trial. *International Journal of Pharmaceutical & Biological Archive*, *2*(6), pp.1651-1657.

[86]. Selvam, T.P. and Kumar, P.V., 2011. Quinazoline marketed drugs. *Research in Pharmacy*, *1*(1), pp 101-104.

[87]. Mahato, A.K., Srivastava, B. and Nithya, S., 2011. Chemistry, structure activity relationship and biological activity of quinazoline-4 (3H)-one derivatives. *Inventi Rapid Medicinal Chemistry*, *2*, pp.400-2.

[88]. Kuneš, J., Bažant, J., Pour, M., Waisser, K., Šlosárek, M. and Janota, J., 2000. Quinazoline derivatives with antitubercular activity. *Il Farmaco*, *55*(11-12), pp.725-729.

[89]. Kuroiwa, K., Ishii, H., Matsuno, K., Asai, A. and Suzuki, Y., 2015. Synthesis and structure–activity relationship study of 1-phenyl-1-(quinazolin-4-yl) ethanols as anticancer agents. *ACS Medicinal Chemistry Letters*, *6*(3), pp.287-291.

[90]. Rajput, R. and Mishra, A.P., 2012. A review on biological activity of quinazolinones. *International Journal of Pharmaceutical Sciences*, *4*(2), pp.66-70.

[91]. Raffa, D., Daidone, G., Maggio, B., Cascioferro, S., Plescia, F. and Schillaci, D., 2004. Synthesis and antileukemic activity of new 3-(5-methylisoxazol-3-yl) and 3-(pyrimidin-2-yl)-2-styrylquinazolin-4 (3H)-ones. *Il Farmaco*, *59*(6), pp.451-455.

[92]. Patel, N.B. and Patel, J.C., 2011. Synthesis and antimicrobial activity of Schiff bases and 2-azetidinones derived from quinazolin-4 (3H)-one. *Arabian Journal of Chemistry*, *4*(4), pp.403-411.

[93]. Cakici, M., Catir, M., Karabuga, S., Kilic, H., Ulukanli, S., Gulluce, M. and Orhan, F., 2010. Synthesis and biological evaluation of (S)-4-aminoquinazoline alcohols. *Tetrahedron: Asymmetry*, *21*(16), pp.2027-2031.

[94]. Sasmal, S., Balaji, G., Reddy, H.R.K., Balasubrahmanyam, D., Srinivas, G., Kyasa, S., Sasmal, P.K., Khanna, I., Talwar, R., Suresh, J. and Jadhav, V.P., 2012. Design and optimization of quinazoline derivatives as melanin concentrating hormone receptor 1 (MCHR1) antagonists. *Bioorganic & Medicinal Chemistry Letters*, *22*(9), pp.3157-3162.

[95]. Lacouture, M.E., 2006. Mechanisms of cutaneous toxicities to EGFR inhibitors. *Nature Reviews Cancer*, *6*(10), p.803.

[96]. Chandregowda, V., Kush, A.K. and Reddy, G.C., 2009. Synthesis and in vitro antitumor activities of novel 4-anilinoquinazoline derivatives. *European Journal of Medicinal Chemistry*, *44*(7), pp.3046-3055.

[97]. Li, H.Q., Li, D.D., Lu, X., Xu, Y.Y. and Zhu, H.L., 2012. Design and synthesis of 4, 6-substituted-(diaphenylamino) quinazolines as potent EGFR inhibitors with antitumor activity. *Bioorganic & Medicinal Chemistry*, *20*(1), pp.317-323.

[98]. Fernandes, C., Oliveira, C., Gano, L., Bourkoula, A., Pirmettis, I. and Santos, I., 2007. Radioiodination of new EGFR inhibitors as potential SPECT agents for molecular imaging of breast cancer. *Bioorganic & Medicinal Chemistry*, *15*(12), pp.3974-3980.

[99]. Shepherd, F.A., Rodrigues Pereira, J., Ciuleanu, T., Tan, E.H., Hirsh, V., Thongprasert, S., Campos, D., Maoleekoonpiroj, S., Smylie, M., Martins, R. and van Kooten, M., 2005. Erlotinib in previously treated non–small-cell lung cancer. *New England Journal of Medicine*, *353*(2), pp.123-132.

[100]. Paez, J.G., Jänne, P.A., Lee, J.C., Tracy, S., Greulich, H., Gabriel, S., Herman, P., Kaye, F.J., Lindeman, N., Boggon, T.J. and Naoki, K., 2004. EGFR mutations in

lung cancer: correlation with clinical response to gefitinib therapy. *Science*, *304*(5676), pp.1497-1500.

[101]. Wells Jr, S.A., Robinson, B.G., Gagel, R.F., Dralle, H., Fagin, J.A., Santoro, M., Baudin, E., Elisei, R., Jarzab, B., Vasselli, J.R. and Read, J., 2012. Vandetanib in patients with locally advanced or metastatic medullary thyroid cancer: a randomized, double-blind phase III trial. *Journal of Clinical Oncology*, *30*(2), p.134.

[102]. Deshidi, R., Devari, S. and Shah, B.A., 2015. Iodine-Promoted Oxidative Amidation of Terminal Alkenes–Synthesis of α-Ketoamides, Benzothiazoles, and Quinazolines. *European Journal of Organic Chemistry*, *2015*(7), pp.1428-1432.

[103]. Ozaki, K.I., Yamada, Y., Oine, T., Ishizuka, T. and Iwasawa, Y., 1985. Studies on 4 (1H)-quinazolinones. 5. Synthesis and antiinflammatory activity of 4 (1H)-quinazolinone derivatives. *Journal of Medicinal Chemistry*, *28*(5), pp.568-576.

[104]. Rosowsky, A. and Modest, E.J., 1966. Quinazolines. III. Synthesis of 1, 3-Diaminobenzo [f] quinazoline and Related Compounds1-3. *The Journal of Organic Chemistry*, *31*(8), pp.2607-2613.

[105]. Tajbakhsh, M., Hosseinzadeh, R., Rezaee, P. and Tajbakhsh, M., 2014. H3PW12O40 catalyzed synthesis of benzoxazine and quinazoline in aqueous media. *Chinese Journal of Catalysis*, *35*(1), pp.58-65.

[106]. Yu, Z.Y., Chen, M.Y., He, J.X., Tao, D.J., Yuan, J.J., Peng, Y.Y. and Song, Z.B., 2017. Controllable Brønsted acid-promoted aerobic oxidation via solvation-induced proton transfer: metal-free construction of quinazolinones and dihydroquinazolinones. *Molecular Catalysis*, *434*, pp.134-139.

[107]. Simon, M.O. and Li, C.J., 2012. Green chemistry oriented organic synthesis in water. *Chemical Society Reviews*, *41*(4), pp.1415-1427.

[108]. Wang, M., Gao, J.J., Song, Z.G. and Wang, L., 2011. Cerium (IV) ammonium nitrate catalyzed green synthesis of 2-substituted 2, 3-dihydro-quinazolin-4 (1H)-ones using a grinding technique. *Chemistry of Heterocyclic Compounds*, *47*(7), pp.851-855.

[109]. Ghiviriga, I., El-Gendy, B.E.D.M., Steel, P.J. and Katritzky, A.R., 2009. Tautomerism of guanidines studied by 15N NMR: 2-hydrazono-3-phenylquinazolin-4

(3 H)-ones and related compounds. *Organic & Biomolecular Chemistry*, *7*(19), pp.4110-4119.

[110]. Mayer, J.P., Lewis, G.S., Curtis, M.J. and Zhang, J., 1997. Solid phase synthesis of quinazolinones. *Tetrahedron Letters*, *38*(49), pp.8445-8448.

[111]. Chakrabarty, M., Batabyal, A., Morales-Ríos, M.S. and Joseph-Nathan, P., 1995. NMR studies of 4 (3H)-quinazolinones and 4 (3H)-quinazolinethiones. *Monatshefte für Chemie/Chemical Monthly*, *126*(6-7), pp.789-794.

[112]. Mahdavi, M., Foroughi, N., Saeedi, M., Karimi, M., Alinezhad, H., Foroumadi, A., Shafiee, A. and Akbarzadeh, T., 2014. Letter Synthesis of Novel Benzo [6, 7][1, 4] oxazepino [4, 5-a] quinazolinone Derivatives via Transition-Metal-Free Intramolecular Hydroamination. *Synthetic Letters*, *25*, pp.0385-0388.

[113]. Cheng, R., Tang, L., Guo, T., Zhang-Negrerie, D., Du, Y. and Zhao, K., 2014. Oxidant-and metal-free synthesis of 4 (3 H)-quinazolinones from 2-amino-N-methoxybenzamides and aldehydes via acid-promoted cyclocondensation and elimination. *RSC Advances*, *4*(50), pp.26434-26438.

[114]. Han, B., Yang, X.L., Wang, C., Bai, Y.W., Pan, T.C., Chen, X. and Yu, W., 2011. CuCl/DABCO/4-HO-TEMPO-Catalyzed Aerobic Oxidative Synthesis of 2-Substituted Quinazolines and 4 H-3, 1-Benzoxazines. *The Journal of Organic Chemistry*, *77*(2), pp.1136-1142.

[115]. McGowan, M.A., McAvoy, C.Z. and Buchwald, S.L., 2012. Palladium-catalyzed N-monoarylation of amidines and a one-pot synthesis of quinazoline derivatives. *Organic Letters*, *14*(14), pp.3800-3803.

[116]. Romero, A.H., Salazar, J. and López, S.E., 2013. A Simple One-Pot Synthesis of 2-Substituted Quinazolin-4 (3H)-ones from 2-Nitrobenzamides by Using Sodium Dithionite. *Synthesis*, *45*(14), pp.2043-2050.

[117]. Parua, S., Das, S., Sikari, R., Sinha, S. and Paul, N.D., 2017. One-Pot Cascade Synthesis of Quinazolin-4 (3 H)-ones via Nickel-Catalyzed Dehydrogenative Coupling of o-Aminobenzamides with Alcohols. *The Journal of Organic Chemistry*, *82*(14), pp.7165-7175.

[118]. Fang, J. and Zhou, J., 2012. Efficient syntheses of 2, 3-disubstituted natural quinazolinones via iridium catalysis. *Organic & Biomolecular Chemistry*, *10*(12), pp.2389-2391.

[119]. Musiol, R., Jampilek, J., Pesko, M., Kralova, K., Kowalczyk, W., Finster, J. and Polanski, J., 2011, October. Preparation and Herbicidal Properties of Ring-Substituted 4-Chloro-2-styrylquinazolines. In *15th International Electron Conference of Synthetic Organic Chemistry,* (Vol. 15). MDPI.

[120]. Micale, N., Postorino, G., Grasso, S., Zappala, M., Zuccala, G., Ferreri, G. and De Sarro, G., 2006. Synthesis of Novel 3-(Alkylcarbamoyl)-2-aryl-1, 2-dihydro-6, 7-(methylenedioxy)-3H-quinazolin-4-ones as Anticonvulsant Agents. *Chemistry & biodiversity*, *3*(3), pp.304-311.

[121]. Kantin, G. and Krasavin, M., 2016. N-Arylation of Amidines and Guanidines: An Update. *Current Organic Chemistry*, *20*(13), pp.1370-1388.

[122]. Mphahlele, M.J., Paumo, H.K., El-Nahas, A.M. and El-Hendawy, M.M., 2014. Synthesis and photophysical property studies of the 2, 6, 8-triaryl-4-(phenylethynyl) quinazolines. *Molecules*, *19*(1), pp.795-818.

[123]. Kieffer, C., Verhaeghe, P., Primas, N., Castera-Ducros, C., Gellis, A., Rosas, R., Rault, S., Rathelot, P. and Vanelle, P., 2013. Sonogashira cross-coupling reaction in 4-chloro-2-trichloromethylquinazoline series is possible despite a side dimerization reaction. *Tetrahedron*, *69*(14), pp.2987-2995.

[124]. Mirallai, S.I., Manos, M.J. and Koutentis, P.A., 2013. One-Step Conversion of 2-Amino-N′-arylbenzamidines into 3-Aryl-4-imino-3, 4-dihydroquinazoline-2-carbonitriles Using 4, 5-Dichloro-1, 2, 3-dithiazolium Chloride. *The Journal of Organic Chemistry*, *78*(19), pp.9906-9913.

[125]. Panja, S.K. and Saha, S., 2013. Recyclable, magnetic ionic liquid bmim [FeCl 4]-catalyzed, multicomponent, solvent-free, green synthesis of quinazolines. *RSC Advances*, *3*(34), pp.14495-14500.

[126]. Yao, T., Zhang, X. and Larock, R.C., 2004. AuCl3-catalyzed synthesis of highly substituted furans from 2-(1-alkynyl)-2-alken-1-ones. *Journal of the American Chemical Society*, *126*(36), pp.11164-11165.

[127]. Milne, J.E. and Buchwald, S.L., 2004. An extremely active catalyst for the Negishi cross-coupling reaction. *Journal of the American Chemical Society*, *126*(40), pp.13028-13032.

[128]. Li, J.H., Liang, Y., Wang, D.P., Liu, W.J., Xie, Y.X. and Yin, D.L., 2005. Efficient Stille cross-coupling reaction catalyzed by the Pd $(OAc)_2$/Dabco catalytic system. *The Journal of Organic Chemistry*, *70*(7), pp.2832-2834.

[129]. Fuwa, H., Ebine, M. and Sasaki, M., 2011. Recent Applications of the Suzuki-Miyaura Cross-coupling to Complex Polycyclic Ether Synthesis. *Journal of Synthetic Organic Chemistry, Japan*, *69*(11), pp.1251-1262.

[130]. Sonogashira, K., 1998. Cross-coupling reactions to sp carbon atoms. *Metal-Catalyzed Cross-Coupling Reactions*, pp.203-229.

[131]. Chinchilla, R. and Nájera, C., 2007. The Sonogashira reaction: a booming methodology in synthetic organic chemistry. *Chemical Reviews*, *107*(3), pp.874-922.

[132]. Langille, N.F., Dakin, L.A. and Panek, J.S., 2002. Sonogashira coupling of functionalized trifloyl oxazoles and thiazoles with terminal alkynes: synthesis of disubstituted heterocycles. *Organic letters*, *4*(15), pp.2485-2488.

[133]. Mangalagiu, I., Benneche, T. and Undheim, K., 1996. Ethenylation and alkynylation in palladium-catalyzed carbosubstitution in heteroazines. *Acta Chemica Scandinavica*, *50*, pp.914-917.

[134]. Armarego, W.L.F., 1963. Quinazolines. In *Advances in heterocyclic chemistry* (Vol. 1, pp. 253-309). Academic Press.

[135]. Paumo, H.K., Makhafola, T.J. and Mphahlele, M.J., 2016. Synthesis and in vitro cytotoxic properties of polycarbo-substituted 4-(arylamino) quinazolines. *Molecules*, *21*(10), p.1366.

[136]. Kaim, W. and Schwederski, B., 2010. Non-innocent ligands in bioinorganic chemistry—An overview. *Coordination Chemistry Reviews*, *254*(13-14), pp.1580-1588.

[137]. Müller, A., Diemann, E., Jostes, R. and Bögge, H., 1981. Transition metal thiometalates: properties and significance in complex and bioinorganic chemistry. *Angewandte Chemie International Edition in English*, *20*(11), pp.934-955.

[138]. van Rijt, S.H. and Sadler, P.J., 2009. Current applications and future potential for bioinorganic chemistry in the development of anticancer drugs. *Drug Discovery Today*, *14*(23-24), pp.1089-1097.

[139]. Arba, M., Ihsan, S. and Tjahjono, D.H., 2017. In silico study of porphyrin-anthraquinone hybrids as CDK2 inhibitor. *Computational Biology and Chemistry*, *67*, pp.9-14.

[140]. Glišić, B.Đ., Senerovic, L., Comba, P., Wadepohl, H., Veselinovic, A., Milivojevic, D.R., Djuran, M.I. and Nikodinovic-Runic, J., 2016. Silver (I) complexes with phthalazine and quinazoline as effective agents against pathogenic Pseudomonas aeruginosa strains. *Journal of Inorganic Biochemistry*, *155*, pp.115-128.

[141]. Khamrang, T., Hung, K.C., Hsia, C.H., Hsieh, C.Y., Velusamy, M., Jayakumar, T. and Sheu, J.R., 2017. Antiplatelet activity of a newly synthesized novel ruthenium (II): A potential role for Akt/JNK signaling. *International Journal of Molecular sciences*, *18*(5), p.916.

[142]. Lin, Z., Liu, T., Kamp, D.W., Wang, Y., He, H., Zhou, X., Li, D., Yang, L., Zhao, B. and Liu, G., 2014. AKT/mTOR and c-jun N-terminal kinase signaling pathways are required for chrysotile asbestos-induced autophagy. *Free Radical Biology and Medicine*, *72*, pp.296-307.

[143]. Yang, Z.J., Chee, C.E., Huang, S. and Sinicrope, F.A., 2011. The role of autophagy in cancer: therapeutic implications. *Molecular cancer therapeutics*, *10*(9), pp.1533-1541.

[144]. Zhang, Y., Zheng, W., Luo, Q., Zhao, Y., Zhang, E., Liu, S. and Wang, F., 2015. Dual-targeting organometallic ruthenium (II) anticancer complexes bearing EGFR-inhibiting 4-anilinoquinazoline ligands. *Dalton Transactions*, *44*(29), pp.13100-13111.

[145]. Nadendla, R.R., 2004. Molecular modeling: A powerful tool for drug design and molecular docking. *Resonance*, *9*(5), pp.51-60.

[146]. Zhang, J.H., Chung, T.D. and Oldenburg, K.R., 1999. A simple statistical parameter for use in evaluation and validation of high throughput screening assays. *Journal of Biomolecular Screening*, *4*(2), pp.67-73.

[147]. Adams, C.P. and Brantner, V.V., 2006. Estimating the cost of new drug development: is it really $802 million?. *Health affairs*, *25*(2), pp.420-428.

[148]. Hughes, J.P., Rees, S., Kalindjian, S.B. and Philpott, K.L., 2011. Principles of early drug discovery. *British Journal of Pharmacology*, *162*(6), pp.1239-1249.

[149]. Lipinski, C.A., Lombardo, F., Dominy, B.W. and Feeney, P.J., 1997. Experimental and computational approaches to estimate solubility and permeability in drug discovery and development settings. *Advanced Drug Delivery Reviews*, *23*(1-3), pp.3-25.

[150]. Berman, H.M., Westbrook, J., Feng, Z., Gilliland, G., Bhat, T.N., Weissig, H., Shindyalov, I.N. and Bourne, P.E., 2000. The protein data bank. *Nucleic Acids Research*, *28*(1), pp.235-242.

[151]. Weigelt, J., 2010. Structural genomics—impact on biomedicine and drug discovery. *Experimental Cell Research*, *316*(8), pp.1332-1338.

[152]. Salum, L.B., Polikarpov, I. and Andricopulo, A.D., 2008. Structure-based approach for the study of estrogen receptor binding affinity and subtype selectivity. *Journal of Chemical Information and Modeling*, *48*(11), pp.2243-2253.

[153]. Kalyaanamoorthy, S. and Chen, Y.P.P., 2011. Structure-based drug design to augment hit discovery. *Drug Discovery Today*, *16*(17-18), pp.831-839.

[154]. Acharya, C., Coop, A., E Polli, J. and D MacKerell, A., 2011. Recent advances in ligand-based drug design: relevance and utility of the conformationally sampled pharmacophore approach. *Current Computer-aided Drug Design*, *7*(1), pp.10-22.

[155]. Bacilieri, M. and Moro, S., 2006. Ligand-based drug design methodologies in drug discovery process: an overview. *Current Drug Discovery Technologies*, *3*(3), pp.155-165.

[156]. Drwal, M.N. and Griffith, R., 2013. Combination of ligand-and structure-based methods in virtual screening. *Drug Discovery Today: Technologies*, *10*(3), pp.e395-e401

[157]. Trossini, G.H., Guido, R.V., Oliva, G., Ferreira, E.I. and Andricopulo, A.D., 2009. Quantitative structure–activity relationships for a series of inhibitors of cruzain from

Trypanosoma cruzi: Molecular modeling, CoMFA and CoMSIA studies. *Journal of Molecular Graphics and Modelling*, *28*(1), pp.3-11.

[158]. Valasani, K.R., Vangavaragu, J.R., Day, V.W. and Yan, S.S., 2014. Structure based design, synthesis, pharmacophore modeling, virtual screening, and molecular docking studies for identification of novel cyclophilin D inhibitors. *Journal of Chemical Information and Modeling*, *54*(3), pp.902-912.

[159]. Lindstedt, I., Edvinsson, L., Lindberg, A.L., Olsson, M., Dahlgren, C. and Edvinsson, M.L., 2018. Increased All-cause Mortality, Total Cardiovascular Disease and Morbidity in Hospitalized Elderly Patients with Orthostatic Hypotension. *Archives of General Internal Medicine*, *2*(1), pp. 1-5.

[160]. World Health Organisation. *Global Tuberculosis Report* 2017, Geneva: World Health Organization; 2017. Licence: CC BY-NCSA.

[161]. Menzies, D., Adjobimey, M., Ruslami, R., Trajman, A., Sow, O., Kim, H., Obeng Baah, J., Marks, G.B., Long, R., Hoeppner, V. and Elwood, K., 2018. Four months of rifampin or nine months of isoniazid for latent tuberculosis in adults. *New England Journal of Medicine*, *379*(5), pp.440-453.

[162]. Pontali, E., Sotgiu, G., Tiberi, S., Tadolini, M., Visca, D., D'Ambrosio, L., Centis, R., Spanevello, A. and Migliori, G.B., 2018. Combined treatment of drug-resistant tuberculosis with bedaquiline and delamanid: a systematic review. *European Respiratory Journal*, p.1800934.

[163]. World Health Organisation.,published, 12 September 2018., *cancer*.,accessed 26 October 2018., {www.who.int}.

[164]. Ormel, H.L., van der Schoot, G.G.F., Sluiter, W.J., Jalving, M., Gietema, J.A. and Walenkamp, A.M.E., 2018. Predictors of adherence to exercise interventions during and after cancer treatment: a systematic review. *Psycho‐oncology*, *27*(3), pp.713-724.

[165]. Jiang, P., Sellers, W.R. and Liu, X.S., 2018. Big Data Approaches for Modeling Response and Resistance to Cancer Drugs. *Annual Review of Biomedical Data Science*, *1*, pp.1-27.

[166]. Agha, L. and Molitor, D., 2018. The local influence of pioneer investigators on technology adoption: evidence from new cancer drugs. *Review of Economics and Statistics*, *100*(1), pp.29-44.

CHAPTER 3: EXPERIMENTAL

3.1 General

Chemical reagents were purchased from Sigma-Aldrich or Merck (Johannesburg, South Africa) and used without further purification. Tetrahydrofuran (THF) was distilled over sodium metal lumps and benzophenone [1] and stored over activated molecular sieves before use. Melting points were obtained using Lasec/SA-melting point apparatus from Lasec company, SA (Johannesburg, South Africa). IR spectra for comppunds 120a-e, **121a-e**, **123a-e**, **125a-e** and **126a-e** were recorded using Anglient technologies Carry 600 series, FTIR spectrometer. For compounds **119a-d**, the FTIR spectra were recorded on Bruker, FTIR spectrometer with a platinum ATR. NMR spectra were obtained as $CDCl_3$, DMSO-d_6 and Methanol-d_4 solutions using Bruker 400 MHz NMR spectrometer (Bruker Biospin GmhH, Karlsrushe, Germany) operating at 400 MHz (^{1}H) and 100 MHz (^{13}C), and ^{1}H-^{13}C-HMBC NMR chemical shifts were quoted relative to the TMS peak. High-resolution mass spectra were recorded at an ionisation potential of 70 eV using Waters Synapt G2 Quadrupole Time-of-flight mass spectrometer (Waters Corp., Milford, MA, USA) at the University of Stellenbosch Central Analytical Facility. The synthesis of ligands **125a-e**, **119a-d** and attempted synthesis of **119c**** was performed under nitrogen atmosphere purchased from Afrox (Polokwane gas and gear) and used without further purification.

3.2 Typical procedure for the synthesis of Schiff base ligands 119a-d

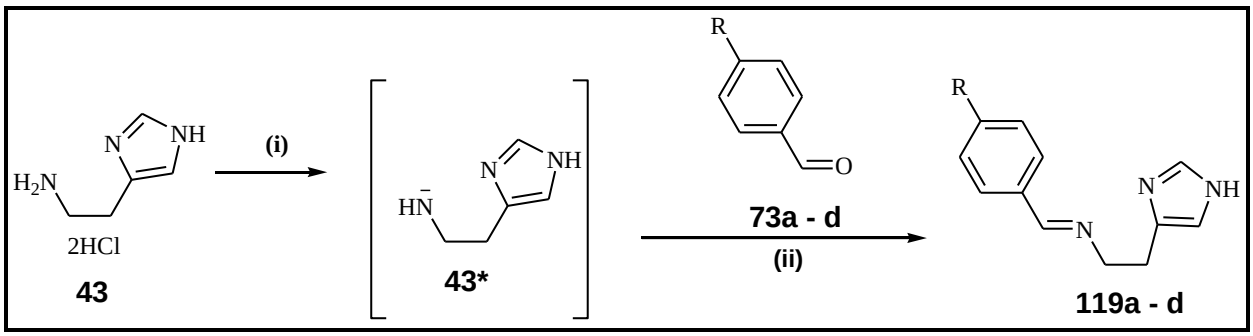

R = -H (**119a**), -OH (**119b**), -F (**119c**) and –NO_2 (**119d**)

To a 50 mL Schlenk flask equipped with a stirrer bar, was added 2.5 mmol histamine dihydrochloride and 5 mmol sodium hydroxide. The mixture was stirred for 1.5 h at

room temperature in 15 mL methanol to obtain a sodium chloride precipitate which was filtered through a syringe plugged with cotton wool. The filtrate was taken into a 250 mL Schlenk flask charged with 15 mL methanol and 2.5 mmol aldehyde. The mixture was stirred for 5 minutes before the addition of 2.5 mmol sodium hydrogen carbonate, the flask was then purged with nitrogen gas for 2 minutes before stirring at room temperature for 24 h after which stirring was stopped and allowed to cool to room temperature. The solvent was removed under reduced pressure to obtain a paste of colours white, brown and yellow. The paste was washed thoroughly with hexane and diethyl ether to acquire the corresponding Schiff bases **119a**-**d**.

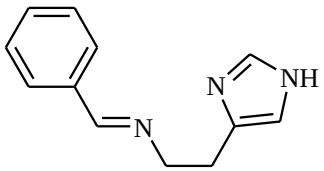

119a

3.2.1 *(E)-N-benzylidene-2-(1H-imidazol-4-yl)ethanamine* (**119a**). A mixture of histamine dihydrochloride **43** (460.1675 mg, 2.5 mmol), benzaldehyde **73a** (265.30 mg, 2.50 mmol), sodium hydroxide (199.99 mg, 5.00 mmol) and sodium hydrogen carbonate (210.02 mg, 2.50 mmol) in methanol 30 mL afforded **119a** as white solid (275.21 mg, 92%); m.p. 247.4 – 248.6 ^{o}C; FTIR(ν_{max}) 598, 763, 824, 1089, 1162, 1251, 1354, 1537, 1627, 2450, 3394 cm^{-1}; ^{1}H-NMR (400 MHz, MeOD-d_4, ppm) 2.99 (t, J = 14.23 Hz, 2H), 3.87 – 3.90 (td, $^{3}J_{H\text{-}H}$ = 12 Hz and $^{4}J_{H\text{-}H}$ = 1.12 Hz, 2H), 6.82 (s, 1H), 7.44 – 7.48 (m, 3H), 7.60 (s, 1H), 7.71 – 7.73 (dd, J = 1.69 Hz and J = 1.71 Hz, 2H), 8.24 (s, 1H); ^{13}C-NMR (100 MHz, MeOD-d_4, ppm) 29.3, 61.8, 118.5, 129.9, 130.9, 132.3, 136.1, 137.1, 161.6, 165.0; HRMS (ESI): calculated 119.1109, $[MH]^{+}$, $C_{12}H_{13}N_3^{+}$, found 200.1180.

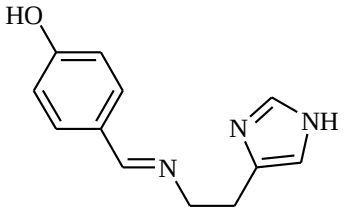

119b

3.2.2 *4-((E)-(2-(1H-imidazol-4-yl)ethylimino)methyl)phenol* (**119b**). A mixture of histamine dihydrochloride **43** (460.17 mg, 2.50 mmol), 4-hydroxybenzaldehyde (**73b**)

(305.30 mg, 2.50 mmol), sodium hydroxide (199.99 mg, 5.00 mmol) and sodium hydrogen carbonate (210.02 mg, 2.50 mmol) in methanol 30 mL afforded **119b** as brown solid (481.87 mg, 90%); m.p. 262.5 – 263.1 ^{o}C; FTIR(ν_{max}) 599, 720, 834, 1126, 1221, 1257, 1358, 1537, 1668, 2948, 3327, 3928 cm^{-1}; ^{1}H-NMR (400 MHz, MeOD-d_4, ppm) 2.95 (t, J = 14.4 Hz, 2H), 3.80 (t, J = 14 Hz, 2H), 6.75 (d, J = 8.66 Hz, 2H), 6.81 (s, 1H), 7.52 (d, J = 8.63 Hz, 2H), 7.60 (s, 1H), 8.05 (s, 1H); ^{13}C-NMR (100 MHz, MeOD-d_4, ppm) 29.7, 61.5, 118.8, 120.3, 122.7, 131.6, 136, 161.6, 165.9, 173.0; HRMS (ESI): calculated 215.1059, [MH]$^{+}$, $C_{12}H_{13}N_3O^{+}$, found 216.1126.

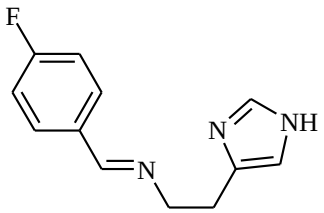

119c

3.2.3 *(E)-N-(4-fluorobenzylidene)-2-(1H-imidazol-4-yl)ethanamine* (**119c**). A mixture of histamine dihydrochloride **43** (460.1675 mg, 2.5 mmol), 4-fluorobenzaldehyde (**73c**) (310.29 mg, 2.5 mmol), sodium hydroxide (199.99 mg, 5.00 mmol) and sodium hydrogen carbonate (210.02 mg, 2.50 mmol) in methanol 30 mL afforded **119c** as white solid (488.56, 90%); m.p. 284.9 – 286.1 ^{o}C; FTIR(ν_{max}) 598, 822, 895, 1088, 1126, 1254, 1362, 1624, 2951, 3340 cm^{-1}; ^{1}H-NMR (400 MHz, MeOD-d_4, ppm) 2.98 (t, J = 14.30 Hz, 2H), 3.86 – 3.89 (td, $^{3}J_{H\text{-}H}$ = 12 Hz and $^{4}J_{H\text{-}H}$ = 0.88 Hz), 6.82 (s, 1H), 7.16 – 7.20 (m, 2H), 7.59 (s, 1H), 7.60-7.89 (dd, $^{3}J_{HF}$ = 5.60 Hz and $^{3}J_{HF}$ = 5.54 Hz, 2H), 8.23 (s, 1H); ^{13}C-NMR (100 MHz, MeOD-d_4, ppm) 29.3, 61.8, 115.4 ($^{2}J_{CF}$ = 22.2 Hz), 118.5, 131.6 ($^{3}J_{CF}$ = 8.6 Hz), 130.1 ($^{3}J_{CF}$ = 9 Hz), 133.7 ($^{4}J_{CF}$ = 2.9 Hz), 136.1, 161.6, 163.5, 166.0 (d, $^{1}J_{CF}$ = 250 Hz); HRMS (ESI): calculated 217.1015, [MH]$^{+}$, $C_{12}H_{12}FN_3^{+}$, found 218.1078.

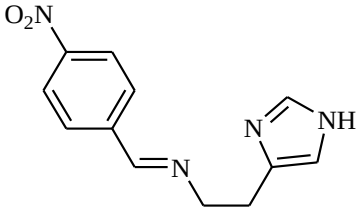

119d

3.2.4 *(E)-N-(4-nitrobenzylidene)-2-(1H-imidazol-4-yl)ethanamine* (**119d**). A mixture of histamine dihydrochloride **43** (460.17 mg, 2.50 mmol), 4-nitrobenzaldehyde (**73d**)

(377.80 mg, 2.50 mmol), sodium hydroxide (199.99 mg, 5.00 mmol) and sodium hydrogen carbonate (210.02 mg, 2.50 mmol) in methanol 30 mL afforded **119d** as yellow solid (594.17, 90%); m.p. 266.2 – 267.4 ^{o}C; FTIR(ν_{max}) 599, 761, 824, 1090, 1121, 1207, 1365, 1537, 1628. 2949, 3348 (-NH) cm^{-1}; ^{1}H-NMR (400 MHz, MeOD-d_4, ppm) 3.016 (t, 14.13 Hz, 2H), 3.94-3.98 (td, $^{3}J_{H\text{-}H}$ = 16 and $^{4}J_{H\text{-}H}$ = 1.25 Hz, 2H), 6.84 (s, 1H), 7.60 (d, ^{4}J = 1.12 Hz, 1H), 7.96-7.98 (dd, J = 2 Hz and J = 2 Hz, 2H), 8.30-8.33 (dd, J = 2 Hz and J = 1.6 Hz, 2H), 8.38 (s, 1H); ^{13}C-NMR (100 MHz, MeOD-d_4, ppm) 29.3, 62.2, 118.4, 125.0, 130.3, 131.1, 143.0, 150.7, 161.6, 162.3; HRMS (ESI): calculated 244.096, $[MH]^{+}$, $C_{12}H_{12}N_4O_2^{+}$, found 245.1031.

3.3 Attempted synthesis of Zn(II) ethanamineimidazolyl-Schiff base complexes

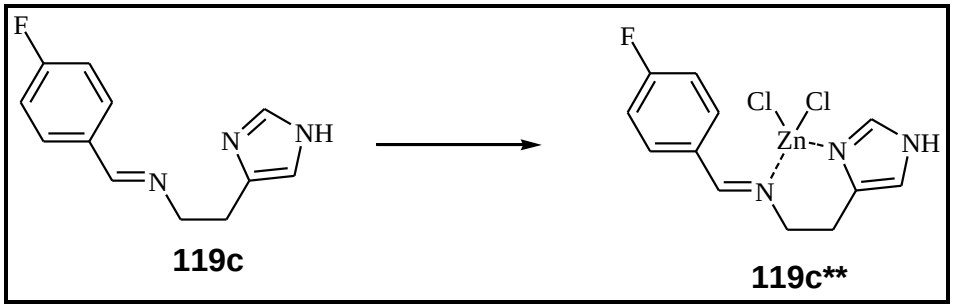

Into an NMR tube was added, (1.00 mg**,** 0.0001 mmol) of **119c** and (0.63 mg, 0.0001 mmol) of $ZnCl_2$. The mixture was left to stand at room temperature for 24 h in 0.6 mL of MeOD-d_4. The ^{1}H-NMR was recorded at (400 MHz, ppm) 2.90 (br-s, 2H), 4.04 (br-s, 2H), 6.85 (br-s, 1H), 2.25 (m, 2H), 7.55(br-s, 1H), 8.12 (d, J = 3.72 Hz, 2H), 8.70 (br-s, 1H).

N.B Compounds **120a-e** are reported inliterature and referenced thereof.

3.4 General synthesis of 2-arylquinazoline-4-one derivatives 120a – e

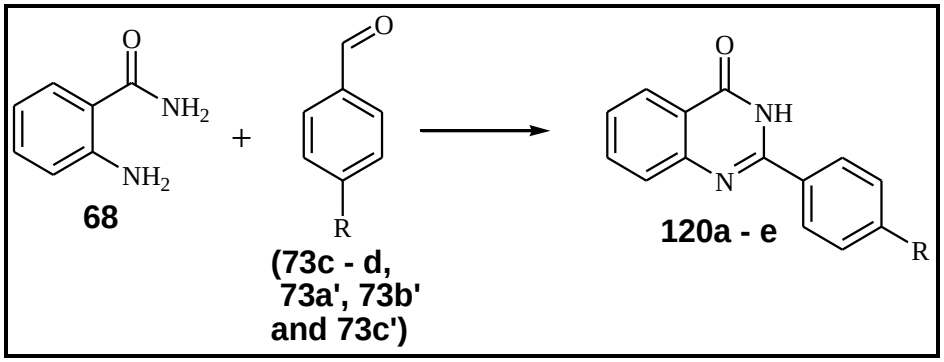

R = -Cl (**120a**), -Br (**120b**), -F (**120c**), -NO_2 (**120d**), -OMe (**120e**)

Quinazoline derivatives were prepared following a literature method reported by Mphahlele and co-workers [2]. To a 100 mL round bottom flask, anthranilamide **68** (1 mmol), benzaldehyde derivatives (**73c – d, 73a', 73b' and 73c'**) (1 mmol) and iodine (2 equiv.) in ethanol (30 mL per mmol of **68**) was refluxed at 80 ^{o}C for 6 h. The mixture was left to cool to room temperature and quenched with cold saturated sodium metabisulfate solution. The resulting precipitate was filtered and washed thoroughly with water. The solid product was recrystalised from acetonitrile and oven dried to yield the corresponding quinazoline-4(3H)-ones **120a - e**. The following products were prepared accordingly:

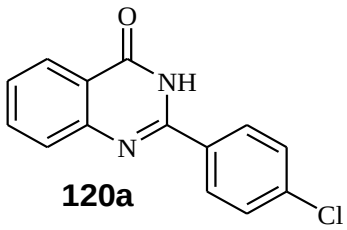

120a

3.4.1 *2-(4-Chlorophenyl)quinazolin-4(3H)-one* (**120a**): A mixture of **68** (1500.00 mg, 11.02 mmol), benzaldehyde (**73a'**) (1550.00 mg, 11.02 mmol) and iodine (2.80 g, 22.04 mmol) in ethanol (100 mL) yielded **120a** as a white solid (2450.00 mg, 87%); m.p. 295.2 – 297.1 ^{o}C, lit (298 – 299 ^{o}C) [3]; FTIR(ν_{max}) 764, 840, 1168, 1232, 1259, 1531, 1606, 1666, 3052, 3174 cm^{-1}; ^{1}H-NMR (400 MHz, DMSO-d$_6$, ppm) 7.53 (t, *J* = 14.4 Hz, 1H), 7.73 – 7.77 (m, 3H), 7.84 (t, *J* = 14.4 Hz, 1H), 8.12-8.19 (m, 3H), 12.63 (s, 1H); ^{13}C-NMR (100 MHz, DMSO-*d$_6$*, ppm) 121.0, 125.2, 125.9, 126.8, 127.4, 129.8, 131.6, 131.9, 134.6, 148.5, 151.5, 162.2.

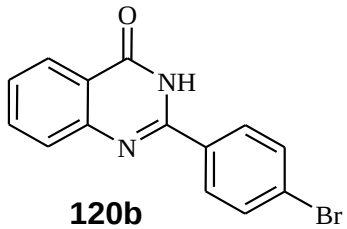

120b

3.4.2 *2-(4-Bromophenyl)quinazolin-4(3H)-one* (**120b**): A mixture of **68** (1500.00 mg, 11.02 mmol), benzaldehyde (**73b'**) (2000.00 mg, 11.02 mmol) and iodine (2800.00 mg, 22.04 mmol) in ethanol (100 mL) yielded **120b** as a white solid (3001.00 mg, 91%); m.p. >350 ^{o}C, lit (>350 ^{o}C) [3]; FTIR(ν_{max}) 766, 840, 1232, 1369, 1486, 1610, 1544, 1656, 3064, 3186 cm^{-1}; ^{1}H-NMR (400 MHz, DMSO-d$_6$, ppm) 7.53 (t, *J* = 14.8 Hz, 1H), 7.63 (d, *J* = 8.4 Hz, 2H), 7.74 (d, *J* = 8 Hz, 1H), 7.84 (t, *J* = 14.8 Hz, 1H) 8.15 (d, *J* = 8

Hz, 1H), 8.20 (d, *J* = 8.4 Hz, 2H) 12.63 (s, 1H); ^{13}C-NMR (100 MHz, DMSO-d_6, ppm) 121.0, 125.9, 126.8, 127.5, 128.7, 129.6, 131.6, 134.7, 136.3, 148.5 151.4, 162.2.

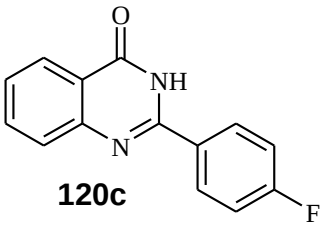

120c

3.4.3 *2-(4-Fluorophenyl)quinazolin-4(3H)-one* (**120c**): A mixture of **68** (1500.00 mg, 11.02 mmol), benzaldehyde (**73c**) (1370.00 mg, 11.02 mmol) and iodine (2800.00 mg, 22.04 mmol) in ethanol (100 mL) yielded **120c** as a white solid (2.46 g, 93%); m.p. 261.3 – 263.2 ^{o}C, lit (257 – 259 ^{o}C) [3]; FTIR(ν_{max}) 764, 840, 1166, 1305, 1484, 1555, 1605, 1668, 3098, 3204 cm^{-1}; ^{1}H-NMR (400 MHz, DMSO-d$_6$, ppm) 7.24-7.35 (m, 3H), 7.71-7.77 (m, 2H), 8.09-8.15 (m, 3H), 12.58 (s, 1H) ; ^{13}C-NMR (100 MHz, DMSO-d_6, ppm) 115.4 (d, $^{2}J_{CF}$ = 22.2 Hz), 120.9, 125.9, 126.5, 128.9 (d, $^{4}J_{CF}$ = 2.9 Hz), 129.5, 130.1 (d, $^{3}J_{CF}$ = 9 Hz), 134.6, 148.7, 151.7, 163.8 (d, $^{1}J_{CF}$ = 249.2 Hz).

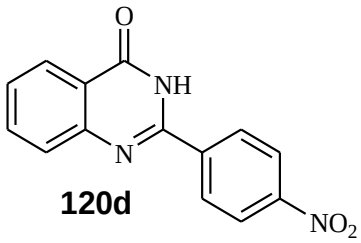

120d

3.4.4 *2-(4-Nitrophenyl)quinazolin-4(3H)-one* (**120d**): A mixture of **68** (1500.00 mg, 11.02 mmol), benzaldehyde (**73d**) (1670.00 mg, 11.02 mmol) and iodine (2800.00 mg, 22.04 mmol) in ethanol (100 mL) yielded **120d** as a white solid (2.65 g, 90%); m.p. > 300 ^{o}C, lit (>300 ^{o}C) [3]; FTIR(ν_{max}) 741, 833, 1018, 1261, 1399, 1583, 1601, 1684, 3057, 3200; ^{1}H-NMR (400 MHz, DMSO-d$_6$, ppm) 7.38-7.68 (m, 1H), 7.72-7.51 (m, 2H), 8.21-8.42 (m, 5H), 12.882 (s, 1H); ^{13}C-NMR (100 MHz, DMSO-d_6, ppm) 121.4, 123.3, 123.6, 126.0, 126.8, 127.6, 129.0, 134.3, 134.5, 139.9, 148.8, 152.1.

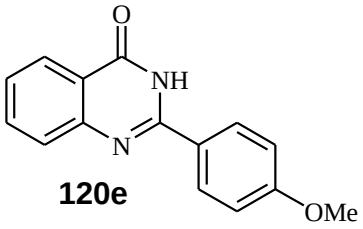

120e

3.4.5 *2-(4-Methoxyphenyl)quinazolin-4(3H)-one* (**120e**): A mixture of **68** (1500.00 mg, 11.02 mmol), benzaldehyde (**73c'**) (1500.00 mg, 11.02 mmol) and iodine (2800.00 mg, 22.04 mmol) in ethanol (100 mL) yielded **120e** as a white solid (2.58 g, 93%); 242.7 – 243.4 ^{o}C, lit (240 – 241 ^{o}C) [3]; FTIR(ν_{max}) 703, 888, 1086, 1380, 1477, 1566, 1691, 1699, 3011, 3247; ^{1}H-NMR (400 MHz, DMSO-d_6, ppm) 3.84 (s, 3H), 7.08 (d, *J* = 14.8 Hz, 2H), 7.48 (t, *J* = 16.0 Hz, 1H), 7.70 (d, *J* = 7.6 Hz, 1H), 7.80 (d, *J* = 16.0 Hz, 1H), 8.19 (d, *J* = 14.8 Hz, 2H), 12.43 (s, 1H); ^{13}C-NMR (100 MHz, DMSO-d_6, ppm) 55.46, 114.0, 120.7, 124.9, 125.8, 126.1, 127.1, 129.5, 134.5, 148.9, 152.0, 161.9, 162.4.

3.5 Oxidative aromatisation of 121a - e in $SOCl_2$-DMF mixture

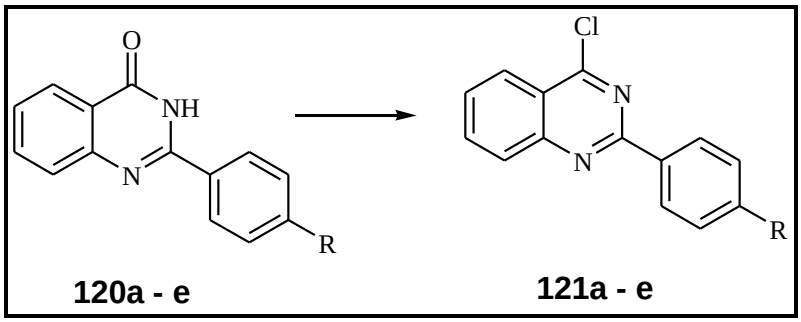

120a - e **121a - e**

R = -Cl (**121a**), -Br (**121b**), -F (**121c**), -NO_2 (**121d**), -OMe (**121e**)

N.B Compounds **121a-e** are reported in literature and referenced thereof.

3.5a Typical procedure for the synthesis of 4-chloro-2-arylquinozaline derivatives (121a- e)

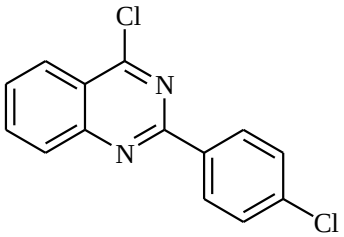

121a

Quinazoline derivatives were prepared following a literature method reported by Mphahlele and co-workers [1]. To a stirring suspension of **120a** (1000.00 mg, 3.90

mmol) in thionyl chloride (30 mL) at room temperature, DMF (1 mL) was added dropwise. The mixture was refluxed for 4 h and allowed to cool to room temperature before quenching with cold water and was extracted with dichloromethane. The dichloromethane was dried over anhydrous sodium sulphate, filtered and evaporated under reduced pressure to yield (The same procedure was applied to afford **120b – e**):

3.5.1 *4-Chloro-2-(4-chlorophenyl)quinazoline* (**121a)** [4] as a white solid (940.00 mg, 88%); m.p. 143.2 – 145.4 ^{o}C; FTIR(ν_{max}) 758, 842, 954, 1152, 1234, 1336, 1519, 1537; ^{1}H-NMR(400 MHz, $CDCl_3$, ppm) 7.47 (d, *J* = 8.8 Hz, 2H), 7.66 (t, *J* = 16. Hz, 1H), 7.92 (t, *J* = 16.4 Hz, 1H), 8.05 (d, *J* = 8 Hz, 1H), 8.23 (d, *J* = 8 Hz, 1H), 8.56 (d, *J* = 8.8 Hz, 2H); ^{13}C-NMR (100 MHz, $CDCl_3$, ppm) 122.4, 125.8, 128.4, 128.9, 130.1, 135.0, 137.4, 143.7, 151.7, 159.0, 162.6.

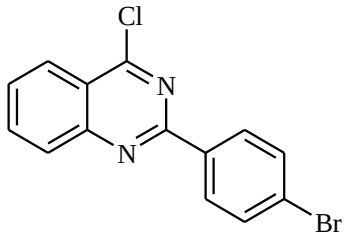

121b

3.5.2 *2-(4-Bromophenyl)-4-chloroquinazoline* (**121b**) [5]. A stirred mixture of **120b** (1000.00 mg, 3.30 mmol) and DMF (1 mL) in thionyl chloride (30 mL) yielded **121b** as a white solid (1130.00 mg, 93%); m.p. 151.7 – 153.4 ^{o}C; FTIR(ν_{max}) 647, 699, 742, 785, 844, 902, 1152, 1264, 1339, 1600; ^{1}H-NMR (400 MHz, $CDCl_3$, ppm) 7.48-7.54 (m, 3H) 7.92 (t, *J* = 16.4 Hz, 1H) 8.05 (d, *J* = 8.4 Hz, 1H), 8.22 (d, *J* = 8.4 Hz, 1H), 8.43 (d, *J* = 8.8 Hz, 2H); ^{13}C-NMR(100 MHz, $CDCl_3$, ppm) 122.4, 125.8, 128.8, 130.0, 131.8, 135.0, 135.5, 137.3, 151.6, 159.0, 162.6.

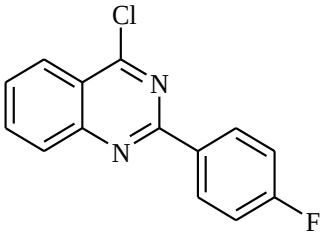

121c

3.5.3 *4-Chloro-2-(4-fluorophenyl)quinazoline* (**121c**) [6]. A stirred mixture of **120c** (1.00 g, 4.18 mmol) and DMF (1 mL) in thionyl chloride (30 mL) yielded **121c** as a white solid (0.97 g, 90%); m.p. 137.2 – 139.3 ^{o}C, lit [139 – 141 ^{o}C]; FTIR(ν_{max}) 655, 688, 726, 760, 844, 933, 1153, 1264, 1510, 1563; ^{1}H-NMR (400 MHz, $CDCl_3$, ppm) 7.11-7.28 (m, 2H), 7.64 (t, *J* = 16.8 Hz, 1H), 7.92 (t, *J* = 16.8 Hz, 1H), 8.05 (d, *J* = 8 Hz, 1H), 8.23 (d, *J* = 8 Hz, 1H), 8.41-8.46 (m, 2H); ^{13}C-NMR (100 MHz, $CDCl_3$, ppm) 115.7 (d, $^{2}J_{CF}$ = 84 Hz), 122.3, 128.2, 128.8, 130.9 (d, $^{3}J_{CF}$ = 8.8 Hz), 132.9 (d, $^{2}J_{CF}$ = 3 Hz), 151.8, 159.0, 162.5, 165.1 (d, $^{1}J_{CF}$ = 248.5 Hz).

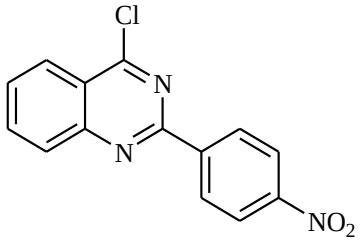

121d

3.5.4 *4-Chloro-2-(4-nitrophenyl)quinazoline* (**121d**) [4]. A stirred mixture of **120d** (1000.00 mg, 3.74 mmol), ν_{max} (ATR) and DMF (1 mL) in thionyl chloride (30 mL) yielded **121d** as a white solid (900 mg, 84%); m.p. 148.1 – 150.2 ^{o}C; FTIR(ν_{max}) 709, 843, 891, 1026, 1248, 1322, 1373, 1509, 1587; ^{1}H-NMR (100 MHz, $CDCl_3$, ppm) 7.74 (t, *J* = 16.8 Hz, 1H), 7.79 (t, *J* = 16.8 Hz, 1H), 8.13 (d, *J* = 8.4 Hz, 1H), 8.29 (d, *J* = 8.4 Hz, 1H), 8.34 (d, *J* = 10.4 Hz, 2H), 8.74 (d, *J* = 10.4 Hz, 2H); ^{13}C-NMR (400 MHz, $CDCl_3$, ppm) 122.7, 123.7, 125.9, 129.5, 129.6, 135.3, 142.3, 144.2, 149.4, 151.6, 157.7, 162.9.

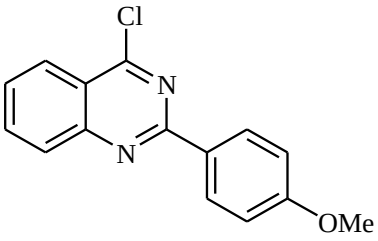

121e

3.5.5 *4-Chloro-2-(4-methoxyphenyl)quinazoline* (**121e**) [7]. A stirred mixture of **120e** (1000 mg, 3.98 mmol) and DMF (1 mL) in thionyl chloride (30 mL) yielded **121e** as a white solid (960 mg, 89%); m.p. 144.3 – 146.6 ^{o}C; FTIR(ν_{max}) 763, 837, 934, 1152,

1290, 1336, 1579, 1603; ^{1}H-NMR (400 MHz, $CDCl_3$, ppm) 3.87 (3H, br-s), 7.08 (d, *J* = 8.8 Hz, 2H), 7.58 (t, *J* = 16.4 Hz, 1H), 7.87 (t, *J* = 16.4 Hz, 1H), 8.01 (d, *J* = 8 Hz, 1H), 8.17 (d, *J* = 8 Hz, 1H), 8.52 (d, *J* = 8.8 Hz, 2H); ^{13}C-NMR (100 MHz, $CDCl_3$, ppm) 55.4, 113.9, 122, 125.8, 127.7, 128.5, 129.2, 130.4, 134.7, 151.8, 159.8, 162.1, 162.2.

3.6 Typical procedure for Dechloro-Amination of 123a - e

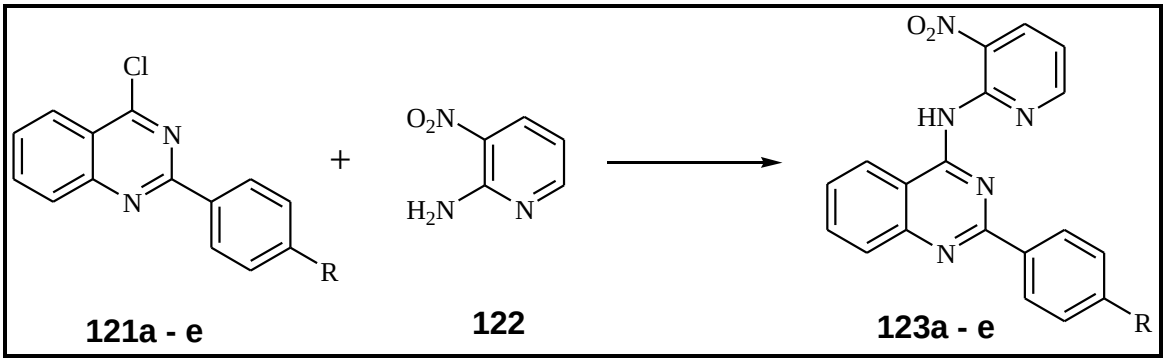

121a - e **122** **123a - e**

R = -Cl (**123a**), -Br (**123b**), -F (**123c**), -NO_2 (**123d**), -OMe (**123e**)

A stirred mixture of **121a** (1 equiv.), 2-amino-3-nitropyridine 1.1 equiv.) **122** and concentrated sulfuric acid (20 drops) in (3:1) THF-DMF 30 ml was heated at 65 ^{o}C for 5 h after which the solution was allowed to cool to RT. The reaction mixture was then added to crushed ice 30 mL, stirred and the product extracted with ethyl acetate. The organic layer washed with aqueous solution of sodium hydrogen carbonate, dried over anhydrous Na_2SO_4, filtered and evaporated under reduced pressure to afford **123a** as yellow solid product **123b-e** were all prepared in a similar fashion.

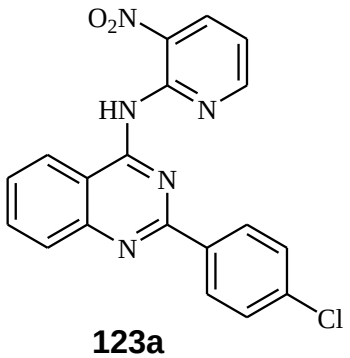

123a

3.6.1 *2-(4-Chlorophenyl)-N-(3-nitropyridin-2-yl)quinazolin-4-amine* (**123a**). A mixture of *4-chloro-2-(4-chlorophenyl)quinazoline* **121a** (300.00 mg, 1.09 mmol), sulphuric acid 20-drops and 2-amino-3-nitropyridine **122** (166.87 mg, 1.20 mmol) afforded **123a** as yellow solid (280.00 mg, 95%) m.p. 281.2 – 282.1 ^{o}C; FT-IR (ν_{max}) 458, 478, 538,

683, 728, 761, 840, 1012, 1074, 1149, 1241, 1280, 1344, 1344, 1443, 1556, 1599, 1669, 3132, 3461; ^{1}H-NMR (400 MHz, DMSO-d_6, ppm) 6.73-6.76 (dd, *J* = 4.8 Hz and 4.4 Hz, 1H), 7.54 (t, *J* = 14.8 Hz, 1H), 7.63 (d, *J* = 8.8 Hz, 2H), 7.75 (d, 8.0 Hz, 1H), 7.85 (t, *J* = 14.8 Hz, 1H), 7.90 (s, 1H), 8.16 (d, *J* = 8.0 Hz, 1H), 8.20 (d, *J* = 8.8 Hz, 2H), 8.38 (t, *J* = 10.8 Hz, 1H), 12.63 (s, 1H); ^{13}C-NMR (100 MHz, DMSO-*d_6,* ppm) 113.0, 121.5, 126.4, 127.3, 128.0, 129.2, 130.1, 132.0, 135.2, 135.4, 136.8, 149, 151.8, 154.2, 156.8, 162.6; HRMS(ESI): calculated 377.0680, $[M\text{-}HCl]^+$, $C_{19}H_{12}N_5O_2^+$, found 341.2670.

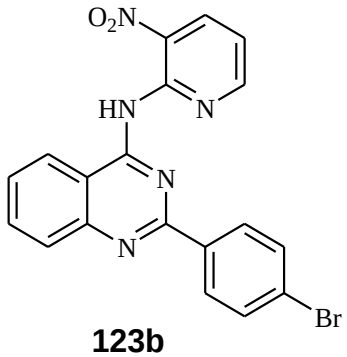

123b

3.6.2 *2-(4-Bromophenyl)-N-(3-nitropyridin-2-yl)quinazolin-4-amine* (**123b**). A mixture of *2-(4-bromophenyl)-4-chloroquinazoline* **121b** (300.00 mg, 0.94 mmol), sulphuric acid 20-drops and 2-amino-3-nitropyridine **122** (143.29 mg, 1.03 mmol) afforded **123b** as yellow solid (210.00 mg, 78%), m.p. 292.1 – 284.1 ^{o}C; FTIR(ν_{max}) 389, 505, 545, 771, 799, 1008, 1064, 1150, 1182, 1336, 1480, 1558, 1600, 1670, 2884, 2919, 2960, 3027, 3268, 3462; ^{1}H-NMR (400 MHz, DMSO-d_6, ppm); 6.73-6.76 (dd, *J* = 4.63 Hz and *J* = 4.44 Hz, 1H), 7.54 (t, *J* = 15.03 Hz, 1H), 7.73-7.78 (m, 3H), 7.85 (t, *J* = 15.51 Hz, 1H), 7.72 (s, 1H), 8.10-8.16 (m, 3H), 8.19-8.40 (m, 1H), 12.64 (s, 1H); ^{13}C-NMR (100 MHz, DMSO-*d_6*, ppm) 112.5, 121.0, 125.3, 125.7, 126.8, 126.8, 127.5, 129.9, 131.7, 132.0, 135.0, 148.6, 151.5, 153.8, 156.3, 162.3; HRMS (ESI): calculated 421.0174. $[M+Na]^+$, $C_{19}H_{12}{}^{79}BrN_5O_2Na^+$, found 444.9536.

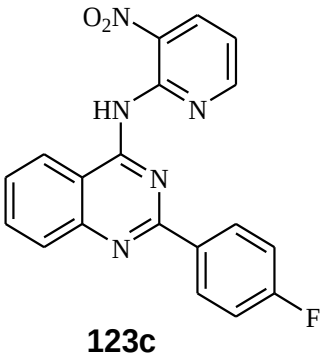

123c

3.6.3 *2-(4-Fluorophenyl)-N-(3-nitropyridin-2-yl)quinazolin-4-amine* (**123c**). A mixture of *4-chloro-2-(4-fluorophenyl)quinazoline* **121c** (300.00 mg, 1.16 mmol), sulphuric acid 20-drops and 2-amino-3-nitropyridine **122** (177.48 mg, 1.28 mmol) afforded **123c** as yellow solid (260.00 mg, 92%),m.p. 273.8 – 274.8 ^{o}C; FTIR(ν_{max}) 426, 496, 540, 685, 735, 763,802, 840, 940, 1019, 1110, 1149, 1233, 1321, 1446, 1518, 1580, 1667, 3090, 3463; ^{1}H-NMR (400 MHz, DMSO-d_6, ppm) 6.73-6.76 (dd, J = 4.4 Hz and 4.4 Hz, 1H), 7.39 (t, J = 17.6 Hz, 2H), 7.52 (t, J = 15.2 Hz, 1H), 7.74 (d, J = 8 Hz, 1H), 7.84 (t, J = 15.6 Hz, 1H), 7.89 (1H, s), 8.15 (d, J = 7.6 Hz, 1H), 8.14-8.23 (m, 2H), 8.38 (t, J = 11.6 Hz, 1H), 12.58 (s, 1H); ^{13}C-NMR (100 MHz, DMSO-d_6, ppm) 113.0, 115.7 (d, $^{2}J_{CF}$ = 21.8 Hz), 121.3, 126.3, 127.1, 127.2, 127.9, 129.3 (d, $^{4}J_{CF}$ = 2.9 Hz), 130.4 (d, $^{3}J_{CF}$ = 9.2 Hz), 135.1, 135.4, 149.1, 151.9, 154.2, 156.7, 164.2 (d, $^{1}J_{CF}$ = 249.4 Hz); HRMS (ESI): calculated 361.0975, $[M]^{+}$, $C_{19}H_{12}FN_5O_2^{+}$, found 361.0641.

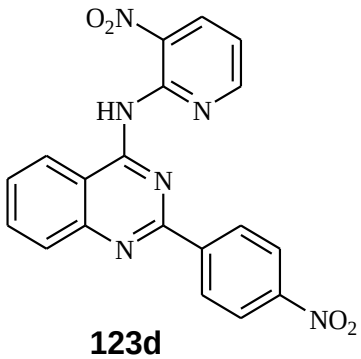

123d

3.6.4 *2-(4-Nitrophenyl)-N-(3-nitropyridin-2-yl)quinazolin-4-amine* (**123d**). A mixture of *4-chloro-2-(4-nitrophenyl)quinazoline* **121d** (300.00 mg, 1.05 mmol), sulphuric acid 20-drops and 2-amino-3-nitropyridine **122** (160.70 mg, 1.16 mmol) afforded **123d** as yellow solid (180.00 mg , 66%), m.p. 269.2 – 271.2 ^{o}C; FTIR(ν_{max}) 501, 539, 762, 802, 820, 941, 1030, 1070, 1099, 1149, 1175, 1241, 1440, 1410, 1515, 1561, 1598, 1674, 3133, 3462; ^{1}H-NMR (400 MHz, DMSO-d_6, ppm); 6.73-6.76 (dd, J = 4.53 Hz and J =

4.59 Hz, 1H), 7.57 (t, *J* = 15.27 Hz, 1H), 7.79 (d, *J* = 7.63 Hz, 1H), 7.87 (t, *J* = 15.27 Hz, 1H), 7.93 (s, 1H), 8.18 (d, *J* = 7.63 Hz, 1H), 7.86-8.44 (m, 6H), 12.89 (s, 1H); ^{13}C-NMR (100 MHz, DMSO-d_6, ppm) 112.5, 121.3, 123.7, 126, 127.8, 127.7, 129.3, 135.0, 139.1, 148.5, 148.9, 151.3, 153.8, 156.3, 162.7; HRMS (ESI): calculated 388.0920, $[M+Na]^+$, $C_{19}H_{12}N_6O_4Na^+$, found 411.0530.

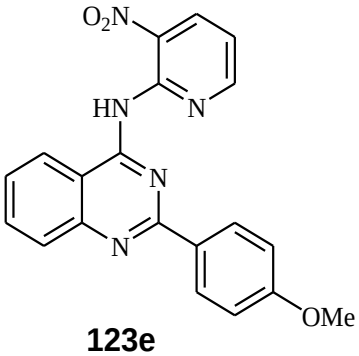

123e

3.6.5 *2-(4-Methoxyphenyl)-N-(3-nitropyridin-2-yl)quinazolin-4-amine* (**123e**). A mixture of *4-chloro-2-(4-methoxyphenyl)quinazoline* **121e** (300.00 mg, 1.11 mmol), sulphuric acid 20-drops and 2-amino-3-nitropyridine **122** (169.59 mg, 1.22 mmol) afforded **123e** as yellow solid (240.00 g, 84%), m.p. 262.4 – 264.4 ^{o}C; FTIR(ν_{max}) 423, 504, 540, 575, 611, 762, 835, 940, 1119, 1244, 1291, 1415, 1441, 1483, 1517, 1558, 1599, 1668, 2994, 3464; ^{1}H-NMR(400 MHz, DMSO-d_6) 3.85 (s, 3H), 6.73-6.76 (dd, *J* = 4.67 Hz and *J* = 4.47 Hz, 1H), 7.09 (d, *J* = 9.14 Hz, 2H), 7.49 (t, *J* = 17.97 Hz, 1H), 7.70 (d, *J* = 8.36 Hz, 1H), 7.82 (t, *J* = 15.36 Hz, 1H), 7.91 (s, 1H), 8.13 (d, *J* = 8.36 Hz, 1H), 8.19 (d, *J* = 9.14 Hz, 2H), 8.20-8.40 (m, 1H), 12.43 (s, 1H); ^{13}C-NMR(100 MHz, DMSO-d_6) 55.5, 112.5, 114.0, 120.7, 124.8, 125.9, 126.2, 126.8, 127.3, 129.5, 134.6, 135.0, 149.0, 151.9, 153.8, 156.3, 161.9, 162.4; HRMS(ESI): calculated 373.1175 $[M]^+$, $C_{20}H_{15}N_5O_4^+$, found 373.1553.

3.7 Typical procedure for Sonogashira Cross-Coupling of 124a - e with ethynylpyridine

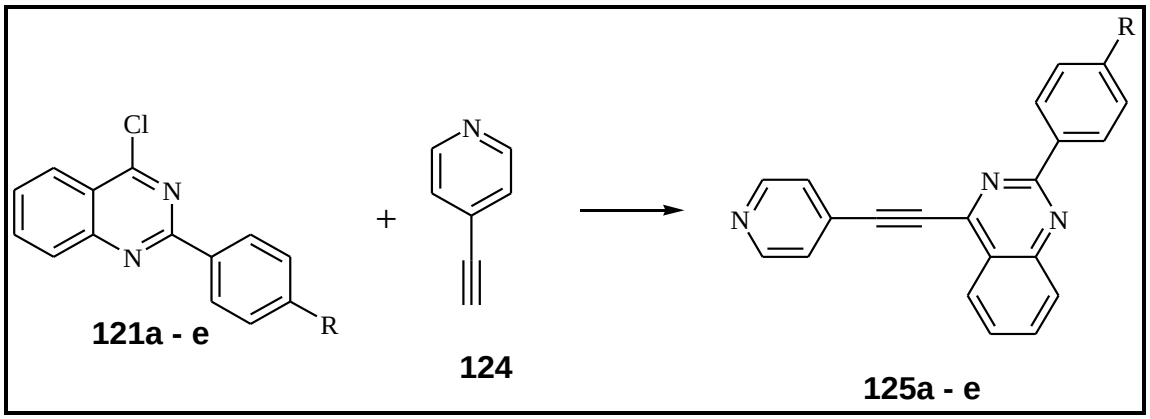

R = -Cl (**125a**), -Br (**125b**), -F (**125c**), -NO_2 (**125d**), -OMe (**125e**)

A mixture of **121** (1 equiv.), $PdCl_2(PPh_3)_2$ (10%), CuI (10%) and Cs_2CO_3 (2 equiv.) in 3:1 THF-water, in a round-bottom flask equipped with a stirrer bar and a condenser equipped with a balloon was flushed for 5 min with nitrogen gas. 1.5 equiv. Ethynylpyridine **124** was added to the flask at once and the mixture was flushed for an additional 10 min. The mixture was refluxed for 24 h at 65 ^oC under nitrogen atmosphere and then quenched with an ice cold water. The precipitate was filtered on a sintered funnel and then taken-up into dichloromethane. The solution was dried with anhydrous sodium sulfate, filtered and then evaporated under reduced pressure. The residue was recrystallised from diethyl ether to afford 4-(ethynylpyridine)quinazolines **125a – e**.

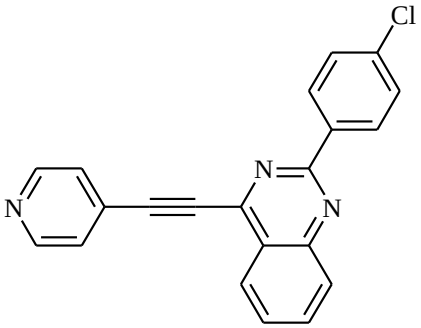

125a

3.7.1 *2-(4-Chlorophenyl)-4-(2-(pyridin-4-yl)ethynyl)quinazoline* (**125a**)*,* A mixture of *4-chloro-2-(4-chlorophenyl)quinazoline* **121a** (500.00 mg, 1.82 mmol), $PdCl_2(PPh_3)_2$ (127.00 mg, 0.18 mmol), CuI (35.00 mg, 0.18 mmol), Cs_2CO_3 (1185.99 mg, 3.64

mmol) and 4-ethynylpyridine **124** (381.05 mg, 2.73 mmol) in THF-water, 30 mL (3:1) afforded **125a** as white solid (460.00 mg, 98%); m.p. 209.2 – 210.0 ^{o}C; FTIR(ν_{max}) 759, 845. 881, 1024, 1228, 1252, 1433, 1537, 2221;^{1}H-NMR (400 MHz, $CDCl_3$, ppm) 7.50 (d, *J* = 8.4 Hz, 2H), 7.61 (d, *J* = 5.2 Hz, 2H), 7.69 (t, *J* = 14.8 Hz, 1H), 7.95 (t, *J* = 14.8 Hz, 1H), 8.10 (d, *J* = 8.4 Hz, 1H), 8.33 (d, *J* = 8.4 Hz, 1H), 8.59 (d, *J* = 8.4 Hz, 2H), 8.74 (d, *J* = 5.2 Hz, 2H); ^{13}C-NMR (100 MHz, $CDCl_3$, ppm) 88.8, 93.7, 123.8, 125.9, 126.1, 128.2, 128.9, 129.2, 129.4, 130.0, 134.7, 136.0, 137.1, 150.1, 151.1, 151.9, 159.9; HRMS(ESI): calculated 341.0720, $[MH]^+$, $C_{21}H_{12}{}^{35}ClN_3{}^+$, found 342.0787.

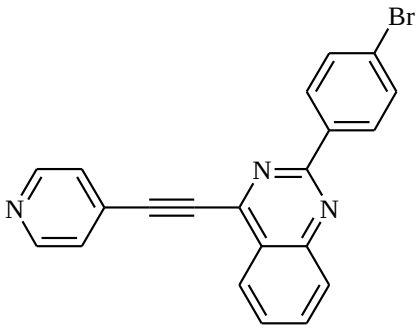

125b

3.7.2 *2-(4-Bromoyphenyl)-4-(2-(pyridin-4-yl)ethynyl)quinazoline* (**125b**), A mixture of *2-(4-bromophenyl)-4-chloroquinazoline* **121b** (500.00 mg, 1.56 mmol), $PdCl_2(PPh_3)_2$ (110.00 mg, 0.16 mmol), CuI (30 mg, 0.16 mmol), Cs_2CO_3 (1016.56 mg, 3.12 mmol) and 4-ethynylpyridine **124** (327.57 mg, 2.35 mmol) in THF-water, 30 mL (3:1) afforded **125b** white solid (400.00 mg, 90%); m.p. 234.6 – 236.3 ^{o}C ; FTIR(ν_{max}) 767, 1005, 1023, 1264, 1336, 1532, 2225; ^{1}H-NMR (400 MHz, $CDCl_3$, ppm) 7.60 (d, *J* = 6 Hz, 2H), 7.64-7.70 (m, 3H), 7.94 (t, *J* = 16.8 Hz, 1H), 8.10 (d, *J* = 8.4 Hz, 1H), 8.33 (d, *J* = 8.4 Hz, 1H), 8.68 (d, *J* = 13.2 Hz, 2H), 8.74 (d, *J* = 6 Hz, 2H); ^{13}C-NMR (100 MHz, $CDCl_3$, ppm) 89.0, 93.7, 123.8, 125.7, 125.9, 126.1, 128.2, 129.1, 129.3, 130.2, 131.8, 134.7, 136.4, 150.1, 151.0, 151.9, 159.9; HRMS(ESI): calculated 386.0215, $[MH]^+$, $C_{19}H_{12}{}^{81}BrN_3{}^+$, found 388.0274.

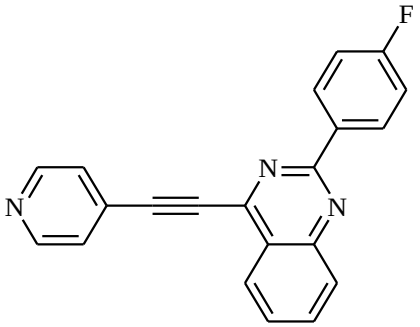

125c

3.7.3 *2-(4-Fluorophenyl)-4-(2-(pyridin-4-yl)ethynyl)quinazoline* (**125c**)*,* A mixture of *4-chloro-2-(4-fluorophenyl)quinazoline* **121c** (500.00 mg, 1.93 mmol), $PdCl_2(PPh_3)_2$ (136.00 mg, 0.19 mmol), CuI (38.00 mg, 0.19 mmol), Cs_2CO_3 (1257.67 mg, 3.86 mmol) and 4-ethynylpyridine **124** (404.08 mg, 2.90 mmol) in THF-water, 30 mL (3:1) afforded **125c** white solid (0.39 g, 94%); m.p. 197.6 – 199.2 ^oC; FTIR(ν_{max}) 758, 819, 925, 1147, 1270, 1336, 1537, 2220; ^{1}H-NMR (400 MHz, $CDCl_3$, ppm) 7.20 (t, $^3J_{HF}$ = 27.6 Hz, 2H), 7.60 (d, *J* = 6 Hz, 2H), 7.67 (t, *J* = 16.4 Hz, 1H), 7.94 (t, *J* = 16.4 Hz, 1H), 8.09 (d, *J* = 8.4 Hz, 1H), 8.32 (d, *J* = 8.4 Hz, 1H), 8.41-8.67 (m, 2H), 8.73 (d, *J* = 6 Hz, 2H); ^{13}C-NMR (100 MHz, $CDCl_3$, ppm) 88.9, 93.6, 115.6 (d, $^2J_{CF}$ = 21.5 Hz), 123.7, 126.0, 128.0, 129.1, 129.4, 130.8 (d, $^3J_{CF}$ = 8.7 Hz), 133.7 (d, $^4J_{CF}$ = 2.9 Hz), 134.7, 150.2, 151.5, 160.0, 164.7 (d, $^1J_{CF}$ = 247.6 Hz); HRMS(ESI): calculated 325.1015, $[MH]^+$, $C_{21}H_{12}FN_3^+$, found 326.1082.

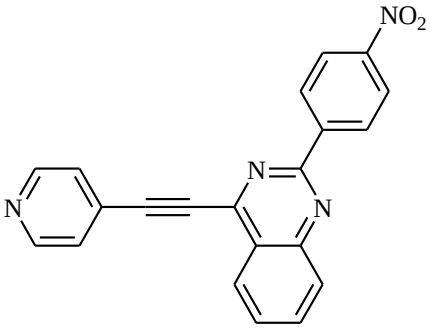

125d

3.7.4 *2-(4-Nitrophenyl)-4-(2-(pyridin-4-yl)ethynyl)quinazoline* (**125d**)*,* A mixture of *4-chloro-2-(4-nitrophenyl)quinazoline* **121d** (500.00 mg, 1.75 mmol), $PdCl_2(PPh_3)_2$ (123.00 mg, 0.18 mmol), CuI (33.00 mg, 0.18 mmol), Cs_2CO_3 (1140.37 mg, 3.50 mmol) and 4-ethynylpyridine **124** (367.10 mg, 2.63 mmol) in THF-water, 30 mL (3:1) afforded **125d** white solid (390.00 mg, 94%); m.p. 272.7 – 274.8 ^oC; FTIR(ν_{max}) 714,

819, 930, 1215, 1250, 13338, 1592, 2207; ^{1}H-NMR (400 MHz, $CDCl_3$, ppm) 7.61 (d, *J* = 5.60 Hz, 2H), 7.76 (t, *J* = 14.62 Hz, 1H), 8.01 (t, *J* = 15.87 Hz, 1H), 8.16 (d, *J* = 8.77 Hz, 1H), 8.16-8.35 (m, 3H), 8.75 (d, *J* = 5.01 Hz, 2H), 8.83 (d, *J* = 9.19 Hz, 2H); ^{13}C-NMR (100 MHz, $CDCl_3$, ppm) 88.4, 94.1, 123.6, 123.9, 125.8, 126, 128.3, 128.4, 128.4, 129.0, 129.2, 129.3, 134.9, 143.1, 149.1, 149.8, 150.0, 150.8, 151.9, 158.4; HRMS(ESI): calculated 352.1015, $[MH]^+$, $C_{21}H_{12}N_4O_4^+$, found 353.1027.

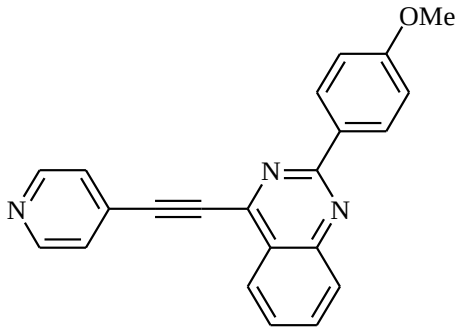

125e

3.7.5 *2-(4-Methoxyphenyl)-4-(2-(pyridin-4-yl)ethynyl)quinazoline* (**125e**) A mixture of *4-chloro-2-(4-nitrophenyl)quinazoline* **121d** (500.00 mg, 1.85 mmol), $PdCl_2(PPh_3)_2$ (130 mg, 0.19 mmol), CuI (35.00 mg, 0.19 mmol), Cs_2CO_3 (1205.53 mg, 3.70 mmol) and 4-ethynylpyridine**124** (388.03 mg, 2.78 mmol) in THF-water, 30 mL (3:1) afforded **125d** yellow solid (495.00 mg, 79 %) ; m.p. 202.6 – 204.6 ^{o}C; FTIR(ν_{max}) 761, 818, 924, 1161, 1252, 1360, 1468, 1535, 2219; ^{1}H-NMR (400 MHz, $CDCl_3$, ppm); 3.88 (s, 3H), 7.03 (d, *J* = 8.87 Hz, 2H), 7.58-7.62 (m, 15.97 Hz, 3H), 7.88 (t, *J* = 15.08 Hz, 1H), 8.05 (d, *J* = 8.87 Hz, 1H), 8.27 (d, *J* = 8.87 Hz, 1H), 8.57 (d, *J* = 8.87 Hz, 2H), 8.72 (d, *J* = 3.52 Hz, 2H); ^{13}C-NMR (100 MHz, $CDCl_3$, ppm) 55.4, 89, 93.2, 113.9, 123.4, 125.9, 126, 127.4, 129.5, 130.1, 130.3, 134.4, 150.1, 151.1, 151.6, 160.6, 161.9; HRMS(ESI): calculated 337.0215, $[MH]^+$, $C_{22}H_{15}N_3O^+$, found 338.1286.

3.8 Synthesis of [(η^6-*p*-cymene)RuCl$_2$-4-(ethynylpyridine)quinazolines] 126a – e

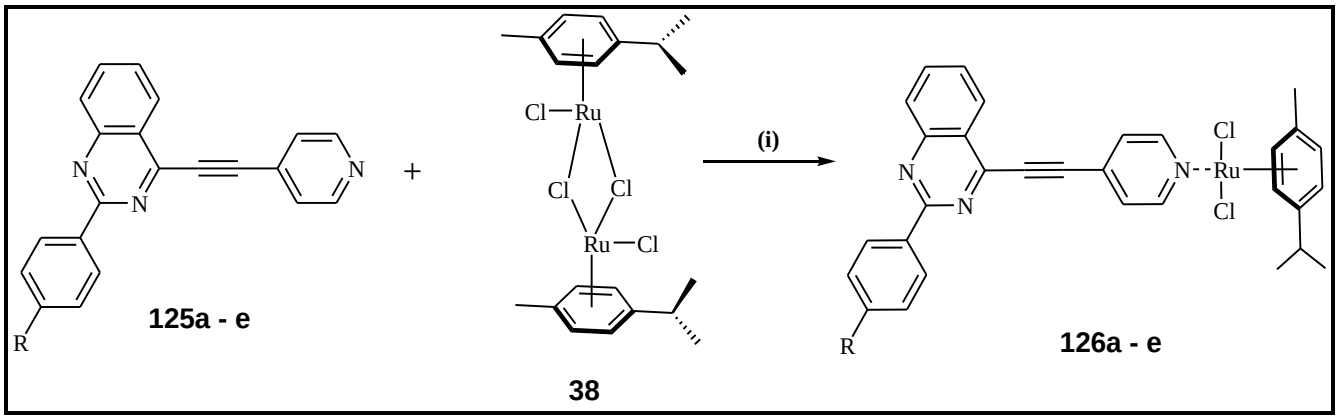

R = -Cl (**126a**), -Br (**126b**), -F (**126c**), -NO_2 (**126d**), -OMe (**126e**)

To a 250 mL Schlenk flask, a mixture of **125** (2.25 equiv.) and dichloro-(p-cymene)-ruthenium (ll) dimer **38** (1 equiv.) was heated to reflux in hexane for 5 h, after which stirring was continued for 12 h at room temperature, the precipitate was collected on a filter-paper and washed thoroughly with methanol and diethyl ether to afford **126a – e.**

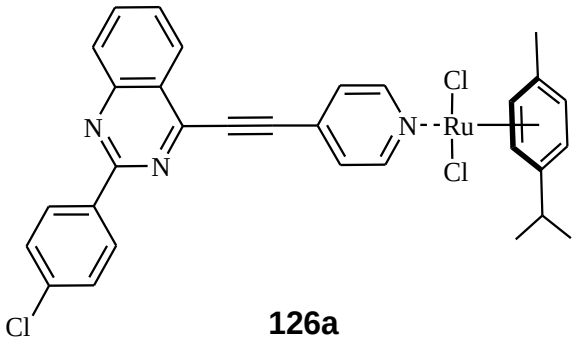

126a

3.8.1 [(η^6-*p*-cymene)RuCl$_2$-*2-(4-chlorophenyl)-4-(2-(pyridin-4-yl)ethynyl)quinazoline*] (**126a**), A mixture of *2-(4-chlorophenyl)-4-(2-(pyridin-4-yl)ethynyl)quinazoline* **125a** (125.40 mg, 0.37 mmol) and dichloro-(*p*-cymene)-ruthenium(ll) dimer **38** (100.00 mg, 0.16 mmol) in hexane 30 mL afforded **126a** as orange solid (94.31 mg, 90%); m.p 402.2 – 404.1 ^{o}C; FTIR(ν_{max}) 768, 834, 937, 1149, 1270, 1339, 1601, 1805, 2218, 2962; ^{1}H-NMR (400 MHz, $CDCl_3$, ppm) 1.33 (d, *J* = 6.8 Hz, 6H), 2.13 (s, 3H), 3.01 (sep, *J* = 28.8 Hz, 1H), 5.27 (d, *J* = 5.6 Hz, 2H), 5.45 (d, *J* = 6 Hz, 2H), 7.60 (d, *J* = 6Hz, 2H), 7.66 (d, *J* = 8.4 Hz, 2H), 7.71 (t, *J* = Hz, 1H), 7.97 (t, *J* = Hz, 1H), 8.11 (d, *J* = 8 Hz, 1H), 8.27 (d, *J* = 8 Hz, 1H), 8.50 (d, *J* = 8.8 Hz, 2H), 9.16 (d, *J* = 6.4 Hz, 2H); ^{13}C-NMR (100 MHz, $CDCl_3$, ppm) 18.4, 22.3, 30.9, 58.4, 82.3, 83.1, 91.7, 97.3, 103.7,

123.7, 125.8, 125.9, 126.6, 128.5, 129.2, 130.2, 131.2, 131.8, 134.9, 136.3, 151.1, 155.0, 159.9; HRMS(ESI): calculated 647.02 $[M\text{-}Cl]^+$, $C_{31}H_{26}{}^{35}Cl_2N_3Ru^+$, found 611.1852.

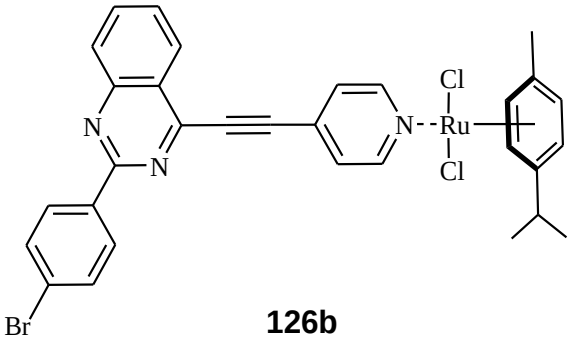

126b

3.8.2 [(η^6-*p*-cymene)$RuCl_2$-*2-(4-bromoyphenyl)-4-(2-(pyridin-4-yl)ethynyl)quinazoline*] (**126b**), A mixture of *2-(4-bromoyphenyl)-4-(2-(pyridin-4-yl)ethynyl)quinazoline* **125b** (151.75, 0.37 mmol) and dichloro-(*p*-cymene)-ruthenium(ll) dimer **38** (100.00 mg, 0.16 mmol) in hexane 30 mL afforded **126b** as orange solid (76.01 mg, 67%); m.p >450 ^oC; FTIR(ν_{max}) 733, 869, 1007, 1171, 1338, 1449, 1536, 1562, 1604, 2219, 2966; ^{1}H-NMR (400 MHz, $CDCl_3$, ppm) 1.33 (br-s, 6H), 2.14 (br-s, 3H), 3.01 (br-s, 1H), 5.27 (br-s, 2H), 5.49 (br-s, 2H), 7.60 (br-s, 1H), 7.66 (d, *J* = 7.2 Hz, 4H), 7.96 (br-s, 1H), 8.11 (d, *J* = 4.4 Hz, 1H), 8.27 (br-s, 1H), 8.50 (d, *J* = 6.4 Hz, 2H), 9.17 (br-s, 2H); ^{13}C-NMR (100 MHz, $CDCl_3$, ppm) 18.4, 22.3, 30.7, 82.4, 83.1, 91.7, 91.8, 97.4, 103.8, 123.8, 125.8, 126.0, 126.6, 128.5, 129.2, 130.2, 131.2, 131.9, 134.9, 136.3, 151.1, 151.2, 155.1, 159.9; HRMS(ESI): calculated 692.44, $[M\text{-}Cl]^+$, $C_{31}H_{26}{}^{79}Br^{35}ClN_3Ru^+$, found 656.0060.

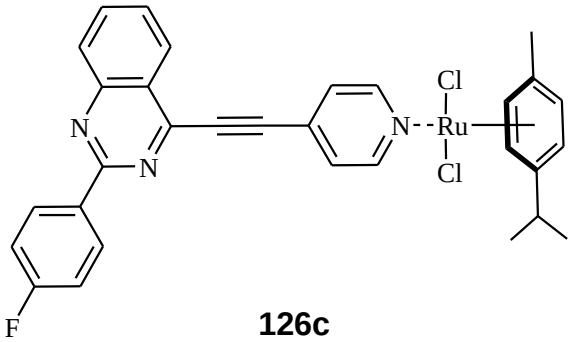

126c

3.8.3 [(η^6-*p*-cymene)$RuCl_2$-*2-(4-fluorophenyl)-4-(2-(pyridin-4-yl)ethynyl)quinazoline*] (**126c**), A mixture of *2-(4-fluorophenyl)-4-(2-(pyridin-4-yl)ethynyl)quinazoline* **125c** (119.40 mg, 0.37 mmol) and dichloro-(*p*-cymene)-ruthenium(ll) dimer **38** (100.00 mg, 0.16 mmol) in hexane 30 mL afforded **126c** as orange solid (82.46 mg, 80%); m.p >

410 ^{o}C; FTIR(ν_{max}) 770, 841, 936, 1151, 1264, 1338, 1537, 1813, 2021, 2359, 2963; ^{1}H-NMR (400 MHz, $CDCl_3$, ppm) 1.31 (d, *J* = 7.2 Hz, 6H), 2.11 (s, 3H), 2.98 (sep, *J* = 26.5 Hz, 1H), 5.27 (d, *J* = 6 Hz, 2H), 5.48 (d, *J* = 6 Hz, 2H), 7.16-7.21 (m, 2H), 7.57 (d, *J* = 6.4 Hz, 2H), 7.67 (t, *J* = 14.4 Hz, 1H), 7.93 (t, *J* = 16.4 Hz, 1H), 8.06 (d, *J* = 4 Hz, 1H), 8.24 (d, *J* = 8 Hz, 1H), 8.25-8.62 (m, 2H), 9.14 (d, *J* = 6.6 Hz, 2H) ^{13}C-NMR (100 MHz, $CDCl_3$, ppm) 18.3, 22.3, 30.7, 82.2, 83, 91.7, 91.6, 97.4, 103.6, 115.6 (d, $^{2}J_{CF}$ = 21.7 Hz), 123.5, 125.9, 126.6, 130.0, 130.7 (d, $^{3}J_{CF}$ = 8.6 Hz), 133.5 (d, $^{4}J_{CF}$ = 2.8 Hz), 134.8, 150.1, 155.0, 159.9, 164.7 (d, $^{1}J_{CF}$ = 250 Hz); HRMS(ESI): calculated 631.05, [M-*p*-cymene]$^{+}$, $C_{21}H_{12}{}^{35}Cl_2FN_3Ru^{+}$, found 497.0965.

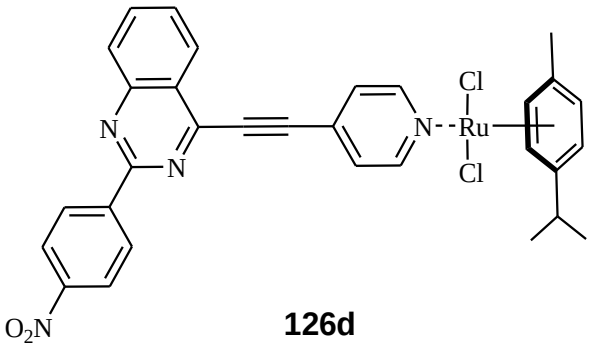

126d

3.8.4 [(η^{6}-*p*-cymene)$RuCl_2$-*2-(4-nitrophenyl)-4-(2-(pyridin-4-yl)ethynyl)quinazoline*] (**126d**) A mixture of *2-(4-nitrophenyl)-4-(2-(pyridin-4-yl)ethynyl)quinazoline* **125d** (129.31 mg, 0.37 mmol) and dichloro-(*p*-cymene)-ruthenium(ll) dimer **38** (100.00 mg, 0.16 mmol) in hexane 30 mL afforded **126d** as orange solid (86.60 mg, 81%); m.p > 410 ^{o}C; FTIR(ν_{max}) 714, 833, 937, 1192, 1338, 1520, 1578, 1778, 2210, 2962; ^{1}H-NMR (400 MHz, $CDCl_3$, ppm) 1.32 (d, *J* = 7.2 Hz, 6H), 2.13 (s, 3H), 3.01 (sep, *J* = 28.8 Hz, 1H), 5.27 (d, *J* = 6 Hz, 2H), 5.49 (d, *J* = 6 Hz, 2H), 7.35 (m, *J* = 18.4 Hz, 3H), 7.60 (t, *J* = 14.8 Hz, 1H), 8.01 (t, *J* = 14.8 Hz, 1H), 8.16 (d, *J* = 8.4 Hz, 1H), 8.35 (d, *J* = 8.4 Hz, 2H), 9.17 (d, *J* = 6.6 Hz, 2H); ^{13}C-NMR (100 MHz, $CDCl_3$, ppm) 18.4, 22.3, 30.7, 82.3, 83.1, 91.3, 97.4, 103.7, 123.8, 126.0, 126.2, 126.6, 129.3, 129.5, 131.0, 135.1, 135.3, 143.1, 149.3, 150.2, 151.0, 155.1, 158.6; HRMS(ESI): calculated 658.05, [M-Cl]$^{+}$, $C_{31}H_{26}{}^{35}ClN_4O_2Ru^{+}$, found 622.0796.

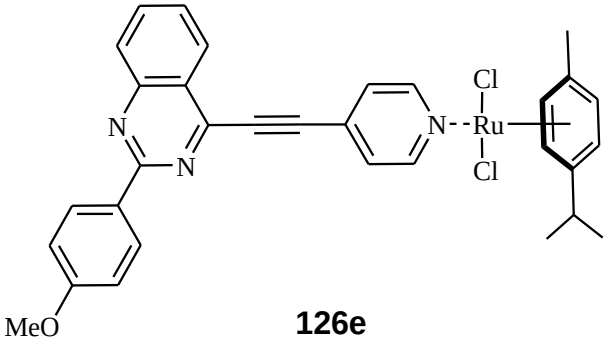

126e

3.8.5 [(η^6-*p*-cymene)$RuCl_2$-*2-(4-methoxy-phenyl)-4-(2-(pyridin-4-yl)-ethynyl)-quinazoline*] (**126e**), A mixture of *2-(4-methoxyphenyl)-4-(2-(pyridin-4-yl)ethynyl)quinazoline* **125e** (123.82 mg, 0.37 mmol) and dichloro-(*p*-cymene)-ruthenium(ll) dimer **38** (100.00 mg, 0.16 mmol) in hexane 30 mL afforded **126e** as orange solid (74.41 mg, 71%); m.p 410 ^oC; FTIR(v_{max}) 714, 829, 930, 1169, 1250, 1354, 1574, 1605, 1774, 2210, 2962; ^{1}H-NMR (400 MHz, $CDCl_3$, ppm) 1.32 (d, *J* = 6.8 Hz, 6H), 2.13 (s, 3H), 3.01 (sep, *J* = 27.6 Hz, 1H), 3.89 (s, 3H), 5.27 (d, *J* = 6 Hz, 2H), 5.48 (d, *J* = 6 Hz, 2H), 7.03 (d, *J* = 8.8 Hz, 2H), 7.59 (d, *J* = 6.4 Hz, 2H), 7.63 (t, *J* = 15.2 Hz, 1H), 7.91 (t, *J* = 14.8 Hz, 1H), 8.06 (d, *J* = 8.8 Hz, 1H), 8.22 (d, *J* = 8.8 Hz, 1H), 8.56 (d, *J* = 8.8 Hz, 2H), 9.15 (d, *J* = 6.8 Hz, 2H); ^{13}C-NMR (100 MHz, $CDCl_3$, ppm) 18.3, 22.3, 30.7, 55.4, 82.3, 83.0, 91.3, 91.9, 97.3, 103.7, 114.0, 123.4, 125.8, 126.6, 127.7, 129.0, 130.0, 130.3, 131.3, 151.0, 151.2, 155, 160.7, 162; HRMS(ESI), calculated 643.07, $[M-Cl]^+$, $C_{32}H_{29}{}^{35}ClN_3ORu^+$, found 607.1059.

3.9 Molecular docking of compounds 119a – d, 123a – e, 125a – e

The molecular docking calculations were achieved using the Schrodinger-2018-1 LLC interface, employing Maestro 11.5 database. All ligands and proteins in the induced-fit docking job were prepared at physiological pH 7.4 using Epik. The conformational search for all ligands was done using optimised potentials for liquid simulations (OPLS_2005) employing water as a solvent. The induced-fit docking (IFD) experiment was run on extra-precision (XP), wherein residues within ligand poses were refined at 5 Å and all ligands were re-docked into structures within 30 Kcal/mol of the best structure, and within the top 20 structures overall.

3.10 In vitro anti-Mycobacterium tuberculosis activity of compounds 119a – d, 121a – e, 123a – e, 125a – e and 126a – e.

3.10.1 Broth micro-dilution method

The inhibitory activity against *Mycobacterium tuberculosis* was achieved at the University of Cape Town, drug discovery and development centre (H3-D), following broth micro-dilution method. The broth micro-dilution method allows a range of antibiotic concentrations to be tested on a single 96-well microtitre plate in order to determine the minimum inhibitory concentration (MIC). Briefly, a 10 mL culture of a mutant *Mtb* (H37Rv) strain constitutively expressing recombinant alamar blue assay of a plasmid integrated at the *attB* locus is grown to an OD600 of 0.6–0.7. The *Mtb*. H37Rv strain culture is then diluted 1:100 in 7H9 GLU CAS TX. In a 96-well microtitre plate, 50 µL of 7H9 GLU CAS TX medium is added to all wells from Rows 2-12. The compounds to be tested are added to Row 2-12 in duplicate, at a final concentration of 640 µM (stocks are made up to a concentration of 12.8 mM in DMSO, and diluted to 640 µM in 7H9 GLU CAS TX medium). A two-fold serial dilution is prepared, by transferring 50 µL of the liquid in Row 1 and 2 to mix. 50 µL of the liquid in Row 2 is then transferred to Row 3 and aspirated. The procedure is repeated until Row 12 is reached, from which 50 µL of the liquid is discarded to bring the final volume in all wells to 50 µL. Finally, 50 µL of the 1:100 diluted *Mtb* cultures are added to all wells in Rows 2-12. Row 1 serves as a contamination control which includes media, 5% DMSO and rifampicin. The microtitre plate is stored in a secondary container and incubated at 37 °C with humidifier to prevent evaporation of the liquid. The lowest concentration of compounds which inhibit growth of more than 90% of the bacterial population is considered to be the MIC_{90} and MIC_{99}. The pellet data is reported as visual score and calculated MIC during 7 and 14 day post inoculation [8].

Reference

[1] Schwartz, A.M., 1978. The benzophenone/ketyl tetrahydrofuran (THF) still. *Chemical Engineering News*, *24*, p.88.

[2]. Mphahlele, M.J., Paumo, H.K., El-Nahas, A.M. and El-Hendawy, M.M., 2014. Synthesis and photophysical property studies of the 2, 6, 8-triaryl-4-(phenylethynyl) quinazolines. *Molecules*, *19*(1), pp.795-818.

[3]. Parua, S., Das, S., Sikari, R., Sinha, S. and Paul, N.D., 2017. One-Pot Cascade Synthesis of Quinazolin-4 (3 H)-ones via Nickel-Catalyzed Dehydrogenative Coupling of o-Aminobenzamides with Alcohols. *The Journal of Organic Chemistry*, *82*(14), pp.7165-7175.

[4]. Patel, K.D., Vekariya, R.H., Prajapati, N.P., Patel, D.B., Patel, H.D., Shaikh, T., Rajani, D.P., Rajani, S., Shah, N.S. and Jhala, D., 2018. Synthesis of N'-(Quinazolin-4-yl) isonicotinohydrazides and their biological screening, docking and ADME studies. *Arabian Journal of Chemistry*.

[5]. Dravyakar, B.R. and Khedekar, P.B., 2012. Study of synthesis of novel N, 2-diphenylquinazolin-4-amine derivatives as an anti-inflammatory and analgesic agent. *Der Pharma Chemica*, *4*, pp.699-706.

[6]. Rahmannejadi, N., Khabnadideh, S. and Yavari, I., 2018. Synthesis, docking, and cytotoxic activities of novel 2-aryl-4-(arylamino) quinazolines. *Monatshefte für Chemie-Chemical Monthly*, *149*(11), pp.2085-2092.

[7]. Maxwell, A.C., Flanagan, S.P., Goddard, R. and Guiry, P.J., 2010. Rhodium-catalysed hydroboration employing new Quinazolinap ligands; an investigation into electronic effects. *Tetrahedron: Asymmetry*, *21*(11-12), pp.1458-1473.

[8]. Yang, J., Pi, W., Xiong, L., Ang, W., Yang, T., He, J., Liu, Y., Chang, Y., Ye, W., Wang, Z. and Luo, Y., 2013. 3H-1, 2, 4-Dithiazol-3-one compounds as novel potential affordable antitubercular agents. *Bioorganic & Medicinal Chemistry Letters*, *23*(5), pp.1424-1427.

CHAPTER 4: RESULTS AND DISCUSSION

Bidentate Schiff base ligands of the *N^N* type were synthesised in good yields and their respective metal coordinated complexes where M is Zn(II) were also attempted. This was later followed by the synthesis of ethynylpyridine bridged quinozaline organic moiety derivatives which were coordinated to monomeric *p*-cymene ruthenium(ll) centre.

4.1 Synthesis of ethanamineimidazolyl-Schiff base ligands and their reaction with M(II) metals

The retrosynthetic analysis strategy for the synthesis of the target ligands **119a-d** to be coordinated to metal centres Ru/Zn is shown below in **Scheme 4.1**.

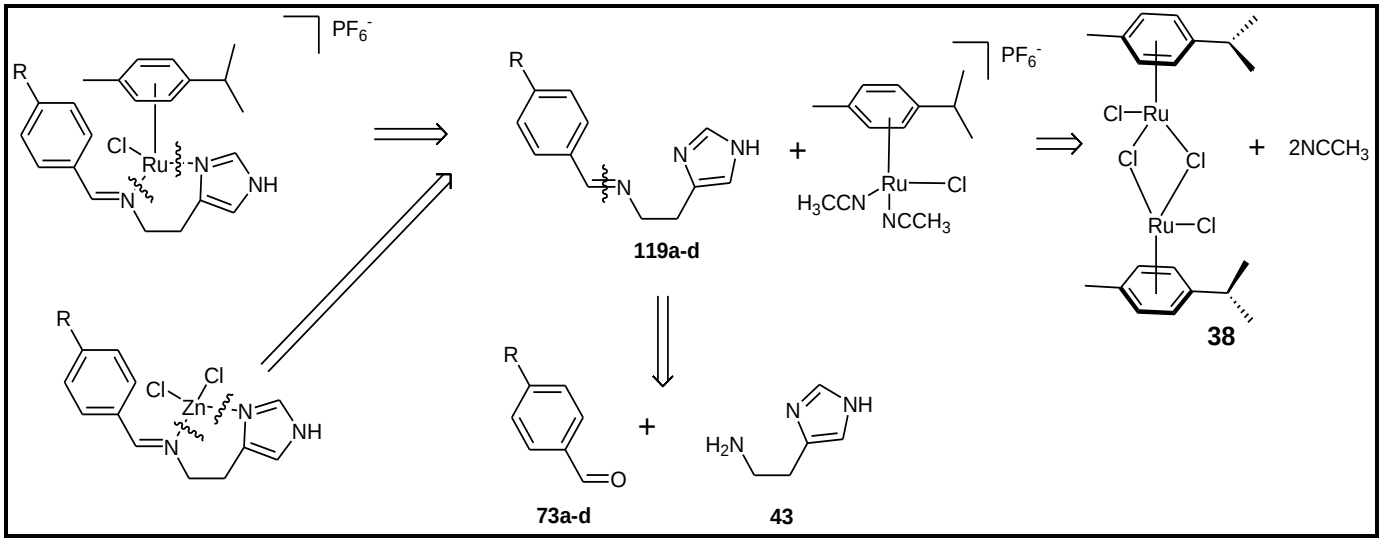

R = -H, -OH, -F, -NO_2

Scheme 4.1: Retrosynthetic strategy for the synthesis of the proposed ethanamineimidazolyl Schiff base complex.

Schiff base ligands are generally accessible by following a direct acid or base catalysed condensation reaction between aldehyde derivatives and primary amine in the presence of a drying agent ($MgSO_4$, Na_2SO_4 and $NaHCO_3$) [1]. The drying agent in this case helps in absorbing the water molecules from the reaction and in-turn form an alkaline solution which does not temper with the progression of the reaction [2]. On the other hand, metal complexes of Schiff bases are formed by treating metal salts with stoichiometric amount of the ligand under moisture free conditions depending on the nature of the ligand and the metal salt employed in the reaction [3].

The synthesis of Schiff base derivatives **119a-d** was initiated by a trial series of acid catalysed reactions. A reaction of *para*-substituted aldehyde derivaties **73a-d**, histamine dihydrochloride **43**, formic acid 5 - 10% (7 - 12 drops) and sodium hydrogen carbonate ($NaHCO_3$) in dry methanol while stirring at room temperature for 24 h was unsuccessful. Only starting materials, *i.e*. aldehyde **73a-d** and the histamine dihydrochloride **43**, were isolated. Further attempts using different acids such as hydrochloric acid (HCl, 5 - 10%) [5], sulphuric acid (H_2SO_4, 5 - 10%) [6] and acetic acid (CH_3COOH, 5 - 10%) [7] yielded trace amount of the desired product. Reaction of the aldehydes (**73a-d**) and histamine in basic conditions i.e. triethylamine solution (TEA) showed the formation of the expected product. However, purification was a challenge as chromatographic purification techniques (prep-TLC and column chromatography) proved detrimental to the ligands. The Schiff base ligands cannot be purified using column/ preparative thin layer chromatographic (TLC) techniques, as they are moisture sensitive and undergo hydrolysis. The imidazolyl-ethanamine Schiff base ligands **119a-d** were successfully synthesised by condensation of the *para*-substituted (-F, $-NO_2$, -H and –OH) aldehyde derivatives **73a-d** and histamine dihydrochloride **43** in the presence of sodium hydroxide (NaOH) [4]. Histamine dihydrochloride **43** was neutralised with NaOH in methanol for 2 hrs to give a colourless methanolic reaction mixture i.e **43***. The reaction mixture was then added dropwise to a methanolic aldehyde solution equipped with a stirrer bar and stirred for 15 minutes before adding $NaHCO_3$. The reaction mixture was stired for 24 h at room temperature, after which Schiff base derivatives **119a-d** were isolated in high yields ranging from 94 – 98%, **Scheme 4.2**.

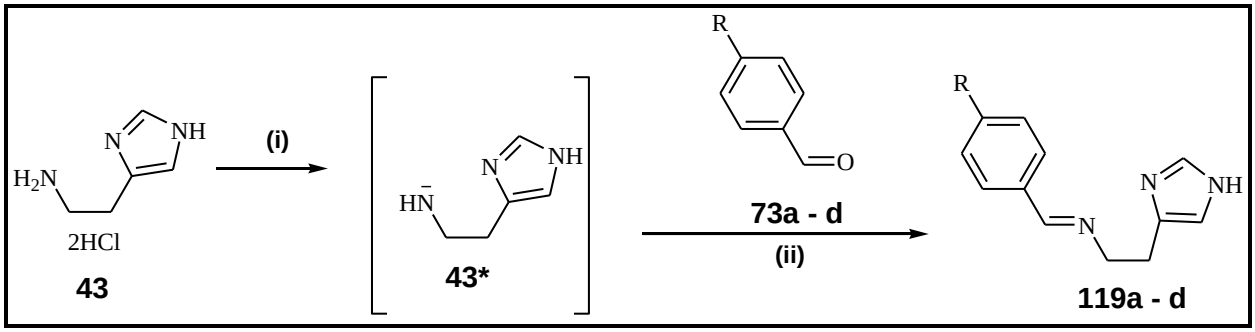

R = -H, -OH, -F, $-NO_2$.

Reagents and solutions: (i) NaOH, MeOH, rt, 2h, (ii) MeOH, rt, 24h.

Scheme 4.2: Reaction scheme for the synthesis of Schiff base ligands **119a-d.**

A representative ligand, 4-((E)-(2-(1H-imidazol-4-yl)ethylimino)methyl)phenol **119b** is here described. The ^{1}H-NMR spectrum (**Figure 4.1**) reveals the presence of an expected set of two singlets and doublets corresponding to the imidazolyl protons and the symmetrical aromatic protons respectively in the region (δ_H 6.74 – 7.60 ppm). Another expected set of two triplets relatively upfield both integrating for 2H each while the slightly de-shielded –CH_2^b of the ethanamine group reasonating at δ 3.80 ppm (*J* = 14.00 Hz) is also observed. An intense singlet of the imine proton at δ 8.05 ppm confirms the condensation between 4-hydroxybenzaldehyde derivative **73b** and histamine **43**. The presence of the azomethine group (-CH*=N-) was further confirmed using the ^{1}H-^{1}H COSY experiment. The spectrum revealed a correlation between the imine proton and the de-shielded triplet –CH_2^b (correlation peak circled red, (**Figure 4.2**)). The ^{1}H-HMBC spectrum (**Figure 4.3**) revealed a correlation between the imine hydrogen (red circles) and the carbon of the –CH_2^b group resonating at 63 ppm via ^{4}J-spin coupling. The FTIR spectrum (**Figure 4.4**) of the 4-((E)-(2-(1H-imidazol-4-yl)ethylimino)methyl)phenol **119b** revealed the azomethine group (-CH=N-) at 1668 cm^{-1} further confirming the presence of the (-CH=N-) link. Similar findings of other derivatives summarised in **Table 4.1**.

Table 4.1: Summarised characterisation of compounds **119a-d**.

119	**R**	**Imine proton (ppm)**	**ν_{max} (-CH*=N-) link (cm^{-1})**	**%yield**	**mp. (°C)**
a	-H	8.243	1696	94	247.4 – 248.6
b	-OH	8.048	1668	97	262.5 – 263.1
c	-F	8.229	1666	95	284.9 – 286.1
d	-NO2	8.375	1628	98	266.2 – 267.4

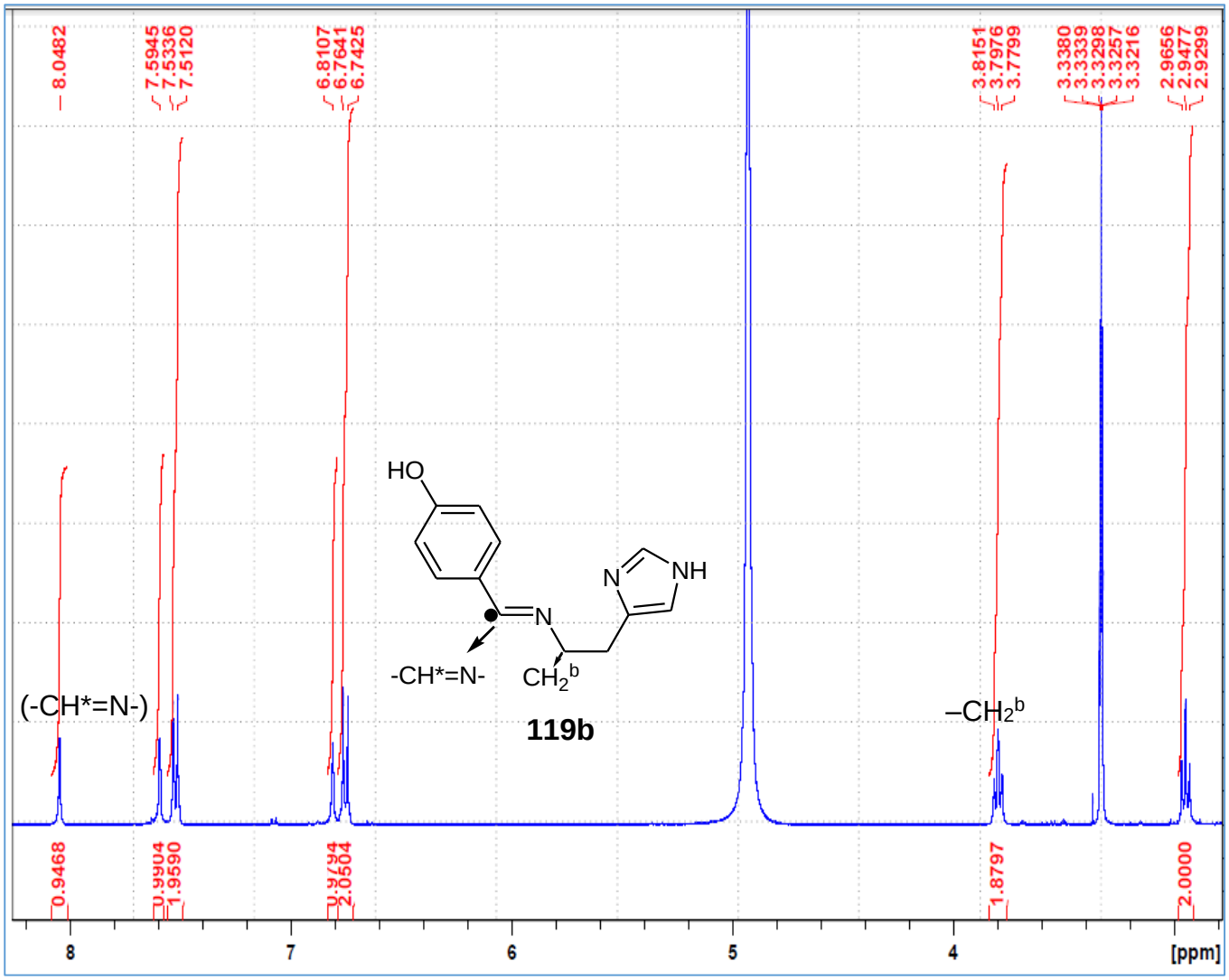

Figure 4.1: 1H-NMR spectrum of **119b** in MeOD-*d*$_3$ at 400 MHz.

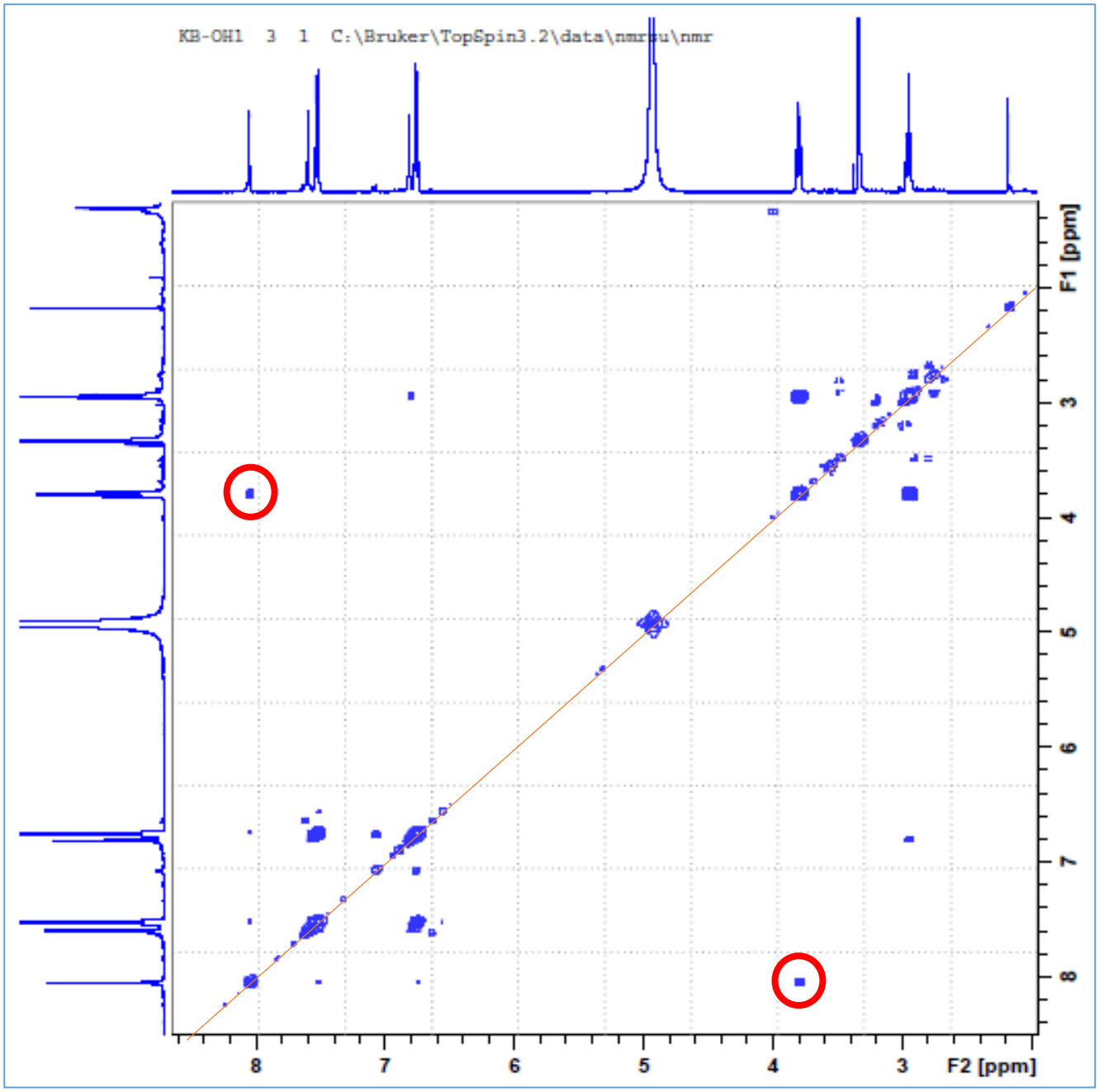

Figure 4.2: ^{1}H-^{1}H-COSY spectrum of **119b** in MeOD-d_3 at 400 MHz.

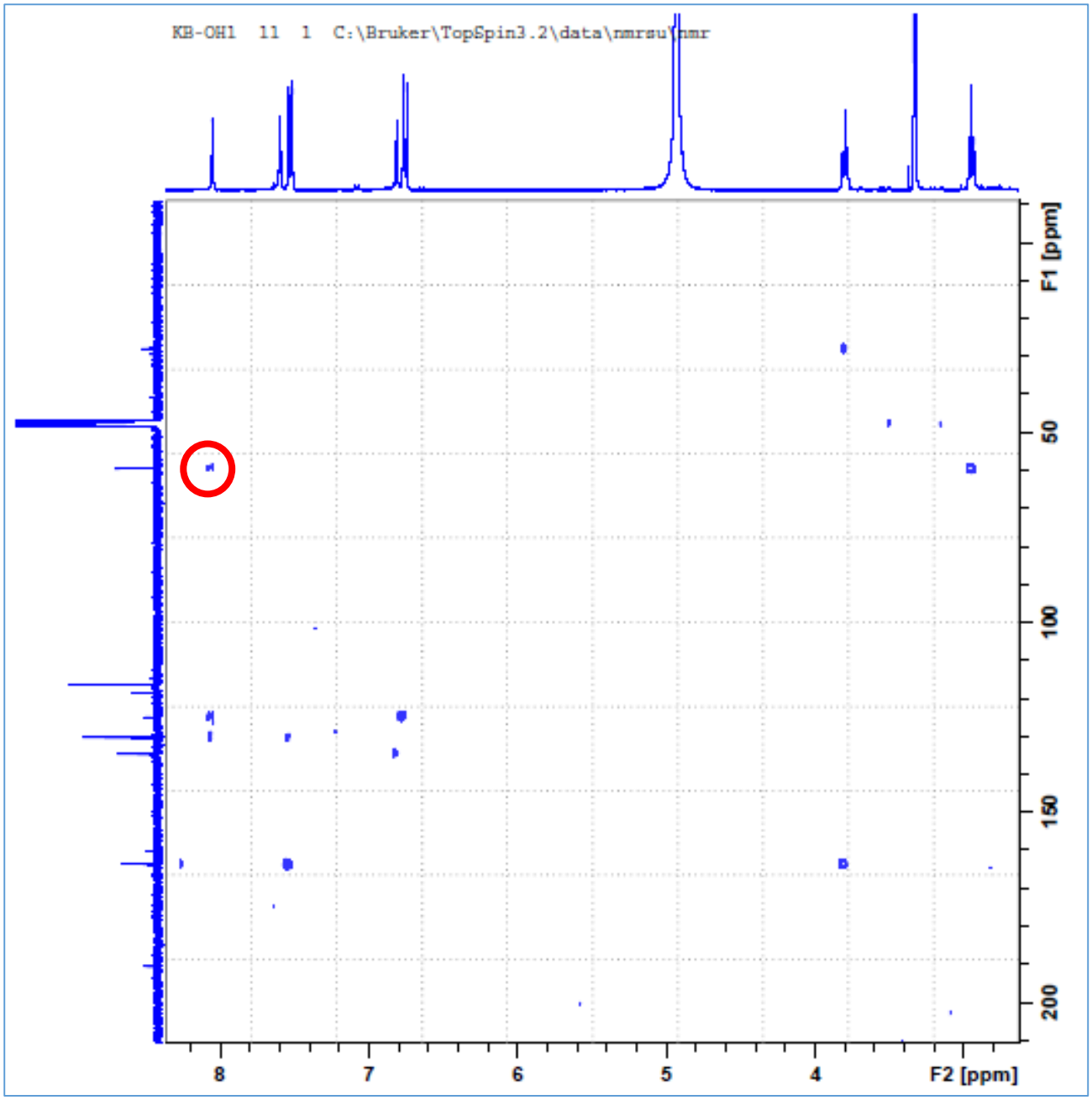

Figure 4.3: Expanded 2D-HMBC spectrum of **119b** in MeOD-d_3 at 400 MHz.

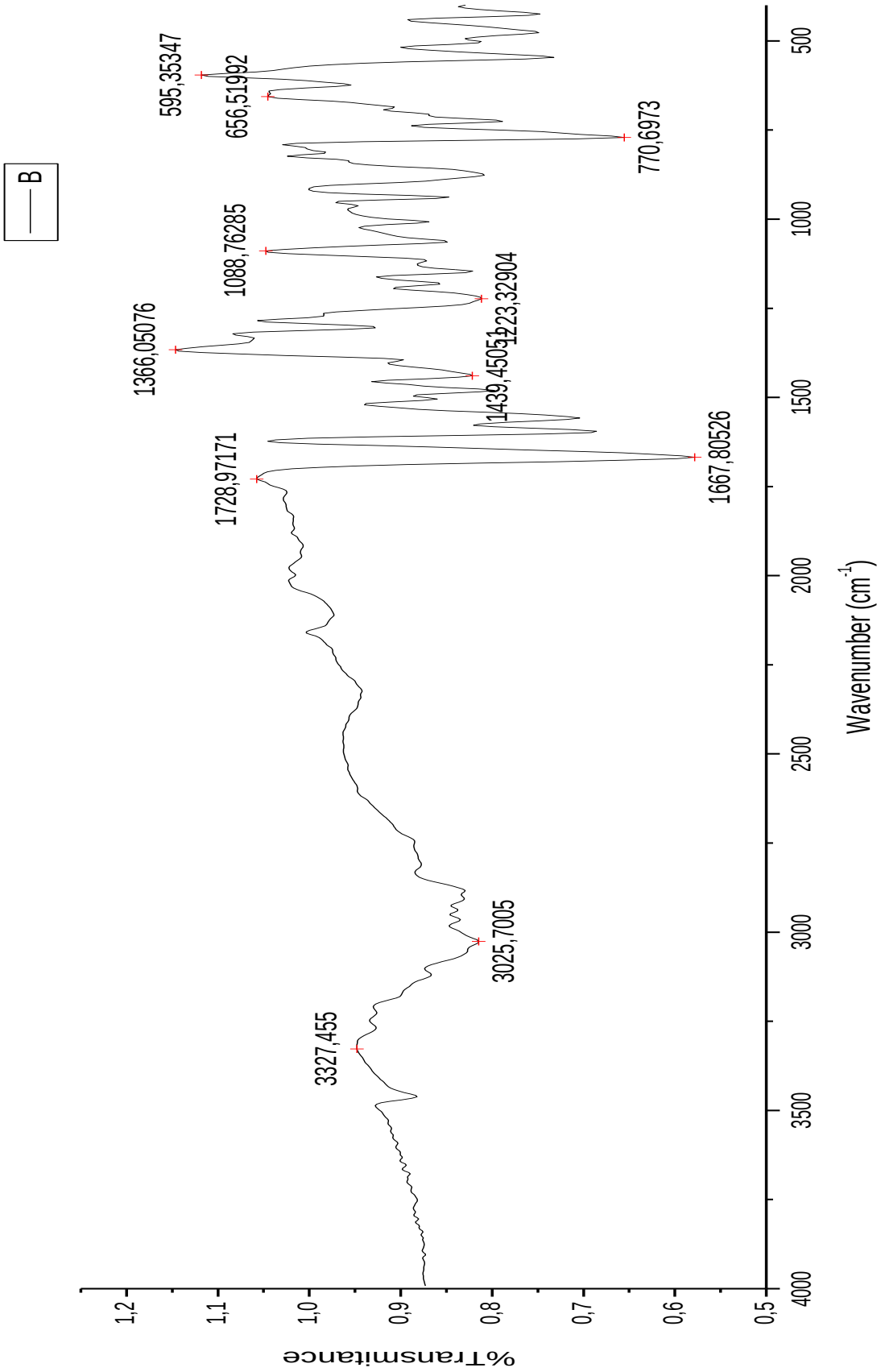

Figure 4.4: FTIR spectrum of **119b**.

4.2. Attempted synthesis of novel Zn(ll)-*N^N*-Schiff base complexes.

Coordination of Schiff base ligand (**119c**) to $ZnCl_2$ salt was attempted following literature method [8] in 100 % HPLC grade methanol by adding 1:1 mmol of (E)-N-(4-fluorobenzylidene)-2-(1H-imidazol-4-yl)ethanamine **119c** and $ZnCl_2$. The progress of reaction was monitored at room temperature in an NMR-tube for between 12 h and 24 h by ^{1}H-NMR. The ^{1}H-NMR spectra below indicate a loss in multiplicity from **Figure 4.5a-c** because the zinc has a spin 5/2 (I = 5/2) with a natural abundance of 4.102 %. From the ^{1}H-NMR, we observed signs of product formation as the $-CH_2^b$ and the imine proton both shifting downfield from the original chemical shift position of the ligand, i.e. from 3.87 ppm to 4.0 ppm and 8.23 ppm to 8.65 ppm. This effect is due to the electron donation imine nitrogen towards the metal centre. We also observe that, as the coordination to the metal centre proceeds, the ligand suffers decomposition as the aldehydic proton at 10.01 ppm and the two triplets peaks from the phenyl of the aldehyde in the aromatic region 7.01 ppm and 7.81 ppm reappear, which corresponds to the commercial starting material. Before the aforedescribed observation, a trial series of coordination reactions to the $ZnCl_2$ metal centre were investigated for ligands **119a-d**. In the first attempt, ligands **119a-d** were separately reacted with $ZnCl_2$ (1:1 mmol) in methanol at room temperature for 12 h. To our dismay, all variations gave a mixture of the aldehyde derivatives with histamine. We then investigated the effect of temperature, wherein we heated the reaction mixture to reflux (70-75 $^{\circ}$C) under nitrogen atmosphere for 24 h.To our disappointment the ^{1}H-NMR spectrum obtained was difficult to interpret as the data observed yielded unresolved broad peaks. We then reasoned that perhaps the poor results are due to the $ZnCl_2$ being subjected to moisture and would then prove detrimental to the ligands while stirriling in methanol. To avert this misfortune, the $ZnCl_2$ was oven-dried at 120 $^{\circ}$C and used immediately thereof. Even with this measure, the reaction presented yielded undesirable spectral data. We then changed the zinc salt to zinc(ll) acetate and repeated the above mentioned trials. However, to our dismay, a similar trend was observed across all ligands *i.e*. decomposition of the Schiff base ligand to give and aldehyde derivative and histamine.

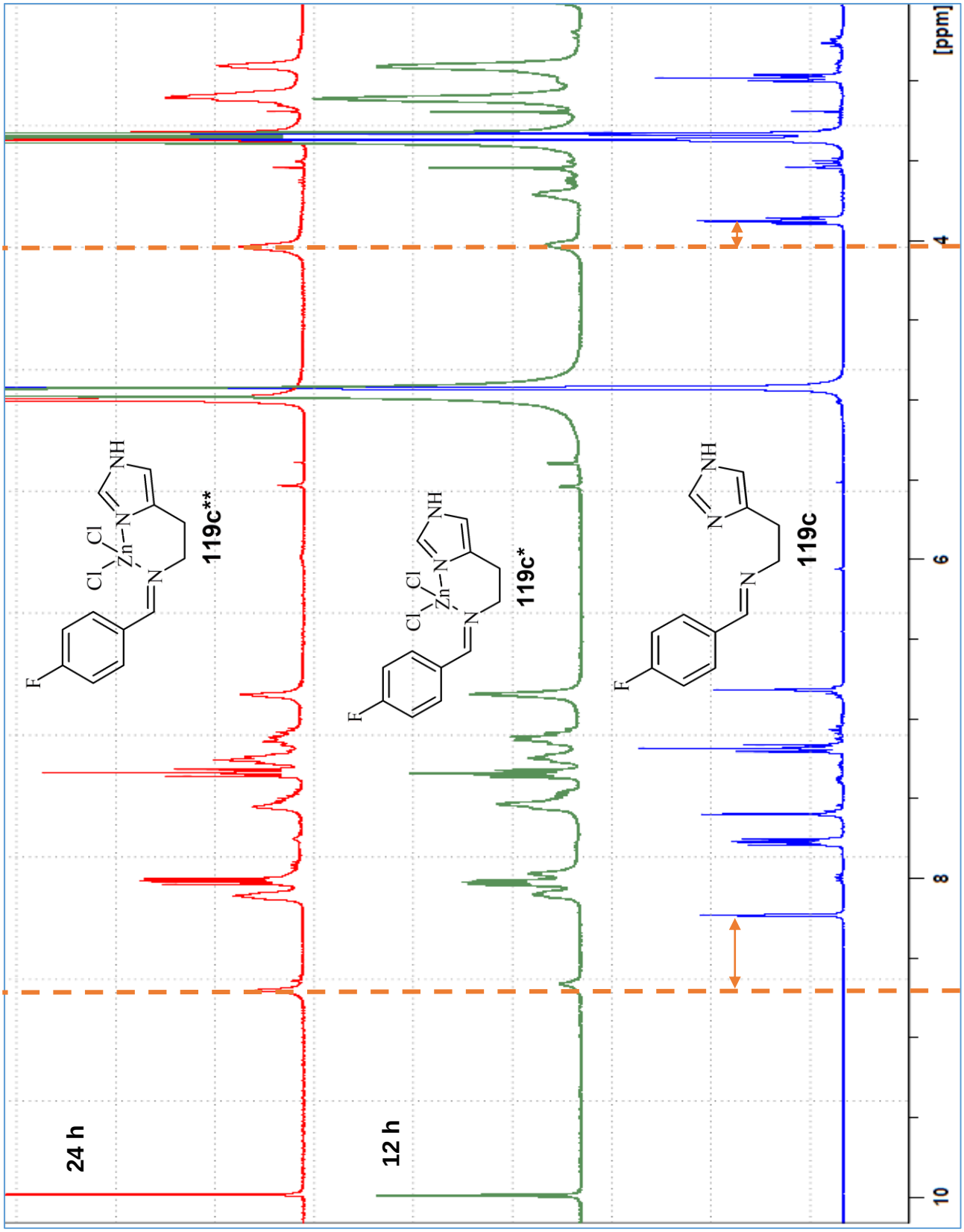

Figure 4.5: Overlaid ^{1}H-NMR spectra of ligand (**119c**) and the attempted reaction time for complexation by $ZnCl_2$ after 12 h (green) and 24 h (red).

4.3. Synthesis of quinazoline derivatives

The retrosynthetic analysis strategy for the synthesis of the target ligands **125a – e** for coordination to the monomeric *p*-cymene Ru(ll) piano stool centre is shown below in **Scheme 4.3** (except ligands **123a – e**).

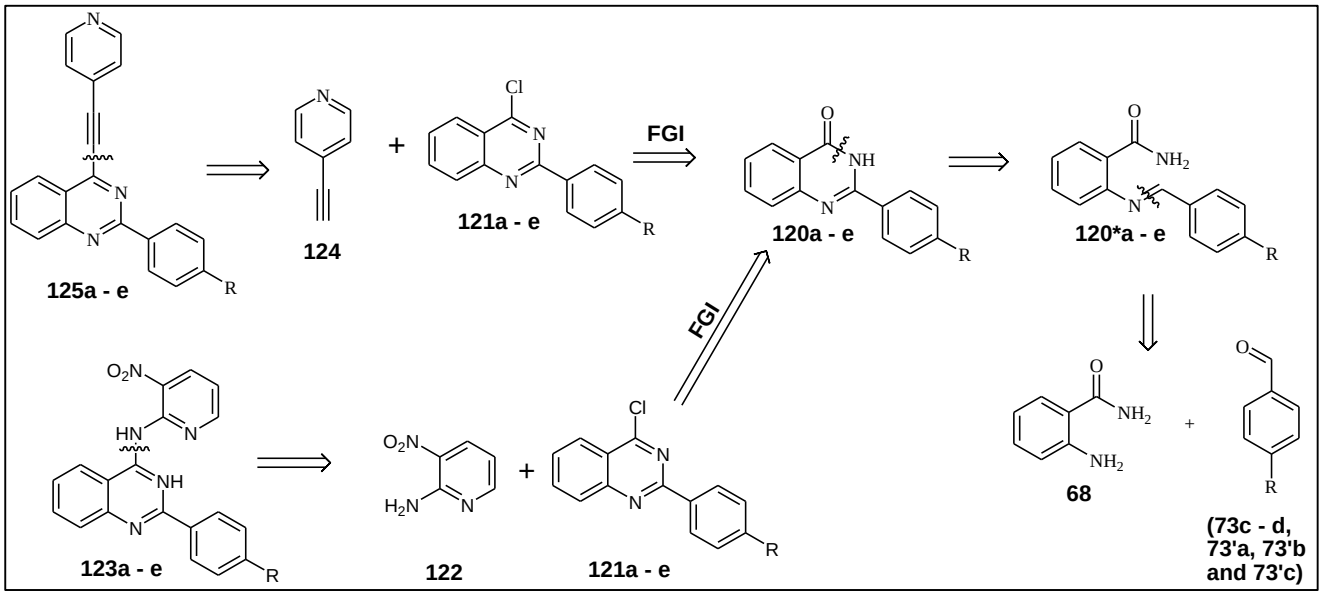

Scheme 4.3: Retrosynthetic strategy for the synthesis of the proposed 4-pyridyl-quinazoline ligands.

4.3.1 Synthesis of 2-aryl-quinazolin-4(3*H*)-ones

Compounds **120a – e**, were synthesised following a literature procedure [9]. The first requirement under this investigation was to synthesise the 2-aryl-quinazolin-4(3*H*)-ones **120a – e** to be used as substrates for the requisites 2-aryl-4-chloroquinazolines **121a – e**. To acquire the desired 2-aryl-quinazolin-4(3*H*)-ones **120a – e**, we performed a one-pot procedure through oxidative cyclocondensation of anthranilamide **68** with *para*-substituted benzaldehyde derivatives (**73c – d, 73a', 73b' and 73c'**) in the presence of molecular iodine (2 equiv.) in ethanol at 80 ^{o}C (**Scheme 4.4**).

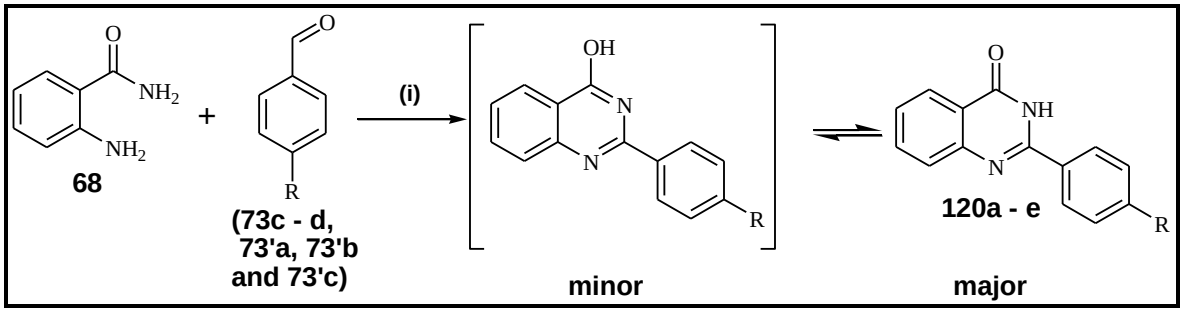

Reagents and conditions: (i) I_2 (2 equiv.), EtOH, 80 ^oC, 6 h.

Scheme 4.4: Iodine-promoted oxidative cyclocondensation of anthranilamide with aldehyde derivatives.

The molecular iodine serves as a promoter to effect cyclocondensation and oxidation reactions by introducing dehydrogenation on the *N-3* position [10]. The quinazolin-4(3*H*)-one framework is generally accessible through a dehydrogenation reaction of 2,3-dihyquinazolin-4(1*H*)-one precursors by treating the latter with oxidants in large excess of DDQ [10] and $KMnO_4$ [11]. Other synthetic methods include a one-pot procedure wherein a direct cyclocondensation between anthranilamide **68** and aldehyde derivatives **73** is catalysed by DDQ [12] or $NaHSO_2$ [13]. The literature procedure followed, induces keto-enol tautomerism, wherein the enol (quinazolinol-minor) is favoured at high temperatures (70-100 ^oC) and the keto (quinazolinone-major) oppositely, is favoured at low temperatures (≤ 20 ^oC) [9]. The tautomerism in this case was avoided by cooling the reaction vessel to room temperature and later bleaching with an ice-cold saturated sodium metabisulphate ($Na_2S_2O_5$). The synthesised compounds **120a – e**, were characterised using ^{1}H-NMR, ^{13}C-NMR, FTIR and melting point techniques. The ^{1}H-NMR spectra of compounds **120a – e** revealed the presence of a broad singlet at 12.75 ppm corresponding to the N-H proton of the alpha-nitrogen. Further expected protons in the aromatic region ranging from 7.53 – 8.20 ppm are assigned to the 2-phenyl substituent and the quinazoline backbone (**Figure 4.6**). The amide nature of the compounds are confirmed by FTIR due to the presence of C-N and C=O in the reagions v_{max} 1531 – 1583 cm^{-1} and v_{max} 1656 – 1691 cm^{-1}, respectively. The melting points recorded are consistent with those reported in literature [14].

Table 4.2: Summarised characterisation of compounds **120a – e**.

120	R	ν_{max} C=O (cm^{-1})	ν_{max} C-N (cm^{-1})	% Yield	m.p. (ºC)
a	4-Cl	1606	1531	87	295.2 – 297., lit (298 – 299) [14]
b	4-Br	1656	1544	91	>350, lit (>350) [14]
c	4-F	1605	1555	93	261.3 – 263.2, lit (257 – 259) [14]
d	4-NO_2	1601	1583	90	> 300, lit (>300) [14]
e	4-OMe	1691	1566	93	242.7 – 243.4, lit (240 – 241) [14]

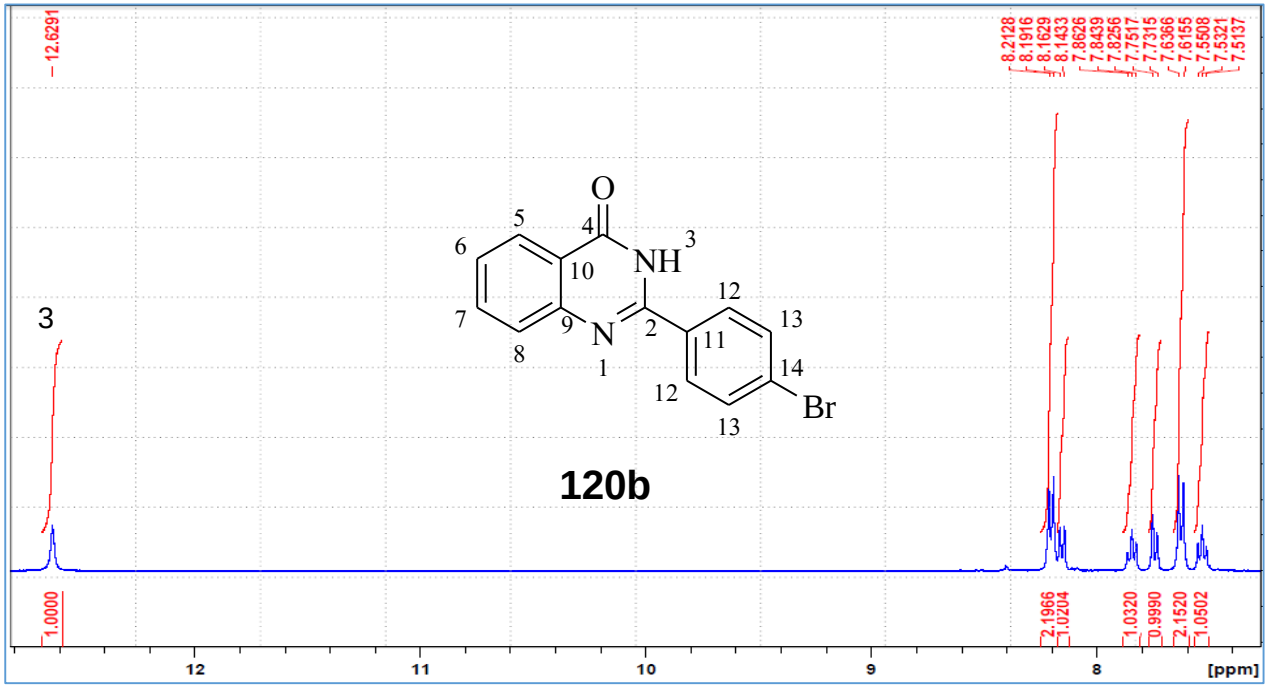

Figure 4.6: ^{1}H-NMR spectrum for compound **120b**.

4.3.2 Synthesis of 2-aryl-4-chloro-quinazolines

The next step was to generate an electrophilic centre at the 4-position of the scaffolds 2-aryl-quinazolin-4(3*H*)-ones **120a – e** through oxidative aromatisation to afford the 2-aryl-4-chloro-quinazolines **121a - e**. The compounds **121a – e** were successfully

synthesised following literature procedure [9], wherein the scaffolds 2-aryl-quinazolin-4(3*H*)-ones **120a – e** were treated with excess thionyl chloride using DMF as a solvent. The reaction was driven to completion by refluxing at 100 ^{o}C for 4 h (**Scheme 4.5**). The full conversion of the latter was confirmed by the absence of an N-H signal on the ^{1}H-NMR spectra of compounds **121a – e**. The FTIR spectra of the compounds **121a – e** revealed the absence of the C=O stretch thus confirming formation of the *C(4)-Cl* bond. Upon obtaining the requisites **121a – e**, we decided to explore the 4-position through dechloro-amination (**section 4.3.3)** and Sonogashira-cross coupling (**section 4.3.4)**. Both functionalities were successfully achieved and the compounds were characterised by ^{1}H-NMR, ^{13}C-NMR, FTIR spectroscopy and HRMS.

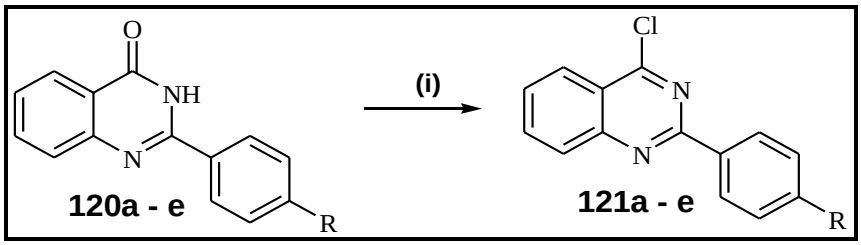

Reagents and conditions: (i) $SOCl_2$, DMF, 100 ^{o}C, 4 h.

Scheme 4.5: Oxidative aromatisation of 2-aryl-4chloro-quinazolines in $SOCl_2$

Table 4.3. Summarised characterisation of compounds **121a – e**.

121	R	% Yield	m.p. (^{o}C)
a	4-Cl	88	143.2 – 145.4
b	4-Br	93	151.7 – 153.4
c	4-F	90	137.2 – 139.3, lit (139 – 141) [15]
d	4-NO_2	84	148.1 – 150.2
e	4-OMe	89	144.3 – 146.6

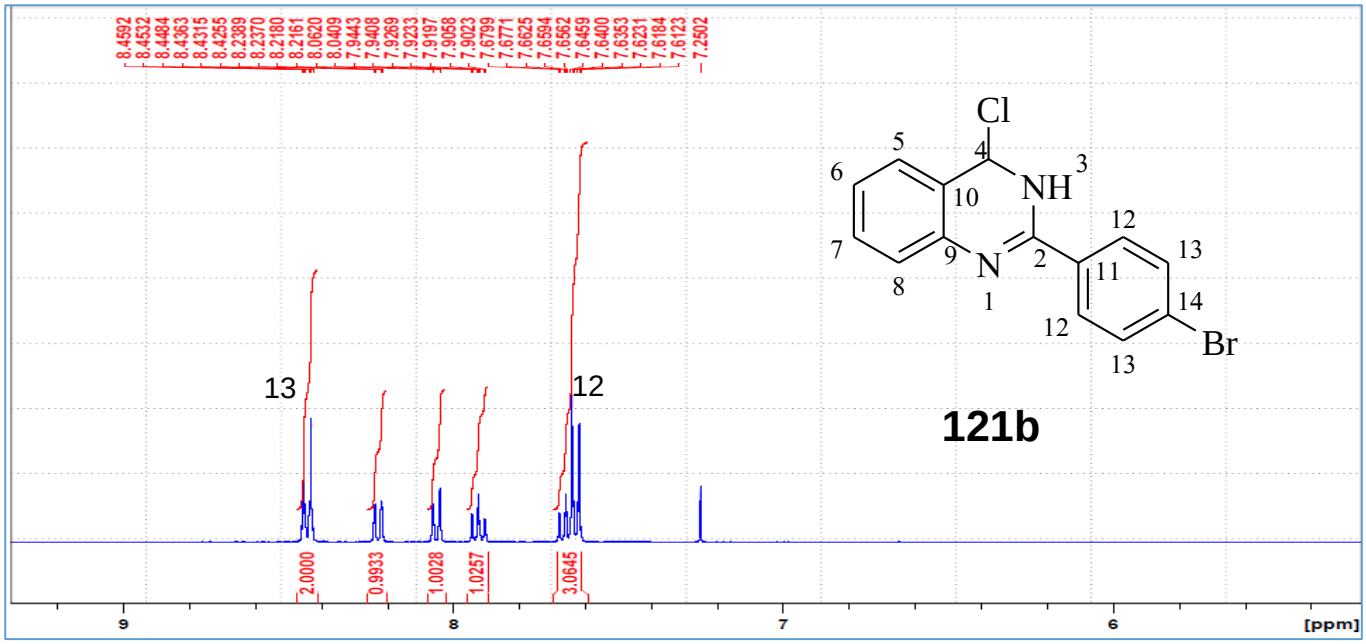

Figure 4.7: ^{1}H-NMR spectrum of compound **121b**.

4.3.3 Dechloro-amination of 2-aryl-4chloro-quinazolines 121a – e

The Synthesis of 2-aryl-*N-(3-nitropyridin-2-yl)quinazolin-4-amine* **123a – e** was achieved through a modified procedure of Paumo and co-workers [16]. The orginal literature procedure employs a combibnation of THF-*i*-PrOH and HCl. The HCl protonates the *N*-1 position of the 4-chloroquinazolines and renders the hetercylclic ring electron deficient and *C*-4 more electrophilic. Based on this observation, we employed **122** and **121b** in the conditions of the literature procedure, unfortunately the reaction yielded trace amounts of the desired product. The reason for undesired yield was due to the poor solubility of **122** in the solvent mixture *i.e*. THF-*i*-PrOH. To improve the solubility, a mixture of THF-DMF (3:1) together with 98% Sulfuric acid serving as a catalyst was applied to afford **123a - e** (**Scheme 4.6**). The formation of compounds **123a - e** was confirmed by the appearance of an N-H signal at 12.6 ppm as observed on the represenative ^{1}H-NMR spectrum (**Figure 4.8**). The presence of the N-H was further confirmed by a signal in the region 3461-3464 cm^{-1} on IR. Furthermore, the FTIR spectra of compounds **123a - e** reflected bands for (C-N) at 1666 cm^{-1}. These type of compounds are easily distinguished by ^{1}H and ^{13}C-NMR spectroscopic techniques from the preceding substrates. Ligand **123b** is here described, from the ^{1}H-NMR spectrum (**Figure 4.8**), additional signals showing multiplicities of dd, br-s and a mulitiplet in the aromatic region from 6.73 ppm to 8.4 ppm are observed. From

the ^{13}C-NMR (**Figure 4.9**), we observe the quaternary carbon (**20-C**) of the nitro-deshielded group resonating at 149 ppm. Furthermore, the molecular ion of the mass spectra revealed the absence of the M+ and M2+ but instead HMRS (ESI+) revealed M+Na (444.9536) for **123b**. Similar findings were observed for **123d** (411.0530). However for **123a** HRMS (ESI+) revealed only $C_{19}H_{12}N_5O_2^+$ indicating replacement of the 4-Cl, due to the absence of chlorine isotopes (m/z 35 and 37).

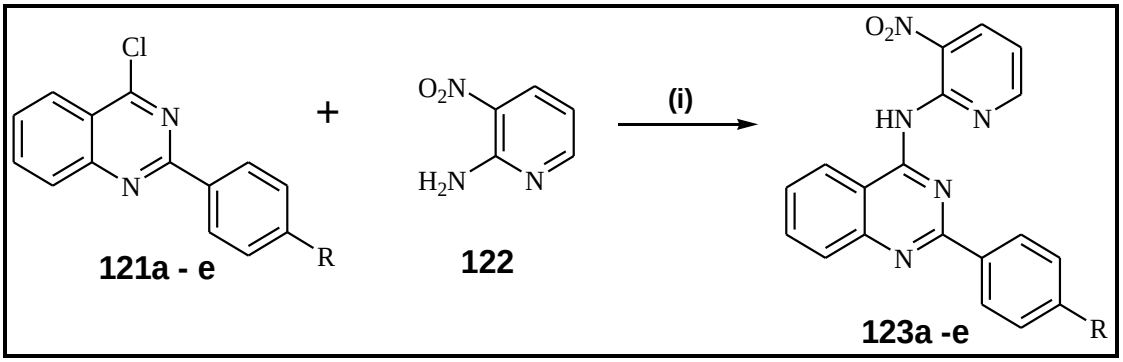

Reagents and conditions: (i) 98% sulphuric acid, TH-DMF, 70 ^{o}C, 5 h.

Scheme 4.6: De-chloro amination of 2-aryl-4chloro-quinazolines **121a-e**.

Table 4.4: Summarised characterisation of compounds **123a – e**.

123	R	N-H v_{max} cm^{-1}	% Yield	m.p. (^{o}C)
a	4-Cl	3461	95%	281.2 – 282.1
b	4-Br	3462	78%	292.1 – 284.1
c	4-F	3463	92%	273.8 – 274.8
d	4-NO_2	3462	66%	269.2 – 271.2
e	4-OMe	3464	84%	262.4 – 264.4

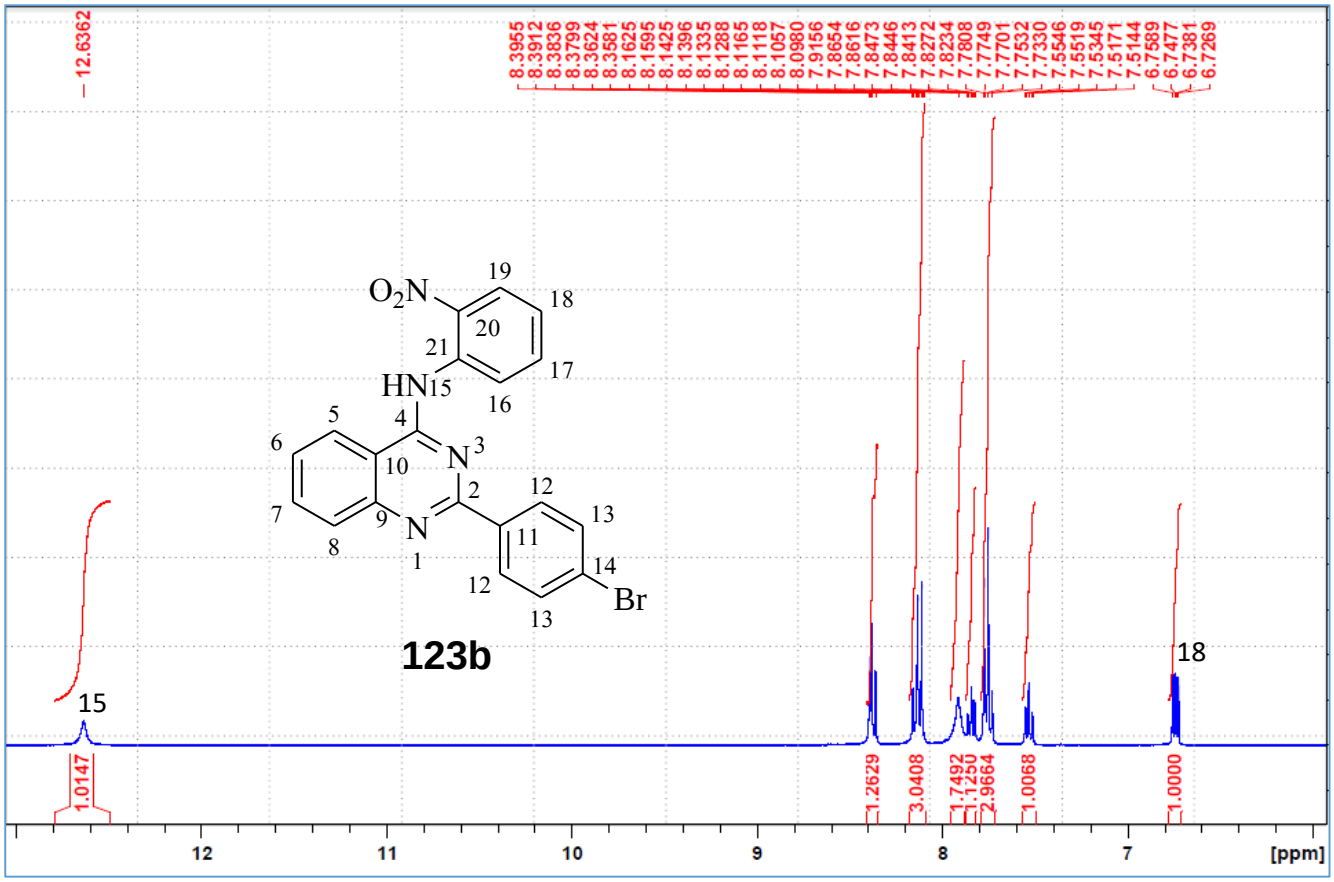

Figure 4.8: ^{1}H-NMR spectrum of compound **123b**.

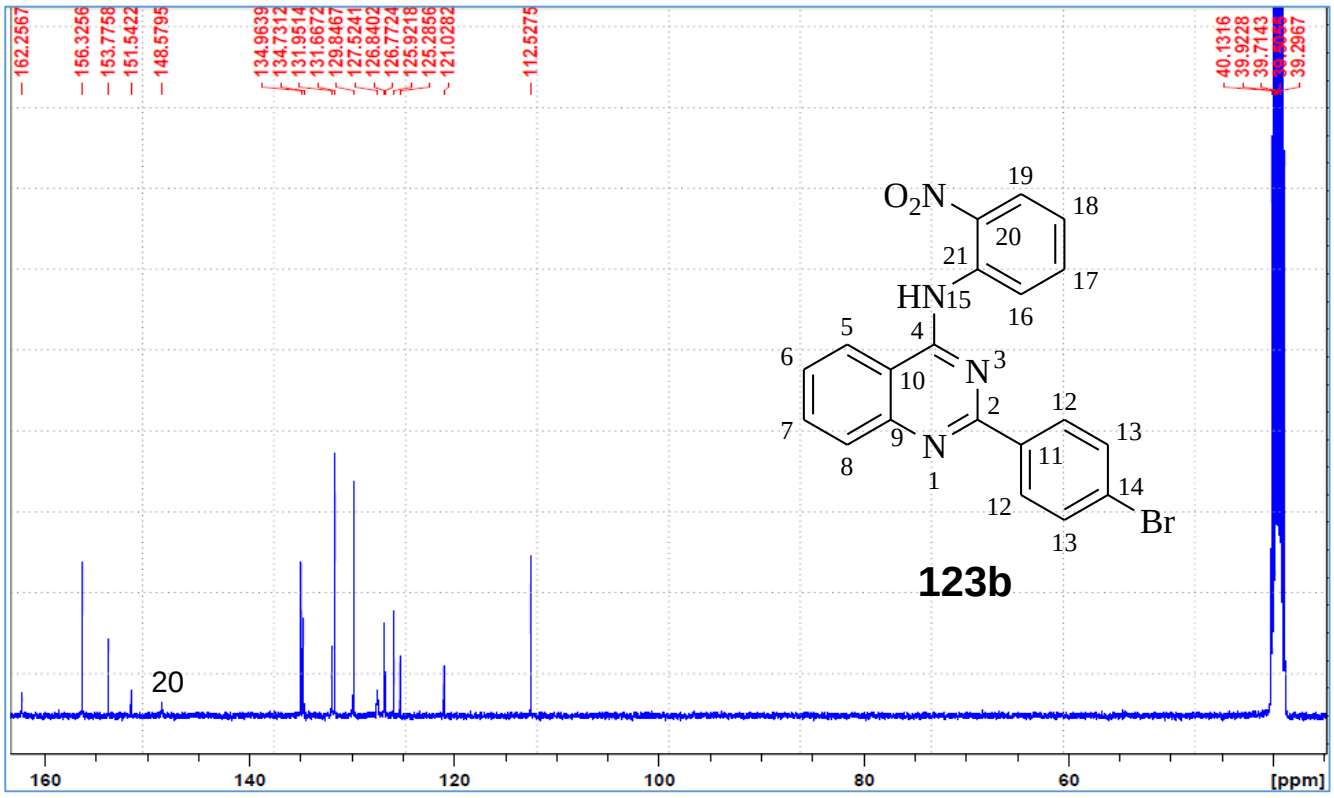

Figure 4.9: ^{13}C-NMR spectrum of compound **123b**.

4.3.4. Sonogashira cross-coupling of 2-aryl-4chloro-quinazolines 121a – e.

The final step in the synthesis of ligands for coordination was to perform Sonogashira cross-coupling reaction on the *C(4)-Cl* position of the 2-aryl-4chloro-quinazolines **121a – e**.The choice of Sonogashira cross-coupling in this case, is to create a two-carbon spacer forming a linear bridge to minimise steric hindrance when coordinating to the monomeric *p*-cymene Ru(ll) piano stool centre. Prior to this step, the substrate 4-ethynylpyridine **124** was successfully coupled following Sonogashira using palladium-catalysed coupling reactions (**Scheme 4.7**). Comparatively, there are few reported cases of Sonogashira coupling reactions between 4-chloroquinazolines and terminal alkynes to significant cases of Suzuki-Miyaura coupling [17]. Accordingly, 4-chloro-2-arylquinozaline was varied with groups such as (R = -Br, -Cl, -F, -NO_2 and -OMe) on the *para* position of the phenyl ring on the 2-position.

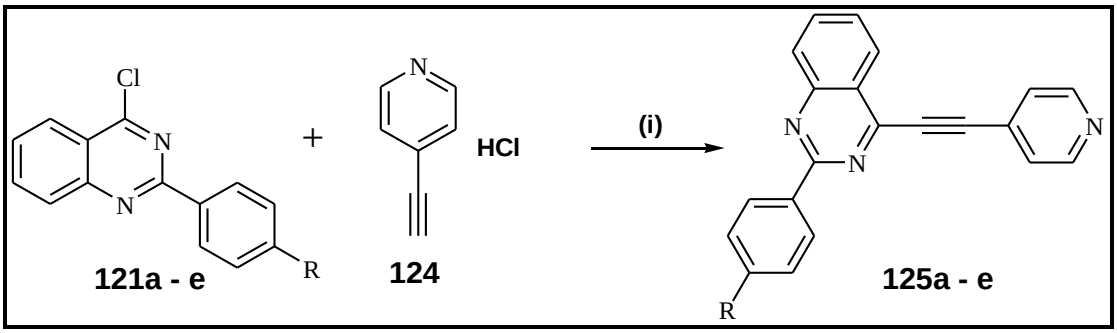

Reagents and conditions: (i) $PdCl_2(PPh_3)_2$, CuI, Cs_2CO_3, THF-water (3:1), 65 ^oC, 24 h

Scheme 4.7: Sonogashira cross-coupling of 2-aryl-4chloro-quinazolines **121a – e** with 4-ethynylpyridine

Our first attempt in the application of Sonogashira cross-coupling conditions at the 4-chloroquinazoline, we employed $Pd(PPh_3)_4$, CuI, Et_3N and 1.5 equiv of 4-ethynylpyridine in dry THF at mild temperatures (40-60 ^oC). Unfortunately we isolated only the starting material **121a** and **124** along with Et_3N. The Pd(0) source, tetrakis(triphenylphosphine)palladium(0) is air and moisture sentive, therefore proving difficult to employ for Sonogashira cross-coupling. We then substituted the palladium source with $PdCl_2(PPh_3)_2$ and kept the other reagents constant, unfortunately this attempt led to recovery of starting material. Further attempts in high boiling solvent such as DMF and Dioxane were also unsuccessful. These results were attributed to Et_3N not being basic enough to deprotonate the terminal alkyne that should in turn

give an anionic nucleophile to form the copper acetylide [18]. Trace amounts of our desired product were obtained when using K_2CO_3, Na_2CO_3 and NaOH as our base during coupling. Since the Sonogashira reaction mechanism requires a relatively strong base to deprotonate the terminal acetylene **124**, we then opted for Cs_2CO_3. In a one-pot, 4-Chloro-2-(4-chlorophenyl)quinazoline **121a** (1 equiv.) was reacted with $PdCl_2(PPh_3)_2$ (10%), CuI (10%) and Cs_2CO_3 (2 equiv.) in 3:1 THF-water, the reaction was left to stir for 24 h at mild heat (40-60 ^oC) under N_2. To our delight we isolated 98% of **125a** after recrystalisation from diethyl ether. Synthesis of ligands **125b – e** followed that of **125a** while varying the *para*-position of the 2-aryl group. The formation of **125a - e** was confirmed using ^1H and ^{13}C-NMR. Ligand **125b** is here described, on the ^1H-NMR spectrum (**Figure 4.10**) we observed additional two additional doublet peaks resonating at 7.60 (18-H) and 8.74 ppm (19-H). On the ^{13}C-NMR spectrum (**figure 4.11**) additional carbons of the two-carbon spacer resonate at 88.216 (15-C) and 93.712 (16-C) ppm are observed. Further characterisation using FTIR spectroscopy showed the presence of *Csp-Csp* band at ν_{max} 2219.44 cm^{-1}.

Table 4.5: Summarised characterisation of compounds **125a – e**.

125	R	ν_{max} *Csp-Csp* cm^{-1}	% Yield	m.p. (^oC)
a	4-Cl	2219.92	98	209.2 – 210.0
b	4-Br	2219.44	90	234.6 – 236.3
c	4-F	2220.15	94	197.6 – 199.2
d	4-NO_2	2219.71	94	272.7 – 274.8
e	4-OMe	2218.70	79	202.6 – 204.6

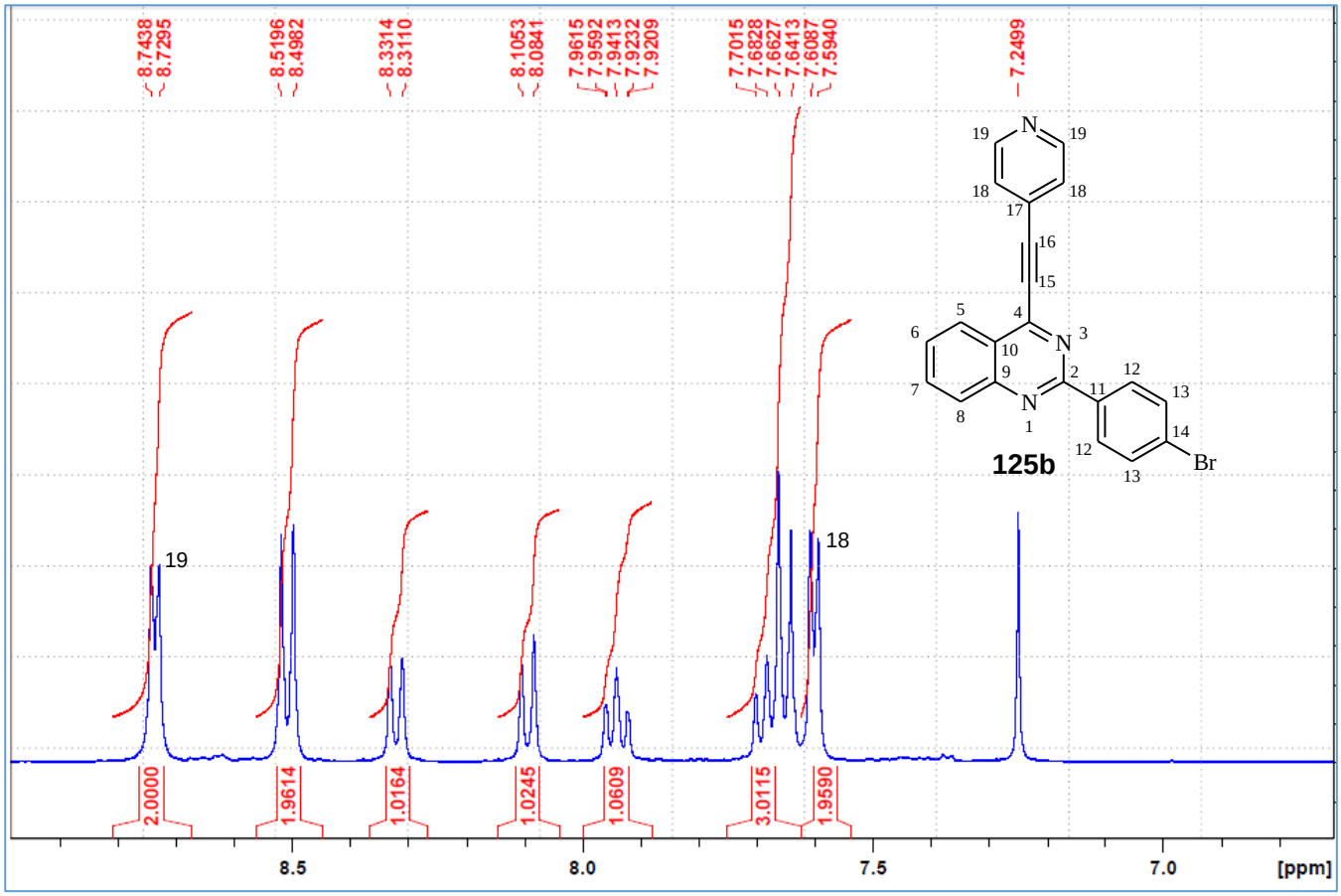

Figure 4.10: ^{1}H-NMR spectrum of compound **125b**.

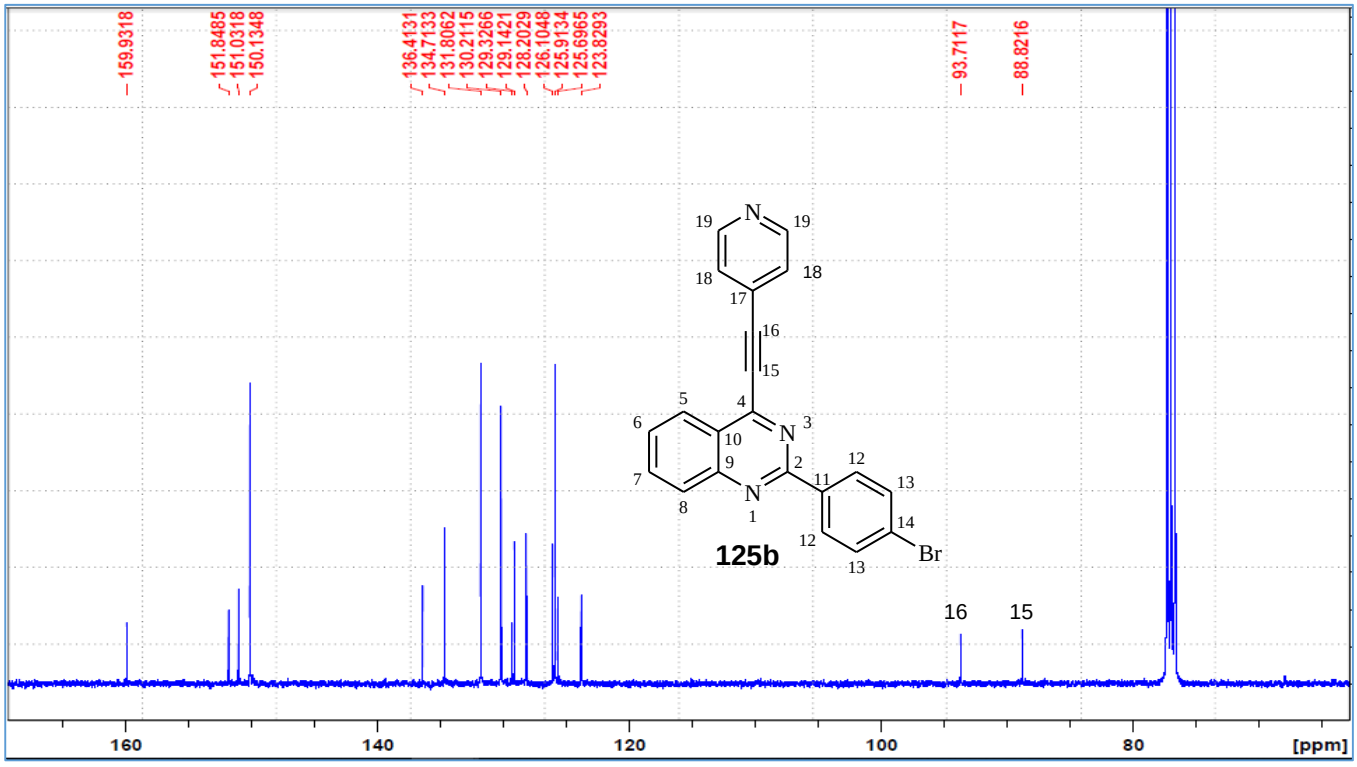

Figure 4.11: ^{13}C-NMR spectrum of compound **125b**.

4.3.5. Coordination of ligands 125a – e to monomeric p-cymene Ru(II) piano stool centre to yield 126a – e.

Three-legged piano-stool Ru(II)/ Ru(III) bearing an arene, *p*-cymene, cyclopentadienyl and heterocyclic caps have come under intense exploration due to their interesting anticancer, anti-metastatic and anti-proliferative properties [19]. These type of complexes are accessible by refluxing a ruthenium dimer and the ligand of interest in a polar solvent [20]. Some ligands however, adopt a double replacement of the lateral chlorine ligands to form a cationic complex which is balanced by anionic counterion. Castonguay and co-workers [21] reported similar complexes wherein, two letrazole ligands were coordinated to monomeric piano-stool arene Ru(II) complex by refluxing in dichloromethane (DCM). The authors reasoned that characterisation of the complex using NMR techniques, ^{1}H-NMR in particular, was less straightforward as the letrazole ligands were found to be labile in $CDCl_3$. This then facilitated replacement of one letrazole ligand by a chloride counterion of the requisite Ru(II) dimer.

Herein, ethynylpyridine-bridged Ru(II)-*p*-cymene bis-chloride complexes were successfully synthesised following a modified procedure reported by Saez and co-workers [22], *i.e.* instead of refluxing the Ru(II) dimer and ligand in methanol, the antecedent reagents were heated to reflux in hexane for 5 hrs to obtain **126a** – **e** in good yields 67 – 90%. The complexes were characterised using NMR (^{1}H, ^{13}C and HMBC) and HRMS.

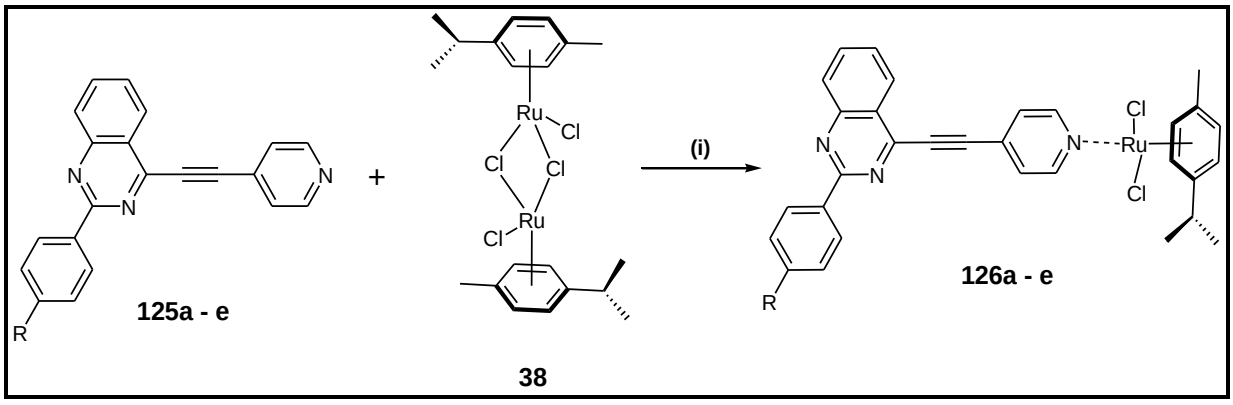

Reagents and solutions: Hexane, 60 ^{o}C, 5 hrs, rt, 12 hrs.

Scheme 4.8: One-pot synthesis of quinazoline monomeric *p*-cymene Ru(II) piano stool centre.

Two representative complexes (**126c** and **126e**) are here described in details. Complex **126e** was characterised using ^{1}H-NMR (**Figure 4.12**). From the ^{1}H-NMR we were able to differentiate the complex (**126e**) from its preceding substrate **125e** due to the addition of *p*-cymene protons within the region 1.320 – 5.483 ppm. The upfield peak resonating at 1.320 ppm is assigned to the two methyl groups 26-H which is spin-couples (^{1}H-^{1}H) with 27-H to give an intense doublet ($^{3}J_{H\text{-}H}$ = 6.8 Hz) peak. The neighbouring singlet at 2.125 ppm is assigned to 21-H and the peak at 2.996 ppm is assigned to 27-H which spin-couples with the two germinal methyl groups to give a septet ($^{3}J_{H\text{-}H}$ = 27.6 Hz). Furthermore, the two set of doublets ($^{2}J_{H\text{-}H}$ = 6 Hz) around 5.2 and 5.4 ppm are assigned to symmetrical protons 23-H and 24-H. The carbons on the cymene ligand (**Figure 4.13**) all resonate relatively upfield within the region 18.276 – 83.022 ppm except the two quartenary carbons 22-C and 25-C. Further interpretations on the ^{1}H-NMR and ^{13}C-NMR spectra include the de-shielding effect brought by coordination to Ru(ll) centre. In 1988, Orellana and co-workers [23] reported a study based on coordination induced shifts (CIS) wherein their study involved ruthenium(II) tris chelates containing pyridyl heterocyclic ligands. During their investigation, they assigned factors that affect CIS, calculated as CIS = $\delta_{complexed}$ - δ_{free}, to be σ-donation, π-back donation, magnetic anisotropy of surrounding ligands, residual paramagnetism and solvent variation. All ^{13}C and ^{1}H-NMR assignments for **126e** are summarised in Table **4.5a**. In this investigation, almost all the ^{1}H and ^{13}C nuclei are de-shielded, this is due to the σ-donation by the 2-(4-methoxyphenyl) group, which in turn promotes de-shielding of the protons and carbons on the quinazoline backbone. Noticeable de-shielded protons and carbons are 20-H and 20-C which are de-shielded by 0.428 and 4.9 ppm respectively. More de-shielded groups include the quaternary carbons (16 and 17-C) of the ethynylpyridine bridge, with a CIS of 8.59 and 10.54 ppm respectively.

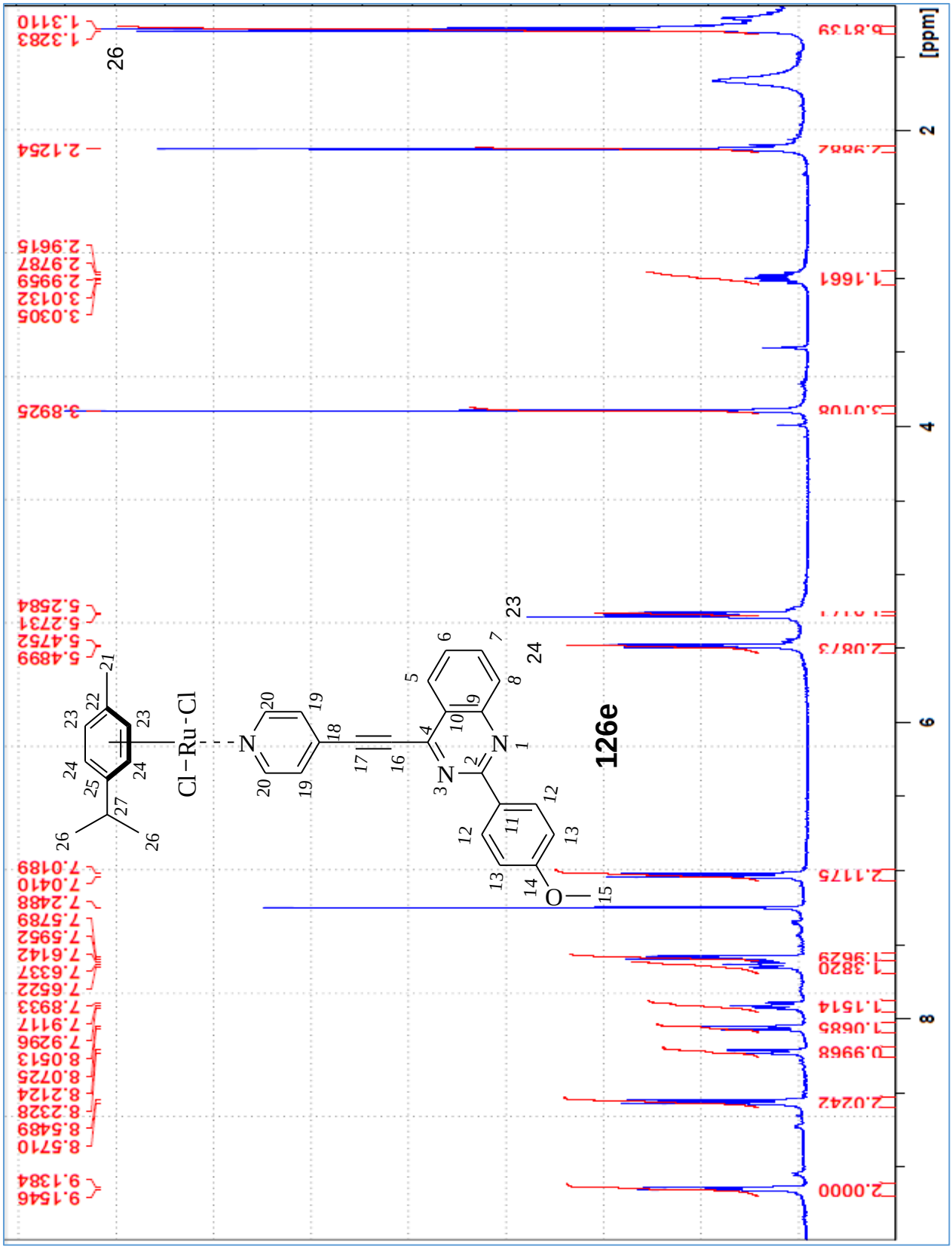

Figure 4.12: ^{1}H-NMR spectrum of compound **126e**.

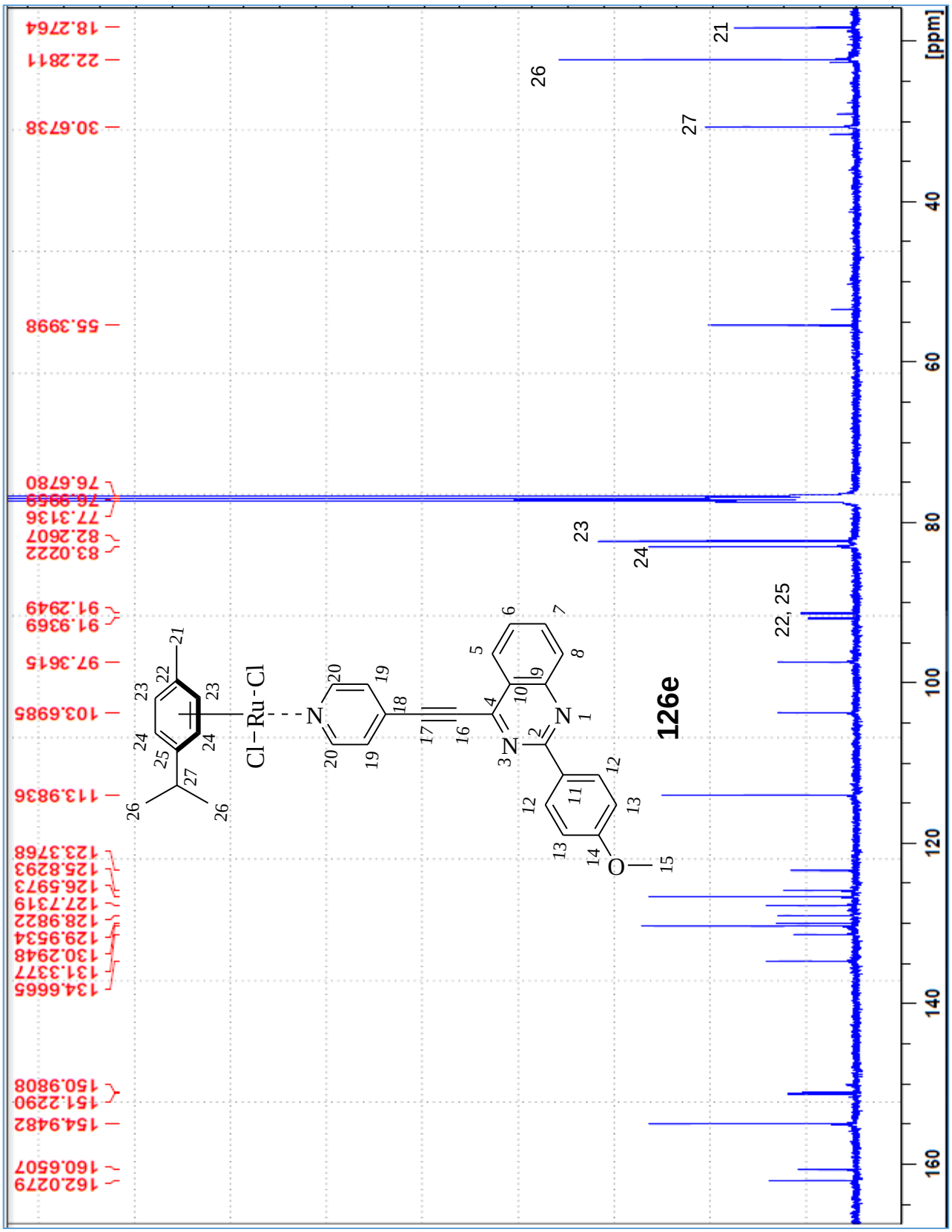

Figure 4.13: ^{13}C-NMR spectrum of compound **126e**.

Table 4.6a. ^{1}H and ^{13}C coordination induced shifts for Ru(ll) complex **126e**

CIS = $\delta_{complexed}$ - δ_{free} for δ_H				**CIS = $\delta_{complexed}$ - δ_{free} for δ_C**		
#	Complexed	Free ligand	^{1}H-CIS (ppm)	Complexed	Free ligand	^{13}C-CIS (ppm)
2				162.03	161.94	0.09
3						
4				151.23	151.60	-0.37
5	8.062	8.043	0.019	125.83	125.90	-0.07
6	7.652	7.619	0.033	126.60	126.00	0.6
7	7.912	7.881	0.031	134.67	134.41	0.26
8	8.223	8.264	-0.041	128.98	128.88	0.1
9				150.98	151.11	-0.13
10				127.73	127.43	0.3
11				129.95	130.08	-0.13
12	8.560	8.572	-0.012	131.34	130.37	0.97
13	7.03	7.024	0.006	113.98	113.91	0.07
14				160.65	160.60	0.05
15	3.893	3.880	0.013	55.40	55.35	0.05
16				97.36	89.04	8.59
17				103.70	93.16	10.54
18				123.38	123.42	-0.04
19	7.587	7.586	0.001	130.29	130.28	0.01
20	9.147	8.719	0.428	154.95	150.05	4.9

Similar to complex **126e, 126c** was analysed for CIS effect. The ^{1}H-NMR spectrum (**Figure 4.14**) of **126c** shows expected additions of cymene protons within the region 1.304 - 5.487 ppm. Within the same line as complex **126e**, the intense doublet ($J_{H\text{-}H}$ = 7.2 Hz) is assigned to 25-H germinal methyl groups, the singlet peak at 2.108 ppm is assigned to 20-H. The septet peak at 2.975 ppm is assigned to proton 26-H ($J_{H\text{-}H}$ =

26.5 Hz). The two set of doublets ($J_{H\text{-}H}$ = 6 Hz) resonating around 5.4 ppm are assigned to the symmetrical protons 22, 23-H. The carbons on the cymene ligand (**Figure 4.15**) resonate relatively upfield within the region 18.254 – 83.020 ppm except the two quartenary carbons 21-C and 24-C. The CIS calculations for complex **126c** gave a great deal of variation (**Table 4.5b**), as almost all the protons and carbons on the quinazoline backbone are shielded upon coordination to the Ru(ll) centre, the reason for this unexpected transition could be due to the electron withdrawing effect of 2-(4-fluorophenyl). However, the quaternary carbons 15 and 16-C carbons of the ethynylbridge, are de-shielded by 8.47 and 9.99 ppm respectively and the same applies to the symmetrical protons and carbons (19-H and 19-C) of the pyridyl group, which have a CIS of 0.405 and 4.8 ppm respectively.

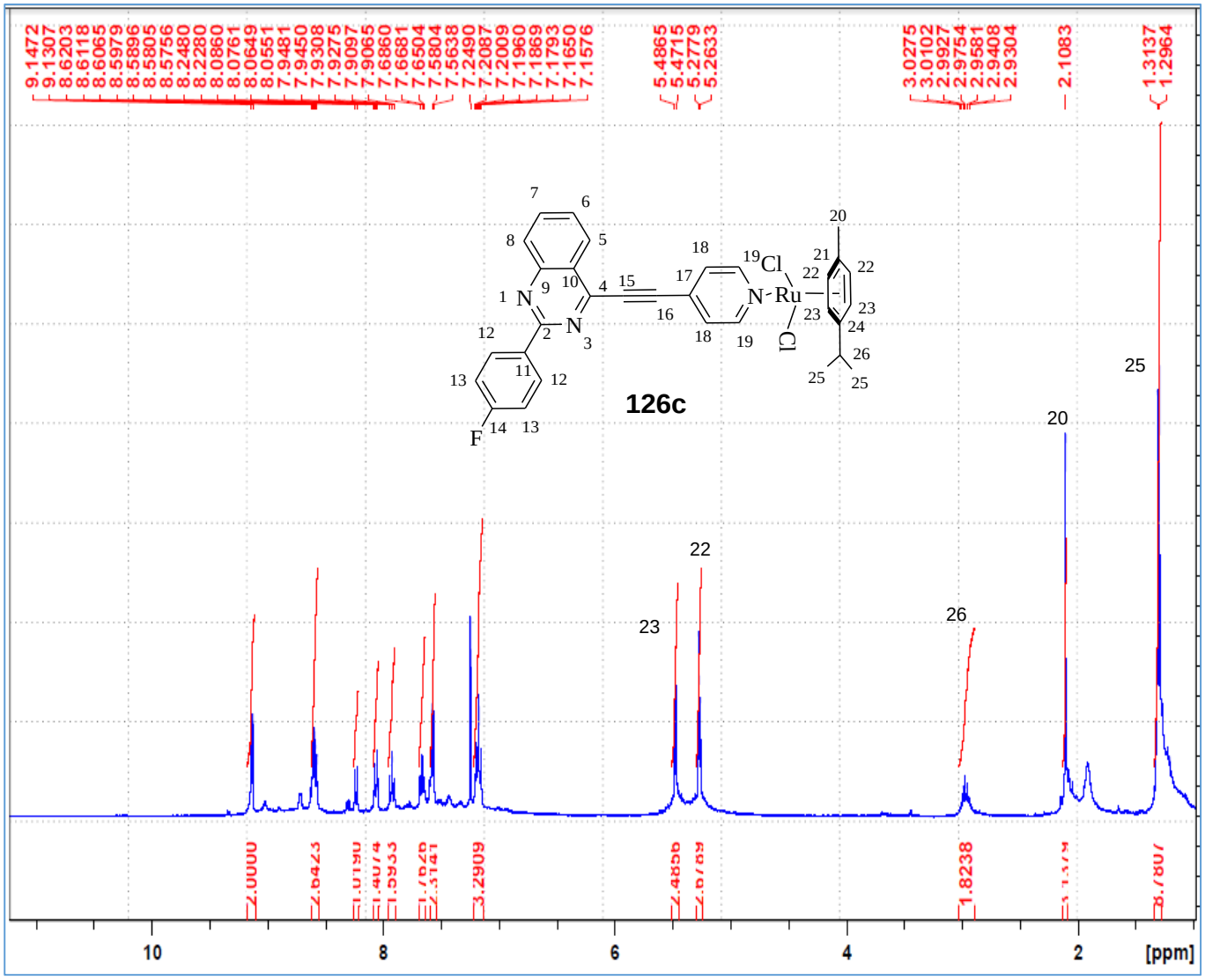

Figure 4.14: ^{1}H-NMR spectrum of compound **126c**.

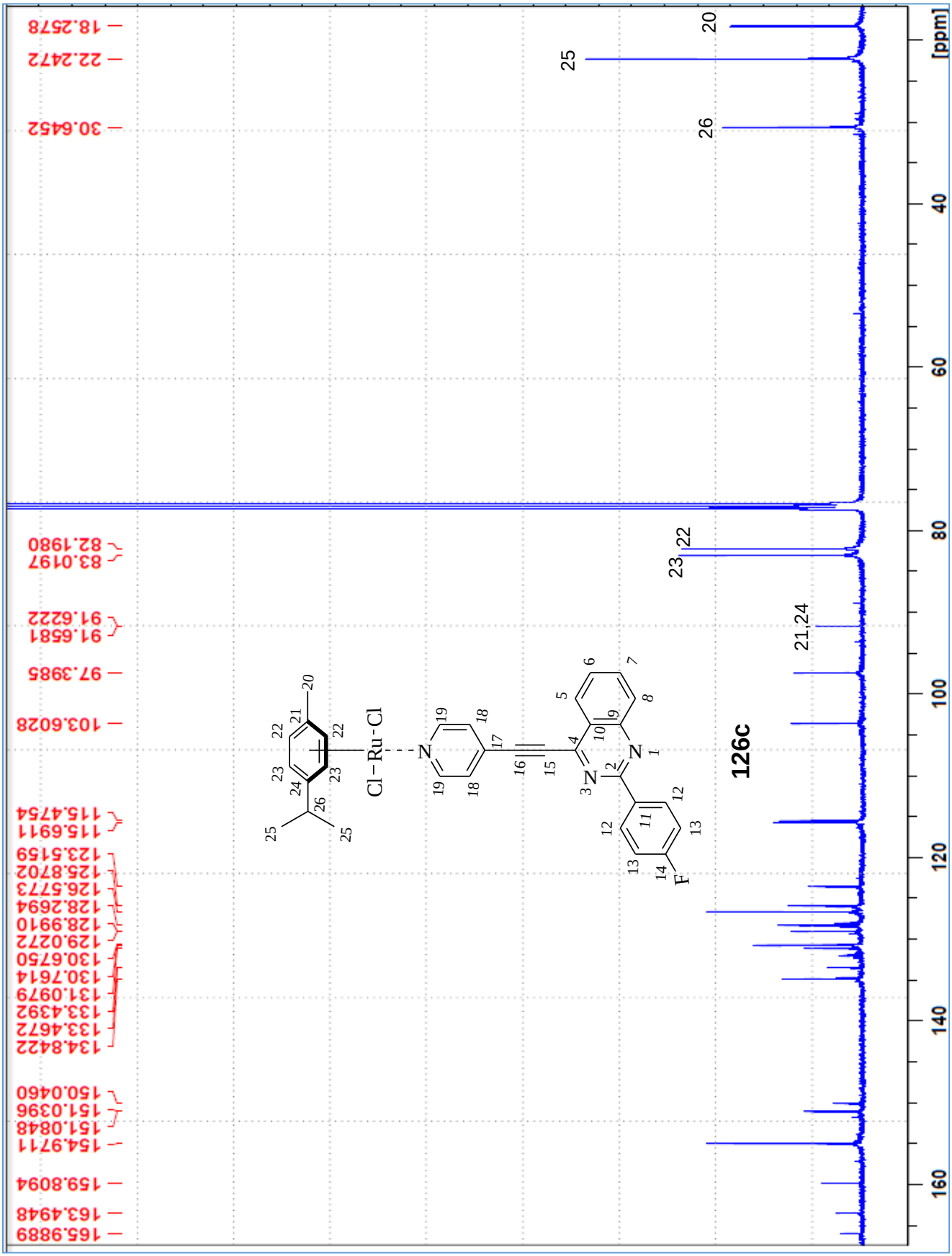

Figure 4.15: ^{13}C-NMR spectrum of compound **126c**.

Table 4.6b: ^{1}H and ^{13}C coordination induced shifts for Ru(ll) complex **126c**

CIS = $\delta_{complexed}$ - δ_{free} for δ_H				**CIS = $\delta_{complexed}$ - δ_{free} for δ_C**		
#	Complexed	Free ligand	^{1}H-CIS (ppm)	Complexed	Free ligand	^{13}C-CIS (ppm)
2				159.83	160.00	-0.17
3						
4				150.05	151.86	-1.81
5	7.668	7.667	0.001	125.87	126.11	-0.24
6	7.928	7.936	-0.008	129.01	128.02	0.99
7	8.06	8.093	-0.876	134.84	134.67	0.17
8	8.238	8.322	-0.084	128.39	129.13	-0.74
9				151.06	151.13	-0.07
10				131.10	129.41	1.69
11				133.47	133.73	-0.26
12	7.187	7.201	-0.014	130.72	130.83	-0.11
13	8.590	8.641	-0.051	115.58	115.62	-0.04
14				164.74	164.85	-0.11
15				97.40	88.93	8.47
16				103.60	93.61	9.99
17				123.52	123.72	-0.2
18	7.572	7.602	-0.03	126.57	125.93	0.64
19	9.139	8.734	0.405	154.97	150.17	4.8

The pyridyl 19-H (20-H) and 19-C (20-C) hydrogen and carbon atoms show great shifts after coordination to Ru(ll) centre. Coordination induced shifts for complexes **126a-e** are summarised on **Table 4.6c**.

Table 4.6c. Summarised selected ^{1}H and ^{13}C shifts for complexes **126a-e**.

126	**R**	**%Yield**	**^{1}H-shift (ppm) (19-H (20-H))**	**^{13}C-shift (ppm) (19-C(20-C))**
a	-Cl	90	9.160	155.03
b	-Br	67	9.170	155.07
c	-F	80	9.139	154.97
d	-NO_2	81	9.165	155.06
e	-OMe	71	9.147	154.95

N.B 20-H and 20-C refer only to complex **126e**

In order to establish the connectivities between the proton and carbon nuclei of the cymene group and the ethynylpyridine quinazoline ligand, we performed a long range 2D ^{1}H-^{13}C-HMBC experiment for complex **126e**. The 2D-HMBC spectrum below (**Figure 4.16**), revealed interesting $^{1\text{-}9}J_{CH}$ couplings between the cymene group and the the ethynylpyridine quinazoline, especially for protons and carbons along the ethynyl bridge. An intense correlation between protons 24, 23-H and carbon 26-C interact through a $^{1}J_{CH}$ coupling. A significant correlation between 24-H, 23-H and the ethynyl carbon 17-C through $^{9}J_{CH}$ coupling is observed. Similarly, another significant proton 21-H correlation with carbon 21-C through $^{1}J_{CH}$ coupling, 24-C through $^{4}J_{CH}$ and with 16-C through $^{8}J_{CH}$ coupling is also observed. Proton 27-H correlates with carbon 16-C through $^{9}J_{CH}$ coupling. Further correlations observed for long range couplings are viewed as 23-H shares a strong correlation with ethynyl carbon 16-C through $^{8}J_{CH}$ coupling, but shares a weak interaction with 17-C through $^{9}J_{CH}$ coupling. By the same note, 24-H shares a strong correlation with 17-C through $^{8}J_{CH}$ coupling and a weak correlation with 16-C through $^{9}J_{CH}$ coupling. The observed $^{8}J_{CH}$ and $^{9}J_{CH}$ coupling are mainly due to the *pi*-connection system which reduces the bond lengths between the carbons and therefore facilitates longer range coupling. Further correlations linking the cymene and the ethynylpyridine brigde are observed as 19-H symmetrical hydrogens interact with quaternary carbon 22-C. These correlations are confirmed for complex **126c** on **Figure 4.17**.

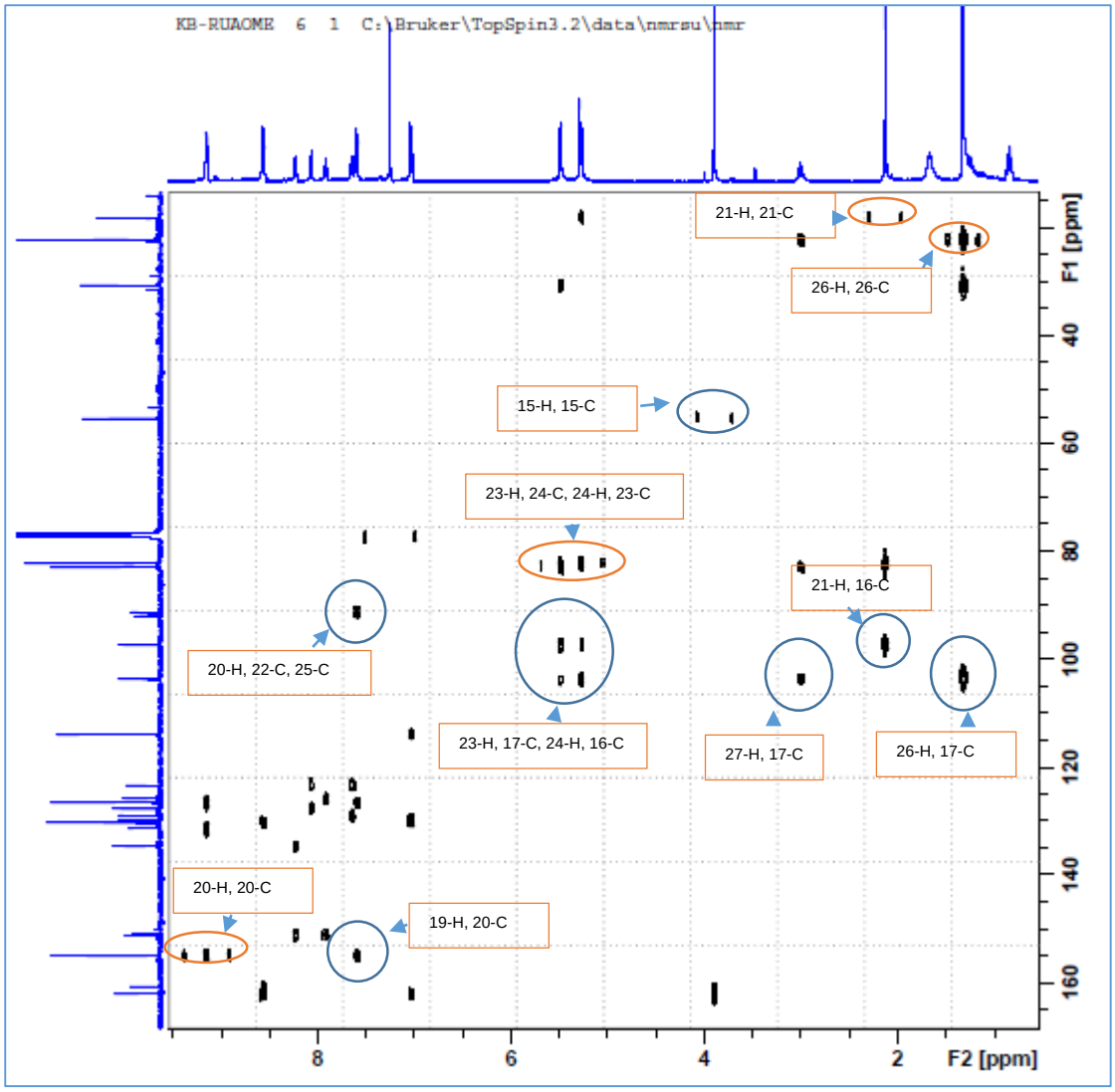

Figure 4.16. 2D-^{1}H-^{13}C-HMBC correlations for Ru(II) complex **126e.**

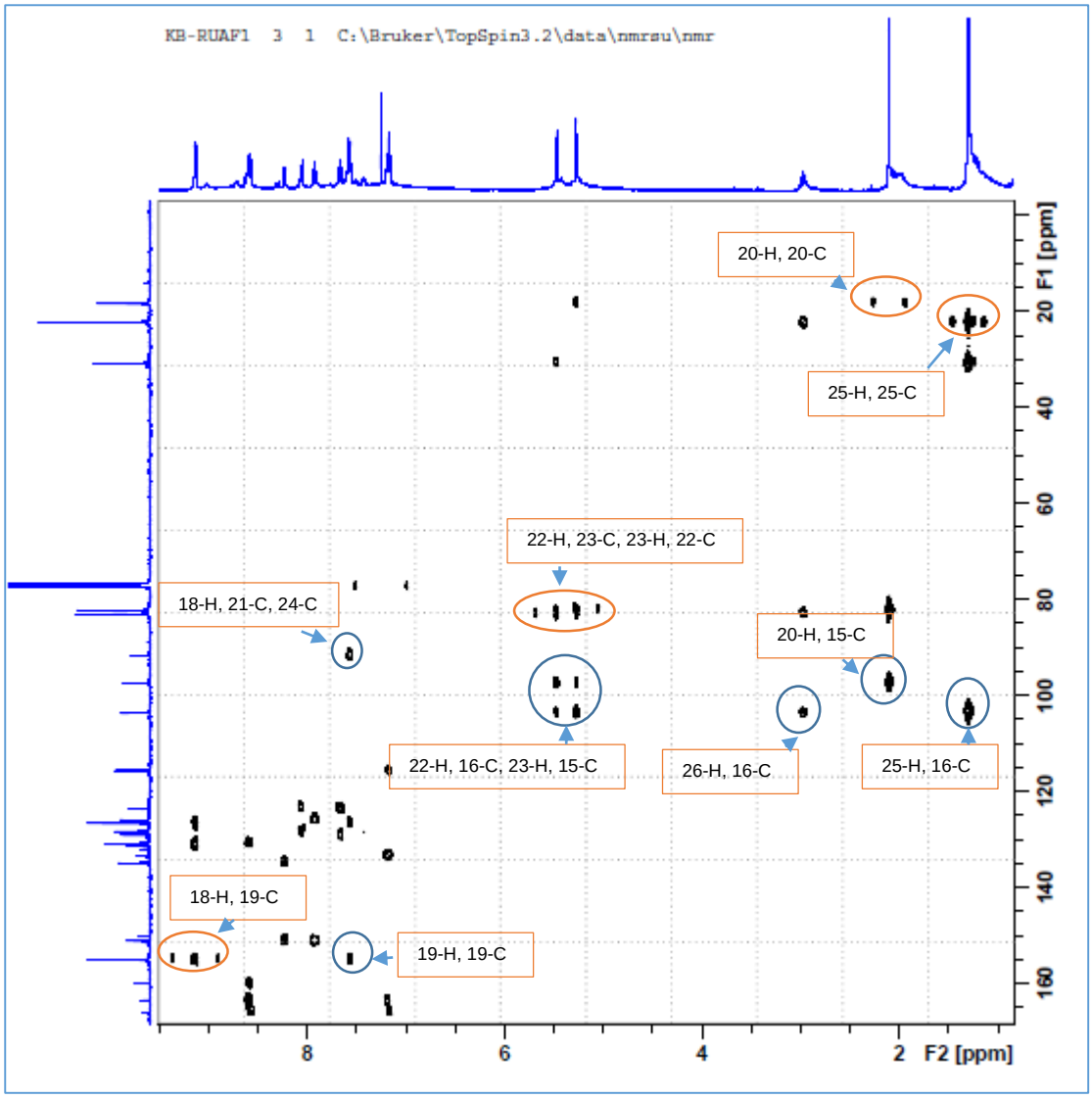

Figure 4.17. 2D-^{1}H-^{13}C-HMBC correlations for Ru(ll) complex **126c.**

4.3.6 Conclusion

Ethanamine Schiff base ligands of the *N^N* type were synthesised in good yield in a basic medium, attempted coordination of ligand **119b** to zinc chloride showed a hint of formation as the reaction was carried out in NMR tube while monitoring during 12 and 24 h period using ^{1}H-NMR. Unfortunately the reaction proceedings showed decomposition of ligand **119b**. The requisite 2-aryl-4-chloro-quinazolines served as a substrate for dechloro-amination and sonogashira cross-coupling reaction at *C(4)-Cl* position which afforded 4-(pyridylamino) and 4-(ethynylpyridine)quinazolines in good yields. Successful coordination to Ru(ll) *p*-cymene centre was achieved and the complexes were isolated in good yield. The newly synthesised Ru(ll) complexes

showed new long range couplings *of* $^{6,7,8,9}J_{CH}$. Furthermore coordination induced shifts were observed across all ligands with different *para*-substituent of –Br, -Cl, -OMe, -F and $–NO_2$.

Reference

[1]. Naeimi, H., Safari, J. and Heidarnezhad, A., 2007. Synthesis of Schiff base ligands derived from condensation of salicylaldehyde derivatives and synthetic diamine. *Dyes and Pigments*, *73*(2), pp.251-253.

[2]. Cordes, E.H. and Jencks, W.P., 1962. On the mechanism of Schiff base formation and hydrolysis. *Journal of the American Chemical Society*, *84*(5), pp.832-837.

[3]. Bernardo, K., Leppard, S., Robert, A., Commenges, G., Dahan, F. and Meunier, B., 1996. Synthesis and characterization of new chiral Schiff base complexes with diiminobinaphthyl or diiminocyclohexyl moieties as potential enantioselective epoxidation catalysts. *Inorganic Chemistry*, *35*(2), pp.387-396.

[4]. Ojwach, S.O., Guzei, I.A., Benade, L.L., Mapolie, S.F. and Darkwa, J., 2009. (Pyrazol-1-ylmethyl) pyridine Nickel Complexes: Ethylene Oligomerization and Unusual Friedel− Crafts Alkylation Catalysts. *Organometallics*, *28*(7), pp.2127-2133.

[5]. Ooi, T., Taniguchi, M., Kameda, M. and Maruoka, K., 2002. Direct asymmetric aldol reactions of glycine Schiff base with aldehydes catalyzed by chiral quaternary ammonium salts. *Angewandte Chemie International Edition*, *41*(23), pp.4542-4544.

[6]. Catanescu, O., Grigoras, M., Colotin, G., Dobreanu, A., Hurduc, N. and Simionescu, C.I., 2001. Synthesis and characterization of some aliphatic–aromatic poly(Schiff bases) . *European Polymer Journal*, *37*(11), pp.2213-2216.

[7]. Babu, G., Sridhar, N. and Perumal, P.T., 2000. A convenient method of synthesis of bis-indolylmethanes: Indium trichloride catalyzed reactions of indole with aldehydes and schiff's bases. *Synthetic Communications*, *30*(9), pp.1609-1614.

[8]. Trost, B.M., Godleski, S.A. and Genet, J.P., 1978. A total synthesis of racemic and optically active ibogamine. Utilization and mechanism of a new silver ion assisted palladium catalyzed cyclization. *Journal of the American Chemical Society*, *100*(12), pp.3930-3931.

[9]. Hati, S., Holzgrabe, U. and Sen, S., 2017. Oxidative dehydrogenation of CC and CN bonds: A convenient approach to access diverse (dihydro) heteroaromatic compounds. *Beilstein Journal of Organic Chemistry*, *13*, pp.1670-1692.

[10]. Fatiadi, A.J., 1986. The oxidation of organic compounds by active manganese dioxide. In *Organic Syntheses by Oxidation with Metal Compounds* (pp. 119-260). Springer, Boston, MA.

[11]. Kanışkan, N., Kökten, Ş. and Çelik, İ., 2012. A new protocol for the synthesis of primary, secondary and tertiary anthranilamides utilizing N-(2-aminoarylacyl) benzotriazoles. *Arkivoc*, *8*, pp.198-213.

[12]. Verma, A., Giridhar, R., Kanhed, A., Sinha, A., Modh, P. and Yadav, M.R., 2012. Novel 2-Aminobenzamides as Potential Orally Active Antithrombotic Agents. *ACS Medicinal Chemistry Letters*, *4*(1), pp.32-36.

[13]. Mphahlele, M.J., Paumo, H.K., El-Nahas, A.M. and El-Hendawy, M.M., 2014. Synthesis and photophysical property studies of the 2, 6, 8-triaryl-4-(phenylethynyl) quinazolines. *Molecules*, *19*(1), pp.795-818.

[14]. Parua, S., Das, S., Sikari, R., Sinha, S. and Paul, N.D., 2017. One-Pot Cascade Synthesis of Quinazolin-4 (3 H)-ones via Nickel-Catalyzed Dehydrogenative Coupling of o-Aminobenzamides with Alcohols. *The Journal of Organic Chemistry*, *82*(14), pp.7165-7175.

[15]. Mphahlele, M., Mmonwa, M., Aro, A., McGaw, L. and Choong, Y., 2018. Synthesis, Biological Evaluation and Molecular Docking of Novel Indole-Aminoquinazoline Hybrids For Anticancer Properties. *International Journal Of Molecular Sciences*, *19*(8), p.2232.

[16]. Paumo, H.K., Makhafola, T.J. and Mphahlele, M.J., 2016. Synthesis and in vitro cytotoxic properties of polycarbo-substituted 4-(arylamino) quinazolines. *Molecules*, *21*(10), p.1366.

[17]. Kabri, Y., Gellis, A. and Vanelle, P., 2009. Synthesis of Original 2-Substituted 4-Arylquinazolines by Microwave-Irradiated Suzuki–Miyaura Cross-Coupling Reactions. *European Journal of Organic Chemistry*, *2009*(24), pp.4059-4066.

[18]. Chinchilla, R. and Nájera, C., 2007. The Sonogashira reaction: a booming methodology in synthetic organic chemistry. *Chemical Reviews*, *107*(3), pp.874-922.

[19]. Singh, A.K., Pandey, D.S., Xu, Q. and Braunstein, P., 2014. Recent advances in supramolecular and biological aspects of arene ruthenium(II) complexes. *Coordination Chemistry Reviews*, *270*, pp.31-56.

[20]. Ramachandran, R., Prakash, G., Viswanathamurthi, P. and Malecki, J.G., 2018. Ruthenium(II) complexes containing phosphino hydrazone/thiosemicarbazone ligand: An efficient catalyst for regioselective N-alkylation of amine via borrowing hydrogen methodology. *Inorganica Chimica Acta*, *477*, pp.122-129.

[21]. Castonguay, A., Doucet, C., Juhas, M. and Maysinger, D., 2012. New ruthenium (II)–letrozole complexes as anticancer therapeutics. *Journal of Medicinal Chemistry*, *55*(20), pp.8799-8806.

[22]. Sáez, R., Lorenzo, J., Prieto, M.J., Font-Bardia, M., Calvet, T., Omeñaca, N., Vilaseca, M. and Moreno, V., 2014. Influence of PPh 3 moiety in the anticancer activity of new organometallic ruthenium complexes. *Journal of Inorganic Biochemistry*, *136*, pp.1-12.

[23]. Orllana, G., Ibarra, C.A. and Santoro, J., 1988. ^{1}H and ^{13}C NMR coordination-Induced Shifts in a series of Tri(α-diimine) ruthenium(ll) complexes containing pyridine, pyrazine and thiazole moieties. *Inorgqnic Chemistry*, 27, pp. 1025-1030.

CHAPTER 5: APPLICATION

5.1 Molecular docking

The molecular docking calculations were done using the Schrodinger-2018-1 LLC interface, employing Maestro 11.5 database. All ligands and proteins in the induced-fit docking (IFD) job were prepared at physiological pH 7.4 using Epik. The conformational search for all ligands was done using optimised potentials for liquid simulations (OPLS_2005) employing water as a solvent. The IFD experiment was run on extra-precision (XP), wherein residues within ligand poses were refined at 5 Å and all ligands were re-docked into structures within 30 Kcal/mol of the best structure, and within the top 20 structures overall.

Induced-fit docking (IFD) of compounds **119a-d**, **123a-e** and **125a-e** using GLIDE was performed to better understand the anticancer and anti-*Mycobacterium tuberculosis* (*Mtb*) activity of the ligands. The molecular docking calculations give a docking or glide score. The glide score is defined as an empirical scoring function designed to maximise separation of compounds with strong binding (more negative) affinity from those with little to no binding ability [1]. A ligand is considered to have affinity towards a protein when the docking score is higher than -5 Kcal/mol cut-off. To aid this study, the compounds were inductively docked into the active pockets of *glutamine synthetase* (PDB:1HTO) for *Mtb*, tyrosine kinase (PDB:2SRC) and oxidoreductase (PDB:3F8P) for cancer.

5.1.1 Induced fit docking of compounds 119a-d, 123e and 125e into *glutamine synthetase* (1HTO) receptor grid.

Glutamine synthetase (PDB:1HTO) is an enzyme essential for cellular nitrogen metabolism and plays a role in both glutamine biosynthesis and ammonia assimilation [2]. *Glutamine synthetase* (GS) has emerged as a potential target for pharmacological target for tuberculosis therapy due to the critical role it plays in nitrogen metabolism in plays in prokaryotes [3]. Synthetic pyridine derivatives such as isoniazid (first line tuberculosis drug) are reported to inhibit *Glutamine synthetase* [4] which catalyses the ATP-dependent condensation of amonium and L-glutamate at the amino acid binding site, resulting in the formation of *glnA1* essential for the growth of *Mtb* in both *in vitro*

and *in vivo* [4]. Any disturbance at the amino acid binding site will in turn breakdown cell wall biosynthesis [5] thus leading to cell death. The ligand-protein interacts are described below

The 2-dimensional (2D) and 3-dimensional (3D) docked poses of compounds **119a-d**, **123e** and **125e** are represented in **Figures 5.1a-m** below. The ethanamine-Schiff base ligands (**119a-d**) appear to undergo protonation at the imine group at pH 7.4, which therefore renders all ligands in the receptor grid as positively charged. The docking poses of the ligands in the 1HTO-receptor grid occupy the polar (blue), hydrophobic (green) and electronegative (red) pockets in the *α*- and *β*-sheets. **Figures 5.1a-m** below indicate increased polar, hydrophobic, electronegative and glycine (H-bond, *π*-*π*-stacking, *π*-cation and salt bridge) interactions existing across all ligands with the 1HTO amino-acid sequence TYR125, TRP275, PHE225, LYS208 and HIE271, ASP404 and ARG366.

Ligand **119a** exhibits a glide score of -9.972 Kcal/mol wherein the pre-mentioned intermolecular *π*-*π* interaction from TRP275 is due to the fused-phenyl ring of the indole group, the *π*-cation interaction is due to the fused-pyrrole ring of TRP275, PHE225 phenyl ring and the *para*-methoxy phenyl ring of the TYR125 **Fig.5.1a**.

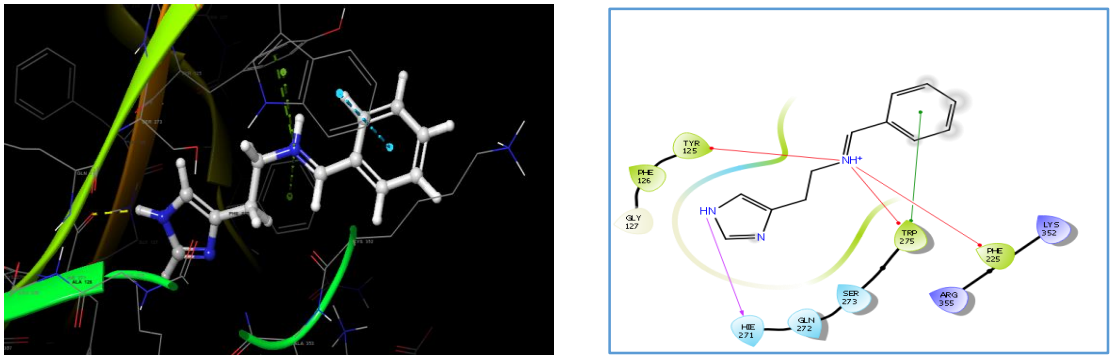

Figure 5.1a and 5.1b: Docking screen (left) and 2D ligand interaction diagram (right) of **119a** in 1HTO.

Ligand **119b** on the other hand exhibits a glide score of -9.634 Kcal/mol wherein the *π*–*π* interaction from PHE225 is due to the phenyl ring of the latter. The H-bond interaction is due to the carbonyl group of HIE271, as the oxygen of the carbonyl group acts as a hydrogen bond acceptor. Interactions with the polar nitrogen of the imidazolyl group on ligand **119b** and LYS208 are of H-bond acceptor due to the *π*-electrons on

the nitrogen and the *π*-cation interactions are due to the fused-pyrrole ring of TRP275, PHE225 phenyl ring and the *para*-methoxy phenyl ring of the TYR125 **Fig.5.1c**.

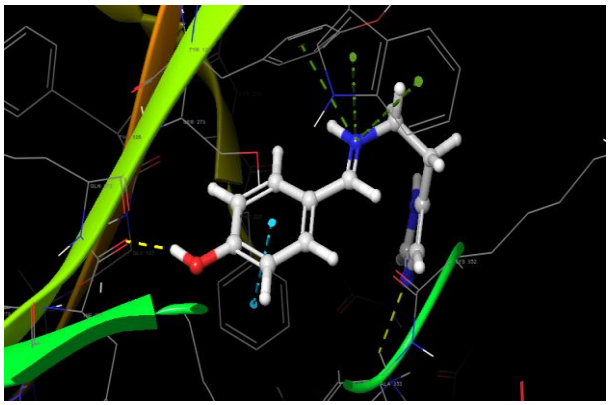

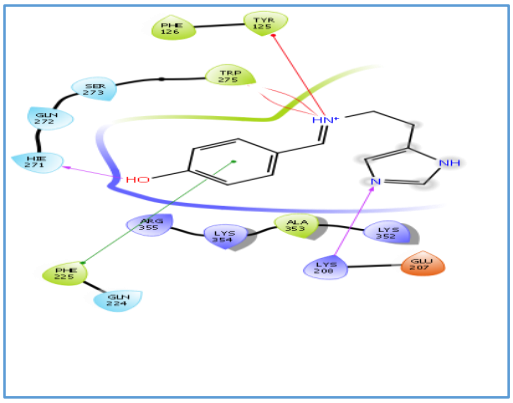

Figure 5.1c and 5.1d: 3D Docking screen (left) and 2D ligand interaction diagram (right) of **119b** in 1HTO.

Ligand **119c** exhibits a glide score of -10.040 Kcal/mol. The observed interactions stem from *π*-*π* interactions of between PHE225 phenyl ring and the *para*-fluoro phenyl ring of the ligand **119c.** Further interactions from TYR125 show a H-bond acceptor between the *para*-methoxy group of TYR125 and –NH group of the imidazolyl group on ligand **119c**. The *π*-cation interactions are due to the fused-pyrrole ring of TRP275, PHE225 phenyl ring and the *para*-methoxy phenyl ring of the TYR125 **Fig.5.1e**

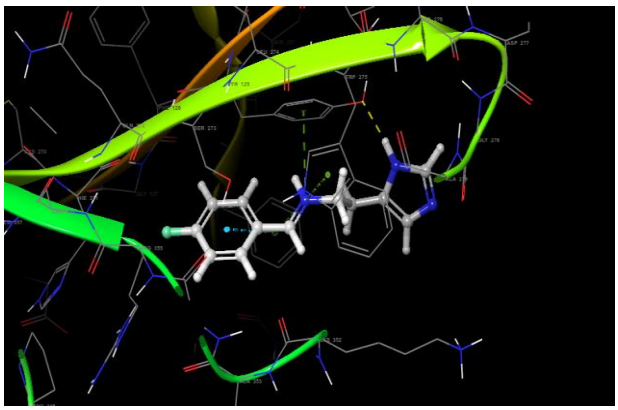

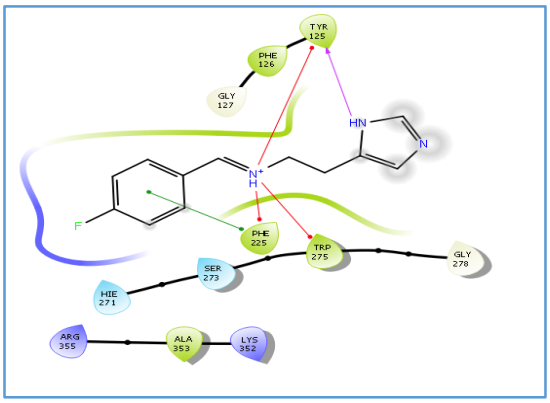

Figure 5.1e and 5.1f: 3D Docking screen (left) and 2D ligand interaction diagram (right) of **119c** in 1HTO.

The best pose for ligand **119d** revealed the absence of *π*-*π* interactions. Instead we view a *π*-cation interaction between with a glide score of -8.679 Kcal/mol the *para*-nitro phenyl ring of ligand **119d** and the phenyl ring of PHE225. The interaction with TYR125 owes to the *para*-methoxy group of the H-bond acceptor from the –NH group

of the imidazolyl ring on ligand **119d**. Added *π*-cation interactions from the cationic imine group of ligand **119d** are due to indole ring of TRP275 and the *para*-methoxy phenyl ring of the TYR125 **Fig.5.1g**. Comparative docking score for the imidazolyl-ethanime Schiff base ligands **119a-d** are summarised on **Table 5.1** below.

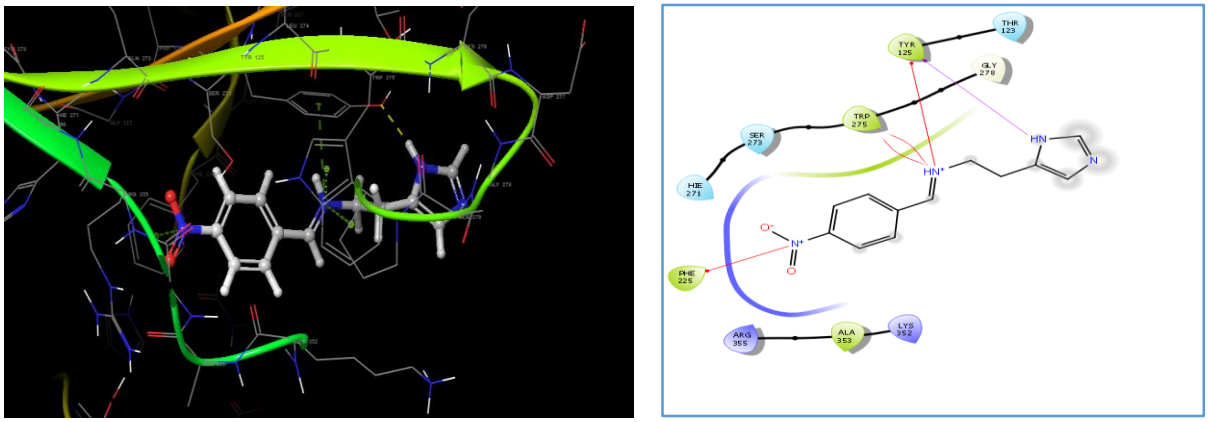

Figure 5.1g and 5.1h: 3D Docking screen (left) and 2D ligand interaction diagram (right) of **119d** in 1HTO.

Table 5.1: Summarised docking scores for ligands **119a-d** (1HTO).

Ligand entry#	Docking score (Kcal/mol)
119a	-9.972
119b	-9.634
119c	-10.040
119d	-8.697

The ethynylpyridine cross-coupled ligand **125e** was found to give the best pose in the glycine, polar and hydrophobic pockets between *α*- and *β*-sheets to give a docking score of -9.176 Kcal/ mol. The ligand interacts with the protein through *π*-*π* stacking and H-bond acceptor. The *π*-*π* interactions are due to the fused pyrimidine and aromatic quinazoline framework and the two rings link phenyl backbone of PHE225. Further *π*-*π* stacking arise from the interaction between the bridged pyridine and tailing pyrrole ring of HIE271. The H-bond acceptor is due to the *para*-methoxy group of the ligand **125e** and –NH_2 group of LYS208 **Fig. 5.1i**. The docking scores of ligands **125a, 125b, 125c and 125d** are here mentioned as -7.566, -6.935, -7.240 and -7.143 Kcal/mol respectively. Comparative docking score for the ethynylpyridine quinazoline ligands 125a-e are summarised on **Table 5.2**.

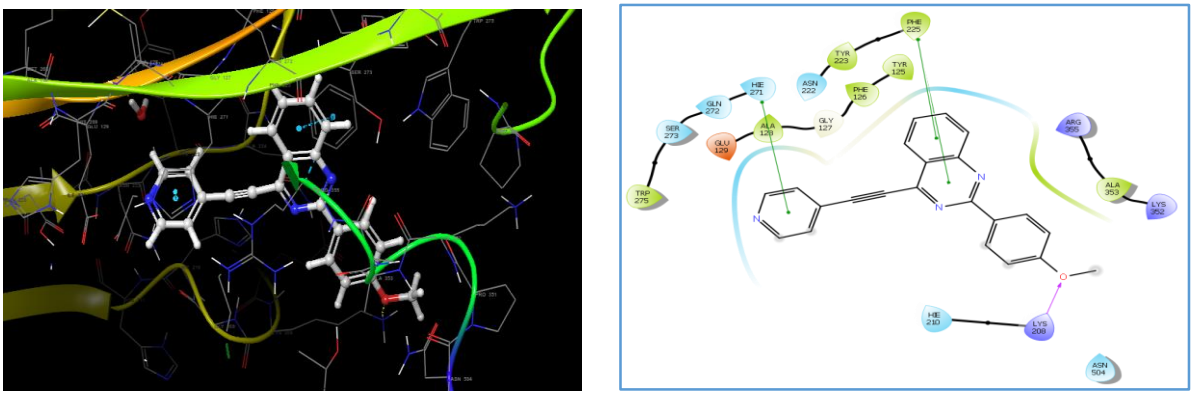

Figure 5.1i and 5.1k: 3D Docking screen (left) and 2D ligand interaction diagram (right) of **125e** in 1HTO.

Table 5.2: Summarised docking scores for ligands **125a-e** (1HTO).

Ligand entry#	Docking score (Kcal/mol)
125a	-7.566
125b	-6.935
125c	-7.240
125d	-7.143
125e	-9.176

Ligand **123e** gave the best pose in the electrophilic, hydrophobic and polar pockets of *α*- and *β*-sheets to give a glide score of -7.650 Kcal/ mol. The terminal carboxyl and carboxamide groups of electronegative ASP404 interact with the anionic oxygen of the nitro group through a salt bridge, while the –NH group of the ligand interacts with the latter through H-bond acceptor. More interactions are observed for the methoxy group of the ligand and the interactions observed are of H-bond acceptor, the lone pairs of electrons on the oxygen interact with germinal $–NH_2$ hydrogens of ARG366 and the free water molecules of the receptor. The water molecules help fix the ligand in the binding site within the receptor grid **Fig.5.1l**. The docking scores for ligands **123a**, **123b**, **123c** and **123d** are here mentioned as -7.413, -6.653, -6.250 and -6.409 Kcal/ mol respectively. Comparative docking scores for the pyridylamino quinazoline ligands **123a-e** are summarised on **Table 5.3** below.

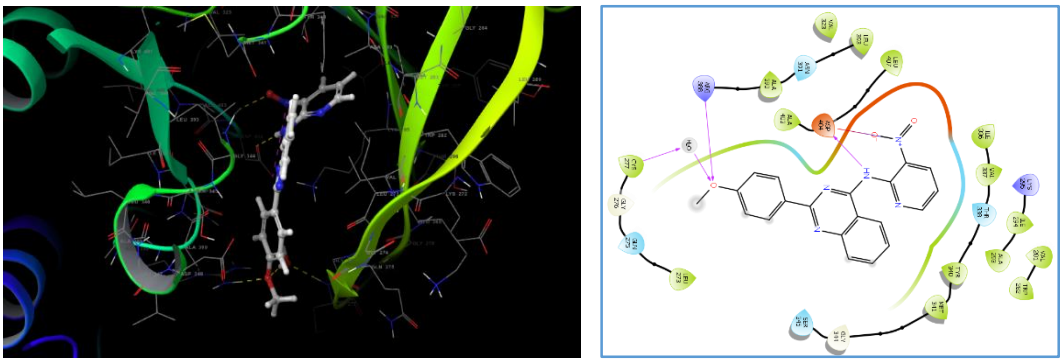

Figure 5.1l and 5.1m: 3D Docking screen (left) and 2D ligand interaction diagram (right) of **123e** in 1HTO.

Table 5.3: Summarised docking scores for ligands **123a-e** (1HTO).

Ligand entry#	Docking score (Kcal/mol)
123a	-7.413
123b	-6.653
123c	-6.250
123d	-6.409
123e	-7.650

5.1.2 Induced fit docking of compounds 119a-d, into oxidoreductase (PDB:3F8P) receptor grid.

Oxidoreductase (PDB:3F8P) is an enzyme from the protein kinase family and it is overexpressed in breast, liver, gastrointestinal tract and kidney cancer [6]. This enzyme is responsible for catalysing oxidation and reduction reactions in cells. Moreover, the enzyme is responsible for both aerobic and anaerobic metabolisms which aid glycolysis, TCA cycle, oxidative phosphorylation and amino acid metabolism [7]. In cancer cells, oxidoreductase is expressed as xanthine oxidoreductase (XOR) and it links with uric acid to proliferate and transform cells to speed the progression of metastasis. Metastasis is described as the development of secondary malignant tumours distant from the site of cancer cells. The XOR and uric acid effect is reported to promote metabolic syndromes. Metabolic syndromes are defined as neoplastic complications that lead to blood pressure, high blood sugar and uncontrollable cholesterol levels. These complications are reported to have anti-therapeutic

protective outcomes [8]. In this light, targeting the active site of this enzyme (3F8P) represent an ideal approach in combating the proliferation of cancer cells. The ligand-protein interactions are described below.

The 2-dimensional (2D) and 3-dimensional (3D) docked poses of compounds **119a-d**, **123e** and **125e** are represented in **Figures 5.2a-h** below. The docking poses of the ligands in the 3F8P-receptor grid occupy the polar (blue), hydrophobic (green), electronegative (red) and glycine (grey) pockets in the *α*- and *β*-sheets. **Figures 5.2a-h** below indicate increased polar, hydrophobic, electronegative and glycine (H-bond, *π*-*π* stacking, *π*-cation and salt bridge) interactions existing across all ligands with the 3F8P amino-acid sequence VAL92, GLN51, PHE225, LYS124 and GLU46.

In this fit, ligand **119b** exhibits a glide score of -9.221 Kcal/mol. The docking screen, **Fig.5.2a** depicts ligand interactions occurring in the hydrophobic and glycine pockets within the *β*-sheets. The ligand interacts with the protein through H-bond acceptor and donor. The H-bond is due to double interaction from carboxamide –NH_2 groups of GLN51. The polar nitrogen of the imidazolyl group of the ligand accesses this interaction through the free lone pair of electrons. Similarly, the hydroxyl group of the ligand accesses the –NH_2 group of VAL92 through the readily accessible lone pair of electrons from the oxygen atom **Fig.26a**. Similar docking scores of ligands **119a**, **119c** and **119d** are here mentioned -7.425, -7.033 and -6.035 Kcal/mol respectively. Comparative docking scores for the imidazolyl-ethanime Schiff base ligands **119a-d** are summarised on **Table 5.4**.

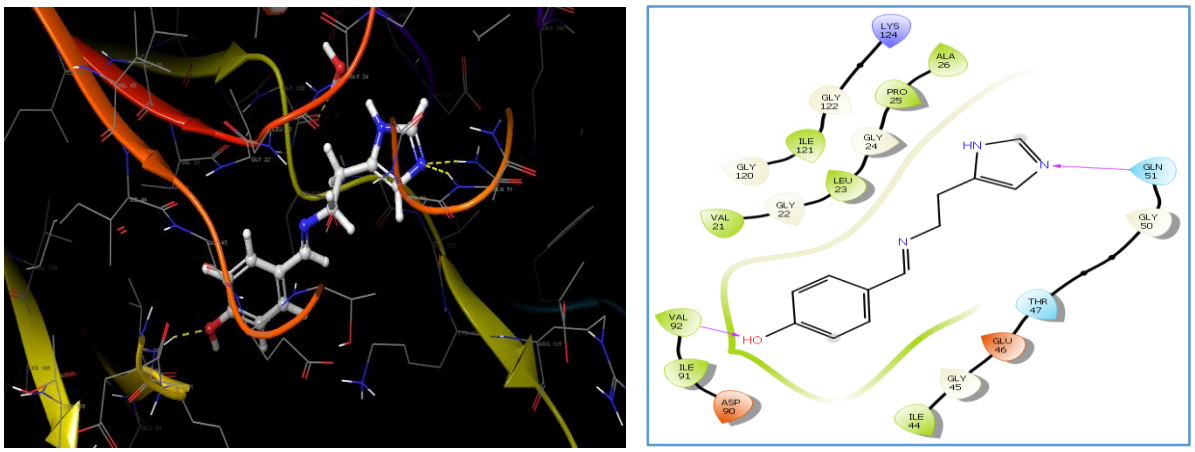

Figure 5.2a and 5.2b: 3D Docking screen (left) and 2D ligand interaction diagram (right) of **119b** in 3F8P.

Table 5.4: Summarised docking scores for ligands **119a-d** (3F8P).

Ligand entry#	Docking score (Kcal/mol)
119a	-7.425
119b	-9.221
119c	-7.033
119d	-6.035

Ligand **123c** gave a glide score of -9.441 Kcal/mol. Protein to ligand interactions are observed in the electrophilic, hydrophobic and polar pockets of *β*-sheets. The interactions observed include *π*-cation, *π*-*π*, H-bond donor and acceptor and salt bridging. The *π*-cation (red lines) and *π*-*π* interactions (green lines) are due to interactions between cationic nitro group, pyrimide group of the quinazoline framework and the phenyl group of hydrophobic PHE225. Furthermore, *π*-cation interactions are due to the 2-(4-fluorophenyl) group of the ligand and the tailing $–NH_2$ group of polar LYS124. The H-bond acceptor is due to the pyridyl nitrogen of the ligand and the –NH group of VAL92. The H-bond donor interaction is due to –NH group of ligand and carbonyl group of VAL92. The salt-bridges are interactions resulting from cationic nitrogen of $-NO_2$ of the ligand interacting with electronegative GLU46 and the anionic oxygen of $–NO_2$ of the ligand which interacts with the $–NH_2$ group of polar LYS124 **Fig.5.2c**. Comparative docking scores for the pyridylamino quinazoline ligands are summarised in **Table 5.5**.

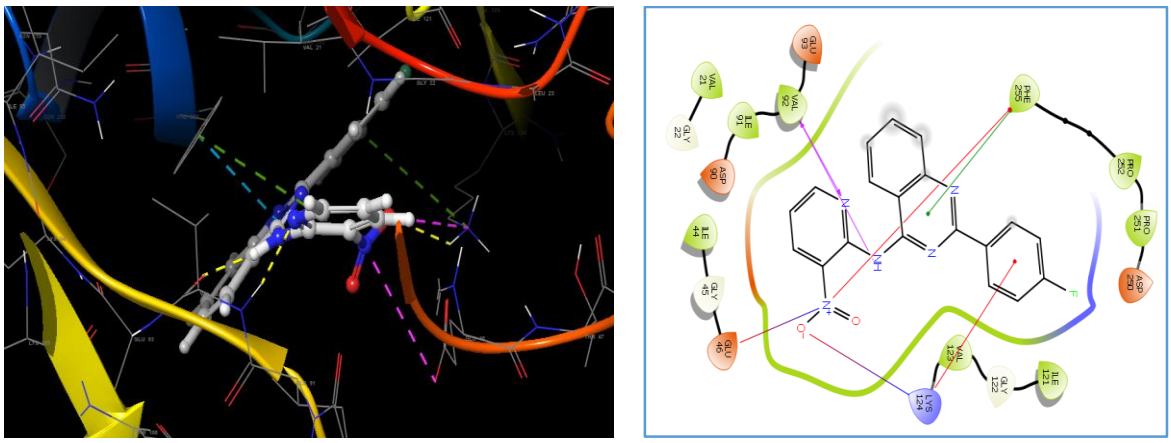

Figure 5.2c and 5.2d: 3D Docking screen (left) and 2D ligand interaction diagram (right) of **123c** in 3F8P.

Table 5.5: Summarised docking scores for ligands **123a-e** (3F8P).

Ligand entry#	Docking score (Kcal/mol)
123a	-5.709
123b	-5.743
123c	-9.441
123d	-5.738
123e	-6.341

Ligand **125a** exhibited a glide score of -9.107 Kcal/mol. The interactions are observed in the electronegative and glycine pockets of the *α*-sheets. However, increased H-bond acceptor and *π*-cation interactions are observed in the glycine pocket. The *π*-cation interaction results from the double interaction of quinazoline framework with tailing $–NH_2$ group of polar LYS124. The H-bond acceptor is due to interaction between *N*-1 and $–NH_2$ group of GLN51 carboxamide group. Further H-bond acceptor interaction results from the terminal nitrogen of ethnylpyridine and –NH group of hydrophobic VAL92 **Fig.5.2e**.

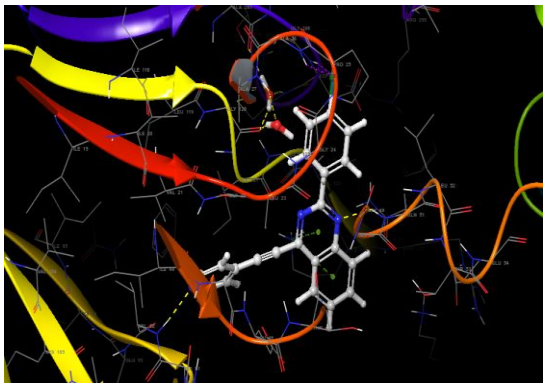

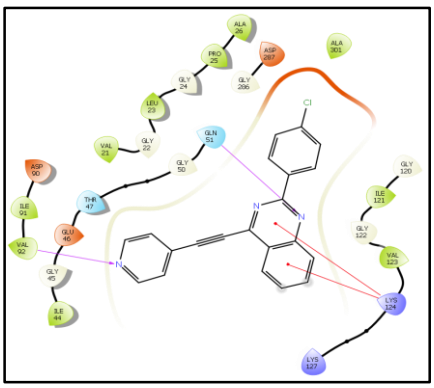

Figure 5.2e and 5.2f: 3D Docking screen (left) and 2D ligand interaction diagram (right) of **125a** in 3F8P.

Ligand **125c** gave a glide score of -10.043 Kcal/mol. Interactions for this ligand are found in the polar, hydrophobic and electronegative pockets of *α*-sheets. However, interactions of H-bond acceptor and *π*-cation are observed in the polar and electronegative pockets. The H-bond acceptor is due to interaction between $–NH_3$ groups of VAL92 and GLN51 for *N*-1 and pyridyl nitrogen retrospectively. The *π*-cation is due to interaction between $-NH_2$ group of polar LYS124 and fused phenyl group of

the quinazoline framework **Fig.5.2g**. Comparative docking scores for the ethynylpyridine quinazolines ligands 125a-e are summarised in **Table 5.6** below.

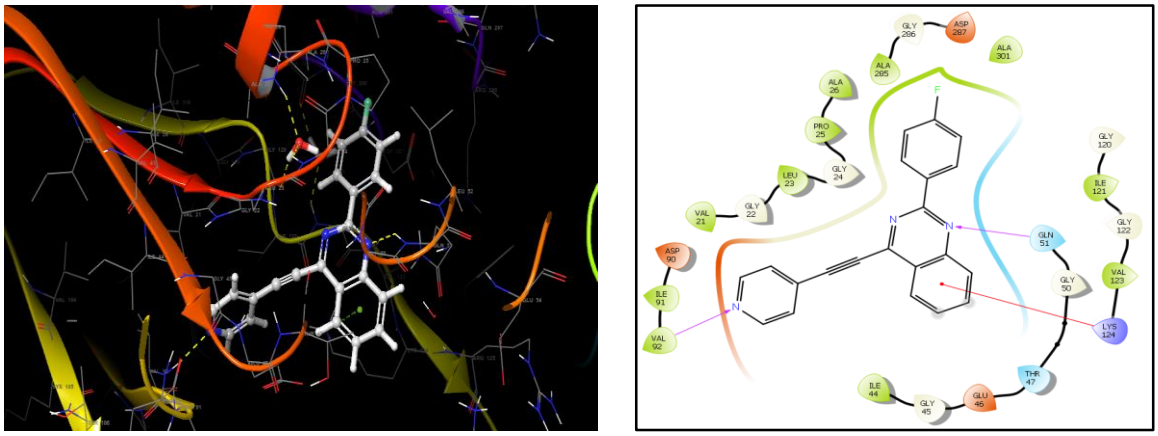

Figure 5.2g and 5.2h: 3D Docking screen (left) and 2D ligand interaction diagram (right) of **125c** in 3F8P.

Table 5.6: Summarised docking scores for ligands **125a-e** (3F8P).

Ligand entry#	Docking score (Kcal/mol)
125a	-9.0107
125b	-8.165
125c	-10.043
125d	-8.522
125e	-8.362

5.1.3 Induced fit docking of compounds 119a-d into Tyrosine kinase (2SRC) receptor grid.

Tyrosine kinases are a subclass of protein kinase family. They are responsible for the transfer of phosphate groups from adenosine triphosphate (ATP) to cellular proteins. They function as an “on” or “off” switch in modulation of growth factor signalling [9]. This signal transduction process helps the rapid widespread of cancer cells [10]. Compounds designed to specifically fit in the active site of tyrosine kinase compete with the ATP binding site of the catalytic domain. Blocking the ATP phosphate transfer results in reduced multiplication of cancer cells and minimises metastasis [11]. The ligand-protein interactions are described below.

The 2-dimensional (2D) and 3-dimensional (3D) docked poses of compounds **119a-d** are represented in **Figures 5.3a-h** below. Ligands **119a** and **119c** were found to give good docking scores when protonated at pH 7.4. The docking poses of the ligands in the 2SRC-receptor grid occupy the polar (blue), hydrophobic (green) and electronegative (red), glycine (grey) pockets in the *α*- and *β*-sheets. **Figures 5.3a-h** below indicate increased polar, hydrophobic, electronegative and glycine (H-bond, π-*π*-stacking, *π*-cation and salt bridge) interactions existing across all ligands with the 2SRC amino-acid sequence PHE225, ASP404, GLU339, MET341, ALA390, VAL323.

In this investigation, ligand **119a** exhibits a glide score of -8.901 Kcal/mol. The ligand-protein interaction is found in the electronegative and hydrophobic pockets of the receptor within the *β*-sheets. The ligand interacts with the receptor through *π*-*π* stacking, H-bond acceptor and salt-bridge linking. The *π*-*π* stacking interaction is due to the phenyl ring of PHE405 and phenyl ring of ligand, the salt-bridge is due to the cationic imino group which interacts with the hydroxyl group of ASP404 carboxyl backbone. The H-bond is through interaction between carboxamide backbone of electronegative GLU339, as the oxygen of the latter acts as hydrogen acceptor of amine hydrogen emanating from imidazolyl group of ligand **119a**, **Fig.5.3a**.

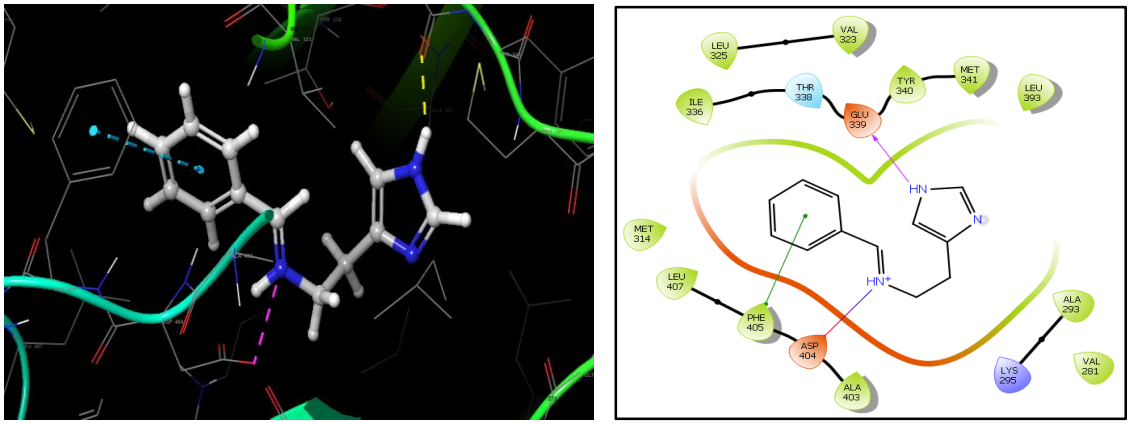

Figure 5.3a and 5.3b: 3D Docking screen (left) and 2D ligand interaction diagram (right) of **119a** in 2SRC.

Ligand **119b** gave a glide score of -8.655 Kcal/mol. All interactions are found in the hydrophobic pocket of the receptor grid. The ligand interacts with the protein by way of H-bond acceptor and donor. The tailing hydroxyl group acts as a hydrogen acceptor for amino carboxamide hydrogen of MET341 and the imidazolyl amine hydrogen interacts with oxygen atoms on carbonyl group of ALA390 **Fig.5.3c**.

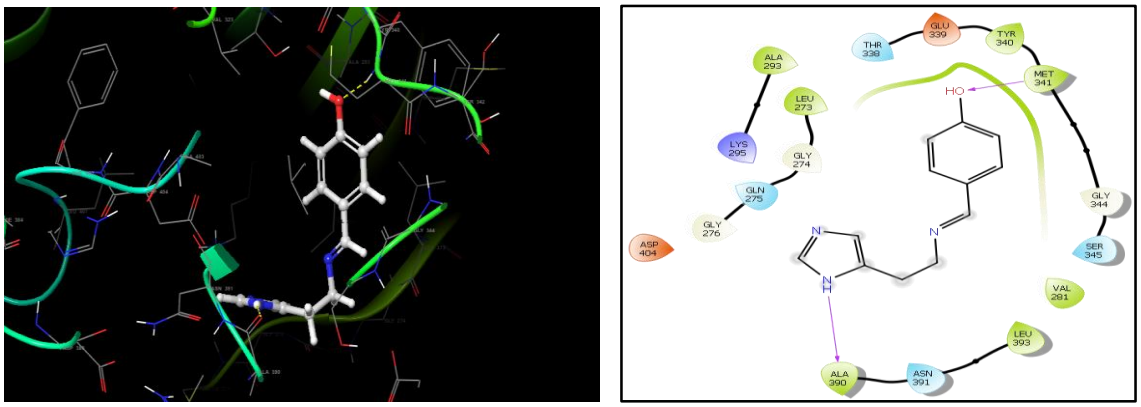

Figure 5.3c and 5.3d: 3D Docking screen (left) and 2D ligand interaction diagram (right) of **119b** in 2SRC.

The best pose for ligand **119c** was found in the polar, hydrophobic and electronegative pockets in the *β*-sheets. A glide score of -9.393 Kcal/mol was obtained for ligand **119c** wherein ligand-protein interactions were found to exhibit salt-bridging and H-bond acceptors. The salt-bridge exists between polar and electronegative pockets. This is due to the cationic imino group of the ligand, which shows a double interaction with the carbonyl oxygen and hydroxyl hydrogen of ASP404. Further interactions observed include H-bond acceptor between –NH group of the imidazolyl group of the ligand and the carboxamide oxygen of GLU339 **Fig.5.3e**.

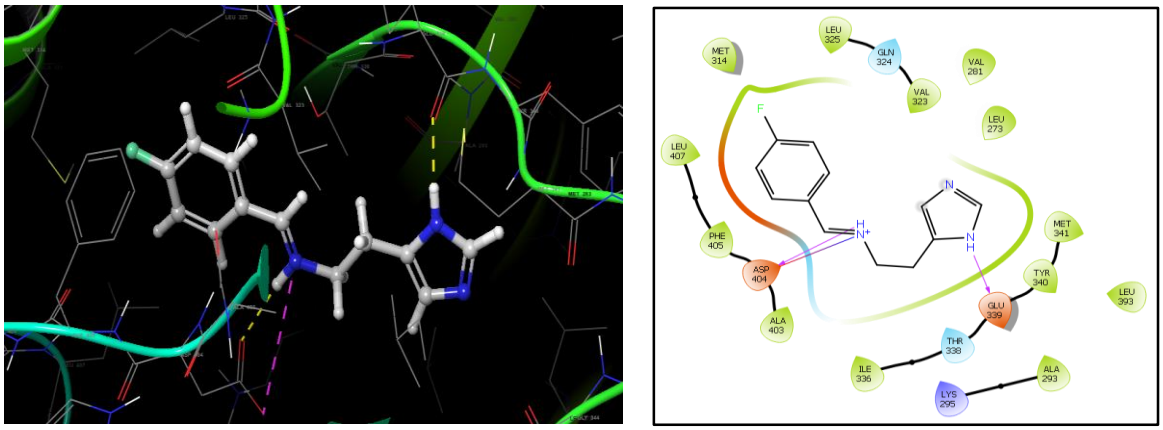

Figure 5.3e and 5.3f: 3D Docking screen (left) and 2D ligand interaction diagram (right) of **119c** in 2SRC.

Ligand **119d** gave the best pose in the polar, hydrophobic and electronegative pockets of the *β*-sheets. However, the ligand-protein interactions were found in the hydrophobic pocket to give a glide score of -8.662 Kcal/mol. The interaction is through both H-bond donor and acceptor. The H-bond acceptor interaction exists between –

NH_2 group of carboxamide backbone of electronegative ASP404 and the sp^2-hybridised nitrogen of the imdazolyl group. The H-bond donor exists between the amino group of the imidazolyl group of ligand and the carboxamide oxygen of hydrophobic VAL323 **Fig.5.3g**. Comparative docking scores for the imidazolyl-ethanamine Schiff base ligands are summarised in **Table 5.7** below.

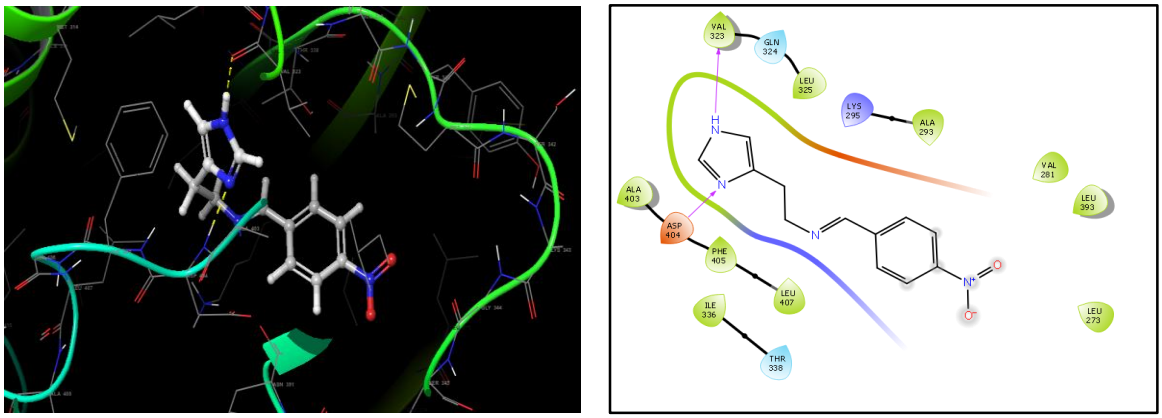

Figure 5.3g and 5.3h: 3D Docking screen (left) and 2D ligand interaction diagram (right) of **119d** in 2SRC.

Table 5.7: Summarised docking scores for ligands **119a-d** (2SRC).

Ligand entry#	Docking score (Kcal/mol)
119a	-8.901
119b	-8.655
119c	-9.393
119d	-8.662

In this fit (2SRC), unfortunately ligands **123a – e** and **125a – e** showed limited binding towards the protein receptor grid. This resulted in poor docking scores which are summarised in **Table 5.8**.

Table 5.8: Summarised docking scores for ligands **123a-e** and **125a-e**.

Ligand entry #	Docking score (Kcal/mol)	**Ligand entry #**	Docking score (Kcal/mol)
123a	-5.958	**125a**	-6.580
123b	-7.163	**125e**	-6.010
123c	-7.408	**125c**	-6.321
123d	-5.118	**125d**	-6.800
123e	-6.949	**125e**	-6.870

Computational chemistry studies are usually backed by experimental biological evaluation data [12]. In this study, the IFD study is supported by *in vitro Mtb* studies of ligands **119a-d**, **123a-e** and **125a-e** in subsection **5.2**.

5.2 In vitro anti-Mycobacterium tuberculosis properties of compounds 119a-d, 121a-e, 123a-e, 125a-e and 126a-e.

The *in vitro* anti-*Mycobacterium tuberculosis* activity of compounds **119a-d**, **121a-e**, **123a-e**, **125a-e** and **126a-e** was performed at the drug discovery and development centre (H3-D), University of Cape Town (UCT). The biological experiments are reported as MIC_{90} and are summarised in tables **5.9** to **5.13** for ligands **119a-d**, **121a-e**, **123a-e**, **125a-e** and **126a-e** respectively prepared in DMSO. MIC_{90} is defined as the minimum inhibitory concentration of a compound that is required to inhibit 90% growth of the bacterium. The preliminary data for *in vitro* anti-*Mycobacterium tuberculosis* was achieved using the alamar blue assay, employing GFP reporter assay 10pt. The media used includes 7H9 CAS GLU Tx and 7H9 ADC GLU Tw. Compounds were assayed within 7 day and 14 day period using the H_{37}Rv strain using Rifampicin as a reference drug. A compound was considered inactive when it showed activity at a concentration >125 µg/mL.

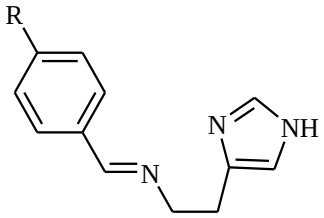

119a - d

Table 5.9: MIC_{90} data for GFP assay for 7 and day 14 data for compounds **119a-d**

R	**Entry #**	**After day 7 data**		**After day 14 data**	
		CAS	ADC	CAS	ADC
-H	119a	>125	>125	>125	>125
-OH	119b	>125	>125	>125	>125
-F	119c	>125	>125	>125	>125
$-NO_2$	119d	>125	>125	>125	>125
#####	Rifampicin	0.009	0.001	0.02	0.02

Schiff base derivatives are multifaceted compounds reported to give numerous biological applications [13]. A representative of this class of compounds in TB application is the second line drug Terizidone [14]. The ethanamine-Schiff base derivatives **119a-d**, on **Table 5.9** above showed no activity during the 7 and 14 day period. This inactivity is attributed to the decomposition of the compounds in DMSO as the compounds are moisture sensitive and degrade almost immediately in biological solvents, *i.e* DMSO and water. Due to this, the induced fit docking results contradict that of experimental with appreciable higher glide score. In subsection **5.1.1**, the compounds appeared to undergo protonation at mimicked physiological pH 7.4, this perhaps sheds light into the stability of these compounds, where pH is a factor.

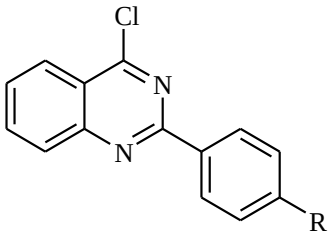

121a - e

Table 5.10: MIC_{90} data for GFP assay for 7 and day 14 data for compounds **121a-e**

R	Entry #	After day 7 data		After day 14 data	
		CAS	ADC	CAS	ADC
-Cl	121a	>125	>125	>125	>125
-Br	121b	>125	>125	>125	>125
-F	121c	>125	>125	>125	>125
$-NO_2$	121d	>125	>125	>125	>125
-OMe	121e	>125	>125	>125	>125
#####	Rifampicin	0.009	0.001	0.002	0.02

Quinazoline derivatives are an important class of compounds in bio-organic chemistry, these compounds are largely applied in cancer application, where compounds such as gefitinib and erlotinib have been marketed and are currently used to treat small lung cancer [15]. In this study we eplore a small structure activity relationship (SAR), the 4-chloroquinazoline derivatives (**121a-e**) were tested against the *Mtb* strain, unfortunately due to the poor solubility of these compounds in DMSO, no desirable activity was obtained.

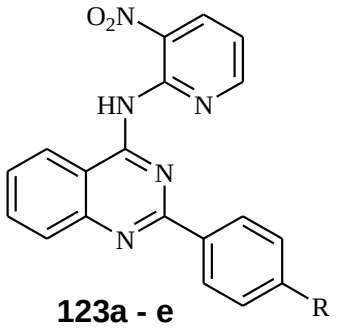

123a - e

Table 5.11: MIC_{90} data for GFP assay for 7 day data for compounds **123a-e**

R	Entry #	After day 7 data	
		CAS	ADC
-Cl	123a	>125	>125
-Br	123b	25	17.244
-F	123c	50	30.969
$-NO_2$	123d	50	42.362
-OMe	123e	12.5	10.698
#####	Rifampicin	0.019	0.075

Compounds **123a-e** were assayed for 7 days, the compounds gave promising preliminary anti-*Mtb* activity. These compounds however, complement the IFD data as compound **123e** gave the highest docking score of -7.650 Kca/mol amongst the compounds in **Table 5.11.** The activity was confirmed by experimental data of the alamar blue assay as the compound gave promising activity of 12.5 and 10.698 µg/mL. The structure activity relationship (SAR) is here observed as the introduction of a pyridylamino group on the *C4*-position proves to have improved solubility of the compounds and activity was observed. The variation of the 4-position of the pyridylamino series shows that electron donating groups improve the activity of the compounds. This is because compounds containing halogens -Cl, -Br and –F on the 4-position of the 2-aryl substituent gave MIC_{90} of 17.2 µg/mL to the undesirable >125 µg/mL. However, an attachement of a 2-aryl substituent bearing a $4\text{-}NO_2$ gave MIC_{90} of 42.36 µg/mL. Good MIC_{90} of 10.698 µg/mL was observed when a 2-aryl substituent bearing a 4-OMe was attached. The methoxy group participates in hydrogen bonding and this helps in fixing the molecule in the receptor grid and thus improving the binding of the molecule in the active binding site. Based on this information, we further expored

the *C(4)-Cl* position of the pre-requisite 4-chloroquinazolines by attaching ethynylpyridine through Sonogashira cross-coupling.

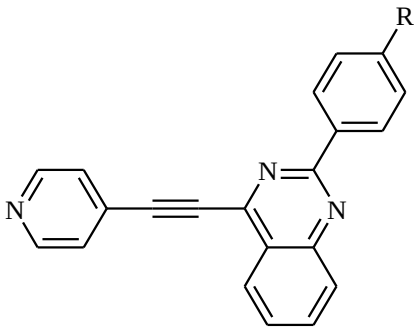

125a - e

Table 5.12: MIC_{90} data for GFP assay for 7 and day 14 data for compounds **125a-e**

R	Entry #	After day 7 data		After day 14 data	
		CAS	ADC	CAS	ADC
-Cl	125a	3.355	23.836	6.338	58.347
-Br	125b	3.625	62.5	6.593	>125
-F	125c	60.25	>125	39.35	>125
$-NO_2$	125d	8.267	>125	10.806	>125
-OMe	125e	<0.244	12.102	<0.244	8.48
#####	Rifampicin	0.01	0.01	0.001	0.001

Compounds with protruding pyridyl groups are considered suitable for application against TB [16]. Examples include first line drug isoniazid and second line drugs ethionamide and prothionamide. The 4-ethynylpyridine cross-coupled quinazoline derivatives gave the most promising preliminary *in vitro* anti-*Mtb* activity with MIC_{90} ranging from 0.723 – (>125) µg/mL. From **Table 5.5**, compound **125d** which bears a 4-NO_2 group on the *para*-postion of the 2-aryl substituent gave an improved MIC_{90} which increased from 42.362 µg/mL to 8.267 µg/mL. Compound **125c** registered a loss in activity as the MIC_{90} decreased from 30.969 µg/mL to an undesirable 60.25 µg/mL concentration. Compound **126e**, which bears a methoxy group on the 4-position of the 2-aryl substituent gave the highest MIC_{90} of <0.244 µg/mL. Varying the 4-position of the 2-aryl substituent appeared to negate the activity of the 4-ethynylpyridine-quinazoline series. This is because an attachment of 2-aryl

substituents with 4-Cl (compound **125a**) and 4-Br (compound **125b**) resulted in a drop in activity with MIC_{90} values of 3.355 µg/mL and 3.625 µg/mL respectively. Coordination of free active ligands to monomeric piano-stool Ru(ll) centre is considered to improve the bioactivity [17].

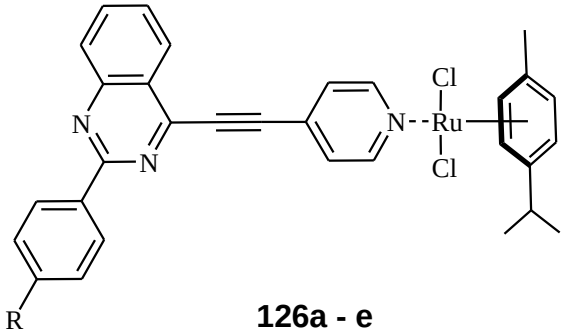

126a - e

Table 5.13: MIC_{90} data for GFP assay for 7 and day 14 data for compounds **126a-e**

R	Entry #	After day 7 data		After day 14 data	
		CAS	ADC	CAS	ADC
-Cl	126a	30.439	>125	31.864	>125
-Br	126b	11.279	>125	16.346	>125
-F	126c	15.8	>125	15.625	>125
$-NO_2$	126d	7.165	>125	3.867	>125
-OMe	126e	8.601	21.865	7.813	20.25
#####	Rifampicin	0.005	0.001	0.002	0.001

In our case we coordinated ligands **125a-e** to *p*-cymene Ru(ll) with hope to increase the activity of the ligands in Table **5.12**. Unfortunately, this theory did not suffice as the activity dropped lower than some of the free ligands. We observe a 3-fold drop for compounds **126a-b**, whose free ligands gave MIC_{90} of 3.355 µg/mL and 3.625 µg/mL. However, an improvement in activity was observed for complex **126c** whose activity improved 4-fold from 60.25 µg/mL of the free ligand **125c** to 15.8 µg/mL of the Ru(ll) complex **126c**. A minute improvement in activity was observed for complex **126d** MIC_{90} 7.165 µg/mL. For this slight improvement, the activity of the complex may as well be systematic as the introduction of the *p*-cymene Ru(ll) group did not seem to effectively incline the activity of the free ligand of which MIC_{90} was 8.267 µg/mL. For the free ligand **125e**, the activity dropped from <0.244 µg/mL to 8.601 µg/mL for

complex **126e** which was undesirable. The reason for a drop in activity could be reasoned as the complexes being affected by efflux, though it may be premature to state, the bulkiness of the complexes may also prevent binding within the receptor grid of the target enzymes. Thus resulting in a loss in activity.

5.3. Conclusion

The imidazolyl-ethanmine Schiff base derivatives **119a-d** molecular docking investigations into cancer protreins 3F8P and 2SRC gave docking scores ranging from –6 to -9 and -8 to -10 Kcal/mol respectively. Further investigations into TB (1HTO) (*Mtb*) protein gave good docking scores ranging from -8 to -10 Kcal/mol. However, the *in vitro* screening results against *Mtb* $H_{37}R_v$ strain showed no activity due to instability of the compounds in DMSO. The 4-aminopyridyl quinazolines **123a-e** gave poor docking scores ranging from -5 to -7 Kcal/mol in the cancer protein 2SRC and this is due to the limited binding in the 2SRC receptor grid. Relatively good docking scores were realised for the 3F8P cancer protein with docking scores ranging from -5 to -9 Kcal/mol. Sensible docking scores for the **123a-e** series were realised for the 1HTO TB protein, with a range of -6 to -7 Kcal/mol. Within the **123a-e** series, ligand **123e** gave the highest docking score of -7.650 Kcal/mol. This was complemented by *in vitro* screening results, where the compound gave MIC_{90} value of 10.698 µg/mL. The ethynylpyrdine quinazoline derivatives **125a-e** gave poor docking scores within -6 Kcal/mol range and this is due to limited binding sites within the receptor grid. Satisfactory docking scores ranging from -8 to -10 Kcal/mol for the 3F8P cancer protein were obtained. The docking calculations into 1HTO TB protein range from -6 to -9 Kcal/mol and the *in silico* data complements that of *in vitro* as compound **125e** gave the highest dockig score of -9.176 Kcal/mol while the *in vitro* data gave MIC_{90} of <0.244 µg/mL. Coordination of **125a-e** to monomeric piano Ru(ll) p-cymene group resulted in a drop in activity towards *Mtb*.

The molecular docking calculations prove to be accurate in identifying possible hits in biological assays. Our data suggests that a good docking score equals good activity to some extent.

Reference

[1]. Guo, J., Hurley, M.M., Wright, J.B. and Lushington, G.H., 2004. A docking score function for estimating ligand− protein interactions: Application to acetylcholinesterase inhibition. *Journal of Medicinal Chemistry*, *47*(22), pp.5492-5500.

[2]. Shapiro, B.M. and Stadtman, E.R., 1970. [130] Glutamine synthetase (Escherichia coli). In *Methods in enzymology* (Vol. 17, pp. 910-922). Academic Press.

[3]. Mehta, R., Pearson, J.T., Mahajan, S., Nath, A., Hickey, M.J., Sherman, D.R. and Atkins, W.M., 2004. Adenylylation and catalytic properties of Mycobacterium tuberculosis glutamine synthetase expressed in Escherichia coli versus mycobacteria. *Journal of Biological Chemistry*, *279*(21), pp.22477-22482.

[4]. Altaf AA, Shahzad A, Gul Z, Rasool N, Badshah A, Lal B, Khan E. A review on the medicinal importance of pyridine derivatives. *Journal of Drug Design and Medicinal Chemistry*. 2015 Sep 29;1(1):1-1.

[5]. Nordqvist A, Nilsson MT, Lagerlund O, Muthas D, Gising J, Yahiaoui S, Odell LR, Srinivasa BR, Larhed M, Mowbray SL, Karlén A. Synthesis, biological evaluation and X-ray crystallographic studies of imidazo [1, 2-a] pyridine-based *Mycobacterium tuberculosis* glutamine synthetase inhibitors. *Medicinal Chemistry Communications*. 2012;3(5):620-6

[6]. Paxman, J.J., Borg, N.A., Horne, J., Thompson, P.E., Chin, Y., Sharma, P., Simpson, J.S., Wielens, J., Piek, S., Kahler, C.M. and Sakellaris, H., 2009. The structure of the bacterial oxidoreductase enzyme DsbA in complex with a peptide reveals a basis for substrate specificity in the catalytic cycle of DsbA enzymes. *Journal of Biological Chemistry*, pp.jbc-M109.

[7]. Schmid, M.C., Hooper, A.B., Klotz, M.G., Woebken, D., Lam, P., Kuypers, M.M., Pommerening-Roeser, A., Op Den Camp, H.J. and Jetten, M.S., 2008. Environmental detection of octahaem cytochrome c hydroxylamine/hydrazine oxidoreductase genes of aerobic and anaerobic ammonium-oxidizing bacteria. *Environmental Microbiology*, *10*(11), pp.3140-3149.

[8]. Battelli, M.G., Bortolotti, M., Polito, L. and Bolognesi, A., 2018. The role of xanthine oxidoreductase and uric acid in metabolic syndrome. *Biochimica et Biophysica Acta (BBA)-Molecular Basis of Disease*.

[9]. Coussens, L., Yang-Feng, T.L., Liao, Y.C., Chen, E., Gray, A., McGrath, J., Seeburg, P.H., Libermann, T.A., Schlessinger, J. and Francke, U., 1985. Tyrosine kinase receptor with extensive homology to EGF receptor shares chromosomal location with neu oncogene. *Science*, *230*(4730), pp.1132-1139.

[10]. Ullrich, A. and Schlessinger, J., 1990. Signal transduction by receptors with tyrosine kinase activity. *Cell*, *61*(2), pp.203-212.

[11]. Arora, A. and Scholar, E.M., 2005. Role of tyrosine kinase inhibitors in cancer therapy. *Journal of Pharmacology and Experimental Therapeutics*, *315*(3), pp.971-979.

[12]. Luo, B., Li, D., Zhang, A.L. and Gao, J.M., 2018. Synthesis, Antifungal Activities and Molecular Docking Studies of Benzoxazole and Benzothiazole Derivatives. *Molecules*, *23*(10), p.2457.

[13]. Maher, K. and Mohammed, S., 2018. Crown Ether Schiff bases and Their Complexes: Recent Advances Review. *Oriental Journal of Chemistry*, *34*(4), pp.1701-1718.

[14]. Chikhale, R.V., Barmade, M.A., Murumkar, P.R. and Yadav, M.R., 2018. Overview of the development of DprE1 inhibitors for combating the menace of tuberculosis. *Journal of Medicinal Chemistry*, *61*(19), pp.8563-8593.

[15]. Rajput, R. and Mishra, A.P., 2012. A review on biological activity of quinazolinones. *International Journal of Pharmaceutical Sciences*, *4*(2), pp.66-70.

[16]. Pao, W., Miller, V., Zakowski, M., Doherty, J., Politi, K., Sarkaria, I., Singh, B., Heelan, R., Rusch, V., Fulton, L. and Mardis, E., 2004. EGF receptor gene mutations are common in lung cancers from “never smokers” and are associated with sensitivity of tumors to gefitinib and erlotinib. *Proceedings of the National Academy of Sciences*, *101*(36), pp.13306-13311.

[17]. Pavan, F.R., Von Poelhsitz, G., do Nascimento, F.B., Leite, S.R., Batista, A.A., Deflon, V.M., Sato, D.N., Franzblau, S.G. and Leite, C.Q., 2010. Ruthenium(II) phosphine/picolinate complexes as antimycobacterial agents. *European Journal of Medicinal Chemistry*, *45*(2), pp.598-601.

CHAPTER 6: CONCLUSIONS AND THE FUTURE PROSPECTS

Imidazolyl ethanamine Schiff base ligands of the *N^N* type were synthesised in good yield. Attempted coordination to $ZnCl_2$ yielded poor results due to decomposition of Schiff base ligands. The 4-pyridylamino- and 4-(ethynylpyridine)quinazoline ligands bearing R = -Cl, Br, -F, $-NO_2$ and -OMe at *para* position were synthesised in good yield through dechlro-amination and sonogashira cross-coupling respectively.

The 4-(ethynylpyridine)quinazoline ligands were coordinated to Ru(ll)-*p*-cymene centre upon which the spectral characterisation by NMR, IR and Mass spectrometrey suggests mono-chelation to the Ru(ll) to adopt a piano-stool type complex.

Selected compounds **119a-d**, **121a-e**, **123a-e**, **125a-e** and **126a-e** were tested for anti-*Mycobacterium tuberculosis* properties and the 4-chloro-quinazoline series **121a-e** gave no activity due to their poor solubility in biological solvent DMSO. Similar results were obtained for the Schiff base series wherein the stability of these compounds in DMSO remains a challenge. However, the 4-(pyridylamino)quinazoline series **123a-e** gave promising activity ranging from 10 to 43 µg/mL. While the 4-(ethynylpyridine)-quinazolines gave good activity against *Mtb* with ligand **125e** giving an activity of <0.244 µg/mL. Coordination of ligands **125a-e** to Ru(ll) p-cymene resulted in a decrease in activity.

Induced-fit molecular docking of ligands **119a-d**, **121a-e**, **123a-e** and **125a-e** into active sites of 1HTO, 2SRC and 3F8P suggested that these compounds may have binding in proteins such as *glutamine synthestase* against *Mtb*, tyrosine kinase and *oxidoreductase* for possible anti-cancer activity.

In future the imidazolyl-ethanamine Schiff base of the *N^N* will be subjected to imino-protonation reactions to yield tertiary-amino two carbon spacer ligands. These ligands will be coordinated to selected transition metal and their protein binding energies will be calculated by way of molecular docking calculations. The molecular docking calculations will determine which compounds to proceed with to *in vitro* biological evaluation. The pyridylamino derivatives will be coordinated to selected transition metals and their biological activity will be investigated. Phenyl-phosphino ligation is reported to improve liphophilicity in biologically active inorganic compounds. The ethynyl-pyridine bridged Ru(ll) complexes will therefore be subjected to phosphine-

group ligation with hope to increase lipophilicity and biological activity of the Ru(ll) complexes. The compounds with promising *in vitro* activity *i.e* activity below 20 µg/mL will be evaluated for safety by way of toxicity assay.

APPENDIX

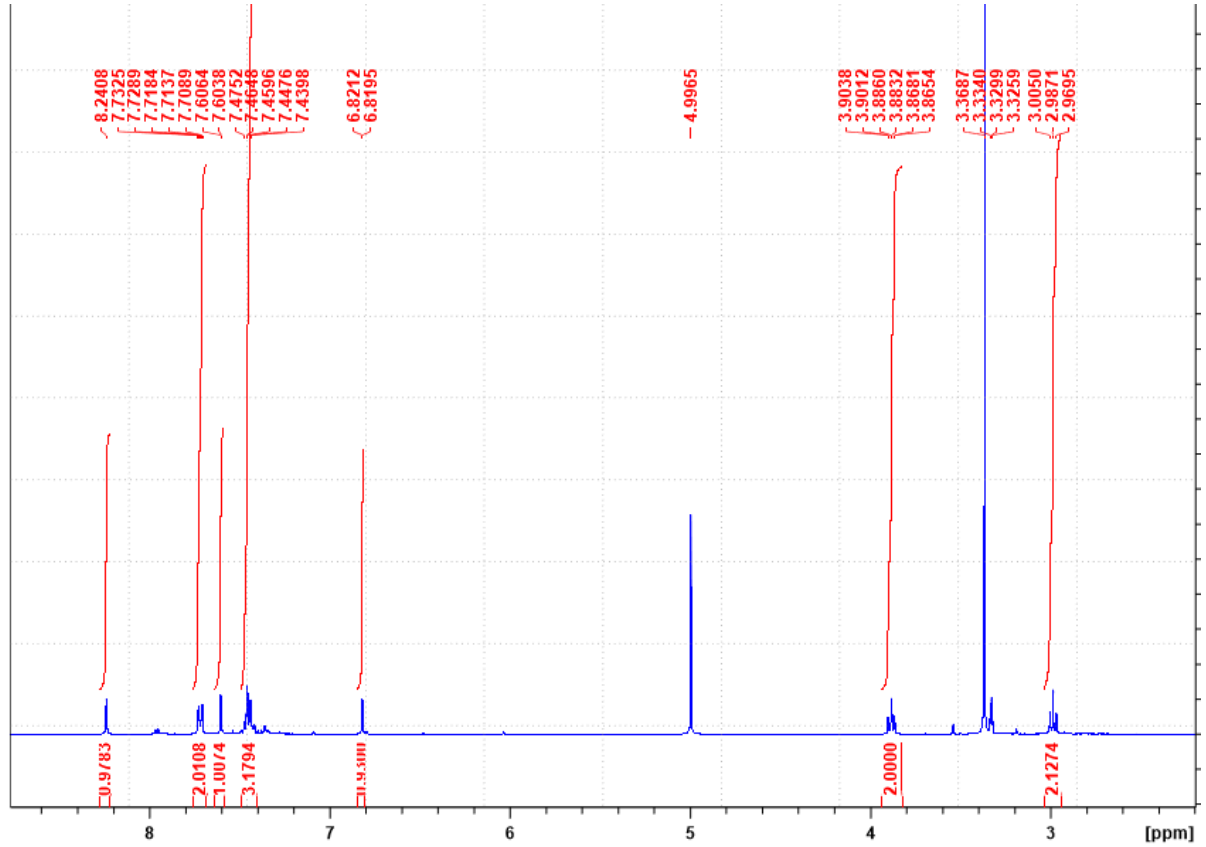

Figure 1: ^{1}H-NMR spectrum of **119a**

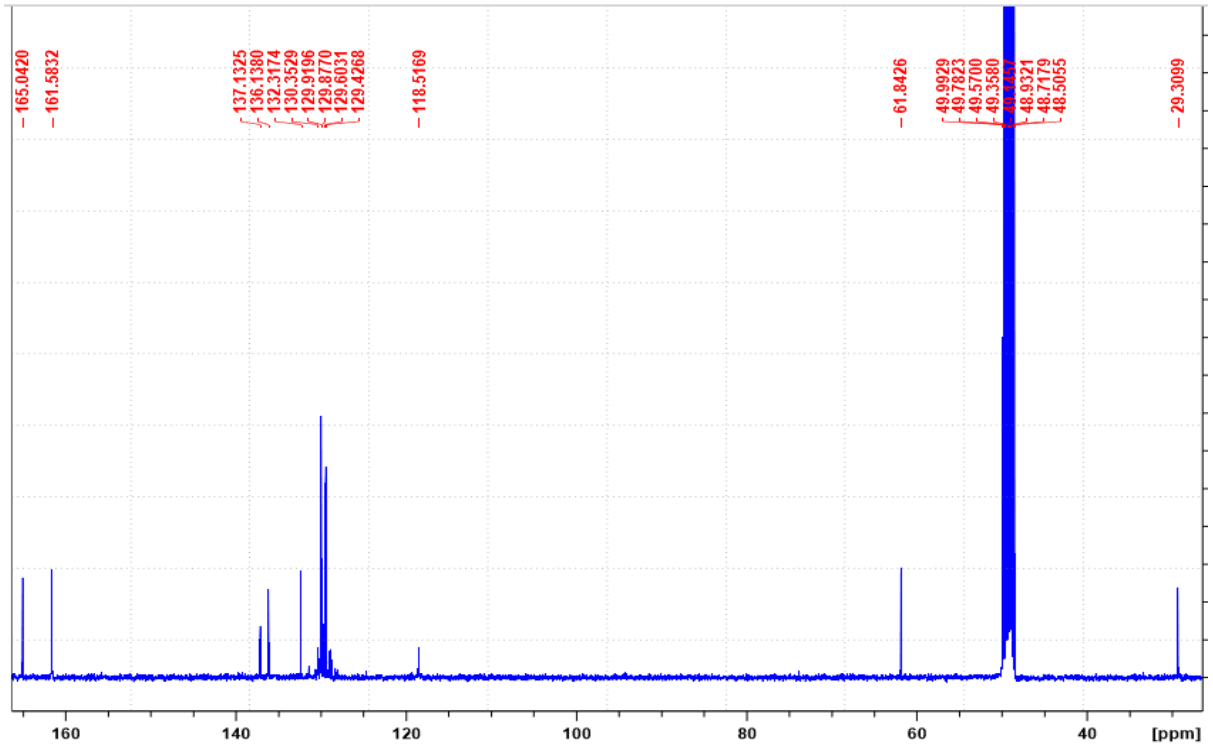

Figure 2: ^{13}C-NMR spectrum of **119a**

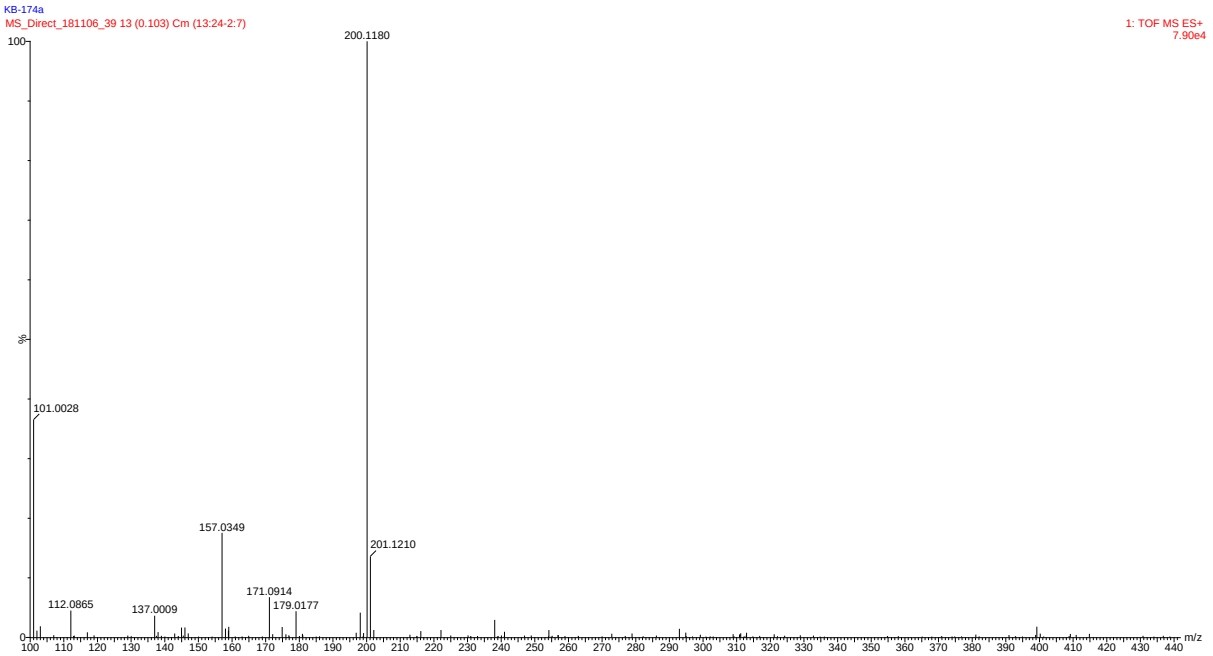

Figure 3: HRMS spectrum of **119a**

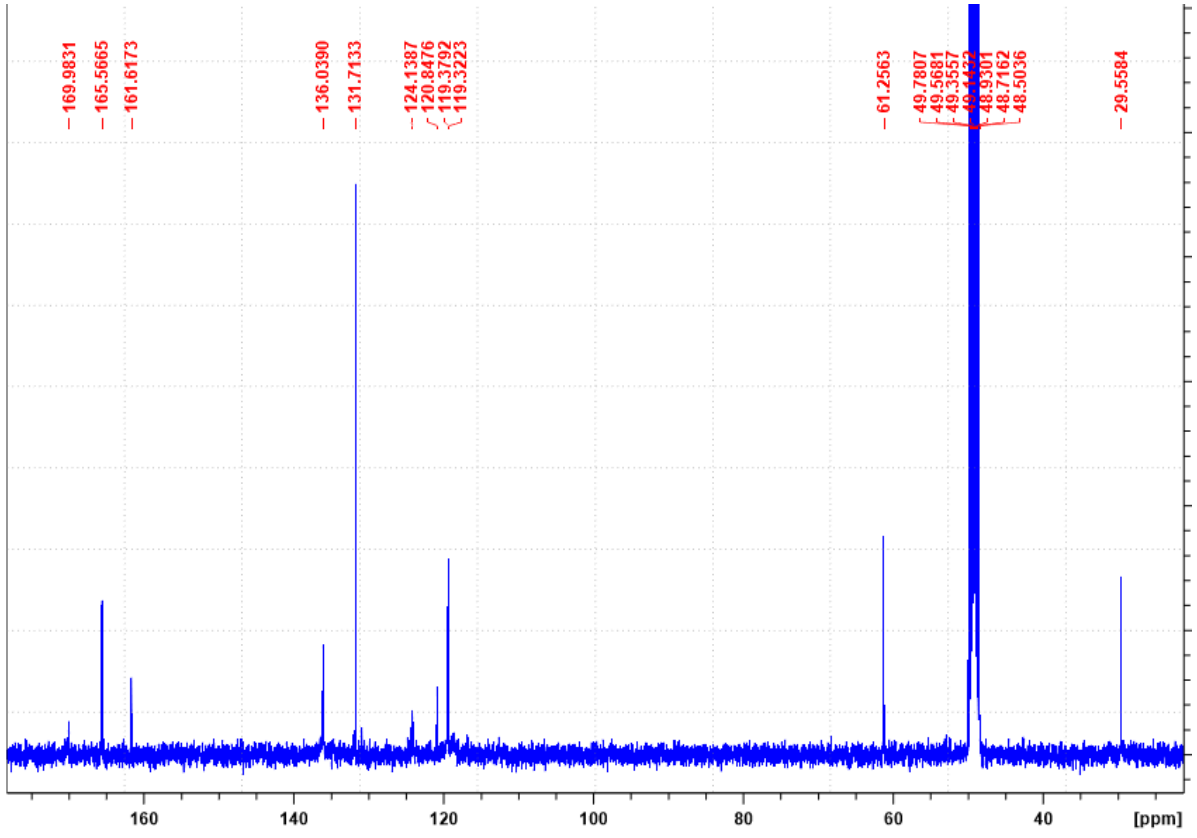

Figure 4: ^{1}H-NMR spectrum of **119b**

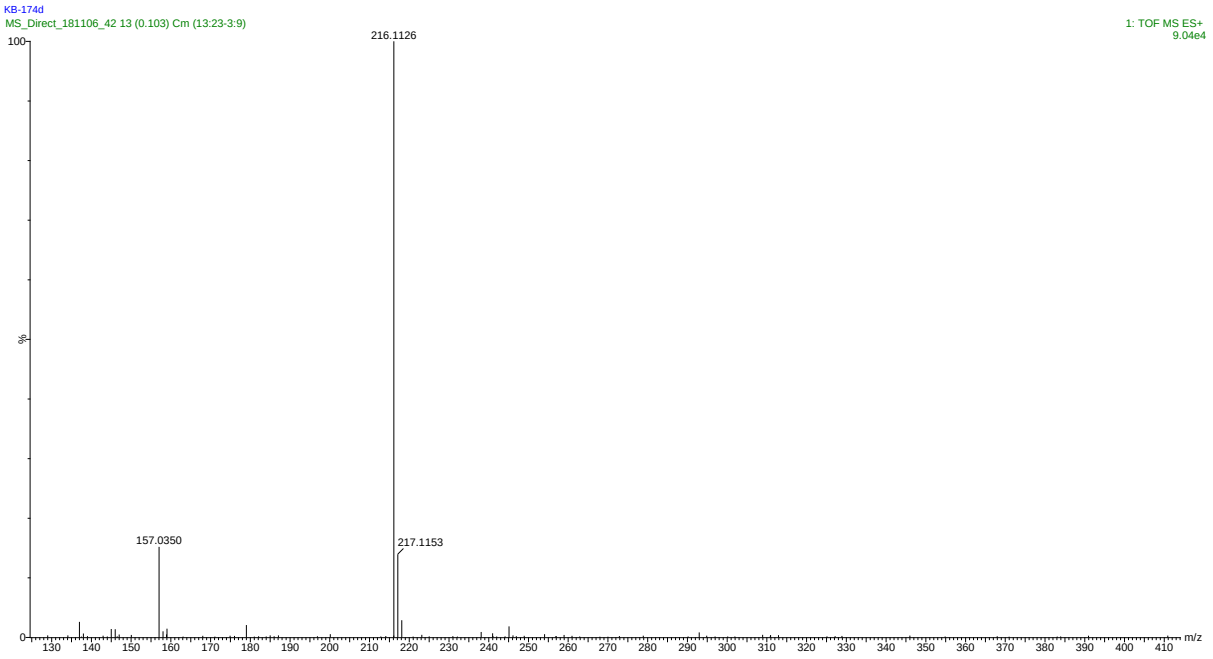

Figure 5: HRMS spectrum of **119b**

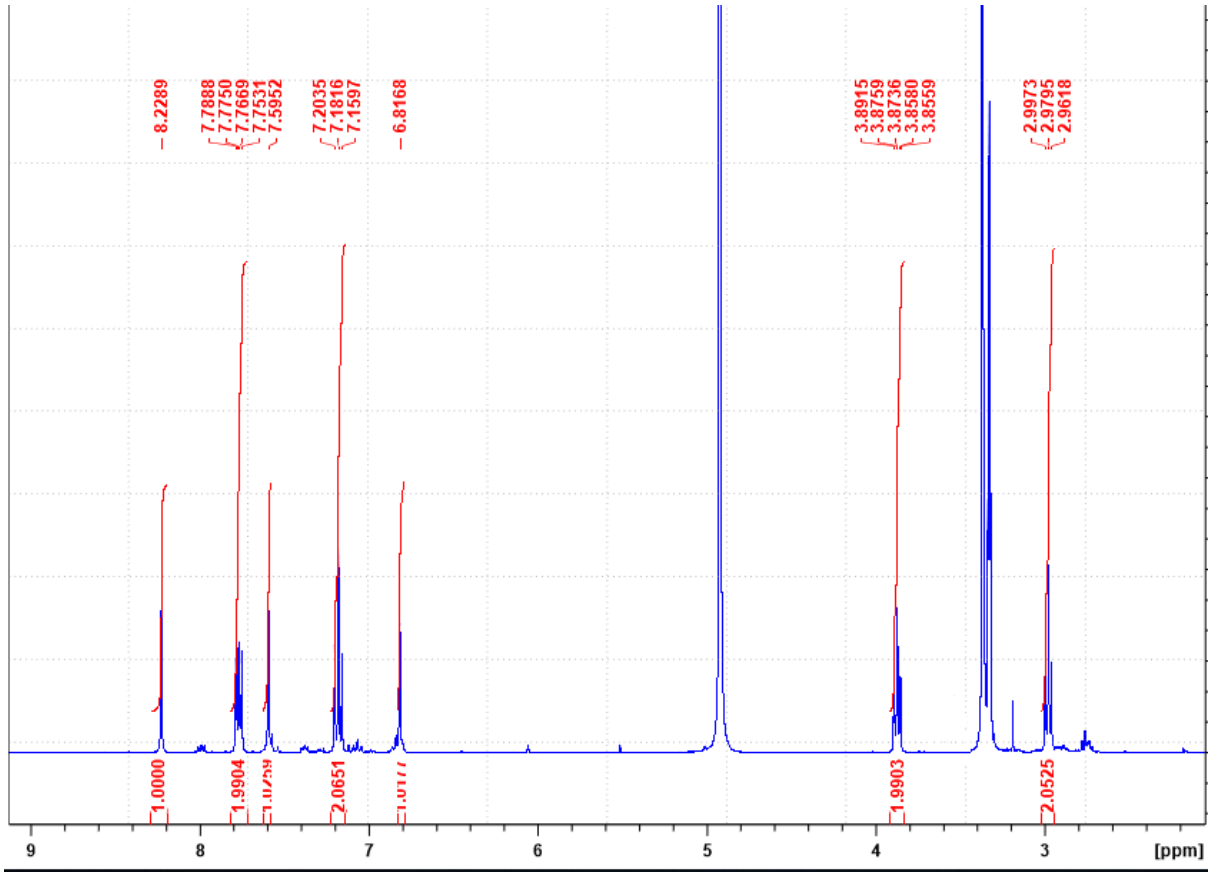

Figure 6: ^{1}H-NMR spectrum of **119c**

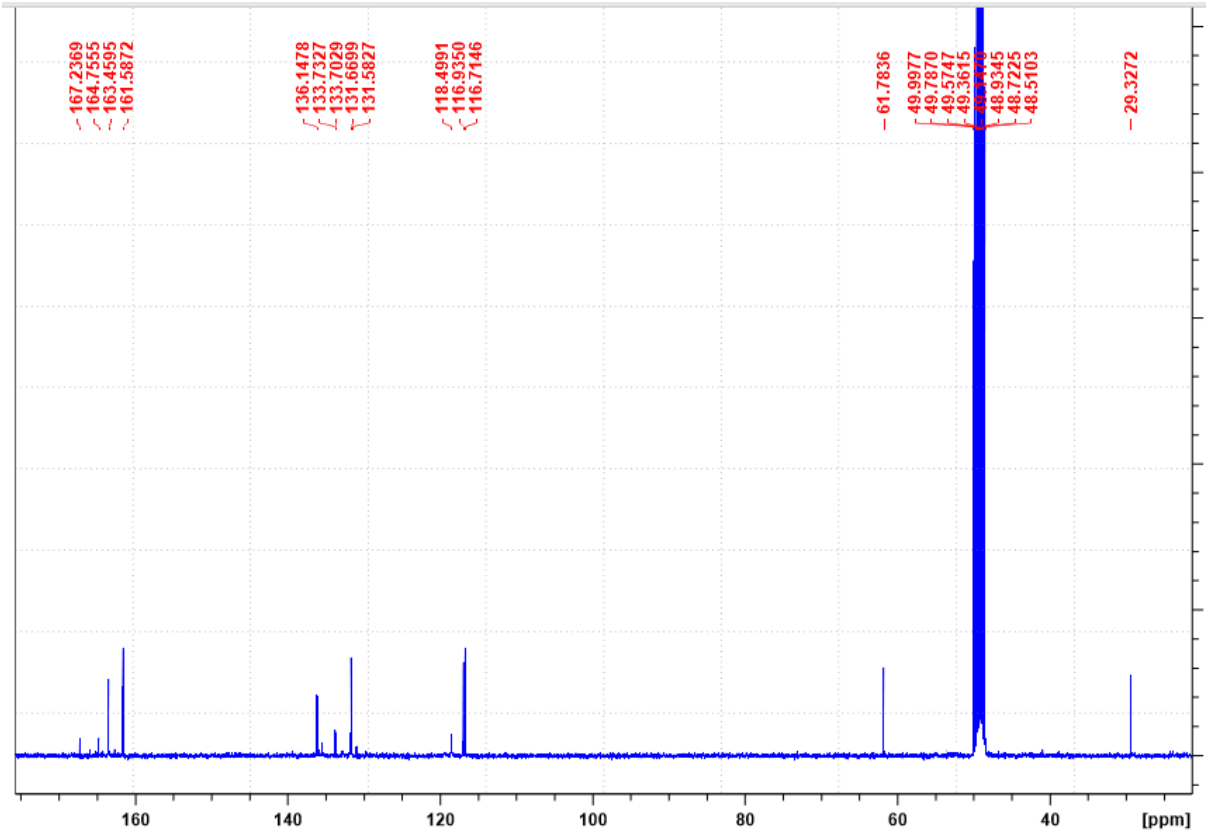

Figure 7: ^{13}C-NMR spectrum of **119c**

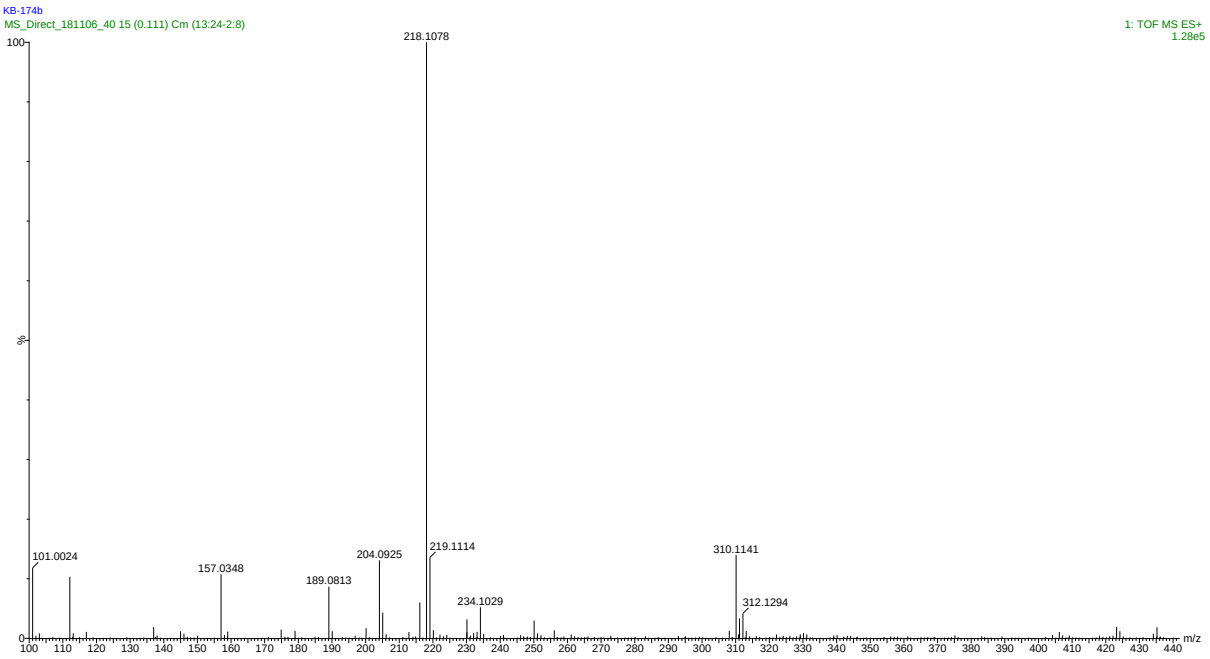

Figure 8: HRMS spectrum of **119c**

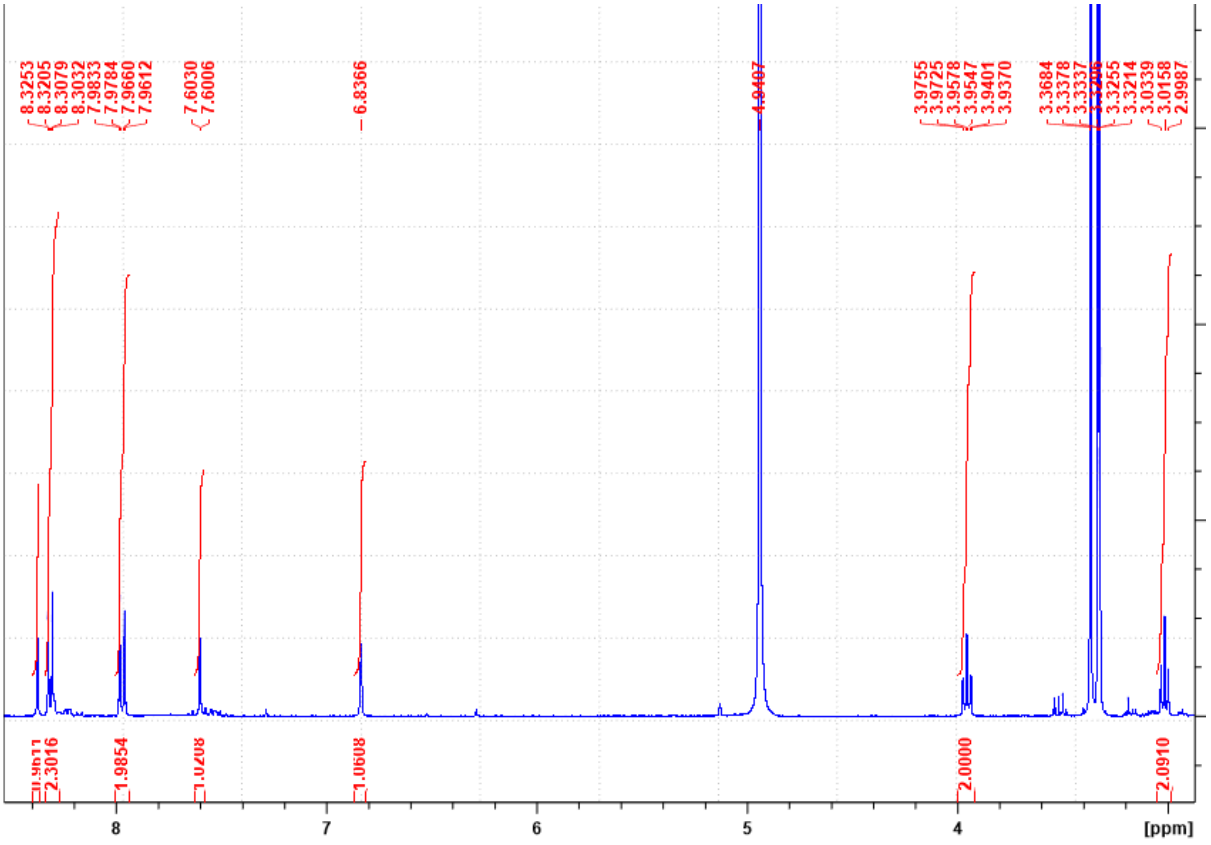

Figure 9: ^{1}H-NMR spectrum of **119d**

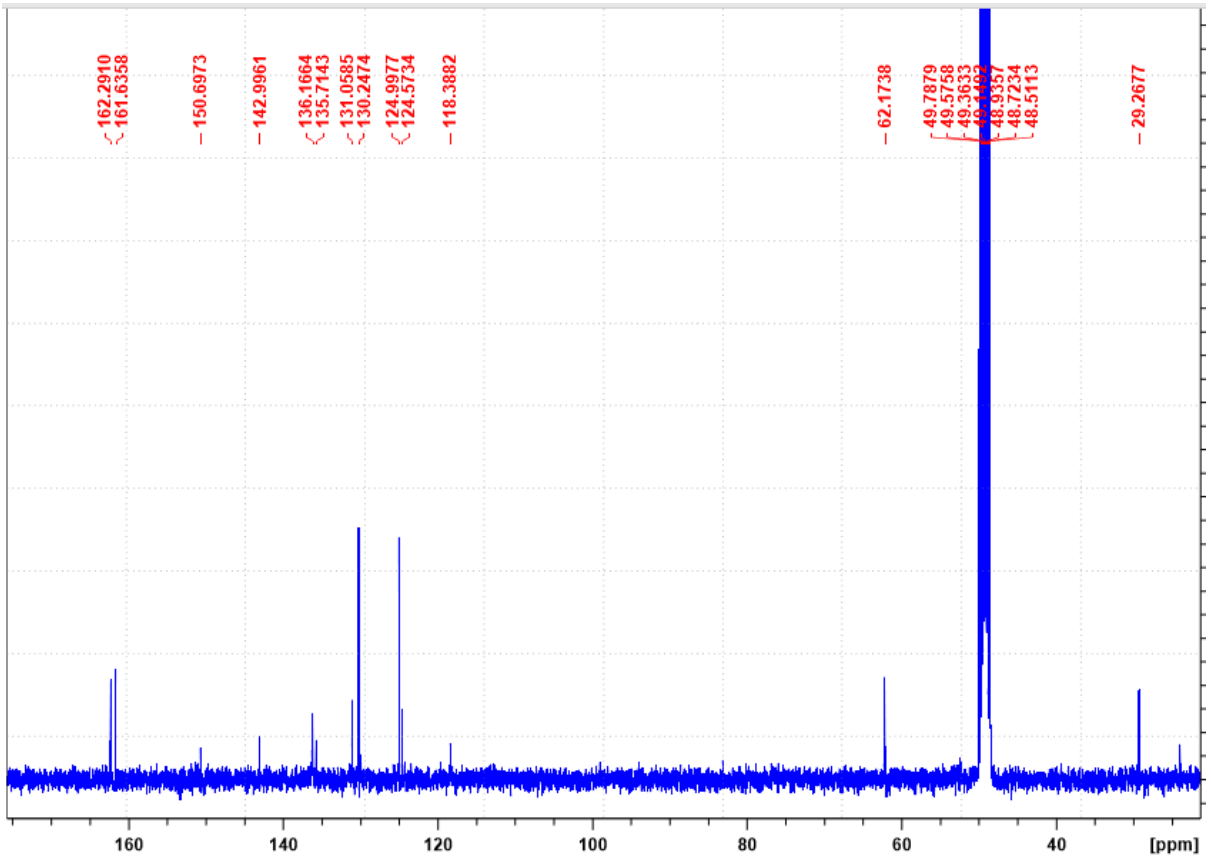

Figure 10: ^{13}C-NMR spectrum of **119d**

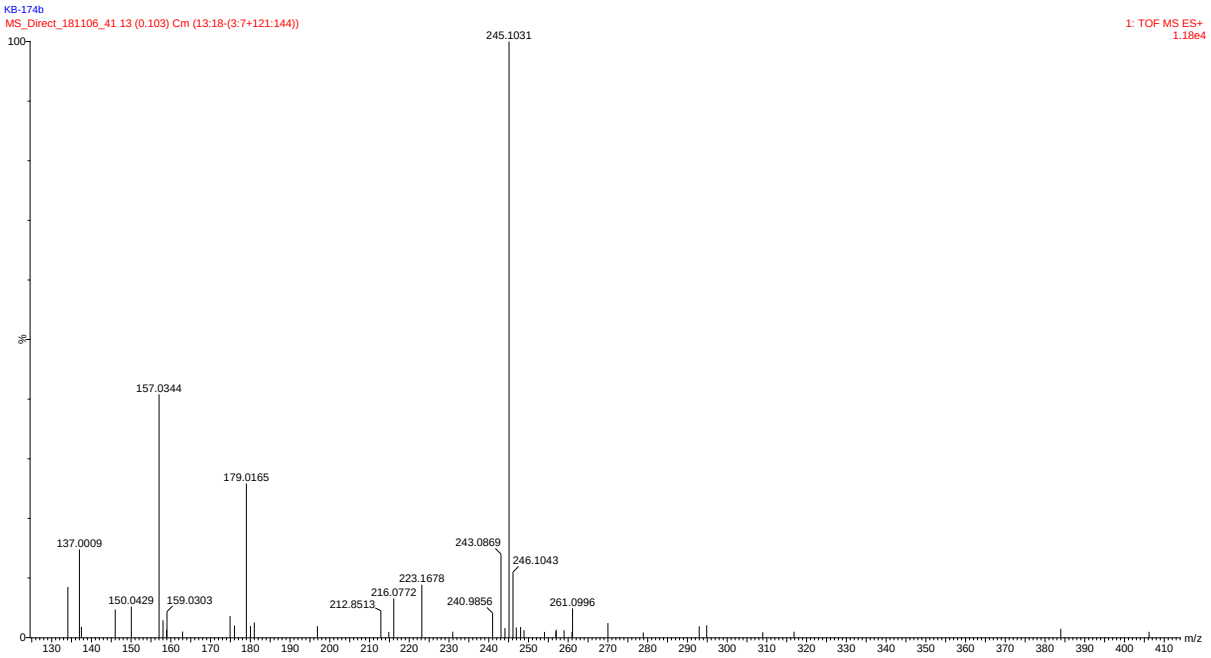

Figure 11: HRMS spectrum of **119d**

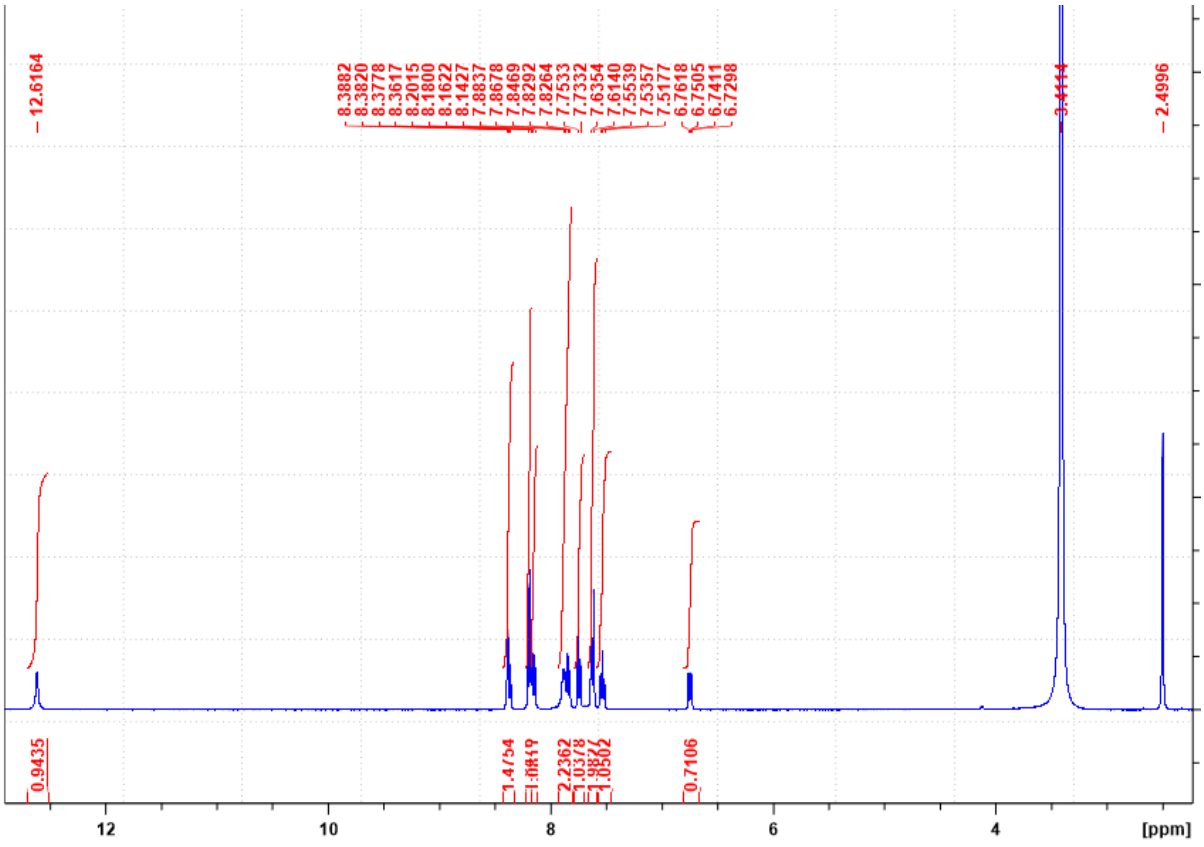

Figure 12: ^{1}H-NMR spectrum of **123a**

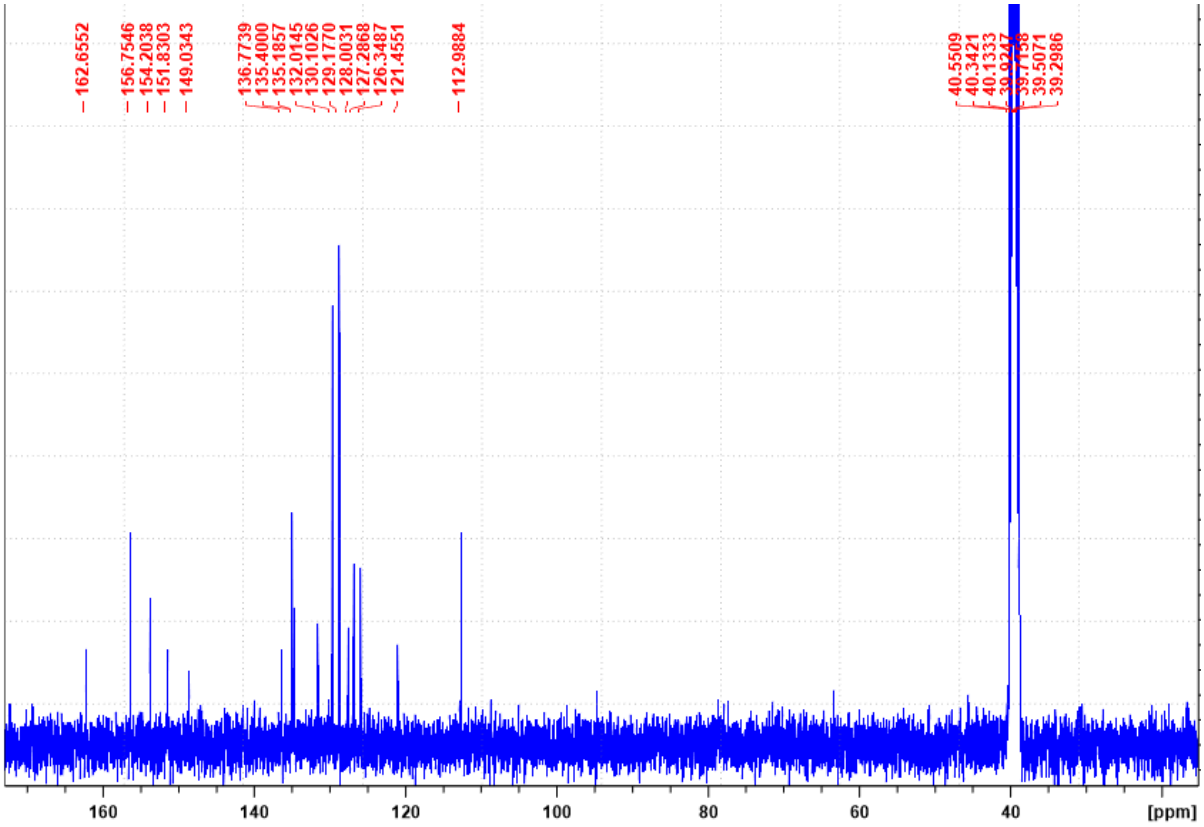

Figure 13: ^{13}C-NMR spectrum of **123a**

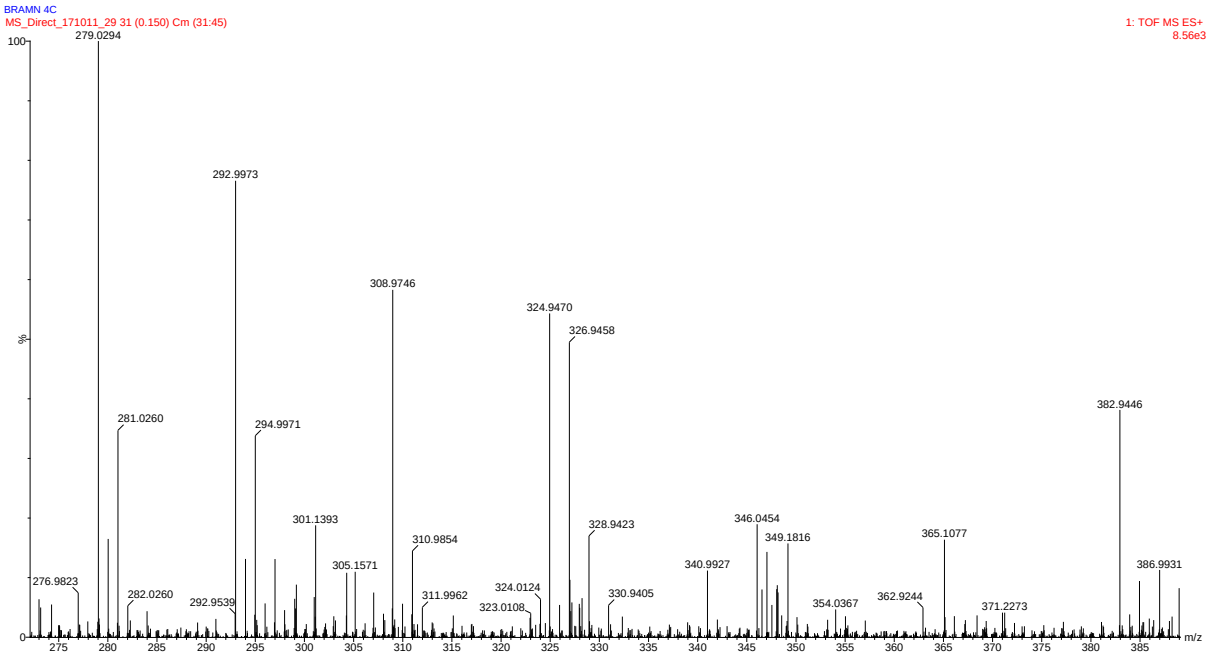

Figure 14: HRMS spectrum of **123a**

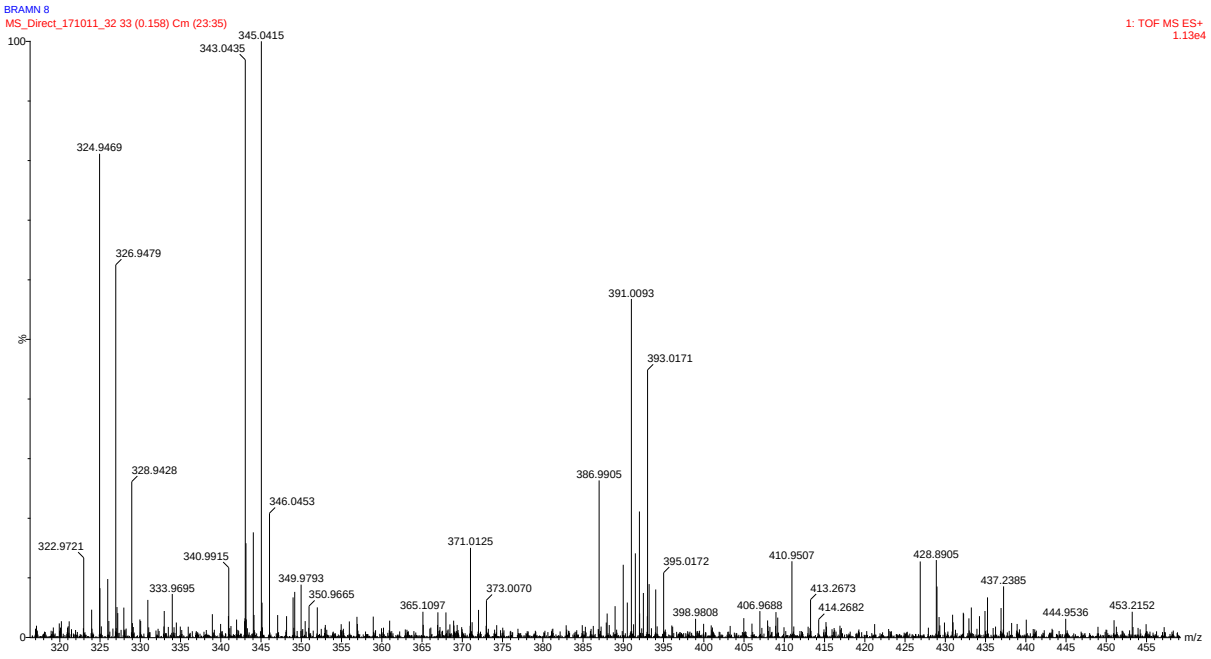

Figure 15: HRMS spectrum of **123b**

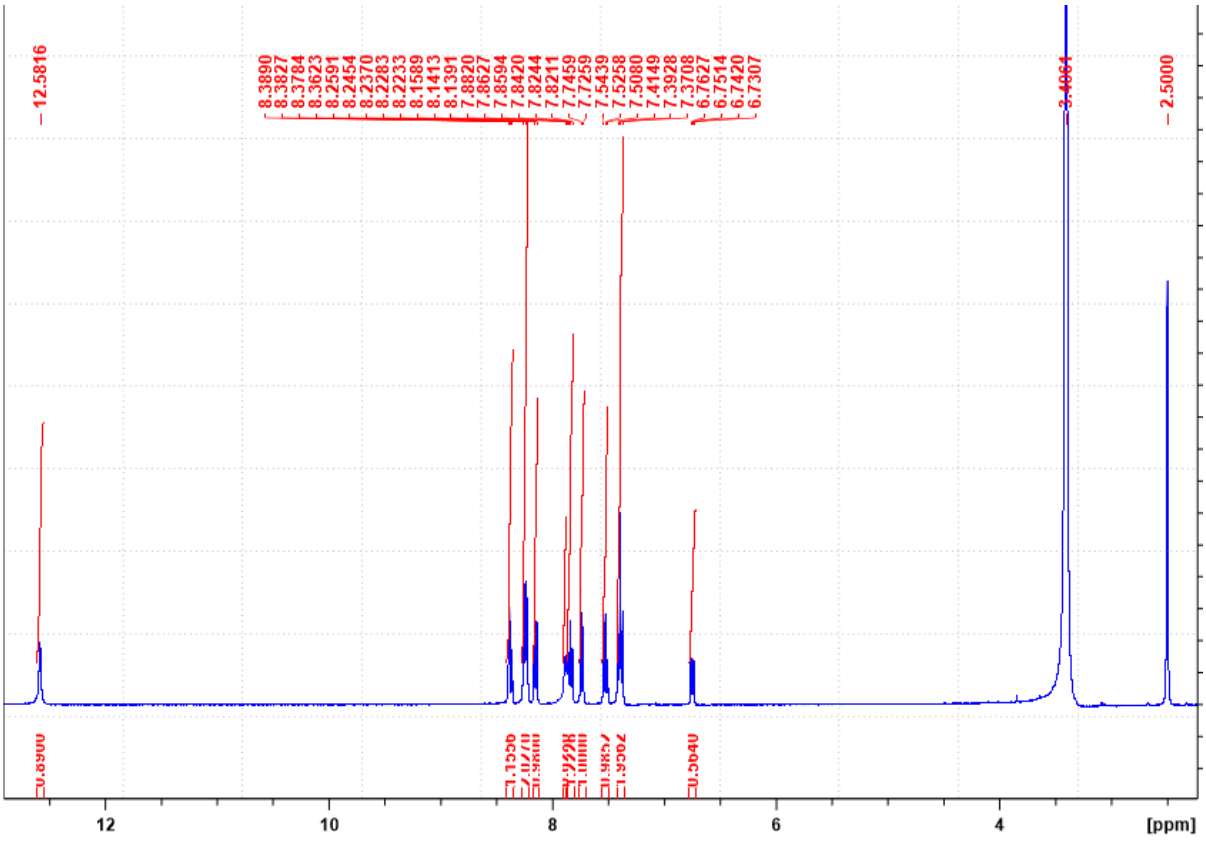

Figure 16: ^{1}H-NMR spectrum of **123c**

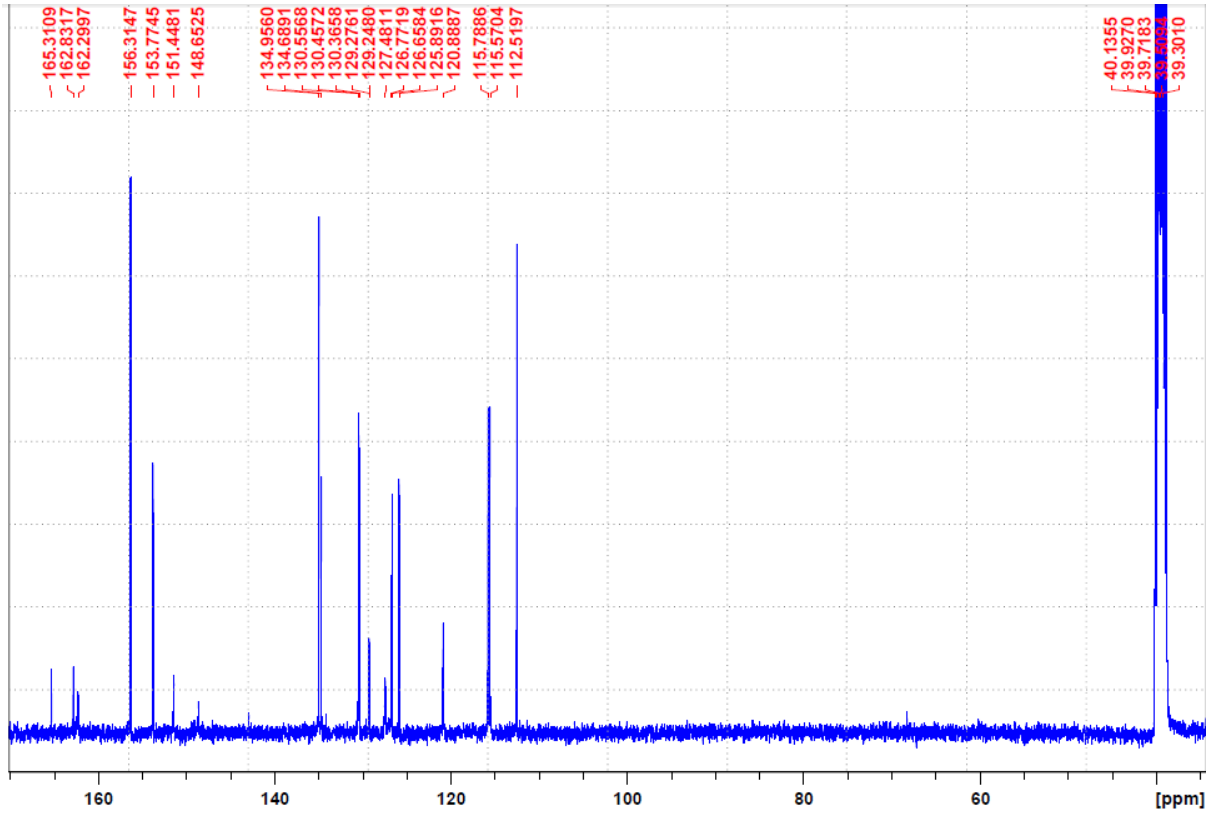

Figure 17: ^{13}C-NMR spectrum of **123c**

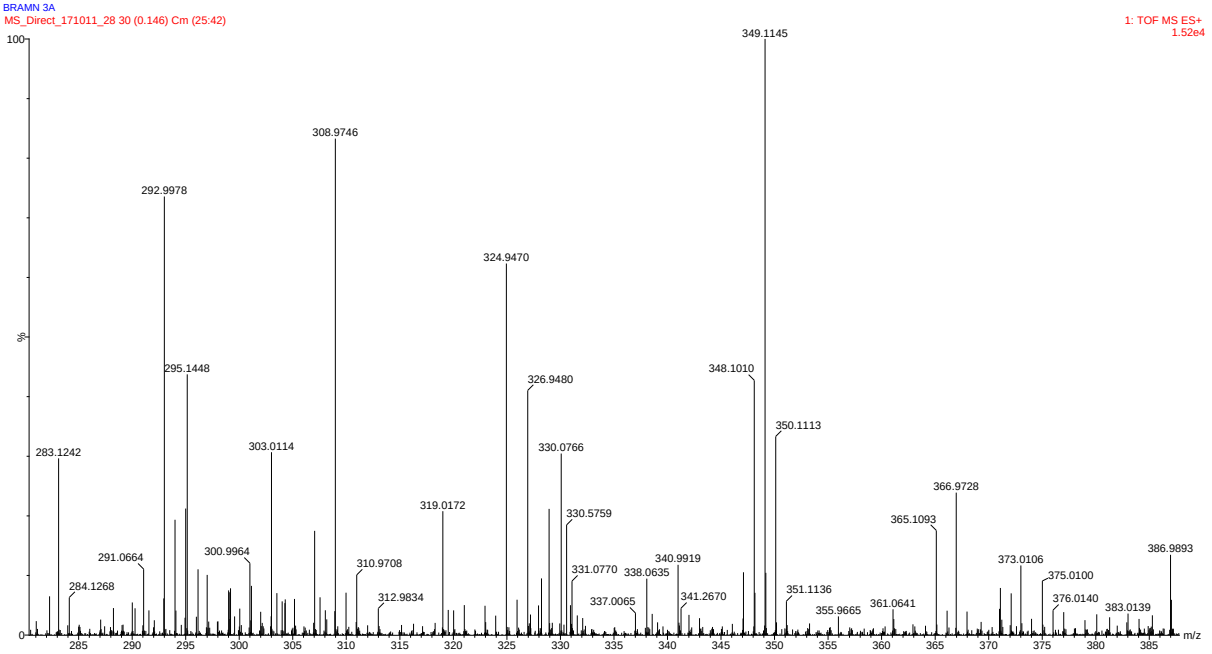

Figure 18: HRMS spectrum of **123c**

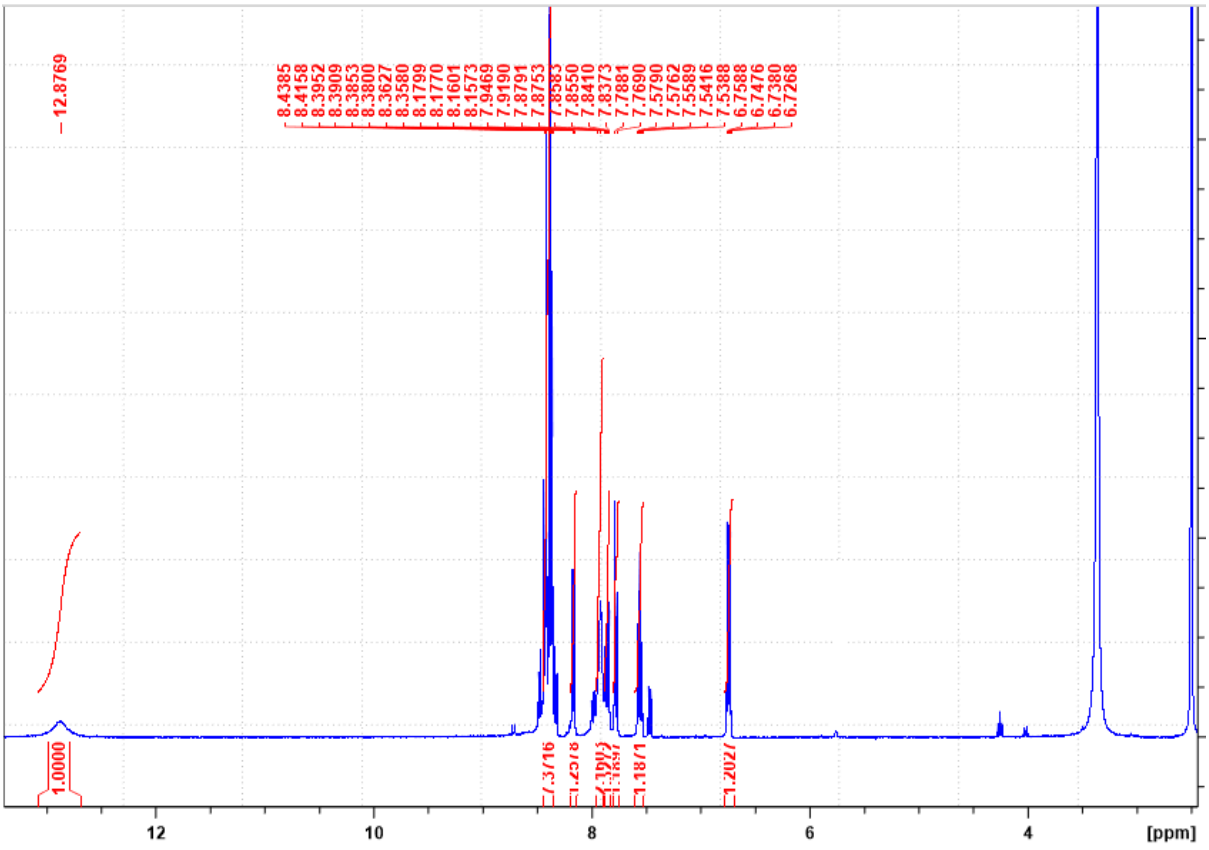

Figure 19: ^{1}H-NMR spectrum of **123d**

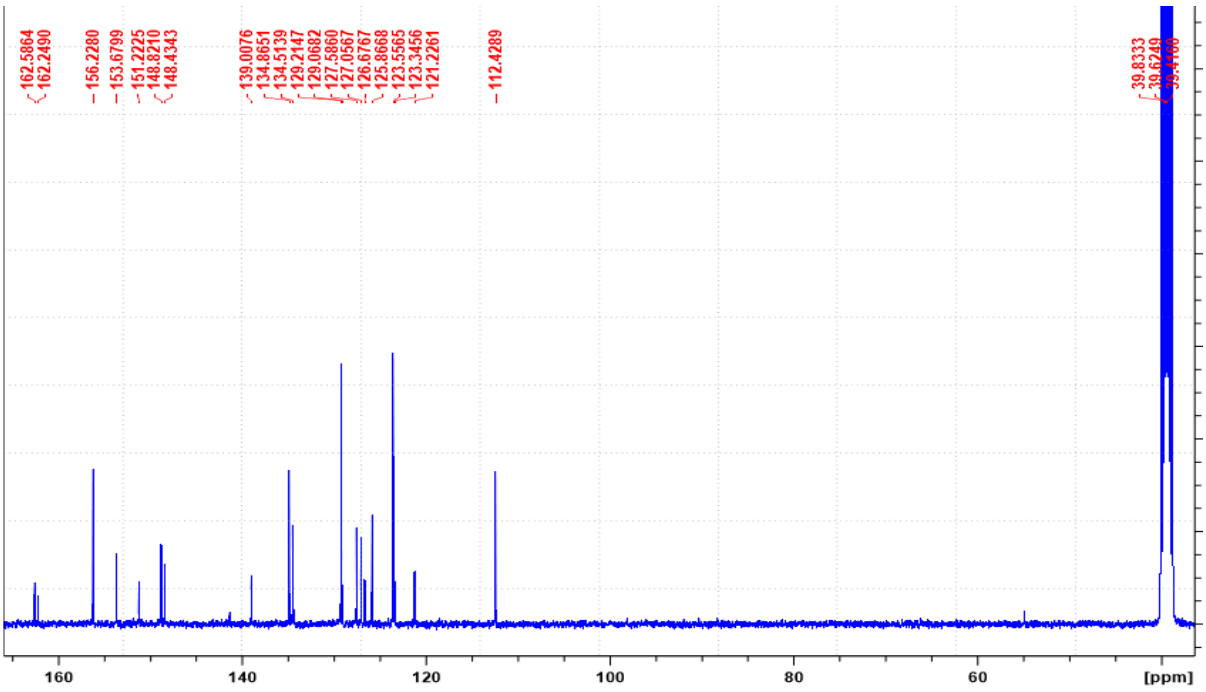

Figure 20: ^{13}C-NMR spectrum of **123d**

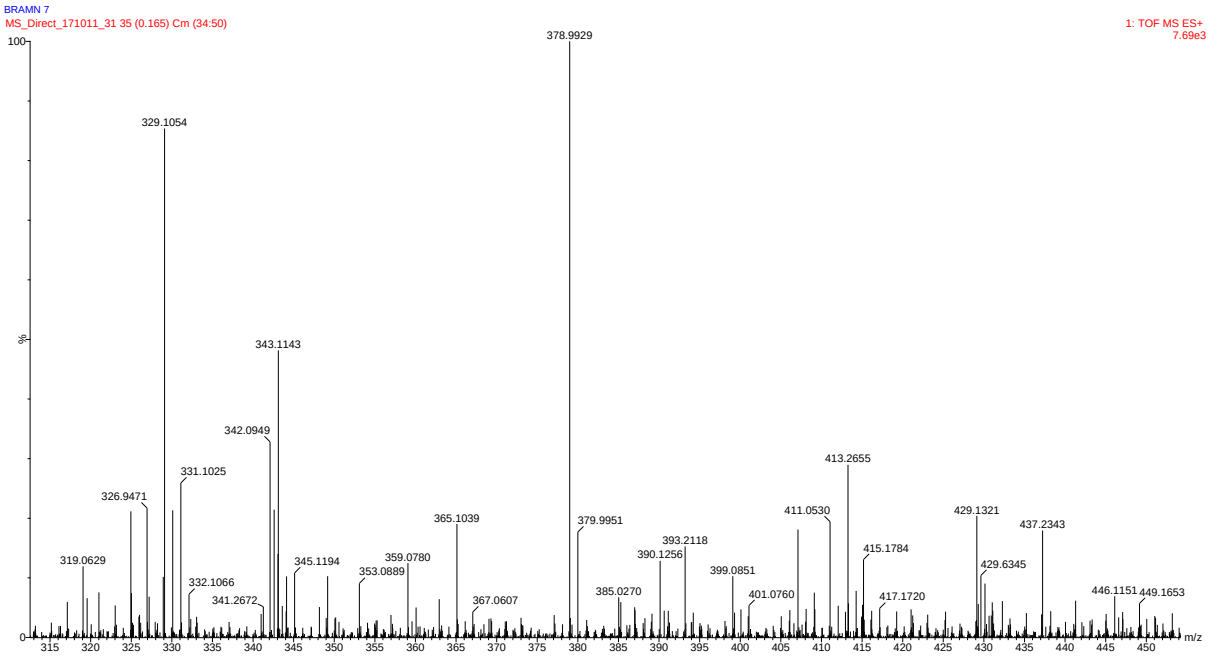

Figure 21: HRMS spectrum of **123d**

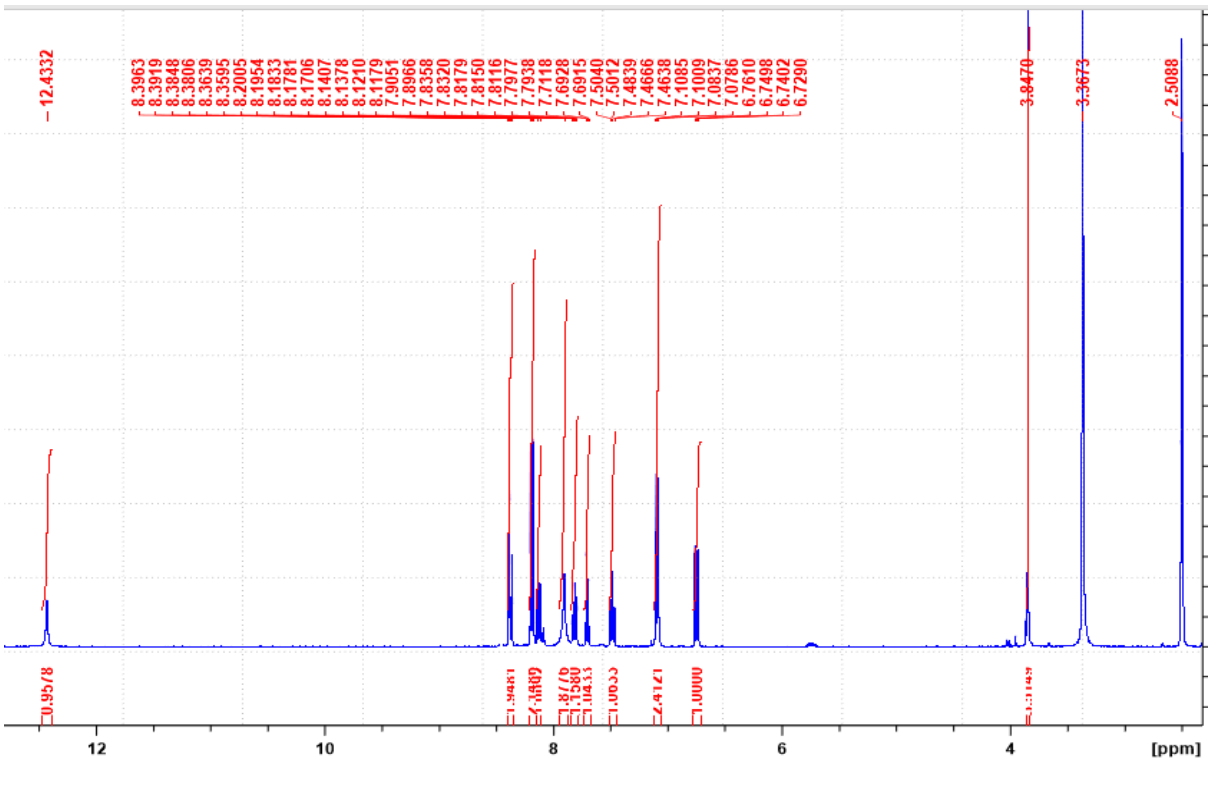

Figure 22: ^{1}H-NMR spectrum of **123e**

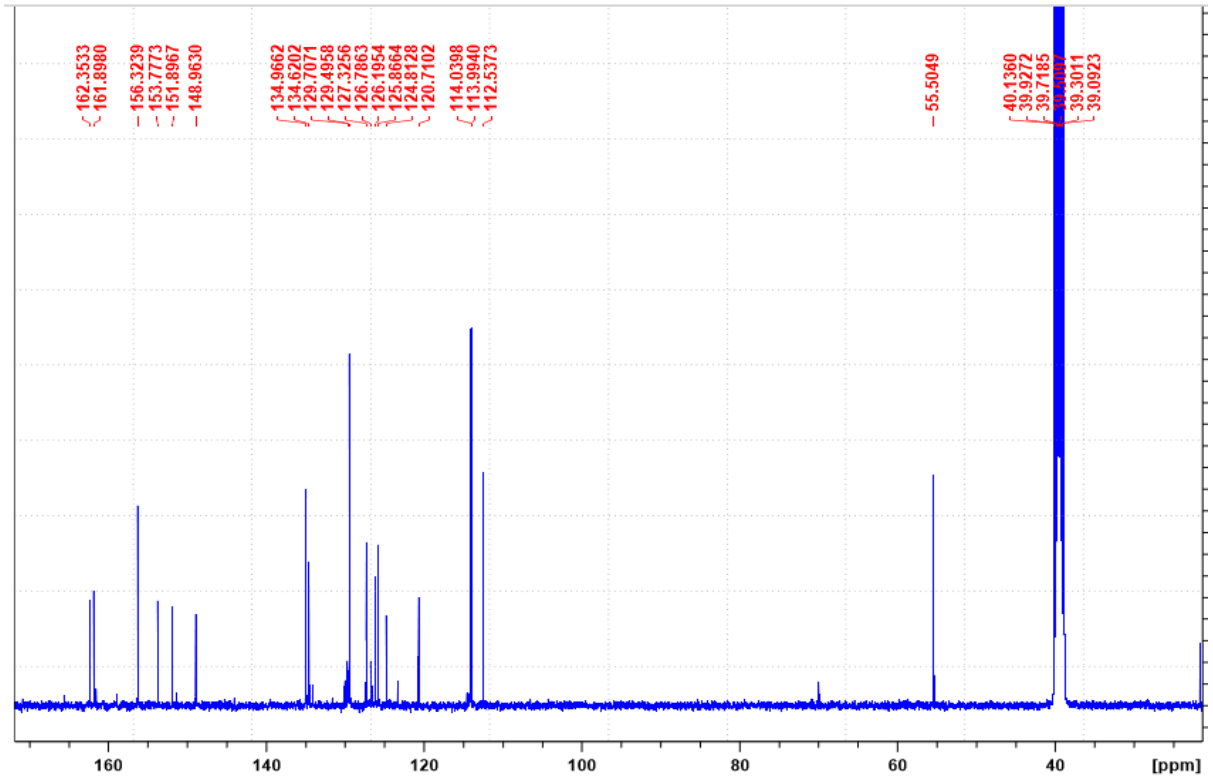

Figure 23: ^{13}C-NMR spectrum of **123e**

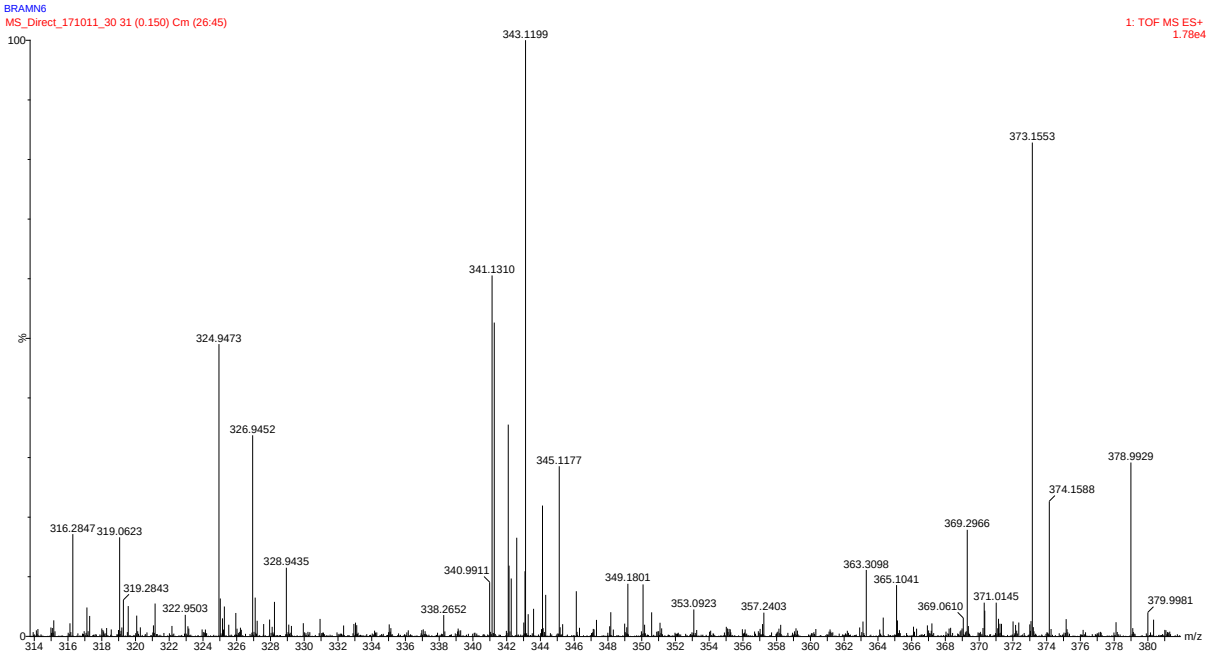

Figure 24: HRMS spectrum of **123e**

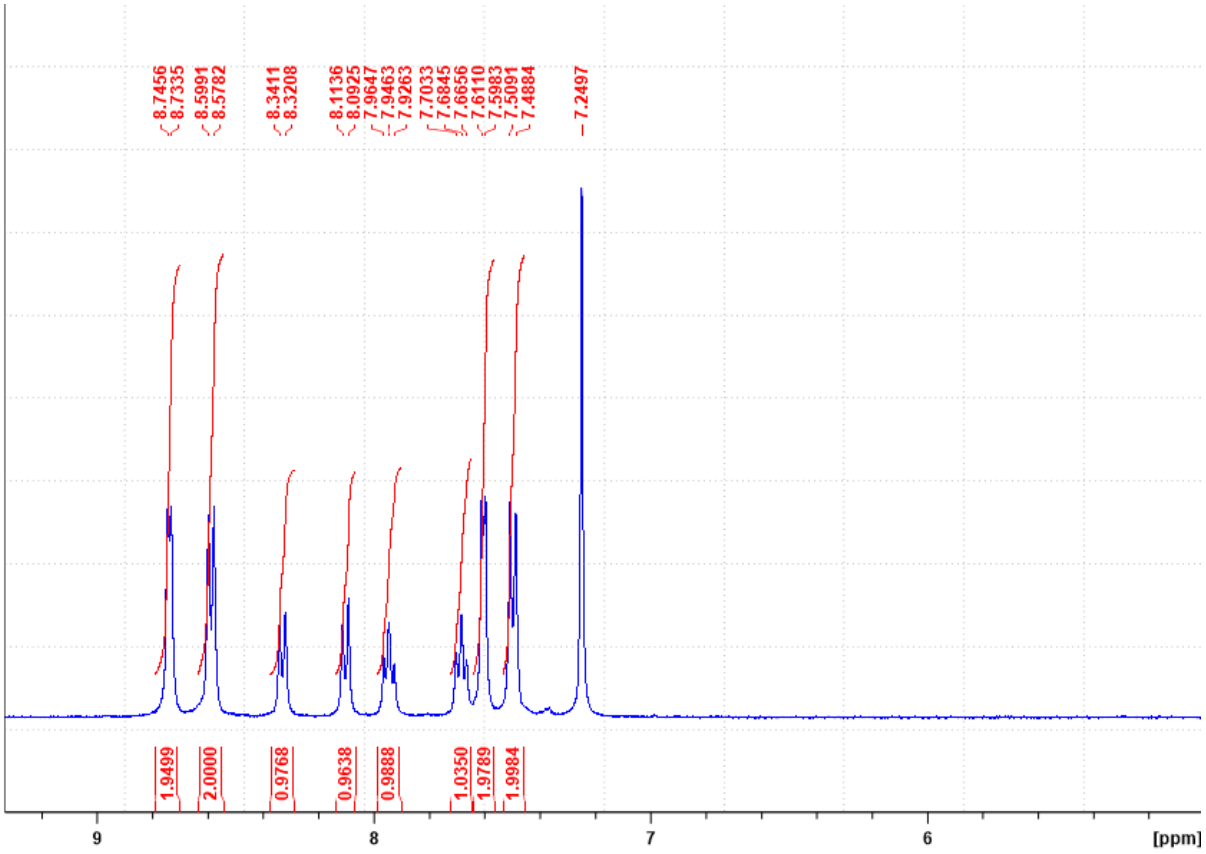

Figure 25: ^{1}H-NMR spectrum of **125a**

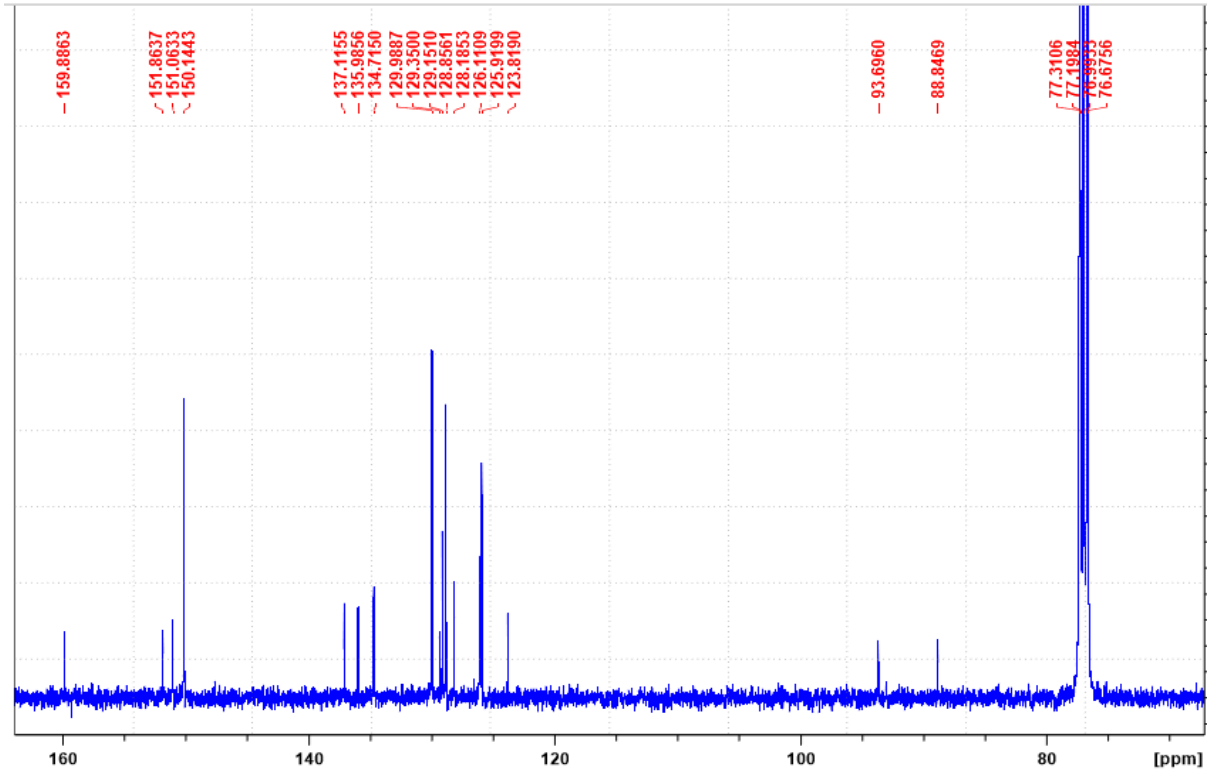

Figure 26: ^{13}C-NMR spectrum of **125a**

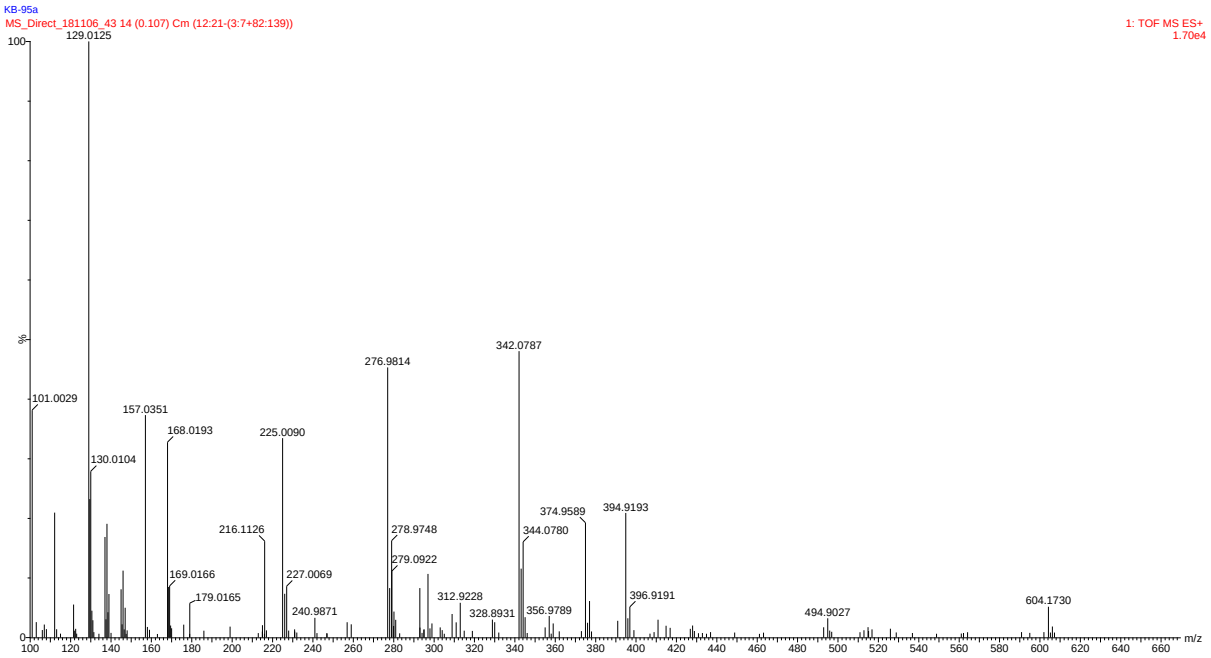

Figure 27: HRMS spectrum of **125a**

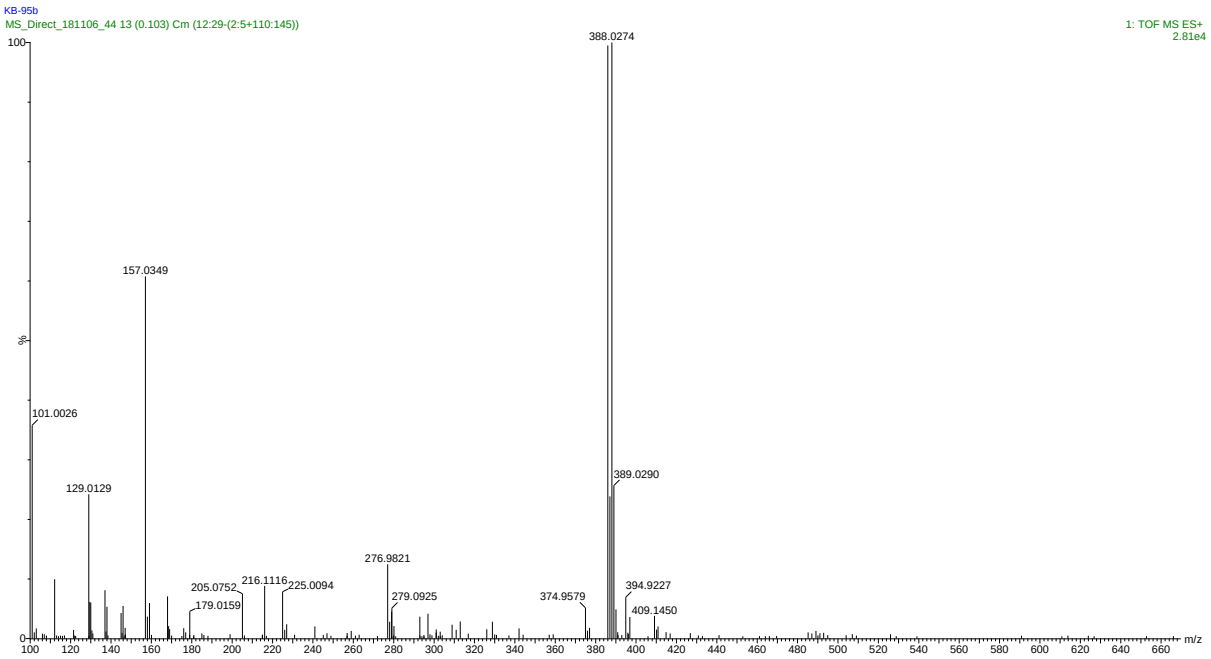

Figure 28: HRMS spectrum of **125b**

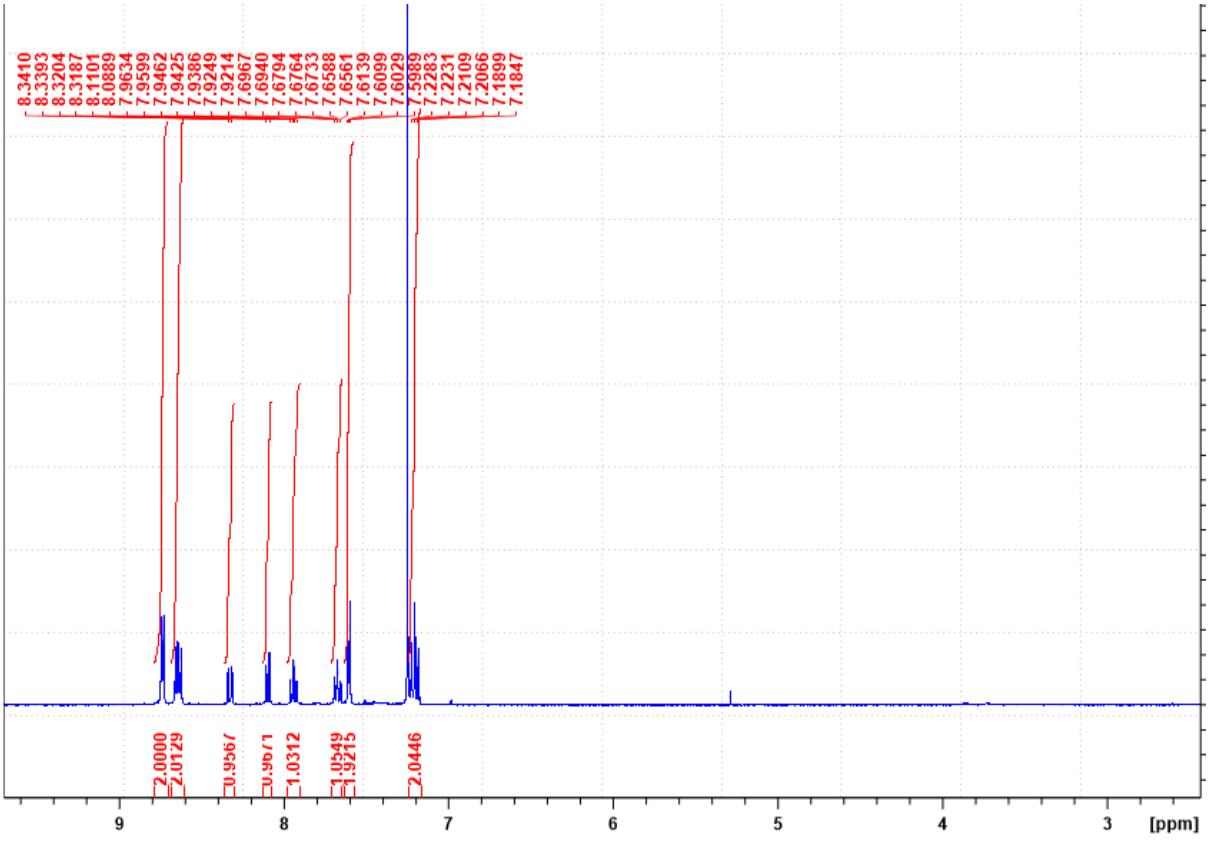

Figure 29: ^{1}H-NMR spectrum of **125c**

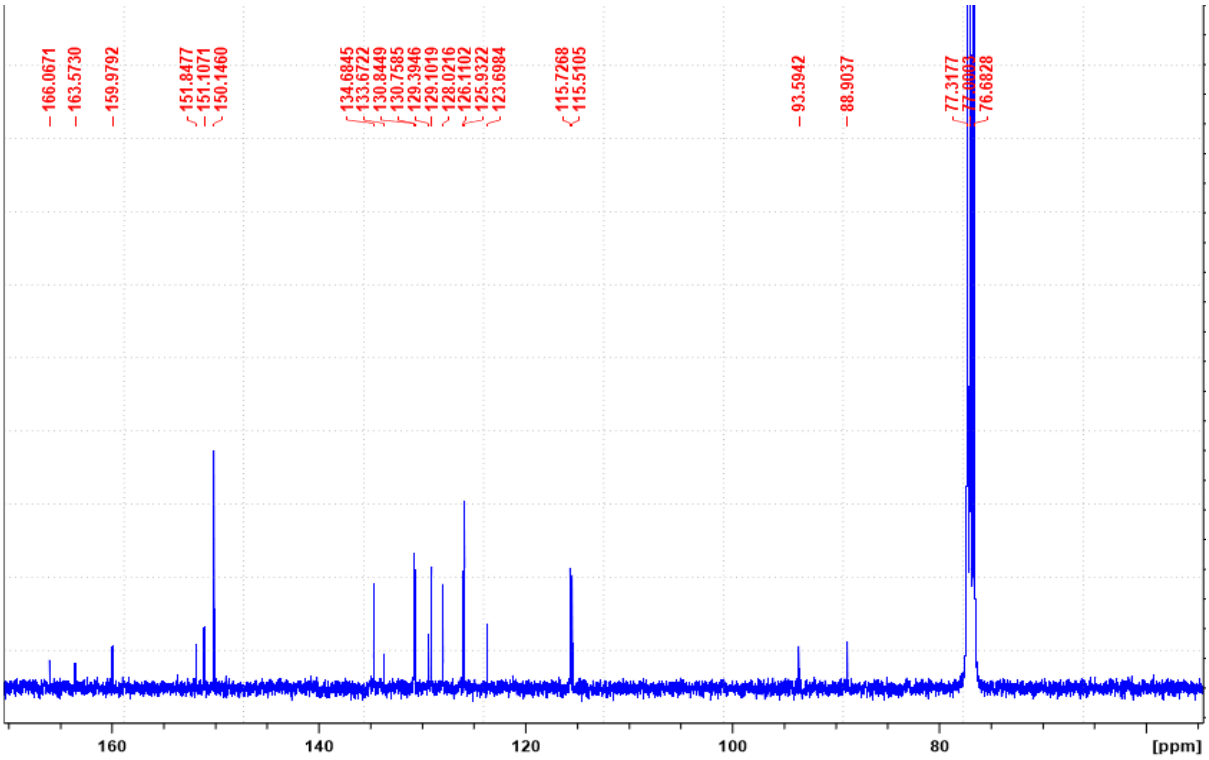

Figure 30: ^{13}C-NMR spectrum of **125c**

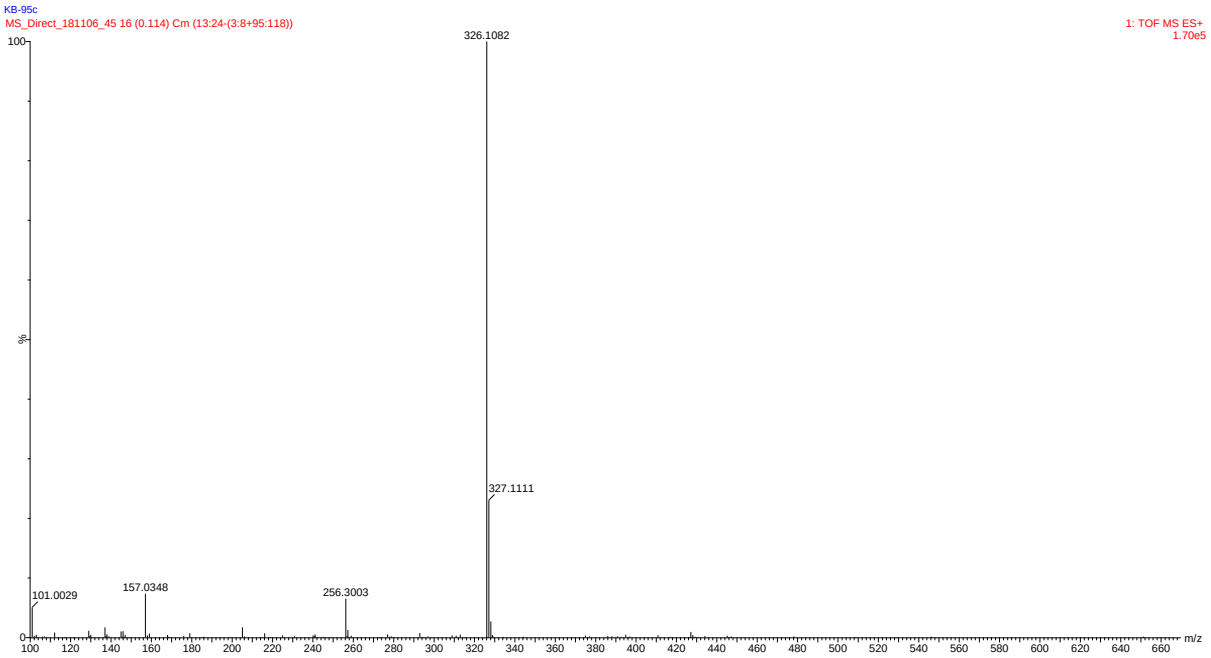

Figure 31: HRMS spectrum of **125c**

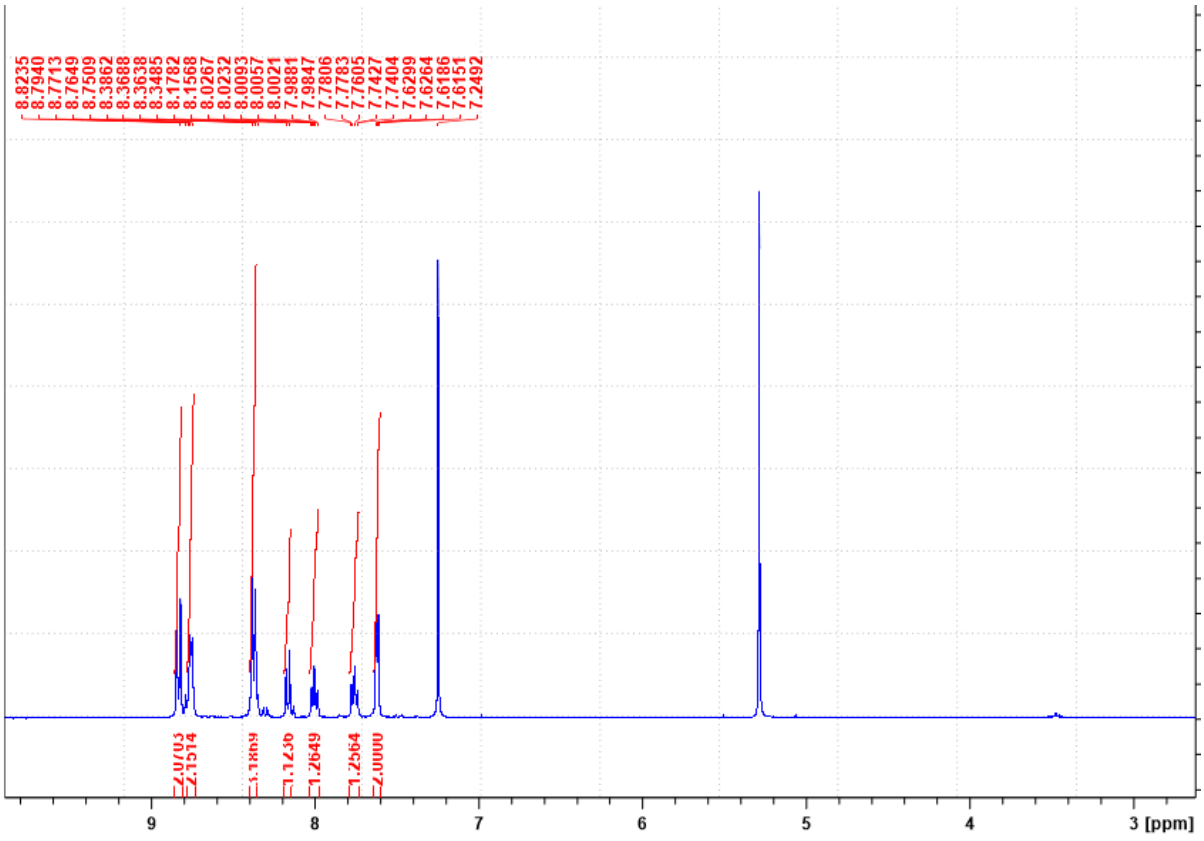

Figure 32: ^{1}H-NMR spectrum of **125d**

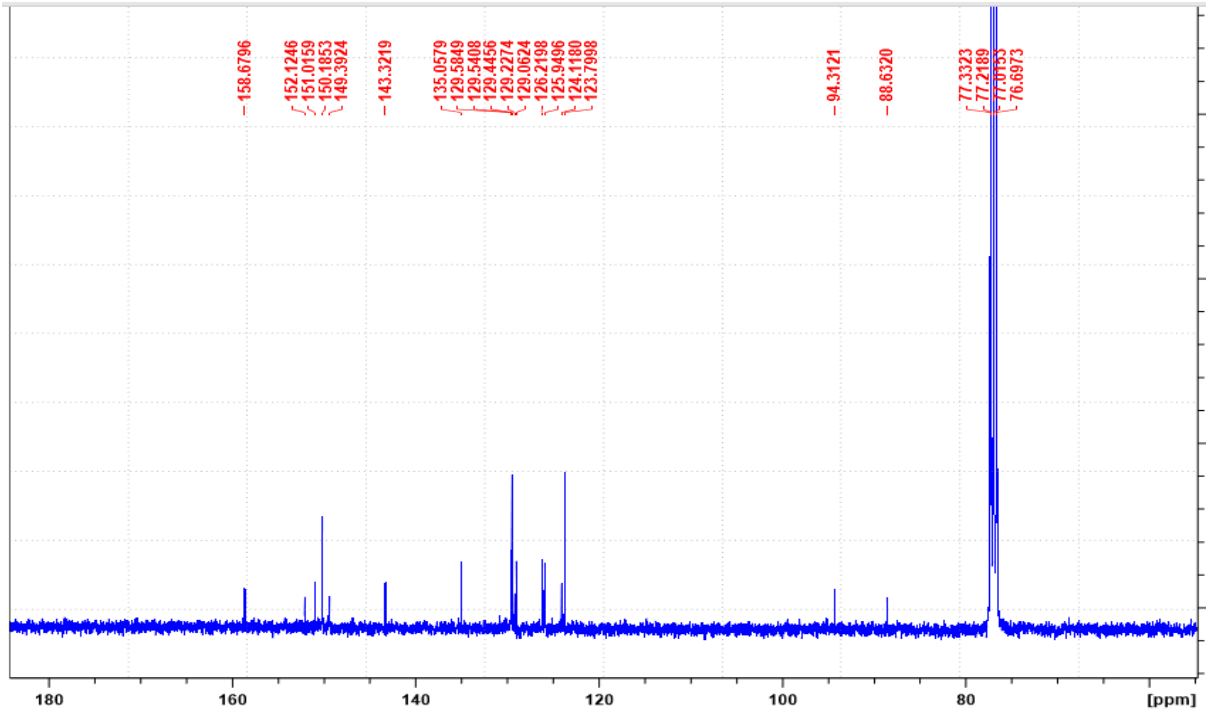

Figure 33: ^{13}C-NMR spectrum of **125d**

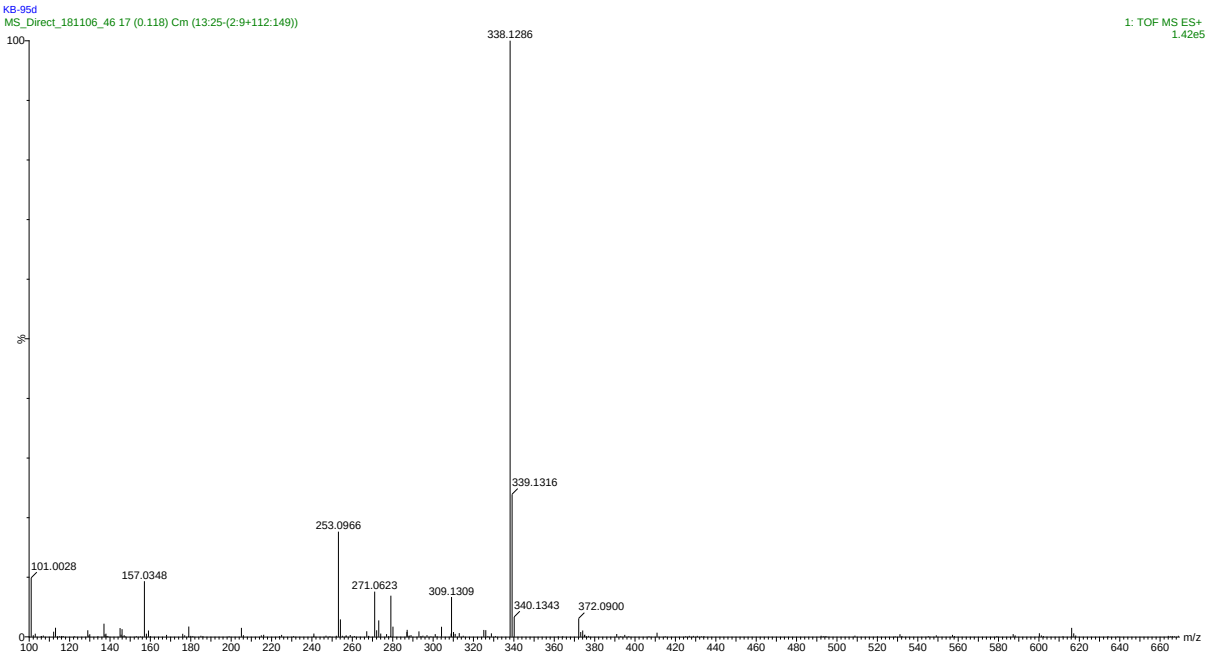

Figure 34: HRMS spectrum of **125d**

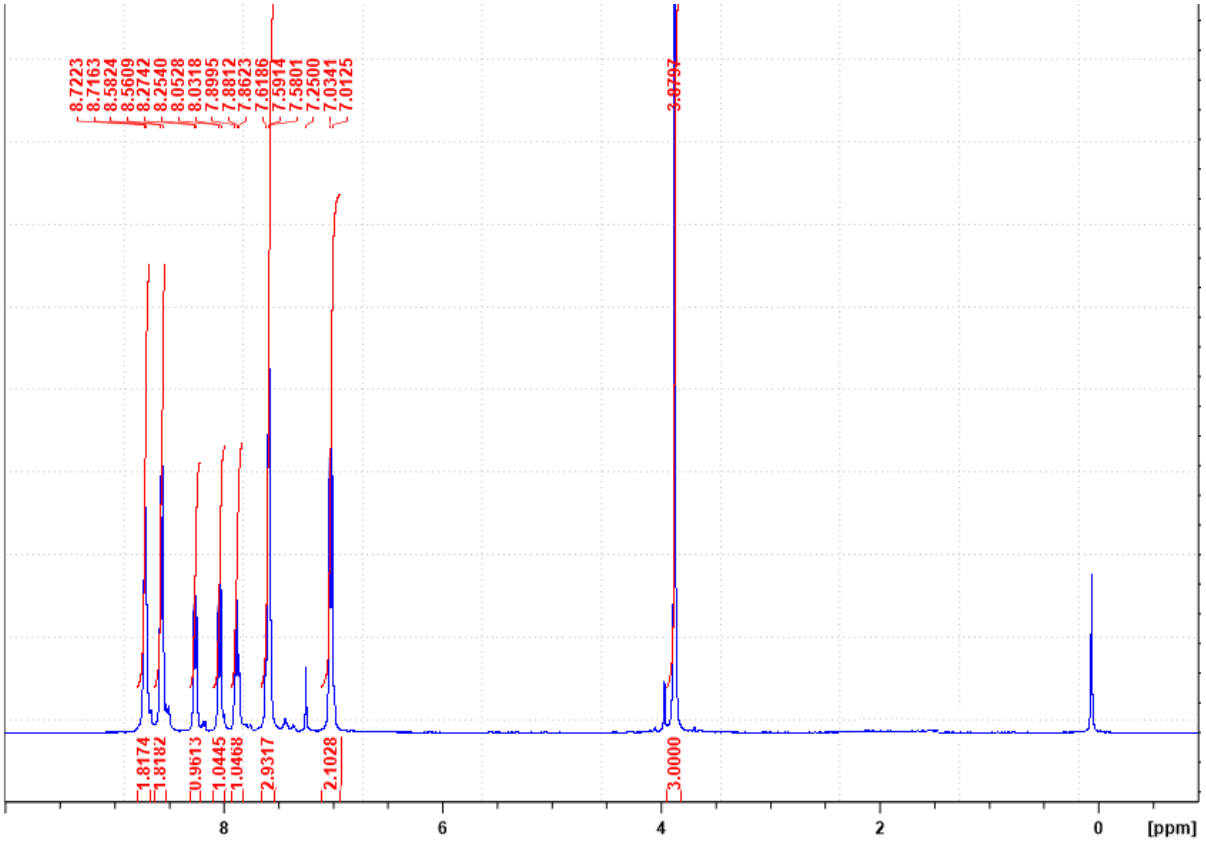

Figure 35: ^{1}H-NMR spectrum of **125e**

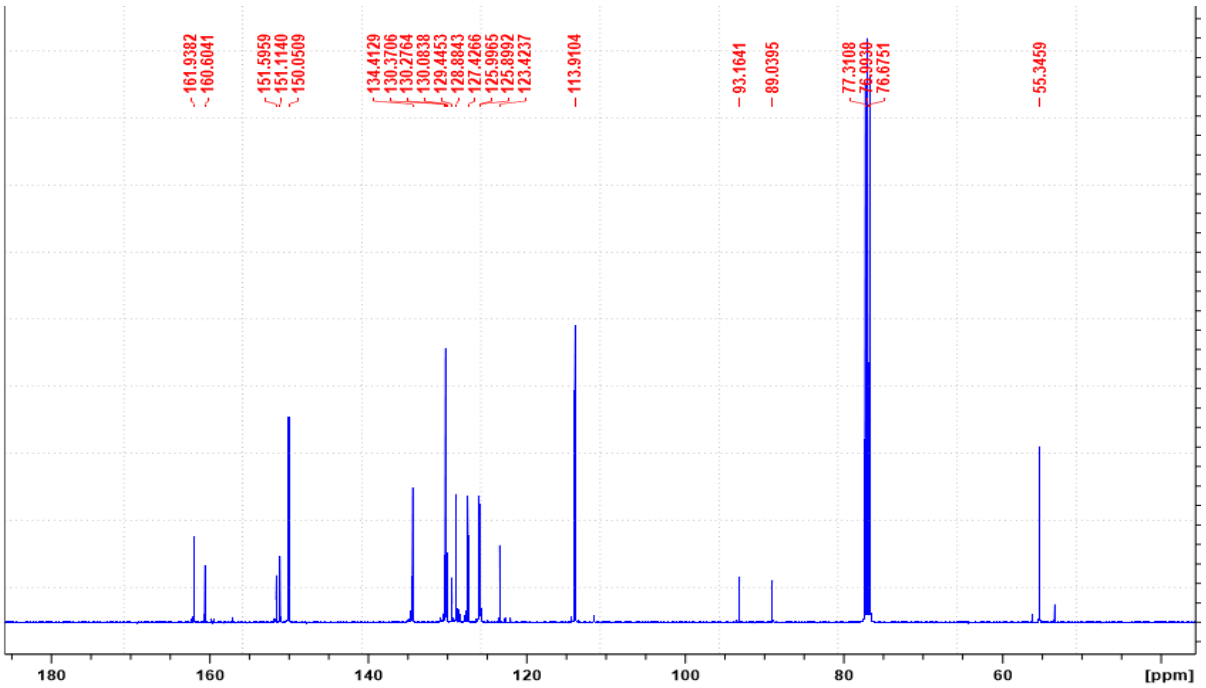

Figure 36: ^{13}C-NMR spectrum of **125e**

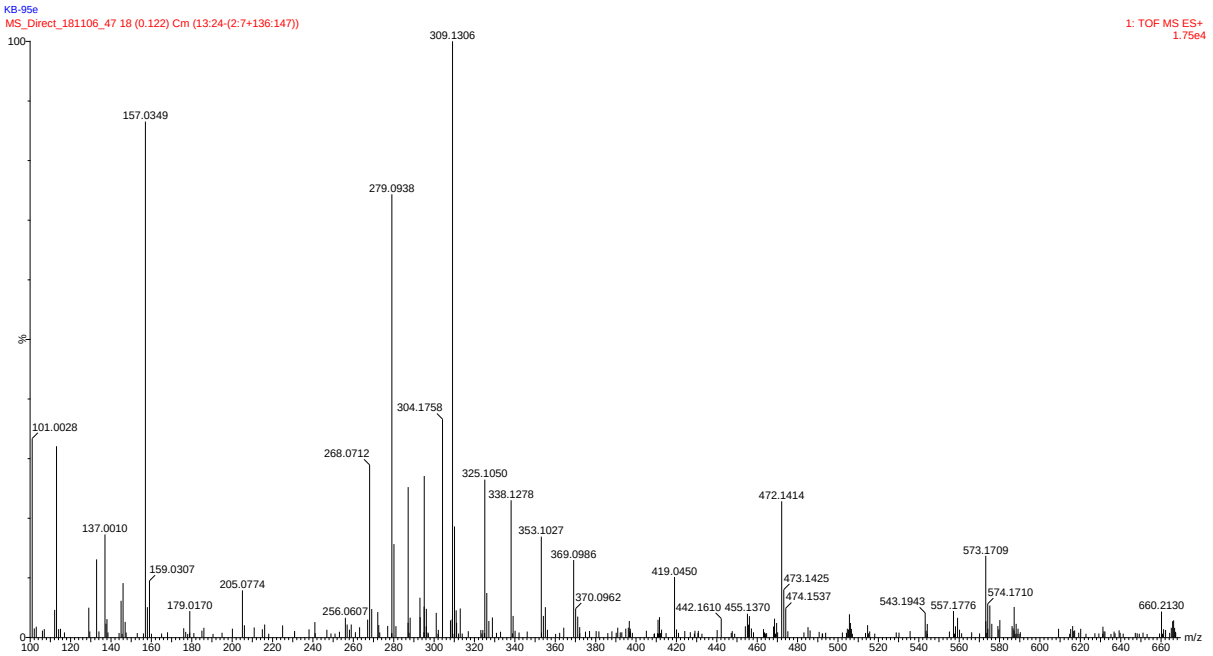

Figure 37: HRMS spectrum of **125e**

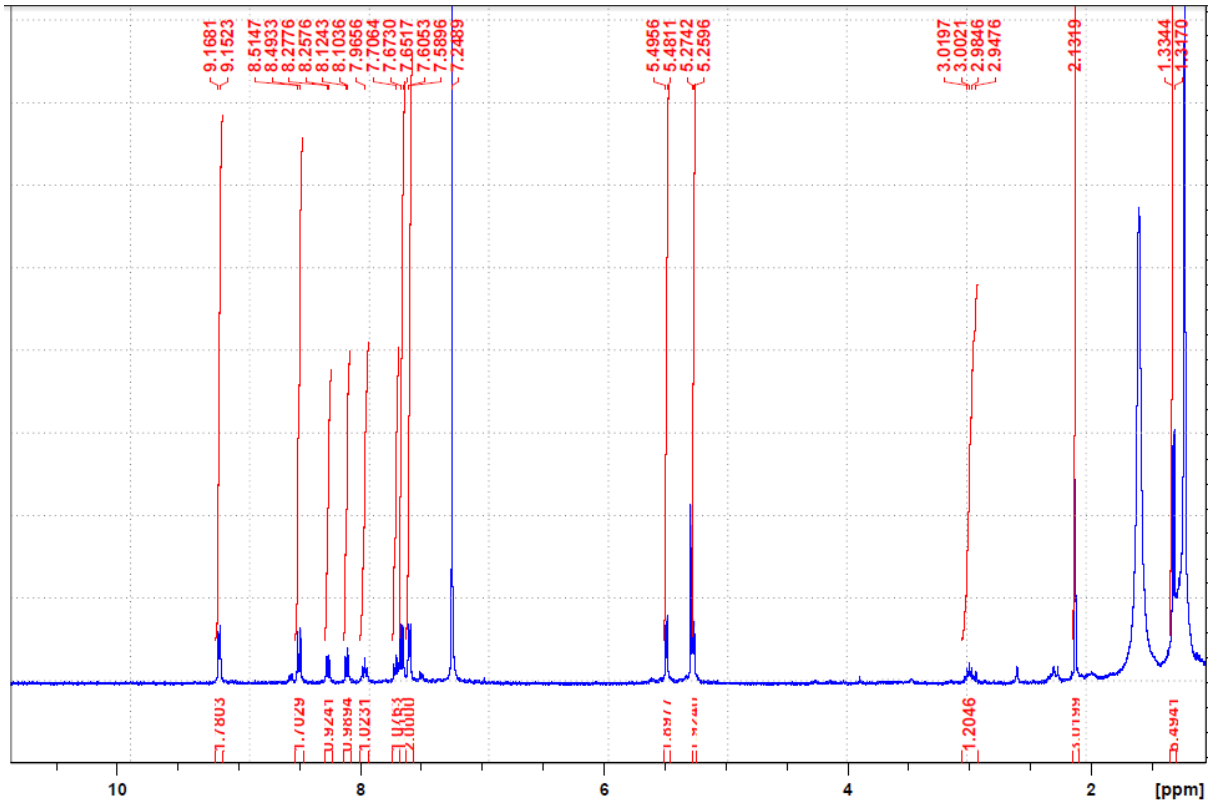

Figure 38: ^{1}H-NMR spectrum of **126a**

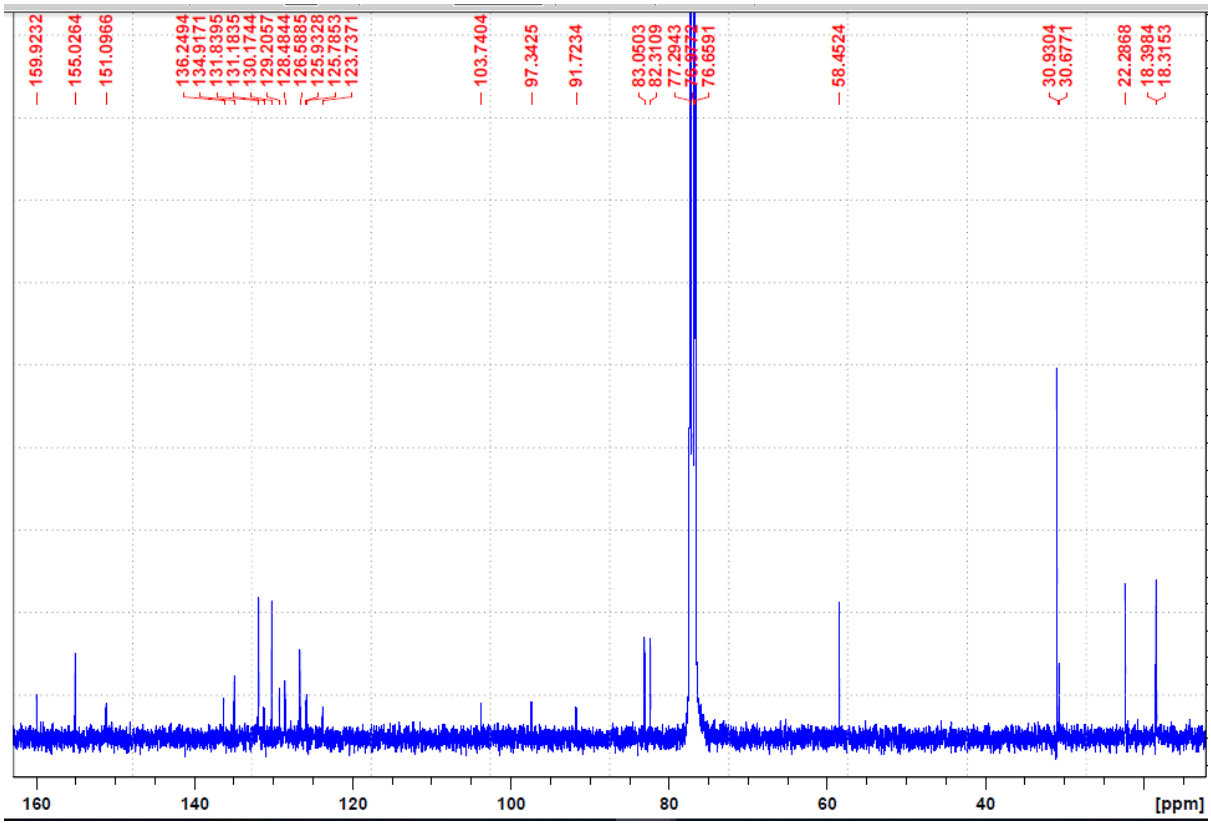

Figure 39: ^{13}C-NMR spectrum of **126a**

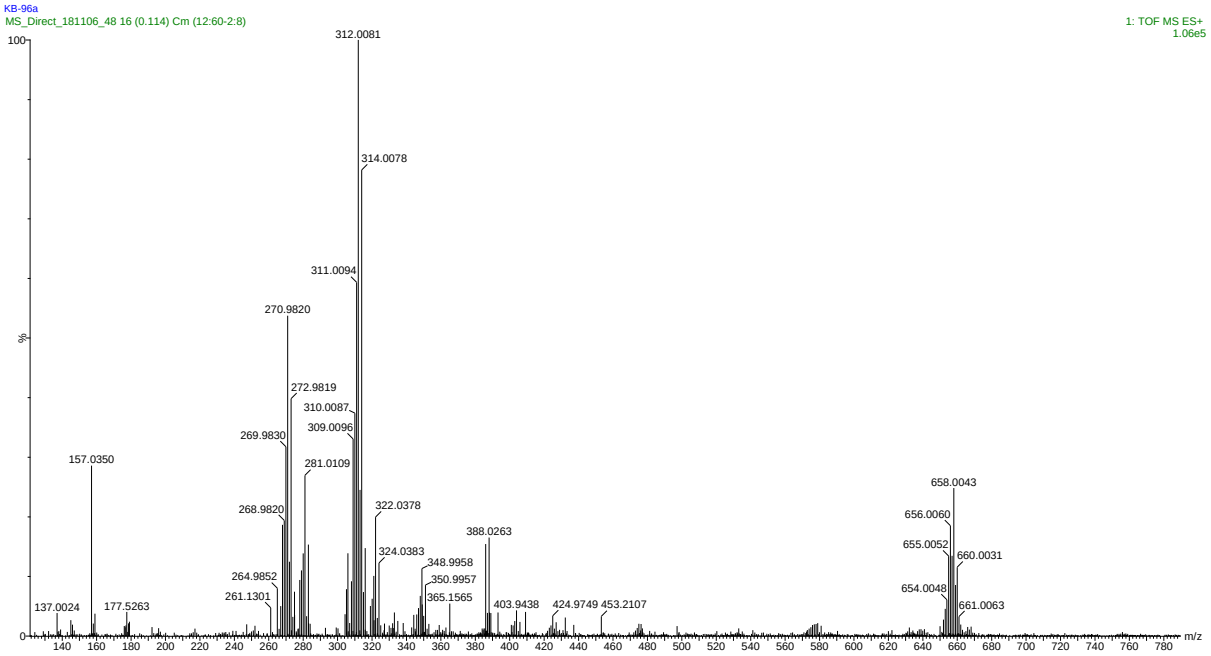

Figure 40: HRMS spectrum of **126a**

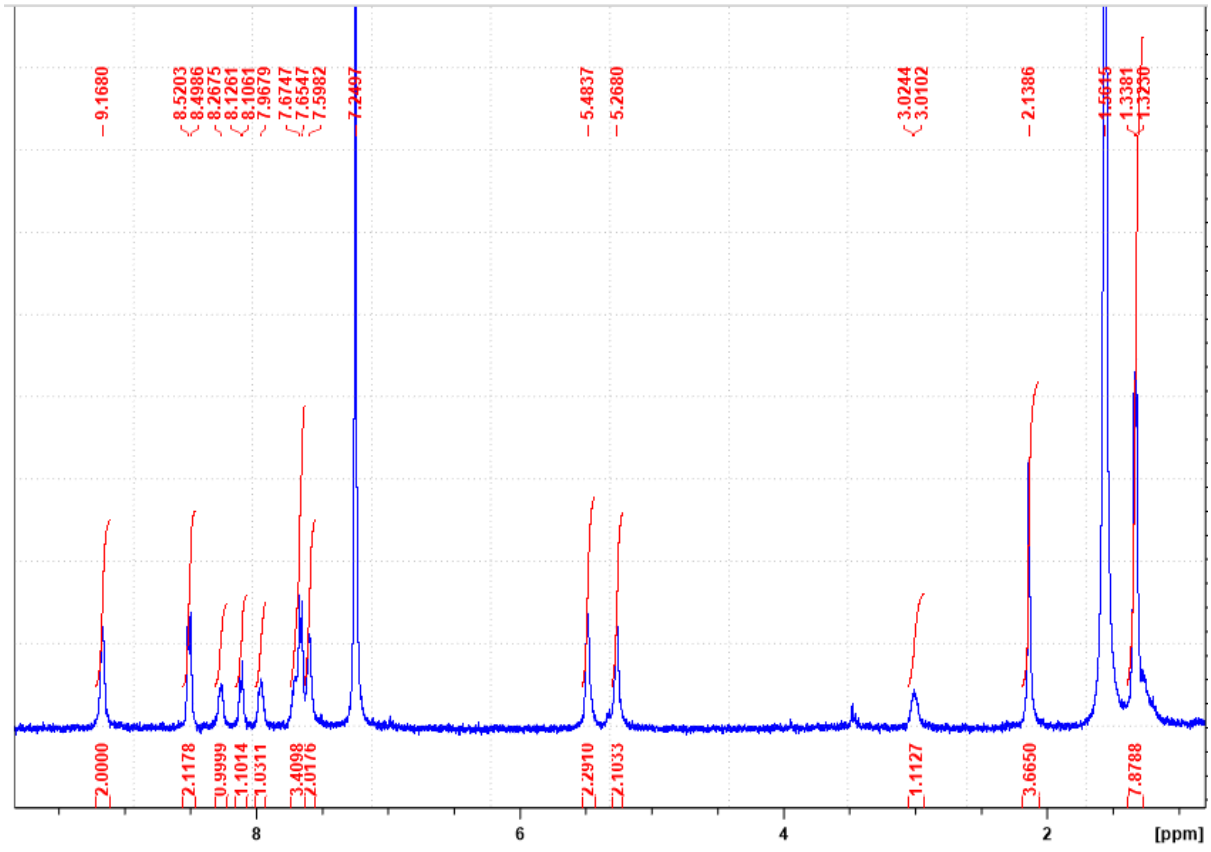

Figure 41: ^{1}H-NMR spectrum of **126b**

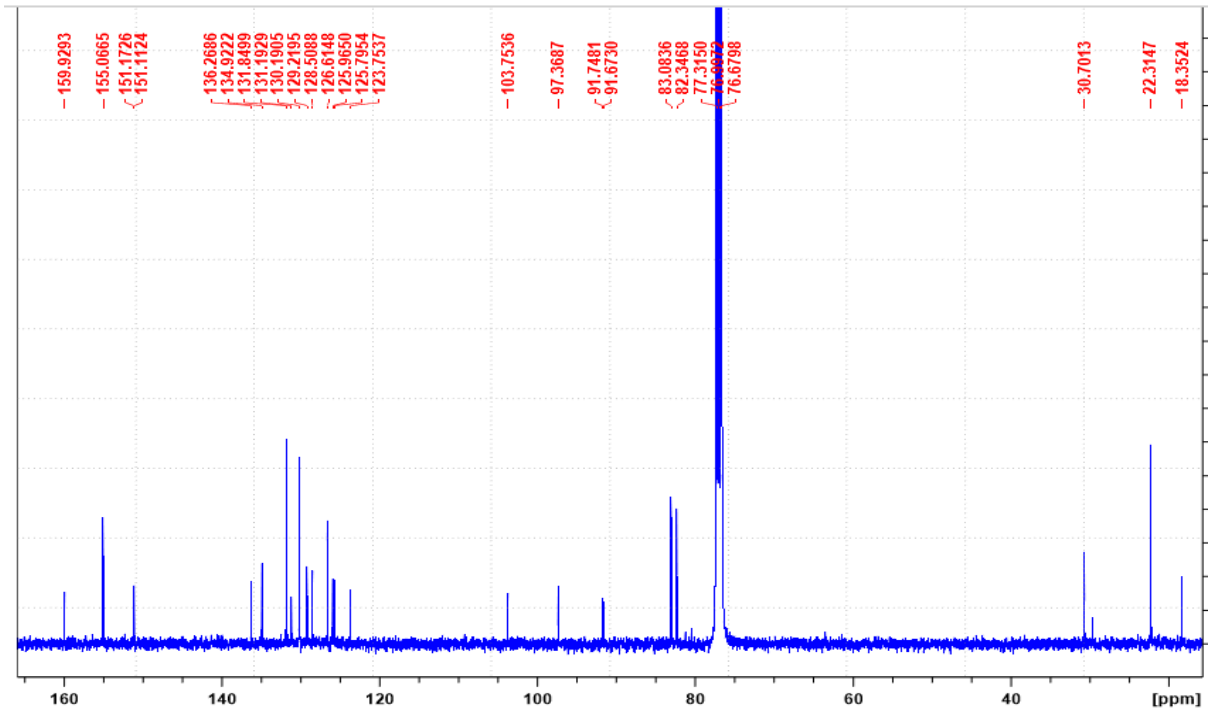

Figure 42: ^{13}C-NMR spectrum of **126b**

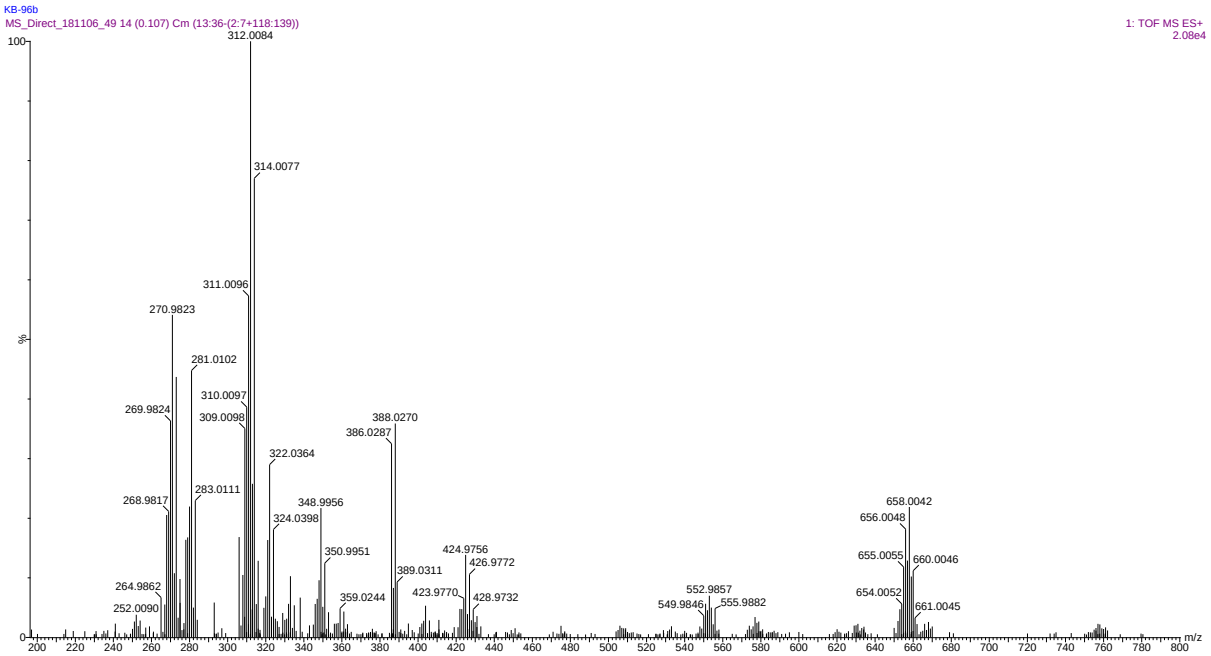

Figure 43: HRMS spectrum of **126b**

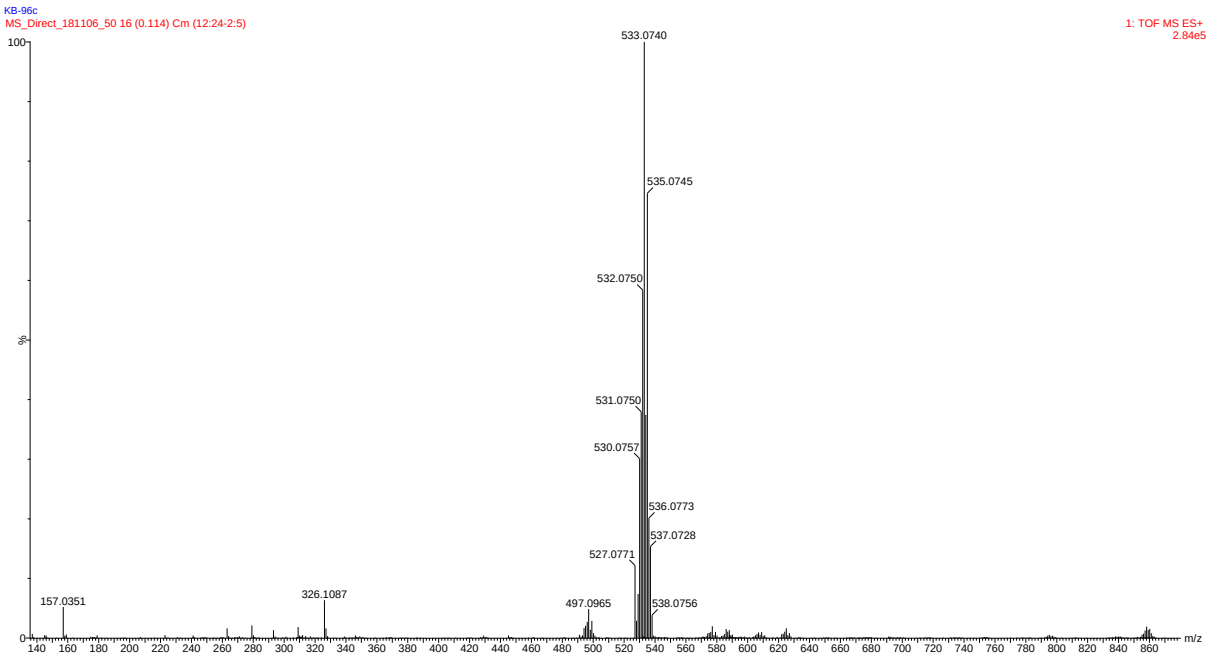

Figure 44: HRMS spectrum of **126c**

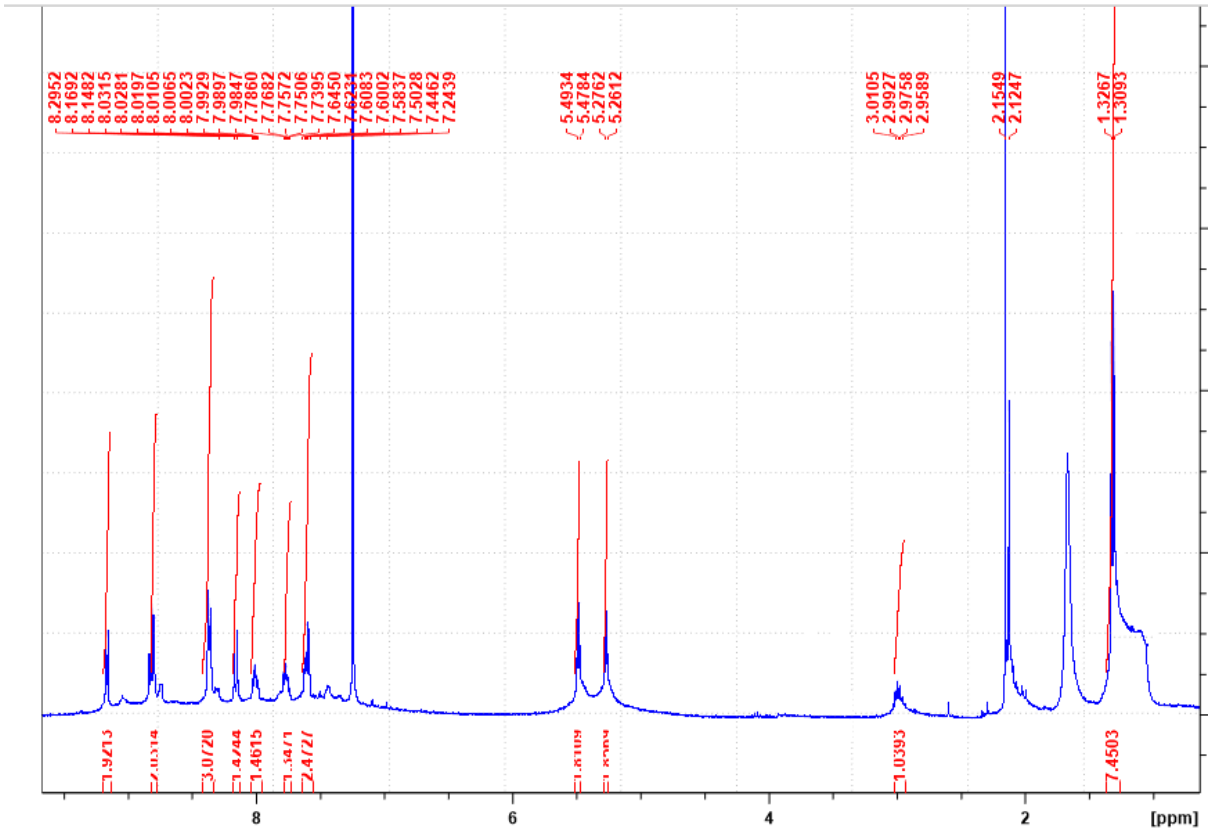

Figure 45: ^{1}H-NMR spectrum of **126d**

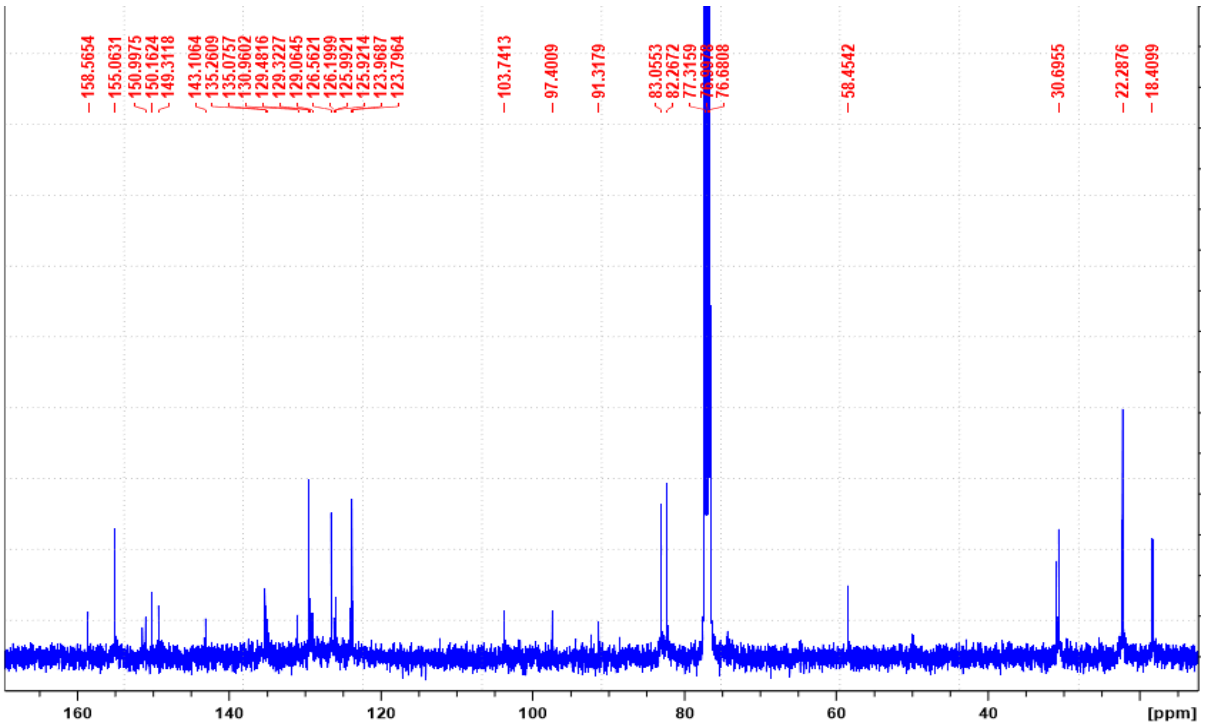

Figure 46: ^{13}C-NMR spectrum of **126d**

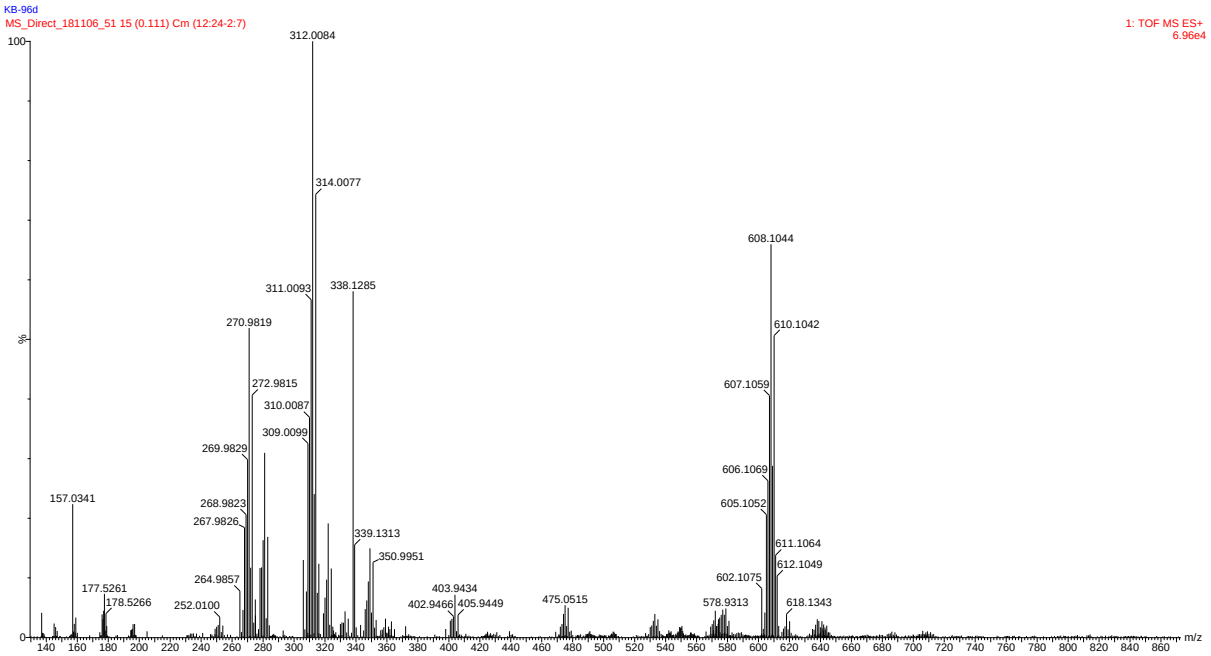

Figure 47: HRMS spectrum of **126d**

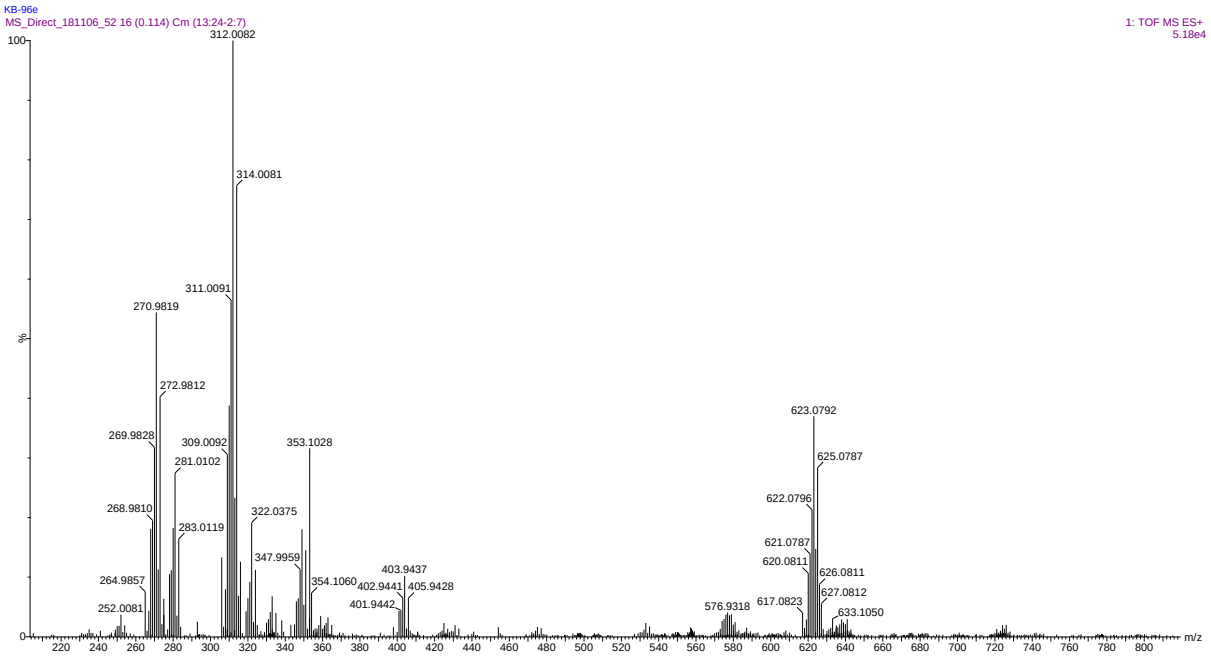

Figure 48: HRMS spectrum of **126e**